

TRANSPORTATION POOLED FUND PROGRAM QUARTERLY PROGRESS REPORT

Lead Agency (FHWA or State DOT): _____

INSTRUCTIONS:

Project Managers and/or research project investigators should complete a quarterly progress report for each calendar quarter during which the projects are active. Please provide a project schedule status of the research activities tied to each task that is defined in the proposal; a percentage completion of each task; a concise discussion (2 or 3 sentences) of the current status, including accomplishments and problems encountered, if any. List all tasks, even if no work was done during this period.

Transportation Pooled Fund Program Project # <i>(i.e., SPR-2(XXX), SPR-3(XXX) or TPF-5(XXX))</i>		Transportation Pooled Fund Program - Report Period: <input type="checkbox"/> Quarter 1 (January 1 – March 31) <input type="checkbox"/> Quarter 2 (April 1 – June 30) <input type="checkbox"/> Quarter 3 (July 1 – September 30) <input type="checkbox"/> Quarter 4 (October 1 – December 31)	
Project Title:			
Name of Project Manager(s):	Phone Number:	E-Mail	
Lead Agency Project ID:	Other Project ID (i.e., contract #):	Project Start Date:	
Original Project End Date:	Current Project End Date:	Number of Extensions:	

Project schedule status:

- On schedule
 On revised schedule
 Ahead of schedule
 Behind schedule

Overall Project Statistics:

Total Project Budget	Total Cost to Date for Project	Percentage of Work Completed to Date

Quarterly Project Statistics:

Total Project Expenses and Percentage This Quarter	Total Amount of Funds Expended This Quarter	Total Percentage of Time Used to Date

Project Description:

Progress this Quarter (includes meetings, work plan status, contract status, significant progress, etc.):

Anticipated work next quarter:

Significant Results:

Circumstance affecting project or budget. (Please describe any challenges encountered or anticipated that might affect the completion of the project within the time, scope and fiscal constraints set forth in the agreement, along with recommended solutions to those problems).

Potential Implementation:

SESSION 1: Purdue University

Progress this Quarter (includes meetings, work plan status, contract status, significant progress, etc.):

The work performed this Quarter at Purdue has been divided in four sections. In addition, previously completed work that is ready in chapter form is provided in the final section of this document.

- 1. Gas Permeability Round Robin: repeatability of the oxygen diffusivity and oxygen permeability tests (Purdue University and EMPA laboratory)
- 2. Chloride Binding study: preliminary results
- 3. Influence of salts on gas transport mechanisms
- 4. Electrical Resistivity testing
- 5. List of papers attached

1. Gas Permeability Round Robin: repeatability of the oxygen diffusivity and oxygen permeability tests (Purdue University and EMPA laboratory)

As anticipated in the previous report, the repeatability study of two gas transport testing instrument have been completed. The results were presented during a recent progress meeting and are being developed into a paper/draft chapter that will be available during the next quarter.

2. Chloride binding study: preliminary results

A study is underway to quantify the amount of bound chlorides for use in assessing the chloride ingress during absorption and diffusion. Specifically, this investigation focus on the development of a technique for the evaluation of the capacity to bind chlorides in cementitious materials.

Materials

Most of the tests were performed using 0.39 w/c paste (Type I ordinary portland cement). Some results that will be presented refer to concrete samples with a w/c of 0.42 whose mixture proportions are presented in Table 1.

Table 1: Mixture proportions of mortar by mass
(assuming SSD condition)

	Mixture proportions
Cement [kg/m ³]	609.93
Sand [kg/m ³]	1385.38
Water [kg/m ³]	253.39
HRWR [kg/m ³]	1.16
w/c	0.42

Paste samples were cast using cylindrical containers (34 mm diameter and 50 mm height); they were then kept sealed in a 50 ± 0.1 °C oven for 3 or 5 months in order to accelerate its hydration.

Experimental details

With reference to the work done by Delagrave [1], Tang [2] an internal procedure has been developed to evaluate the amount of bound chlorides. Further tests will be performed in order to refine some steps. The current methodology adopted is summarized below.

- 1) Paste sample is initially ground to pass 2-mm sieve.
- 2) The powder is vacuum dried for 4 days in a desiccator and subsequently kept at 11% RH for seven days.

Note: this step was skipped in this preliminary investigation.

- 3) The powder samples are then submerged in sodium chloride solutions and kept in a properly closed container to avoid any evaporation.

For most tests presented in this study, 10 g of powder was used with 25 ml of solution in different concentration.

- 4) The chloride concentration of chloride solution is evaluated using an automatic titration unit (Figure 1) at time 0 (before the solution touches the powder) and after 3 weeks of immersion.

In this study the solution was monitored instead every day for the first week and every two days for the following weeks in order to investigate the equilibrium time. 0.5 g of solution was pipetted and analyzed after having added 40 ml of deionized water. In case of low chloride concentration expected, 1 ml of 0.01 M NaCl solution was added.

- 5) After each test, the samples were shook in order to avoid sedimentation.



Figure 1: Automatic titration unit

In the all procedure it has been seen that the critical point is the correct dosage of solution that has to be precisely quantified in the range 0.4990 g to 0.5010 g. In our study a 5 ml syringe and an analytical balance (precision of ± 0.0001 g) has been used. In addition, to avoid contamination among different solutions when tested at the same time, the syringe was rinsed twice with deionized water in between each measurement.

The main steps of the procedure are summarized in Figure 2.



Figure 2: Some steps of the chloride binding test

Results

Repeatability study

In order to establish the accuracy in the evaluation of the bound chloride, three powder samples from the same paste specimen were randomly selected and split in seven parts (10 g). Each part was submerged in 25 ml of 0.1% NaCl solution at the same time and one sample every day was tested in order to evaluate the concentration change of the solution. Additionally, in order to check the homogeneity of the solution, four solution samples were extracted and tested every day. The results are presented in Figure 3 in terms of solution concentration and in Figure 4 in terms of bound chloride. The homogeneity of the solution is instead pictured in Figure 5 where the error bars describe the variation range of the solution measured among the four samples every testing day.

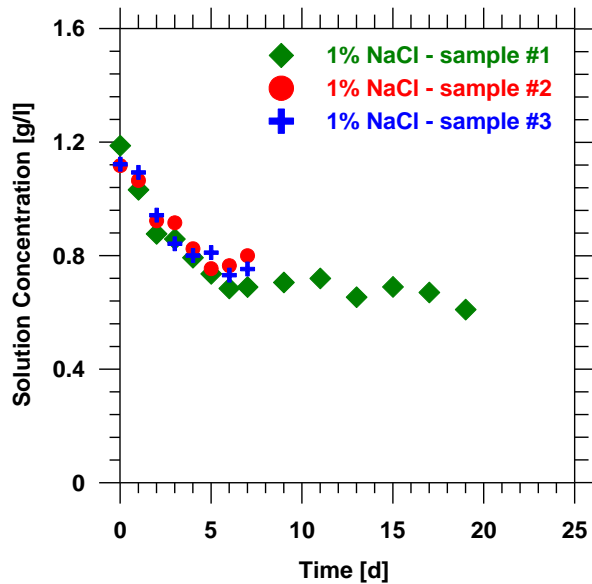


Figure 3: Change in the 1% Sodium chloride solution with time

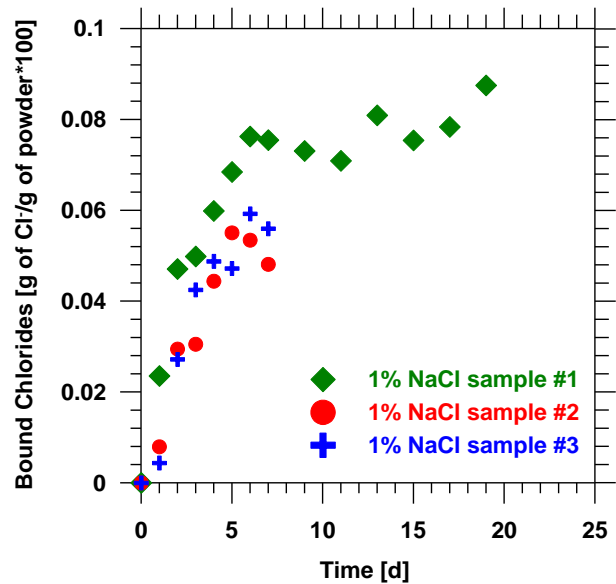


Figure 4: Fraction of bound chlorides with respect to the mass of powder during immersion

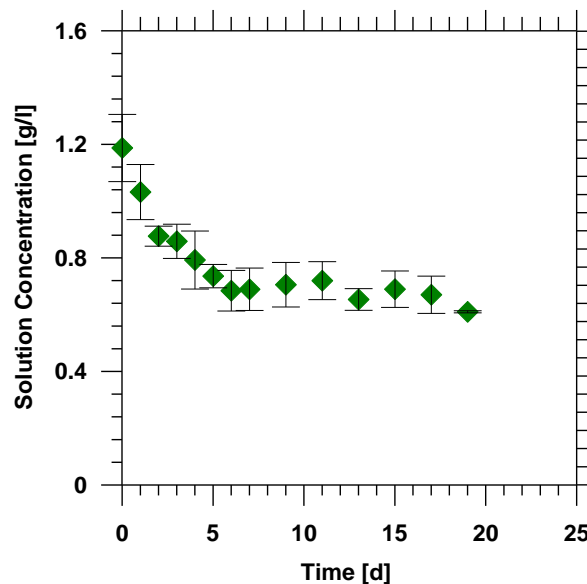


Figure 5: Error bars that indicate the range of variation of each chloride measurement for paste samples

The results presented above show reasonable agreement among the tests and limited variation in the solution concentration.

An additional check has been done using a concrete powder sample. Due to the presence of aggregates it is expectable a higher variation in the chloride binding behavior among different samples coming from the same material. To check this, a concrete cylinder has been grinded and the powder collected every millimeter of depth. Two powder samples (3 g each) were submerged in a 0.3% NaCl solution and the concentration was monitored for 23 days. The

concentration of the solution has been chosen in order to have the same ratio between the total amount of chlorides in solution and the powder of the 1% NaCl solution paste sample that will be presented in the following paragraph. The results are presented in terms of solution concentration and chloride bound in Figure 6 and 7. The comparison between paste and concrete powder test is also showed in Figure 7.

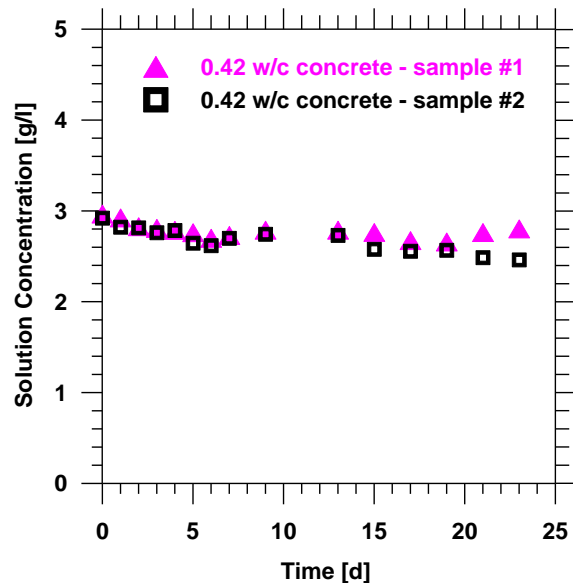


Figure 6: Concrete samples, change in concentration with time in a 0.3% NaCl solution

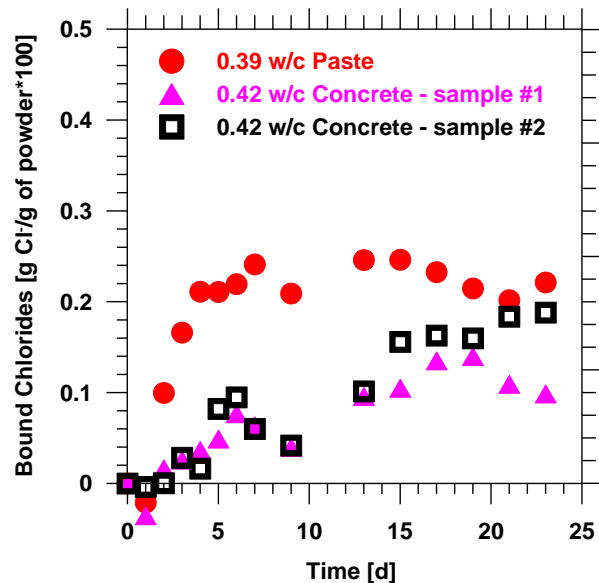


Figure 7: Chloride bound for paste and concrete samples.

It can be seen a very different initial behavior between paste and concrete. The total amount of bound chlorides at 23 days looks, however, similar for both materials. It should be also noted that concrete samples show higher variability compared to paste samples (Figure 3 and 4).

Non-linearity investigation

Previous researches have proved that the chloride binding is a non-linear phenomenon. Indeed, the amount of bound chlorides, chemically bound and physically adsorbed, increases with the increase in the chloride concentration of the surrounding solution.

Powder samples from paste were submerged in 0.1, 1, 2 and 4% sodium chloride solution and the concentration was monitored as described above. In this set of tests only one sample for each solution was used and the solution was pipetted every day from the same container. We should point out that this methodology might cause a slight variation in the binding behavior since the total amount of chlorides present in solution was decreasing every time we were extracting some solution. In the calculation, the change in the amount of solution was however taken into account. The results are presented in Figure 8 where the concentration of the solution is expressed as function of time of immersion of the powder. In Figure 9 instead the percentage of chloride bound are presented versus the immersion time. The percentage of bound chlorides C_b has been evaluated according to Equation 1:

$$C_b(t) = \frac{(C(t) - C_i)}{w} \cdot 100 \quad (1)$$

where $C(t)$ is the chlorides concentration evaluated at time t (g), C_i is the initial chloride concentration of the solution (g) and w is the total amount of powder submerged in the solution (g).

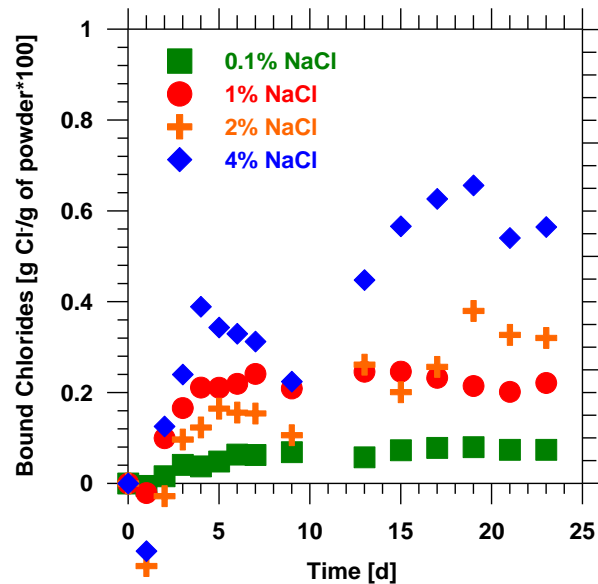


Figure 8: Bound chlorides percentage versus immersion time

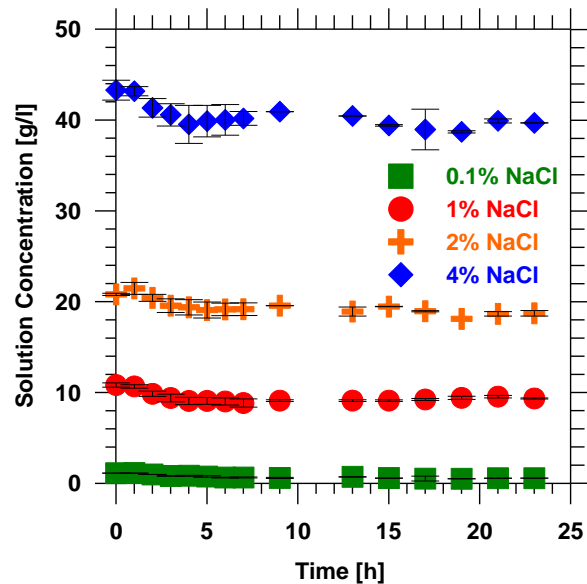


Figure 9: Chloride concentration of the solution versus immersion time

From Figure 8 it can be seen that there is an initial release of chloride ions, followed by the binding mechanisms. It is confirmed the increase in the amount of bound chlorides when the solution concentration increases. In addition, it can be noticed that also the equilibrium time is function of the solution concentration. Indeed, the amount of chlorides bound start to be constant at earlier ages for low solution concentration. 0.1% and 1% solution can be considered in equilibrium already after 10 days, while 2% and 4% might need longer time to reach the equilibrium point. The same observation can be derived from Figure 9.

The results of the chloride binding test are usually presented with the so called chloride binding isotherm. The one relative to the paste sample analyzed in this study is presented in Figure 10. The results obtained are very close to some found in literature (Tang 1993) and presented in Figure 11.

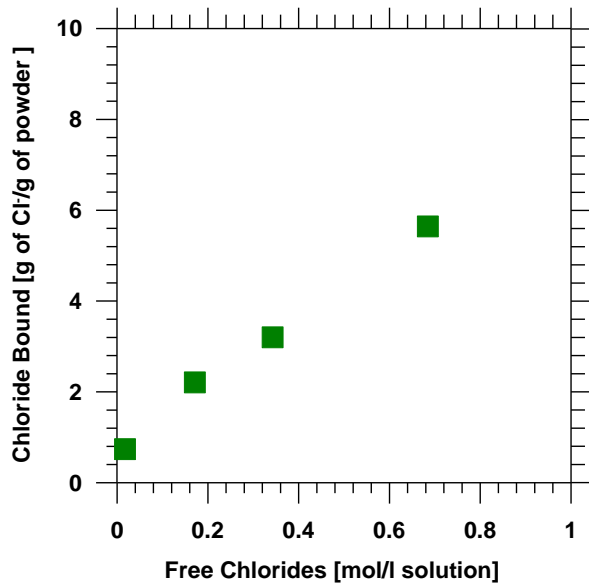


Figure 10: Chloride binding isotherm for 0.39 w/c paste sample

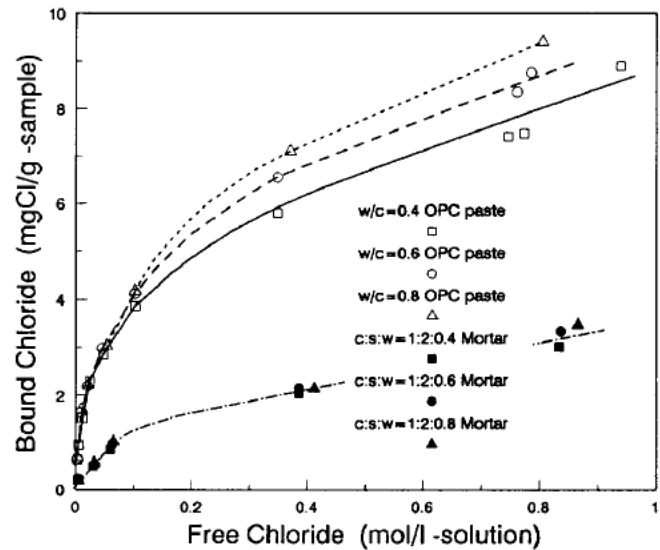


Figure 11: Chloride binding isotherms from literature (Tang 1993)

Future work

Future work will be addressed in order to define the proper range of concentration needed for the definition of the chloride binding isotherm. An additional set of test will be performed to further check the equilibrium of the chosen concentration.

References

- [1] A. Delagrave, J. Marchand, J. Ollivier, S. Julien and K. Hazrati, Chloride binding capacity of various hydrated cement paste systems, *Advanced Cement Based Materials*, Vol. 6 (1997), pp.28-35
- [2] L.Tang and L.O. Nilsson, Chloride binding capacity and binding isotherms of OPC pastes and mortars, *Cement and Concrete Research*, Vol. 23 (1993), pp. 247-253

3. Influence of salts on gas transport mechanisms and resistivity

The transport properties are known to be strongly related to the moisture content and the distribution of moisture in the concrete. This study investigates the influence of deicing salt on the gas permeability and gas diffusivity of concrete.

Materials and samples preparation

The samples used for this study are 0.42 w/c mortar samples whose mixture proportions are presented in Table 2.

Table 2: Mixture proportions of 0.42 w/c mortar by mass (assuming SSD condition)

	Mixture proportions
Cement [kg/m ³]	1026.7
Sand [kg/m ³]	2390.7
Water [kg/m ³]	432.2
w/c	0.42

Mortar samples were cast in 4 x 8 inches cylindrical molds and demolded after 24 hours. They were then sealed in plastic bags for about 6 months; subsequently, they were cored into smaller (68 mm of diameter and 25 mm of height) samples for gas permeability tests. For gas diffusivity, instead, 102 mm of diameter and 50 mm of height cylinders were cut using a wet saw. Oxygen diffusivity samples were also used for resistivity measurements.

All samples were then submerged in different salt solutions and their mass was monitored. In this phase resistivity was also measured. The solutions used in this study were chosen in order to avoid that crystal salts might block some external pores affecting the results. They are the following: 15% magnesium chloride, 16% calcium chloride, 17% sodium chloride and tap water.

Samples were kept submerged until their mass variation was lower than 0.1% for three consecutive days. All samples were then dried in a 50±0.1 °C and 30% RH oven for 7 days (gas permeability samples) and for 14 days (gas diffusivity samples). They were then cooled in a desiccator for two hours and then tested. Additionally, the mass of the samples was monitored during all phases.

After the test oxygen diffusivity samples were vacuum saturated and then were oven dried at 100 °C in order to evaluate the porosity, needed for the degree of saturation evaluation.

Instruments used

The oxygen permeability has been measured using a falling head permeameter (Ballim 1991), usually known as South African apparatus; it is shown in Figure 11. Oxygen diffusivity was instead measured using the instrument pictured in Figure 12 originally developed by Lawrence (Lawrence 1984).



Figure 11: South African instrument



Figure 12: Oxygen diffusivity instrument

The bulk resistivity of the material was evaluated using stainless steel plate electrodes connected to a surface resistivity meter. The instrument set up is shown in Figure 13.

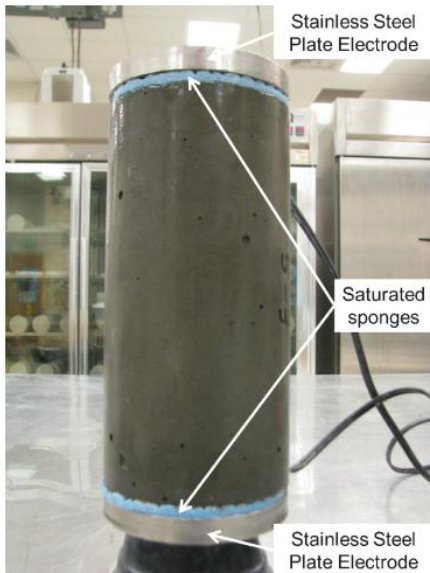
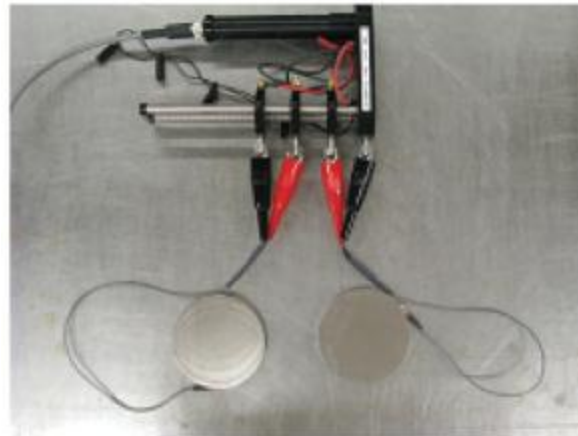


Figure 13: Bulk resistivity instrument



The degree of saturation has been evaluated following a modified version of the procedure described in ASTM C642. The saturation with boiling was indeed replaced by vacuum saturation of samples submerged in water.

Results

The gas permeability results are presented as function of the degree of saturation in Figure 14. Oxygen diffusivity results are instead pictured in Figure 15. The error bars represent the range of variation in the results among the samples testes (four in the case of gas permeability and three in the case of oxygen diffusivity).

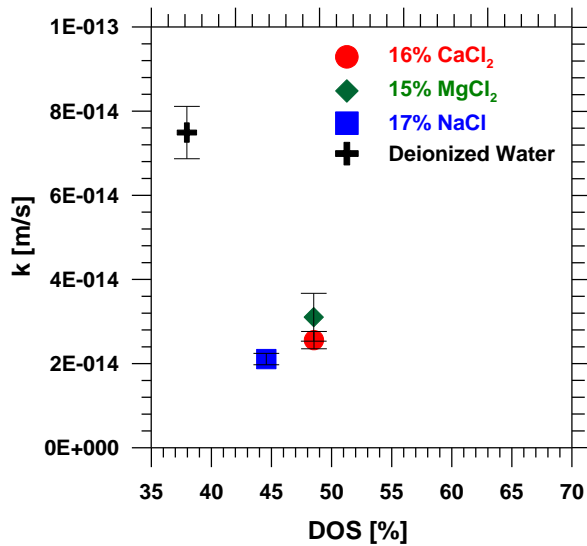


Figure 14: Oxygen permeability versus degree of saturation

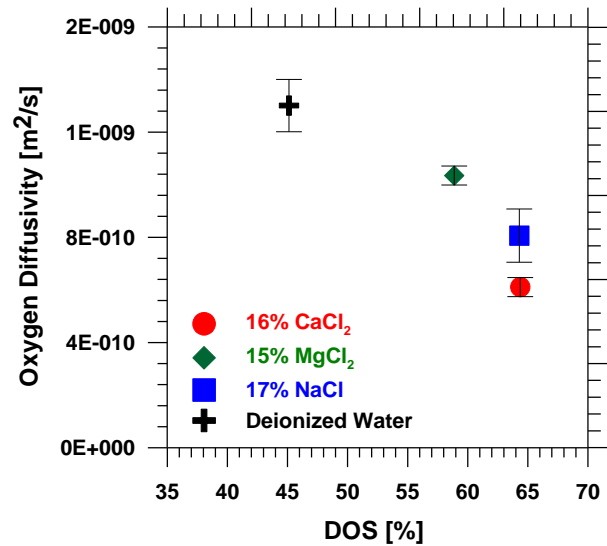


Figure 15: Oxygen diffusivity versus degree of saturation

It is evident the influence of the presence of salt that causes an increase of the degree of saturation and a consequent lower “apparent” oxygen permeability and diffusivity. It is worth to underline that the material is the same and the difference is only due to the presence of salt in the system. Consequently, care must be taken when performing in-situ testing since the presence of deicing salt might alter the real response of the material analyzed.

References

- [1] Y. Ballim, “A low cost, falling head permeameter for measuring concrete gas permeability”, *Concrete Beton*, 61 (1991) 13-18
- [2] C. D. Lawrence, Transport of oxygen through concrete, in D.P. Glasser (Ed.), *The chemistry and Chemical-related Properties of Cement*, British Ceramic Society Proceedings 35 (1984) 277-293

4. Electrical resistivity testing

It is known that several factors influence the electric resistivity measurement and one of the most important is the degree of saturation. Several studies have analyzed how resistivity changes with moisture content, but a single expression was not yet proposed that predicts how drying changes the electrical response. A study was done suggesting the use of a saturation function to take into account or correct resistivity measurements of unsaturated concrete.

Starting from Archie’s equation that is valid for electrical conductivity of a rock soaked in brine, an expression has been proposed to describe electrical conductivity of partially saturated concrete σ_c (Equation 2):

$$\sigma_c(S) = \frac{\sigma_p^0}{S} \frac{1}{F} f(S) \quad (2)$$

where σ_p^0 is the pore solution conductivity at saturation, S is the degree of saturation, F is the formation factor and f(S) represents the saturation factor. Each term of Equation 2 is further explained hereafter:

- the term σ_p^0/S accounts for the pore solution conductivity that depends on the mix design but also on eventual concentration due to water loss. A correction is also proposed in the study, to take into account the ionic strength that increases during drying. The pore solution conductivity is assumed to be proportional to the ionic strength and an alternative formulation of Equation 2 has been proposed:

$$\frac{\sigma_c(S)}{\sigma_c^0} = S^{n-1+\delta} \quad (3)$$

where δ represents the degree to which the pore solution conductivity is not inversely proportional to water content.

- $1/F$ can also be expressed as σ_c^0/σ_p^0 , the inverse of the formation factor which represents the total pore space available;

- and finally f(S) is the saturation factor that accounts for the connectivity of the fluid in the pore space. A power-law relationship is often used (Equation 3):

$$f(S) = S^n \quad (4)$$

n is a fitting parameter called *saturation coefficient*. More research is needed, however the first experimental results show values in the range of 3.5 to 5.0 for cementitious materials and indicate the potential that a single function may work for cementitious materials (with n equals approximately 4). These findings were further confirmed through a VCCTL (Virtual Cement and Concrete Testing Laboratory) software used to estimate the form of the saturation function of different cementitious systems.

The study was completed with two examples of application of the saturation model: the first compares sealed and saturated curing conditions. It shows that the measured conductivity strongly depends on how the sample was cured and conditioned; specifically concrete stored in lime water shows a conductivity that is almost 4 times the one evaluated for sealed samples. With re-saturation, the conductivity becomes instead eight times the one of the sealed sample. This result highlights the importance of taking into account the degree of saturation and the storage condition since it also influence the degree of hydration (and consequently the formation factor which is a material property). The second example instead presents the application of the saturation model in the case of concrete subject to drying conditions. The saturation function showed very good agreement with experimental results and the VCCTL simulation showing similar saturation coefficients. The results suggest also that the model agrees for relative humidity higher than 65%-70%; for RH lower instead it seems the saturation function (connectivity of the fluid in the pore space) becomes very low. It is maybe due to the change in the conduction pathway that involves the the gel pores or the wall of the capillary pores instead of the entire large capillary pore network.

The paper relative to the above presented study is attached (Paper 7).

An additional study has been performed to evaluate the influence of other factors on resistivity measurements. Specifically, the influence of sample geometry, of temperature, of sample storage and conditioning was investigated.

More details concerning each of the factor analyzed are below:

- 1) Resistance was measured on samples with different geometries: it has been proved that with an appropriate correction for geometry (k), the electrical resistivity values obtained are similar. The equation that relates resistance R and resistivity ρ , which is the material property is (Equation 5):

$$\rho = k R \quad (5)$$

- 2) The influence of temperature was instead proved using a variation of the Arrhenius law. The so called activation energy of conduction has been evaluated from the relation (the slope) between the logarithm of resistivity and the inverse of temperature. The increase in temperature causes indeed the increase of the ions mobility of the material's pore solution and consequently the decrease in resistivity. The tests were conducted on mortar samples and on pore solution samples. It has been noticed that activation energies change when measured on bulk cylinders or on the pore solutions, suggesting that also the microstructure plays a role.
- 3) Different curing and storage conditions determine different degree of hydration as well as different degree of saturation, but also the pore solution. Different ratios of the volume of the lime saturated solution to sample were considered. The resistivity has been monitored for both the solution and the samples. It has been seen a decrease in the resistivity of the solution probably due to the movement of ions from the sample to the solution. Not clear trend was seen instead for the resistivity of samples.

Additionally the influence of the DOH on the pore solution resistivity has been studied. A very good linear correlation between resistivity and degree of hydration was shown. The pore solution resistivity measured was also compared to the one evaluated using the Nist model (<http://ciks.cbt.nist.gov/poresolncalc.html>); it seems the experimental results follow the curves of the model corresponding to different dissolved alkali content in the solution, depending on the degree of hydration.

The complete version of the results summarized above are presented in a paper attached (Paper 10).

An AASHTO draft on electrical resistivity measurement is in preparation and will be presented in the next quarter report.

5. List of papers attached

The following draft papers will be attached at the end of this report:

- [1] Castro, J., Spragg, R., and Weiss, W. J., “*Internal Curing for W/C Systems Between 0.30 and 0.45: Impact on Water Absorption and Electrical Conductivity*,” ASCE Journal of Civil Engineering Materials
- [2] Castro, J. Bentz, D., and Weiss, W. J., (2011) “*Effect of Sample Conditioning on the Water Absorption of Concrete*,” Cement & Concrete Composites 33, p. 805–813 (2011)
- [3] Li, W., Pour-Ghaz, M., Castro, J., and Weiss, W. J., (accepted) “*Water Absorption and the Critical Degree of Saturation as it relates to Freeze-Thaw Damage in Concrete Pavement Joints*,” ASCE Journal of Civil Engineering Materials
- [4] M. Pour-Ghaz, R. Spragg, J. Weiss, ‘*Moisture profiles and diffusion coefficient in mortars containing shrinkage reducing admixtures*’, International RILEM Conference on Use of Superabsorbent Polymers, Denmark (2011)
- [5] Poursaee, A., and Weiss, W. J., (2010) “*An Automated Electrical Monitoring System (AEMS) to Assess Concrete Property Development*’, Journal of Automation in Construction, Volume 19, Issue 4, 2010, p. 485-490 (2010)
- [6] Sant, G., Rajabipour, F., and Weiss, W.J., (2008) ‘*The Influence of Temperature on Electrical Conductivity Measurements and Maturity Predictions in Cementitious Materials during Hydration*’, Indian Concrete Journal, p. 10 (2008)
- [7] R.P. Spragg, J. Castro, T Nantung, M. Paredes, and J. Weiss, ‘*Variability analysis of the bulk resistivity measured using concrete cylinders*’, Advances in Civil Engineering Materials, Vol.1
- [8] R. Spragg, J. Castro, W. Li, M.Pour-Ghaz, P.Huang, J. Weiss, *Wetting and Drying Concrete Using Aqueous Solutions Containing Deicing Salts*, Cement and Concrete Composites, Vol. 33, p. 535-542 (2011)
- [9] R.P. Spragg, C. Villani, K. Snyder, D. Bentz, J.W. Bullard and J. Weiss, *Electrical Resistivity Measurements in Cementitious Systems: Observations of Factors that Influence the Measurements*, TRB 92nd annual meeting (2012), submitted
- [10] W. J. Weiss, K. A. Snyder, J. W. Bullard and D. P. Bentz, Using a Saturation Function to Interpret the Electrical Properties of Partially Saturated Concrete, Journal of Materials in Civil Engineering (2012), accepted

Water Absorption and Electrical Conductivity for Internally Cured Mortars with a W/C between 0.30 and 0.45

Javier Castro¹; Robert Spragg²; and Jason Weiss, M.ASCE³

Abstract: Internal curing has emerged over the last decade as an approach to counteract the negative effects associated with self-desiccation in low water-to-cement ratio (w/c) mixtures. Specifically, much of the early research on internal curing focused on the reduction of autogenous shrinkage. Recent work has demonstrated, however, that internal curing can also be beneficial in reducing drying-shrinkage cracking, reducing the propensity for thermal cracking, reducing fluid absorption, and reducing ion diffusion in concrete. However, several aspects of internal curing still require closer examination. One of these aspects is the application of internal curing for mixtures with a wider range of water-to-cement ratios. This paper describes results from experiments that investigated the potential use of internal curing in mortar systems with w/c ratios of 0.30, 0.36, 0.42, and 0.45 that were cured under sealed conditions, in terms of water absorption and electrical conductivity. Test results show that internal curing reduces the water absorption in all the systems. Similarly, results obtained on electrical conductivity at late ages (1 year) also show a benefit. Care needs to be taken to analyze electrical conductivity results at early ages because of the increased amount of fluid resulting from the inclusion of the prewetted lightweight aggregate. DOI: 10.1061/(ASCE)MT.1943-5533.0000377. © 2012 American Society of Civil Engineers.

CE Database subject headings: Aggregates; Hydration; Mortars; Mixtures; Absorption; Electrical conductivity.

Author keywords: Internal curing; Lightweight aggregate; Water absorption; Electrical conductivity.

Background on Internal Curing

Internal curing has emerged over the last decade as a method to improve the performance of low water-to-cement ratio (w/c) mixtures [Rilem 2007; American Concrete Institute (ACI) 2008; ACI Committee 231 2010; Schlitter et al. 2010; Bentz and Weiss 2011]. Specifically, internal curing refers to the use of prewetted lightweight aggregate (LWA) or other water filled inclusions, such as super absorbent polymers (SAP) or cellular fibers that can provide curing water throughout the cross section of the concrete. This differs from conventional water curing in which water is provided after placement, and in which the water is applied only at the surface of the concrete. Internal curing was originally promoted to reduce autogenous shrinkage and autogenous shrinkage cracking (Bentz and Snyder 1999; Jensen and Hansen 2001a; Jensen and Hansen 2001b; Jensen 2005; Cusson and Hoogeveen 2008; Lopez et al. 2009). However, its potential benefits include reducing drying-shrinkage cracking (Henkensiefken et al. 2009a), reducing the likelihood of thermal cracking (Schlitter et al. 2010; Byard et al. 2010) and reducing the likelihood of plastic-shrinkage cracking (Henkensiefken et al. 2010). Internal curing can also improve

freeze-thaw resistance (INDOT 2010), increase the resistance to fluid absorption (Bentz and Snyder 1999; Henkensiefken et al. 2009b; Peled et al. 2010) and reduce ion diffusion (Bentz 2009) in concrete. Internal curing has great potential for the concrete industry to create a longer lasting, more sustainable product. Several aspects of internal curing still require closer examination. One of these aspects is the use of internal curing for mixtures containing a wider range of water-to-cement ratios (e.g., mixtures with a w/c between 0.30 and 0.45), for which only a few publications are available (Espinoza and Lopez 2011).

To fully understand how internal curing works it must be recognized that the hydration of cement paste causes a volume reduction that is known as chemical shrinkage (Le Chatelier 1900; Powers 1935; L'Hermite 1960). While chemical shrinkage begins when the water comes in contact with the cement, it has different impacts on the system before and after the paste sets. Before setting, chemical shrinkage causes bulk shrinkage of the cement paste that is equal to the total external volume change. After setting, however, the cement paste becomes stiff enough to resist a portion of the volume change caused by chemical shrinkage (Barcelo et al. 1999; Sant et al. 2006). Contact between the cement particles does not permit this volume reduction to occur. As a result, vapor-filled pockets form inside the cement paste in the largest pores (Jensen and Hansen 2001b; Couch et al. 2006; Lura et al. 2009). This is known as self-desiccation.

Chemical shrinkage occurs in all cementitious materials, irrespective of the w/c (Geiker 1983). In low w/c mixtures, these vapor-filled cavities can result in substantial relative humidity reduction and shrinkage because the vapor-filled cavities form in relatively small pores with a small radius of curvature (Bentz and Jensen 2004; Radlinska et al. 2008; Lura et al. 2009). In higher w/c mixtures, these vapor-filled spaces also develop, however they occur in much larger pores with less impact on volume change. As a result, it is thought that many of the higher w/c systems would not derive as much benefit from internal curing.

¹Assistant Professor, Pontificia Universidad Catolica de Chile, School of Engineering, Casilla 306, Correo 22, Santiago, Chile (corresponding author). E-mail: jecastro@ing.puc.cl

²Undergraduate Research Assistant, School of Civil Engineering, Purdue Univ., 550 Stadium Mall Dr., West Lafayette, IN 47907. E-mail: rspragg@purdue.edu

³Professor, Director of Pankow Materials Laboratory, Purdue Univ., 550 Stadium Mall Dr., West Lafayette, IN 47907. E-mail: wjweiss@ecn.purdue.edu

Note. This manuscript was submitted on February 21, 2011; approved on August 17, 2011; published online on August 19, 2011. Discussion period open until July 1, 2012; separate discussions must be submitted for individual papers. This paper is part of the *Journal of Materials in Civil Engineering*, Vol. 24, No. 2, February 1, 2012. ©ASCE, ISSN 0899-1561/2012/2-223-231/\$25.00.

Lightweight aggregates are used as a water reservoir that can provide water to replenish the empty pore volume that is created by chemical shrinkage during hydration. Since water is removed from large pores to small pores, the ideal lightweight aggregate would have pore sizes larger than the pore size that develops in the cement paste (Bentz 2009; Castro et al. 2011a). This is the case for many commercially available expanded clays, slates, and shales (Castro et al. 2011a).

Approaches for Mixture Proportioning of Internally Cured Concrete

The design of concrete for internal curing requires that a sufficient amount of water is placed in the concrete to aid in hydration and to overcome the effects of self-desiccation. Different approaches have been used during recent years to determine and quantify the amount of water needed for internal curing. Two of the most widely used approaches are discussed here.

Bentz and Snyder Approach

Bentz and Snyder (1999) developed an approach to determine the volume of prewetted LWA that should be used to “ensure adequate water for complete curing of concrete, which means that the cement reaches the maximum degree of hydration that is possible, given the space limitation for forming hydration products in low w/c systems.” It is derived from the concept of filling the volume of pores created by chemical shrinkage with water from the LWA (Bentz et al. 2005). This approach was first published by Bentz and Snyder (1999), shown as

$$M_{LWA} = \frac{C_f \times CS \times \alpha_{max}}{S \times \phi_{LWA}} \quad (1)$$

where M_{LWA} (kg/m³) = mass of LWA (in a dry state) that needs to be water-filled to provide water to fill in the voids created by chemical shrinkage; C_f (kg/m³) = cement content of the mixture; CS (g of water per g of cement) = chemical shrinkage of the cement; α_{max} (unitless) = expected maximum degree of hydration: [(w/c)/0.36] for w/c below 0.36, or 1 for w/c higher than 0.36; ϕ_{LWA} (kg of water/kg of dry LWA) = absorption capacity of LWA (24 h absorption value); and S (unitless) = expected degree of saturation of the LWA, expressed as a function of absorption value (ϕ_{LWA}). Water absorption and S values from the most used LWA in America were previously reported by Castro et al. (2011a).

In theory, this approach may overestimate the amount of water required for internal curing because it considers the volume change that occurs before setting (Henkensiefken et al. 2009a), however this approach is preferred because of its simplicity.

Jensen and Hansen Approach

Jensen and Hansen (2001a) developed an approach to proportion internally cured mixtures with the intention of limiting the negative effects of self-desiccation in cementitious systems by maximizing the volume of cement that can react. The equations were developed on the basis of the Powers’ model to calculate the minimum amount of water that needs to be stored (entrained) to enable the maximum degree of hydration. It was published by Jensen and Hansen (2001a) and is expressed as

$$(w/c)_e = \begin{cases} 0.18(w/c); & \text{for } w/c < 0.36 \\ 0.42 - (w/c); & \text{for } 0.36 \leq w/c \leq 0.42 \\ 0 & \text{for } w/c > 0.42 \end{cases} \quad (2)$$

where $(w/c)_e$ = amount of additional water for internal curing, expressed as g of water per g of cement; and w/c = original water-to-cement ratio of the system.

Extension of Internal Curing to High W/C Systems

Fig. 1 (after Bentz et al. 2005) illustrates both approaches as a function of w/c. Below a w/c of 0.36, both approaches are identical. The Bentz approach adds water to fill all of the chemical shrinkage volume, which causes it to stay constant above a w/c of 0.36, while the Jensen approach considers adding only the water needed for full hydration—resulting in the recommend quantity of water decreasing above a w/c of 0.36.

Both approaches assume that all of the mixing water will be accessible to react with the unhydrated cement. Issues associated with the distance that the water needs to travel, a lack of adequate mixing, or excessive evaporation from the specimens, are not considered. These issues may decrease the amount of hydration that occurs and may increase the porosity of the system and its connectivity.

Research Objectives

The objective of this research is to examine the potential benefits of internal curing in mortar systems with a w/c of 0.30–0.45. In particular, this research will evaluate the benefits (in terms of water absorption and electrical conductivity) of systems with w/c of 0.30, 0.36, 0.42, or 0.45.

Materials

ASTM C150 Type I ordinary portland cement (OPC) was used in this study, with a Blaine fineness of 370 m²/kg and an estimated Bogue composition of 56% C₃S, 16% C₂S, 12% C₃A, 7% C₄AF, and a Na₂O equivalent of 0.68% by mass.

The sand used was natural river sand with a fineness modulus of 2.71, an apparent specific gravity of 2.58, and water absorption of 1.0% by mass. Portions of the normal weight sand were replaced with expanded shale with a fineness modulus of 3.10 and a specific gravity of 1.45. The 24 h absorption of the fine lightweight aggregate was determined to be 17.5% by the paper towel method (NYDOT 2008, Castro et al. 2011a). This test involves immersing

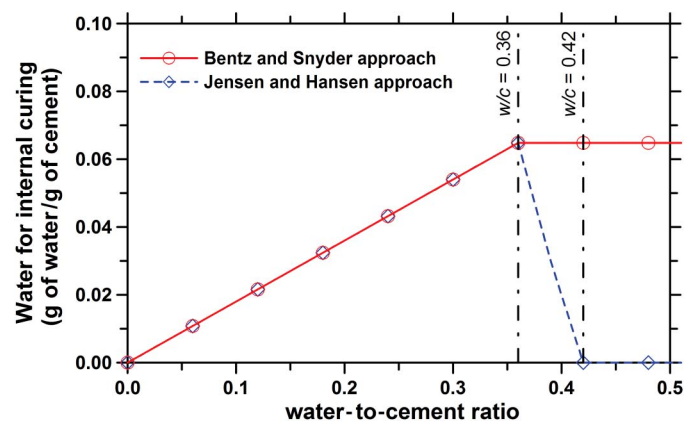


Fig. 1. Water for internal curing required to maintain saturated condition in cement paste (data from Bentz et al. 2005)

the aggregate in water for 24 h, after which time the water is decanted and the surface of the aggregate is patted dry. The paper towel method spreads the aggregate out, and the paper towel is placed across the surface of the aggregate. This process is repeated at different moisture contents [preferably near the surface dry (SD) condition]. Once it appears that the paper towel is no longer picking up moisture (as determined by visual inspection for a change in color of the paper towel) from the aggregate, it is assumed that an SD condition has been reached and the aggregate moisture can be determined.

Mixture Proportioning

Twenty different mixtures were prepared. The mortars had a single volume fraction of fine aggregate (55% of the total volume) and different w/c (0.30, 0.36, 0.42, or 0.45). For each system, fine LWA (FLWA) was used as a replacement for NWA sand at five different levels: 0, 25, 50, 75, and 100% of the values calculated using Eq. (1). The replacement is performed on a total volume basis; the volume of aggregate (FLWA and sand) remained constant at 55% because only the sand was replaced with FLWA. A list of the mixture proportions can be found in Table 1.

Mixing Procedure

The mixing procedure used for the mortar was in accordance with ASTM C305 (ASTM 2006). The FLWA was oven dried, air cooled, and then submerged in water for 24 ± 1 h prior to mixing. The volume of water used to submerge the FLWA included both mixing water and the water the FLWA would absorb in 24 h. The excess water (water not absorbed in 24 h) was then decanted and used as the mixing water. The normal weight sand was oven dried and cooled for 24 h before mixing.

Experimental Procedures

Water Absorption

Six 100 mm \times 200 mm cylinders were cast for water absorption testing for each mixture. After one day of curing, the samples were demolded and then sealed in a double layer of plastic bags for sealed curing. Bags were stored at $23 \pm 1^\circ\text{C}$ until samples reached an age of 90 d. At that point, the cylinders were removed from the bags and three 50 ± 2 mm thick samples were cut from the central portion of each cylinder using a wet saw. Obtaining samples from the central portion of the cylinders allows for testing of the core of the material, instead of testing the finishing of the surface.

After cutting, samples were conditioned by placing them in environmental chambers at $23 \pm 0.5^\circ\text{C}$ and at two different relative humidities ($65 \pm 1\%$ and $80 \pm 1\%$). Samples were kept in the environmental chamber until they reached mass equilibrium, defined as a mass change of less than 0.02% over a 15-day period. Mixtures conditioned at $65 \pm 1\%$ RH required the longest period of time (9 months) to reach mass equilibrium. However, all samples were maintained in the chambers for 9 months to test them all at the same age.

This conditioning procedure was preferred to the procedure described in ASTM C1585 (ASTM 2004) because it has been shown (Castro et al. 2011b) that the standard procedure is unable to eliminate the “moisture history” of the samples. As the mortars used in this research have different amounts of LWA (i.e., different initial amounts of water), the samples will have different initial moisture content, and the ASTM C1585 (ASTM 2004) procedure will be not able to correctly condition the samples.

Once the samples were removed from the chambers, the side surface (i.e., outer circumference) was sealed with aluminum tape, and the top surface was covered with plastic, to avoid evaporation from the sample during testing. After the samples were prepared, absorption testing was conducted in accordance with ASTM C1585

Table 1. Mixture Proportions for the Internally Cured Mixtures

w/c	% LWA	Cement	Mixing water	NWA, SSD	LWA, dry	IC water	Aggregate volume (%)		
	from Eq. (1)	(kg/m ³)	NWA	LWA	Total				
0.30	0%	727.0	218.1	1,429.7	0.0	0.0	55.0	0.0	55.0
	25%	727.0	218.1	1,330.2	55.4	9.7	51.2	3.8	55.0
	50%	727.0	218.1	1,230.6	110.8	19.4	47.3	7.7	55.0
	75%	727.0	218.1	1,131.1	166.2	29.1	43.5	11.5	55.0
	100%	727.0	218.1	1,031.5	221.6	38.8	39.7	15.3	55.0
0.36	0%	662.6	238.6	1,419.7	0.0	0.0	55.0	0.0	55.0
	25%	662.6	238.6	1,320.9	60.6	10.6	50.8	4.2	55.0
	50%	662.6	238.6	1,212.0	121.2	21.2	46.6	8.4	55.0
	75%	662.6	238.6	1,103.1	181.8	31.8	42.4	12.6	55.0
	100%	662.6	238.6	994.2	242.4	42.4	38.2	16.8	55.0
0.42	0%	608.7	255.7	1,429.7	0.0	0.0	55.0	0.0	55.0
	25%	608.7	255.7	1,329.7	55.7	9.7	51.2	3.8	55.0
	50%	608.7	255.7	1,229.7	111.4	19.4	47.3	7.7	55.0
	75%	608.7	255.7	1,129.7	167.1	29.1	43.5	11.5	55.0
	100%	608.7	255.7	1,029.7	222.8	38.8	39.6	15.4	55.0
0.45	0%	584.9	263.2	1,429.7	0.0	0.0	55.0	0.0	55.0
	25%	584.9	263.2	1,333.6	53.5	9.4	51.3	3.7	55.0
	50%	584.9	263.2	1,237.5	107.0	18.8	47.6	7.4	55.0
	75%	584.9	263.2	1,141.4	160.5	28.2	43.9	11.1	55.0
	100%	584.9	263.2	1,045.3	214.0	37.6	40.2	14.8	55.0

(ASTM 2004), with the exception of the conditioning method described above.

The effect of internal curing can be increased under the sealed conditions employed in this study as compared with other curing conditions (unsealed curing or curing under lime water). Using sealed curing, the internally cured specimens will have a greater amount of water available for hydration, and will likely hydrate further, producing a denser microstructure with lower transport coefficients. The authors consider that the sealed curing condition can isolate the effect of internal curing on the specimens. However, the authors also consider that differences in the curing conditions for both internally and not internally cured specimens can affect the performance of the specimens.

Electrical Impedance

The electrical conductivity of mortar samples was measured using cylindrical specimens (70-mm height and 35-mm diameter). Two 2.5-mm diameter rods, spaced 20 mm apart, were embedded longitudinally inside each mold (Fig. 2).

A Solartron 1260 Impedance Gain-Phase analyzer measured the impedance response of each specimen. The measurements were made over a frequency range from 1 MHz to 1 Hz, using a 100 mV AC signal. Measurements were performed at 3 d, 7 d, 90 d, and 365 d.

The electrical conductivity was obtained from the measured bulk resistance as follows:

$$\sigma = \frac{k}{R} \quad (3)$$

where σ = conductivity (S/m); k = geometry factor (1/m); and R = bulk resistance (ohm). A geometry factor of $k = 22.15/\text{m}^{-1}$ was determined for the molds used in this study, through the use of a solution with a known electrical conductivity.

A modified parallel model is normally used to describe the electrical conductivity of the concrete (McCarter and Brousseau 1990; Rajabipour 2006). Because the conductivity of the liquid phase is several orders of magnitude higher than the conductivity of the solid and vapor phases, concrete is normally considered a composite material with a single conductive component, and the modified parallel model can be simplified to Eq. (4). This typically assumes that only the fluid phase is conductive. For internally cured concrete mixtures, however, the water in the LWA may also be conductive and the implications of this will be discussed later in the paper.

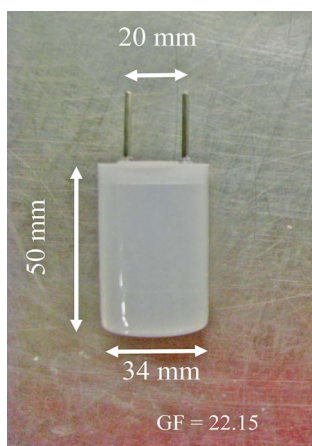


Fig. 2. Mold used for continuous electrical conductivity measurements

$$\sigma = \sigma_o \phi_o \beta_o \quad (4)$$

where σ_o = conductivity of the pore solution, sigma notch (S/m); ϕ_o = volume fraction of pore solution (unitless); and β_o = connectivity of pore structure (unitless).

Experimental Results and Discussion

Water Absorption

Fig. 3 shows the cumulative absorbed water in the samples that were 1 year old (3 months of sealed curing and 9 months of conditioning) after 8 d of testing, for samples conditioned at 65 and 80% relative humidity. Fig. 4 shows the initial sorptivity (i.e., related to the rate of water absorption) for samples conditioned at 65 and 80% relative humidity, calculated as the slope of the absorption versus the square root of time during the first six hours of testing. Fig. 5 shows the secondary sorptivity for samples conditioned at 65 and 80% relative humidity, calculated as the slope of the absorption versus the square root of time from the second to the eighth day of testing.

In Figs. 3–5, the water absorption is very sensitive to both the relative humidity at which the specimens were preconditioned before testing (Castro et al. 2011b) and the w/c of the systems. Samples conditioned at 65% relative humidity show higher values than similar samples conditioned at 80% relative humidity. Samples from mixtures with a higher w/c show higher absorption values

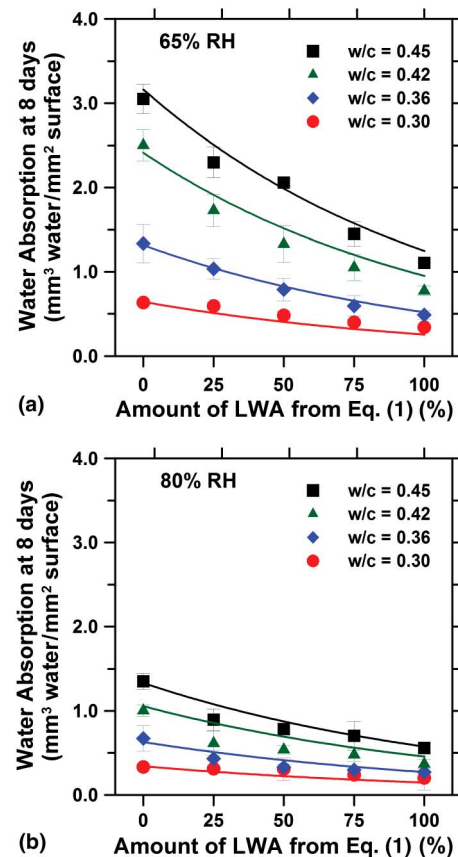


Fig. 3. Cumulative amount of water absorbed after 8 days of testing for samples conditioned at (a) 65% RH, (b) 80% RH; error bars represent standard deviation of 3 samples; continuous lines represent empirical equations described subsequently

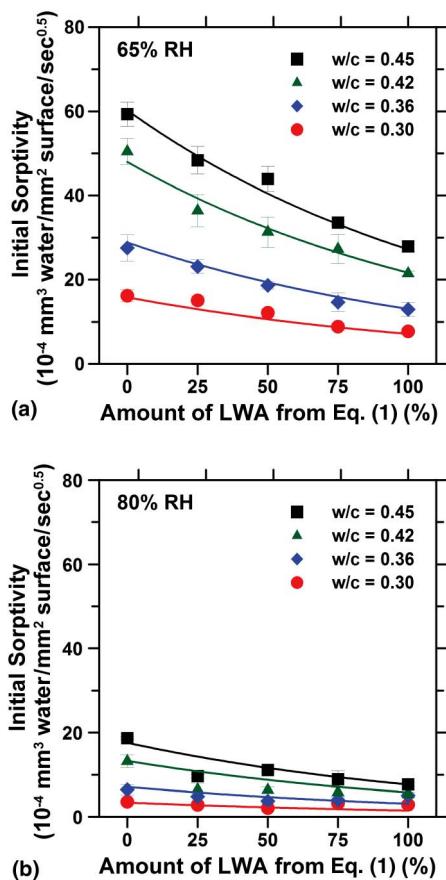


Fig. 4. Initial sorptivity as a function of w/c and the amount of LWA for samples conditioned at (a) 65% RH, (b) 80% RH; error bars represent standard deviation of 3 samples; continuous lines represent empirical equations described subsequently

compared with samples with lower w/c , both conditioned at the same relative humidity.

These trends can be explained by the fact that water ingress in unsaturated concrete is dominated by capillary suction upon initial contact with water (Hall 1989). Capillary absorption is related to the volume of the pores, as well as the size of empty capillary pores. Systems with higher w/c will have a greater proportion of capillary pores. The relationship between the equilibrated relative humidity and the radius of the smallest empty pore is given by the Kelvin-Laplace equation. Using this equation, it is possible to calculate that these capillary pores are filled with water vapor at relative humidities above 80%.

As such, the relative humidity used to condition the sample prior to the sorption test and the w/c of the system can have a significant impact on the results. The higher the w/c of the system, the greater the total volume of the capillary pores. The lower the relative humidity, the greater the total volume of pores that are empty and available to be filled with water during the sorption test. Further, the lower humidity will empty smaller pores, creating a higher suction force in the materials and resulting in a greater sorption rate and a larger overall total absorption.

In Figs. 3–5, the total volume of water and the rate of absorbed water decrease when a higher amount of FLWA is used. This observation is independent of both the relative humidity used for conditioning and the w/c of the system. Even more, it seems that a greater benefit is obtained in those mixtures containing the highest w/c .

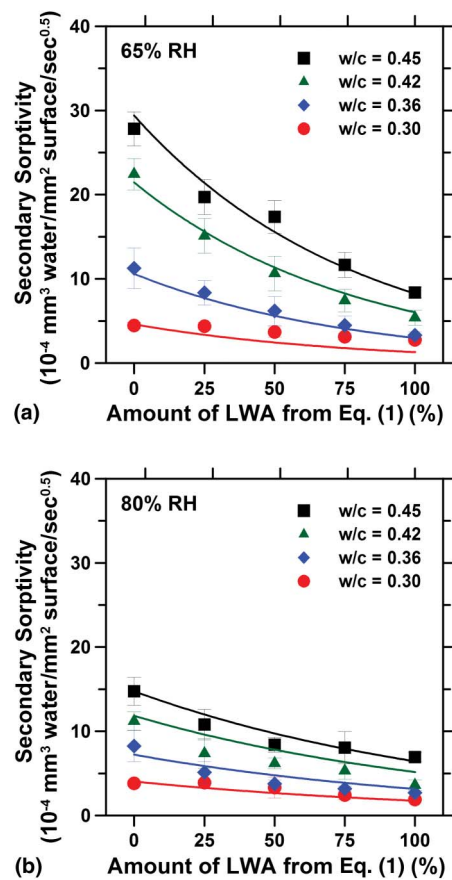


Fig. 5. Secondary sorptivity as a function of the w/c and the amount of LWA for samples conditioned at (a) 65% RH, (b) 80% RH; error bars represent standard deviation of 3 samples; continuous lines represent empirical equations described subsequently

When water leaves the pores of the LWA, it is available in the cement paste to enable additional hydration. This additional hydration results in a paste microstructure that is more dense, which has a large impact on the cement paste matrix (Henkensiefken et al. 2009b). Internal curing can also increase the hydration of the areas surrounding the LWA (Henkensiefken et al. 2009b), producing a more dense interfacial transition zone (ITZ; Zhang and Gjorv 1990; Elsharief et al. 2005). Considering that the ITZ of the normal weight aggregate (NWA) can be percolated across the 3D microstructure, the inclusion of the LWA could depercolate these ITZ pathways (Winslow et al. 1994; Bentz 2009; Peled et al. 2010). If LWA, with the more dense ITZ it creates, was added to the system, the NWA ITZ may not be as percolated, resulting in a lower absorption. As more LWA is used, the potential for percolation of the normal weight aggregate ITZ also decreases. If enough LWA is used, the ITZ of the NWA would depercolate (Bentz 2009). For this reason, it could be expected that the absorption of mortars with LWA could be lower, even in systems with a high w/c .

The benefits of internal curing are most dramatic for specimens cured under sealed conditions like those used in the study (as compared with curing under lime water). Under sealed conditions, the internally cured specimens have a greater amount of water available for hydration than the plain samples. This increased hydration produces a more dense microstructure with lower transport coefficients (Bentz and Weiss 2011).

Electrical Impedance

Fig. 6 shows the electrical conductivity of sealed samples at 3, 7, 90, and 365 days after casting. The systems with higher w/c have a higher conductivity mainly because of the higher volume of pore fluid described by Eq. (4). The conductivity decreases with time as a result of continued hydration, which reduces the volume of conductive pore fluid and also makes the conduction path more tortuous.

The mixture with a w/c of 0.30 shows that internal curing results in a reduction of the measured conductivity that can be explained by the effect of the water provided for internal curing helping to increase the hydration of areas surrounding the FLWA (Henkensiefken et al. 2009b). However, in the systems with higher w/c, an increase in the FLWA content increases the electrical conductivity at early ages. This may be explained by the fact that these systems have water contained in the FLWA particles that remains for a longer time in the FLWA pores without reacting with unhydrated cement. As a result, the total amount of fluid in the system will increase with additional FLWA, thereby increasing the measured electrical conductivity of the samples.

As the samples hydrate (e.g., for 90 days), the system with w/c = 0.36 starts to show the benefits of internal curing, decreasing the conductivity. At this time, systems with higher w/c still show higher conductivity with the use of FLWA (again because of additional water in the system). Finally, at 365 days, all the systems show the benefits of the use of internal curing. At this age, a considerable reduction of the measured electrical conductivity can be observed.

The water for internal curing requires longer times to leave the FLWA pores in higher w/c systems because of the lack of a driving

force (which is the under-pressure build-up resulting from self-desiccation in the case of a low w/c system). However, at some point, the smaller pores of the cement paste will develop a meniscus that will make the water move from the FLWA pores to the cement paste. Eventually, this water will react with the unhydrated cement to increase the amount of hydration product, reducing both the total porosity and the fluid filling the pores of the system. This will produce a reduction in the measured electrical conductivity. If the cement in high w/c systems is able to hydrate further than low w/c systems, high w/c systems will require more cement hydration to depercolate (Powers 1948), which can also explain the benefit of internal curing in these mixtures.

A direct comparison of the electrical conductivity of the systems containing different w/c presents some difficulties, mainly because of complications associated with determining the volume fraction of the pore solution at different ages. For this reason, after the electrical conductivity of the samples was measured in a sealed condition at 365 d, samples were soaked with tap water under vacuum for 3 h at 29 mm Hg and then kept under water until 24 h without release of the vacuum. After saturation, electrical conductivity was measured again and results are shown in Fig. 7.

The conductivities presented in Fig. 7 are proportional to the total volume of accessible pores and their connectivity through the samples. These are parameters that can be used to describe the transport of fluid in concrete (Rajabipour and Weiss 2007). Fig. 7 shows that using internal curing on systems with high w/c helps to reduce the connectivity of the porosity, which helps to reduce the fluid transport in concrete.

Comparing Figs. 6(d) and 7, it can be observed that the electrical conductivity increases when samples were resaturated. This can be

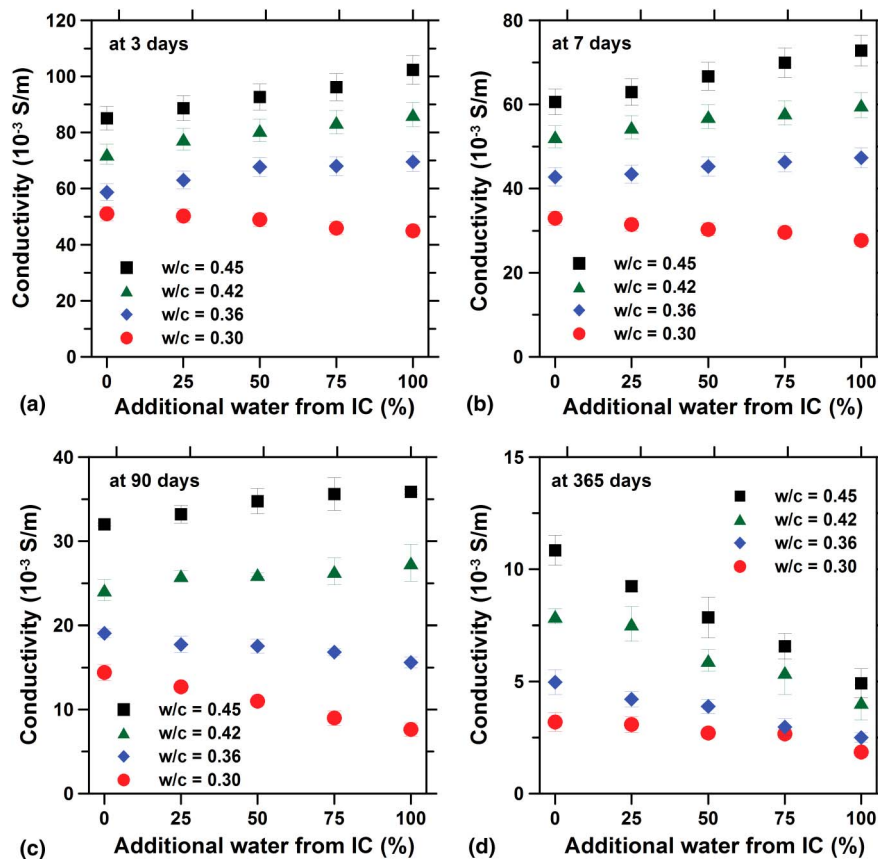


Fig. 6. Electrical conductivity of sealed samples as a function of the amount of LWA at (a) 3 days, (b) 7 days, (c) 90 days, and (d) 365 days; error bars represent the standard deviation of 3 samples

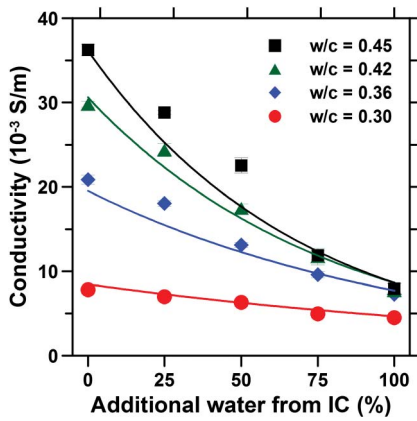


Fig. 7. Electrical conductivity of vacuum-saturated samples at 365 days; error bars represent the standard deviation of 3 samples; continuous lines represent empirical relations described subsequently

explained by the fact that resaturation results in a higher volume of pore fluid, as described by Eq. (4). However, sample resaturation does not seem to fill the FLWA pores, because an increase of conductivity with the percentage of FLWA is not observed.

Empirical Relationship for Water Absorption and Electrical Conductivity

From Figs. 3–5, it is possible to obtain an empirical relationship for the cumulative absorption (for samples conditioned at 65 and 80% RH), which is presented in Eq. (5). A similar form of equation can be used to characterize initial and secondary sorptivities. From Fig. 7, it is possible to obtain an empirical relationship for the saturated electrical conductivity, which is presented in Eq. (6).

$$\text{Absorption} = C_1 \cdot (w/c)^{C_2} \cdot \exp(-C_3 \cdot \text{IC}) \quad (5)$$

$$\text{Conductivity} = [C_4 \cdot (w/c) - C_5] \cdot \exp[(-C_6 \cdot (w/c) + C_7) \cdot \text{IC}] \quad (6)$$

where w/c = water-to-cement ratio (e.g., 0.36); IC = internal curing percentage from Eq. (1) (e.g., IC = 50 means 50% of the IC water predicted from Eq. (1)); and $C_1, C_2, C_3, C_4, C_5, C_6$ and C_7 = regression constants (values in Table 2).

Fig. 8 illustrates the proportional reduction of water absorption, initial sorptivity, and secondary sorptivity for internally cured samples. Fig. 9 illustrates the proportional reduction of electrical conductivity of 1 year old saturated, internally cured samples.

In Fig. 8, when FLWA is added according to the Bentz and Snyder approach [Eq. (1)], the internally cured system shows an average reduction of 55% in the initial sorptivity and the 8-d cumulative absorption, and 70% in the secondary sorptivity,

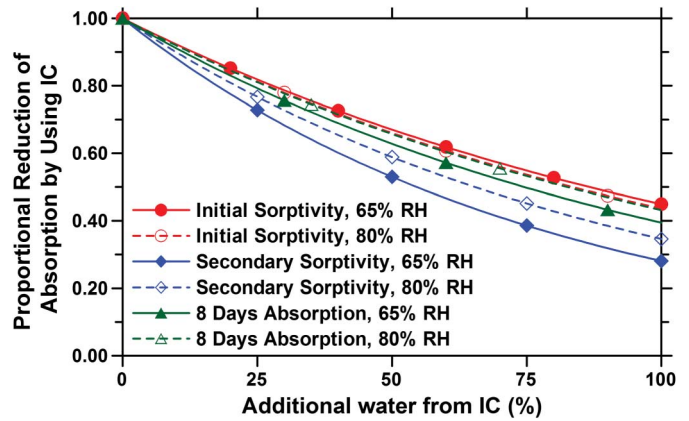


Fig. 8. Proportional reduction of absorption, initial sorptivity, and secondary sorptivity of internally cured samples

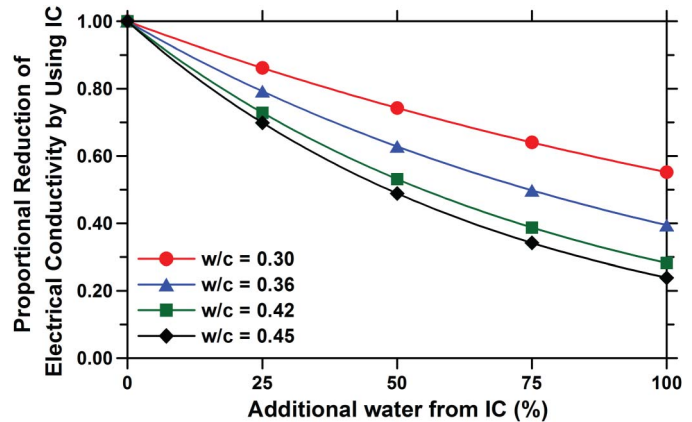


Fig. 9. Proportional reduction of electrical conductivity of 1-year-old saturated, internally cured samples

independent of the relative humidity at which the samples were conditioned prior to testing and the w/c of the mixtures.

In Fig. 9, internal curing is more efficient for reducing the electrical conductivity in high w/c systems than low w/c systems. A 40% reduction in conductivity is observed in the system with a w/c of 0.30, but a reduction of 75% is observed in the system with a w/c of 0.45.

Conclusions

A series of 20 mortars were prepared to evaluate the effect of internal curing on the fluid transport properties of mortars over

Table 2. Parameters for Eqs. (5) and (6)

Parameters	Water absorption at 8 d		Initial sorptivity		Secondary sorptivity		(1 year) Electrical conductivity Saturated
	65% RH	80% RH	65% RH	80% RH	65% RH	80% RH	
C_1	72.776	19.391	0.084	0.045	0.113	0.019	—
C_2	3.93	3.35	3.30	4.06	4.57	3.20	—
C_3	0.0093	0.0084	0.0080	0.0083	0.0127	0.0106	—
C_4	—	—	—	—	—	—	184.59
C_5	—	—	—	—	—	—	46.915
C_6	—	—	—	—	—	—	0.0558
C_7	—	—	—	—	—	—	0.0108

a range of water-to-cement ratios. The effect of internal curing was evaluated using water absorption and electrical conductivity measurements.

The total absorbed water was reduced when the level of internal curing was increased. This reduction in water absorption was known for systems with low w/c, but the results show that the benefits extend to systems with higher w/c. These benefits were also observed in reducing the rate of water absorption, showing a lower initial and secondary sorptivity. An average maximum reduction of 55% was observed in both the initial sorptivity and cumulative absorption, and a maximum reduction of 70% was observed in the secondary sorptivity.

Electrical conductivity tests, performed on sealed samples a year after casting, show a benefit in the use of internal curing in mortar systems containing low w/c as expected, but also in systems with higher w/c. The effect of internal curing is proportionally larger in samples prepared with the highest w/c. A reduction of 40% is observed in the system with a w/c of 0.30; this reduction was observed to increase to 75% in the system with a w/c of 0.45.

The benefits of internal curing are most dramatic for specimens cured in this sealed condition used in this study as compared with curing under lime water. Under sealed conditions, the internally cured specimens have a greater amount of water available for hydration than in plain samples. This increased hydration produces a more dense microstructure with lower transport coefficients.

Precaution is needed to interpret the electrical properties of IC concrete at an early age because of the higher amount of fluid present in the system when prewetted LWA is added.

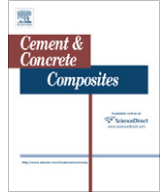
Acknowledgments

This work was supported in part by the Expanded Shale, Clay, and Slate Institute (ESCSI) and by the Joint Transportation Research Program administered by the Indiana Department of Transportation and Purdue University (Project SPR 3211), and the authors gratefully acknowledge that support. The contents of this paper reflect the views of the authors, who are responsible for the facts and the accuracy of the data presented herein, and do not necessarily reflect the official views or policies of the Indiana Dept. of Transportation or ESCSI, nor do the contents constitute a standard, specification, or regulation. The experiments reported in this paper were conducted in the Pankow Materials Laboratories at Purdue University. The authors acknowledge the support that has made this laboratory and its operation possible.

References

- American Concrete Institute (ACI). (2008). "Internal curing of high performance concrete: laboratory and field experiences." *ACI SP-256*, Farmington Hills, MI.
- American Concrete Institute (ACI) Committee 231. (2010). "Report on early-age cracking: Causes, measurement and mitigation." Farmington Hills, MI.
- ASTM. (2004). "Standard test method for measurement of rate of absorption of water by hydraulic-cement concretes." *C1585*, West Conshohocken, PA.
- ASTM. (2006). "Standard practice for mechanical mixing of hydraulic cement pastes and mortars of plastic consistency." *C305*, West Conshohocken, PA.
- Barcelo, L., Boivin, S., Rigaud, S., Acker, P., and Clauvaud, B. (1999). "Linear vs volumetric autogenous shrinkage measurements: Material behavior or experimental artefact." *Proc. of the second int. sem. on self-desiccation and its importance in concrete technology*, B. Persson and G. Fagerlund, Lund University, Sweden, 109–125.
- Bentz, D. P. (2009). "Influence of internal curing using lightweight aggregates on interfacial transition zone percolation and chloride ingress in mortars." *Cem. Concr. Compos.*, 31(5), 285–289.
- Bentz, D. P., and Jensen, O. M. (2004). "Mitigation strategies for autogenous shrinkage cracking." *Cem. Concr. Compos.*, 26(6), 677–685.
- Bentz, D. P., Lura, P., and Roberts, J. W. (2005). "Mixture proportioning for internal curing." *Concr. Inter.*, 27(2), 35–40.
- Bentz, D. P., and Snyder, K. A. (1999). "Protected paste volume in concrete: Extension to internal curing using saturated lightweight fine aggregate." *Cem. Concr. Res.*, 29(11), 1863–1867.
- Bentz, D. P., and Weiss, J. (2011). "Internal curing: A 2010 state of the art review." *National NISTIR 7765*, Institute of Standards and Technology, U.S. Dept. of Commerce, Gaithersburg, MD.
- Byard, B. E., Schindler, A. K., Barnes, R. W., and Rao, A. (2010). "Cracking tendency of bridge deck concrete." *Transportation Research Record 2164*, Transportation Research Board, Washington, DC.
- Castro, J., Bentz, D., and Weiss, J. (2011a). "Effect of sample conditioning on the water absorption of concrete." *Cem. Concr. Compos.*, 33(8), 805–813.
- Castro, J., Keiser, L., Goliás, M., and Weiss, J. (2011b). "Absorption and desorption properties of fine lightweight aggregate for application to internally cured concrete mixtures." *Cem. Concr. Compos.*, 33(10), 1001–1008.
- Couch, J., Lura, P., Jensen, O., and Weiss, J. (2006). "Use of acoustic emission to detect cavitation and solidification (time zero) in cement pastes." *Int. RILEM Conf. on Volume Changes of Hardening Concrete: Testing and Mitigation*, O. Jensen, P. Lura and K. Kovler, eds., RILEM Publications S.A.R.L., Bagneux, France, 393–400.
- Cusson, D., and Hoogveen, T. (2008). "Internal curing of high-performance concrete with pre-soaked lightweight aggregate sand for prevention of autogenous shrinkage cracking." *Cem. Concr. Res.*, 38(6), 757–765.
- Elsharief, A., Cohen, M., and Olek, J. (2005). "Influence of lightweight aggregate on the microstructure and durability of mortar." *Cem. Concr. Res.*, 35(7), 1368–1376.
- Espinoza-Hijazin, G., and Lopez, M. (2011). "Extending internal curing to concrete mixtures with W/C higher than 0.42." *Constr. Build. Mat.*, 25(3), 1236–1242.
- Geiker, M. (1983). "Studies of portland cement hydration by measurements of chemical shrinkage and a systematic evaluation of hydration curves by means of the dispersion model." Ph.D. dissertation, Technical Univ. of Denmark, Lyngby, Denmark.
- Hall, C. (1989). "Water sorptivity of mortars and concretes: A review." *Mag. Concr. Res.*, 41(147), 51–61.
- Henkensiefken, R., Bentz, D., Nantung, T., and Weiss, J. (2009a). "Volume change and cracking in internally cured mixtures made with saturated lightweight aggregate under sealed and unsealed conditions." *Cem. Concr. Compos.*, 31(7), 427–437.
- Henkensiefken, R., Briatka, P., Bentz, D., Nantung, T., and Weiss, J. (2010). "Plastic shrinkage cracking in internally cured mixtures: Prewetted lightweight aggregate can reduce cracking." *Concr. Inter.*, 32(2), 49–54.
- Henkensiefken, R., Castro, J., Bentz, D., Nantung, T., and Weiss, J. (2009b). "Water absorption in internally cured mortar made with water-filled lightweight aggregate." *Cem. Concr. Res.*, 39(10), 883–892.
- Jensen, O. M. (2005). "Autogenous phenomena in cement-based materials." Ph.D. thesis, Aalborg Univ., Aalborg, Denmark.
- Jensen, O. M., and Hansen, P. F. (2001a). "Water-entrained cement-based materials: I. Principles and theoretical background." *Cem Concr Res.*, 31(4), 647–654.
- Jensen, O. M., and Hansen, P. F. (2001b). "Autogenous deformation and RH-change in perspective." *Cem. Concr. Res.*, 31(12), 1859–1865.
- Le Chatelier, H. (1900). "Sur les changements de volume qui accompagnent le durcissement des ciments." *Bulletin Societe de l'encouragement pour l'industrie nationale*, 5eme serie, tome 5, Paris, France, 54–57.
- L'Hermite, R. G. (1960). "Volume changes of concrete." *4th Int. Symp. on the Chemistry of Cement*, U.S. Dept. of Commerce, National Bureau of Standards, Washington, DC, 659–694.
- Lopez, M., Kahn, L. F., and Kurtis, K. E. (2009). "Characterization of elastic and time-dependent deformations in high performance lightweight concrete by image analysis." *Cem. Concr. Res.*, 39(7), 610–619.

- Lura, P., Couch, J., Jensen, O. M., and Weiss, J. (2009). "Early age acoustic emission measurement in hydrating cement paste: Evidence for cavitation during solidification due to self-desiccation." *Cem. Concr. Res.*, 39(10), 861–867.
- McCarter, W., and Brousseau, R. (1990). "The A.C. response of hardened cement paste." *Cem. Concr. Res.*, 20(6), 891–900.
- New York State Dept. of Transportation (NYDOT). (2008). "Test Method No.: NY 703-19 E: Moisture content of lightweight fine aggregate." Materials Bureau, Albany, NY.
- Peled, A., Castro, J., and Weiss, J. (2010). "Atomic force microscopy examinations of mortar made by using water-filled lightweight aggregates." *Transportation Research Record 2141*, Transportation Research Board, Washington, DC.
- Powers, T. (1935). "Absorption of water by portland cement paste during the hardening process." *Ind. Eng. Chem.*, 27(7), 790–794.
- Powers, T. C. (1948). "A discussion of cement hydration in relation to the curing of concrete." *Bulletin 25*, Portland Cement Association, Chicago.
- Radlinska, A., Rajabipour, F., Bucher, B., Henkensiefken, R., Sant, G., and Weiss, J. (2008). "Shrinkage mitigation strategies in cementitious systems: A closer look at sealed and unsealed material behavior." *Transportation Research Record 2070*, Transportation Research Board, Washington, DC.
- Rajabipour, F. (2006). "In situ electrical sensing and material health monitoring in concrete structures." Ph.D. dissertation, Purdue Univ., West Lafayette, IN.
- Rajabipour, F., and Weiss, J. (2007). "Electrical conductivity of drying cement paste." *Mater. Struct.*, 40(10), 1143–1160.
- RILEM. (2007). "Internal curing of concrete—State of the art." *Rep. 41*, K. Kovler, and O. M. Jensen, eds., RILEM Publications S.A.R.L., Bagneux, France.
- Sant, G., Lura, P., and Weiss, J. (2006). "Measurement of volume change in cementitious materials at early ages: Review of testing protocols and interpretation of results." *Transportation Research Record 1979*, Transportation Research Board, Washington, DC.
- Schlitter, J., Henkensiefken, R., Castro, J., Raoufi, K., Weiss, J., and Nantung, T. (2010). "Development of internally cured concrete for increased service life." *Rep. SPR-3211*, Joint Transportation Research Program, Indiana Dept. of Transportation and Purdue Univ., West Lafayette, IN.
- Winslow, D. N., Cohen, M., Bentz, D., Snyder, K., and Garboczi, E. (1994). "Percolation and pore structure in mortars and concrete." *Cem. Concr. Res.*, 24(1), 25–37.
- Zhang, M.-H., and Gjörv, O. E. (1990). "Microstructure of the interfacial zone between lightweight aggregate and cement paste." *Cem. Concr. Res.*, 20(4), 610–618.



Effect of sample conditioning on the water absorption of concrete

Javier Castro^{a,*}, Dale Bentz^{b,1}, Jason Weiss^{c,2}

^a Pontificia Universidad Católica de Chile, School of Engineering, Casilla 306, Correo 22, Santiago, Chile

^b National Institute of Standards and Technology, Materials and Construction Research Division, Engineering Laboratory, 100 Bureau Drive, Stop 7313, Gaithersburg, MD 20899-7313, USA

^c School of Civil Engineering, Purdue University, 550 Stadium Mall, West Lafayette, IN 47907-2051, USA

ARTICLE INFO

Article history:

Received 23 November 2010

Received in revised form 17 May 2011

Accepted 19 May 2011

Available online 25 May 2011

Keywords:

Water absorption
Sample conditioning
Moisture effect
Relative humidity

ABSTRACT

ASTM C1585 is commonly used to determine the absorption and rate of absorption of water in unsaturated hydraulic cement concretes. Unfortunately, a wide range of relative humidities can exist in the samples after this relatively short conditioning period and such variation may considerably influence the test results. Three main variables were studied in this program: the water to cement ratio, the paste volume fraction, and the effect of sample conditioning. The results confirm that water absorption testing is considerably influenced by sample preparation. Samples conditioned at 50% relative humidity can show up to six times greater total absorption than similar samples conditioned at 80% relative humidity. Samples that were conditioned in the oven at 105 °C do not appear to follow a similar trend when compared with specimens conditioned in chambers at lower temperatures for a longer duration. The absorption is also influenced by the volume of paste in the samples. The experiments show that a lack of control on moisture content or lack of consideration of the material composition may lead to a misunderstanding of the actual absorption behavior.

© 2011 Elsevier Ltd. All rights reserved.

1. Introduction

The durability of concrete subjected to aggressive environments depends largely on transport properties, which are influenced by the pore system [1–7]. Three main mechanisms govern transport in cementitious systems: permeability, diffusion and absorption. Permeability is the measure of the flow of fluids under a pressure gradient, while diffusion is the movement of ions due to a concentration gradient. Absorption can be described as the ability to take in water by means of capillary suction. All three mechanisms are heavily influenced by the volume of pores as well as the connectivity of the pore network. A large fraction of concrete in service is only partly saturated and the initial ingress of water and dissolved salts is influenced, at least in part, by capillary absorption [7]. As such, water absorption has been used as an important factor for quantifying the durability of cementitious systems [4–11]. Water absorption is the primary focus of this study since it is being increasingly used by specifiers and in forensic studies to provide a parameter that can describe an aspect of concrete durability. It is also important that these properties be adequately described for use in service life models [6,11].

1.1. Water absorption test

ASTM C1585 [1] is commonly used to determine the absorption and rate of absorption (commonly referred to as sorptivity) of water in unsaturated hydraulic cement concretes. This test method, based on work reviewed by Hall [12], consists of preconditioning cylindrical samples (2" (51 mm) in thickness and 4" (102 mm) in diameter) to a known moisture content, then exposing the bottom surface of the sample to liquid water and measuring the increase in mass resulting from water absorption. According to the standard conditioning procedure, samples are conditioned for 18 days. This conditioning period begins by first placing the sample in a 50 °C and 80% relative humidity (RH) environment for 3 days. The samples are then removed from this environment and placed in individually sealed containers where they remain for a minimum 15 days at 23 °C, to allow internal moisture to redistribute throughout the specimens before the test begins.

The absorption test involves recording incremental mass change measurements at relatively frequent intervals during the first 6 h after the sample comes in contact with water and subsequently taking one measurement every day for the next 8 days. The amount of absorbed water is normalized by the cross-section area of the specimen exposed to the fluid using Eq. (1):

$$i = \frac{m_t}{(a \cdot \rho)} \quad (1)$$

* Corresponding author. Tel.: +56 2 354 4245.

E-mail addresses: jecastro@ing.puc.cl (J. Castro), dale.bentz@nist.gov (D. Bentz), wjweiss@purdue.edu (J. Weiss).

¹ Tel.: +1 301 975 5865.

² Tel.: +1 765 494 2215.

where i is the normalized absorbed fluid volume, m_t is the change in specimen mass at time t ; a is the area of the specimen exposed to the fluid (i.e., that of the bottom face), and ρ is the density of the absorbed fluid (taken to be 1000 kg/m^3 at 23°C for water).

These absorbed fluid volumes are then plotted as a function of the square root of time. The initial sorptivity is determined as the slope of the curve during the first 6 h, while secondary sorptivity is determined using the slope of the same measurements between 1 and 8 days, as outlined in ASTM C1585 [1]. It should be noted that these times work well for water though they may not work as well for other fluids with different surface tension and/or viscosity [13].

The initial and secondary sorptivities can be used to evaluate the connectivity of the pore network [9]. Additionally, the secondary sorptivity, combined with exposure conditions, has been used for performing service life predictions [11].

1.2. The role of the relative humidity

Water ingress in unsaturated concrete is dominated by capillary suction upon initial contact with water [7,12–18]. Capillary absorption can be related to the volume of the pores and pore size distribution, as well as the size (i.e. radius) of the partially empty capillary pores (Fig. 1a). The relation between the equilibrated relative humidity and the radius of the smallest empty pore is given by the Kelvin-Laplace equation (Eq. (2)).

$$\ln(RH) = \frac{2\sigma V_m}{r_m RT} \quad (2)$$

where: RH is the relative humidity, σ is the surface tension of water (pore solution), V_m is the molar volume of water, r_m is the average radius of curvature, R is the universal gas constant, and T is the absolute temperature.

It should be noted that this expression is simplified as it does not consider the effect of water that is absorbed on the walls of the pores. Largely the concrete community has considered two sizes of pores as introduced by Powers [19]. The gel pores are considered to be small pores (<10 nm diameter) that are a part of the hydration products. Capillary pores are larger pores that occur due to excess water. Capillary porosity is particularly of concern in transport, as is the interconnectivity of the capillary pores.

Fig. 1b shows a conceptual illustration based on Powers [19] that uses a desorption isotherm to illustrate the volume of water located in the different size pores at different relative humidities.

The relative humidity used to condition the sample prior to the sorption test can have a significant impact on the results [1]. Previous test results by Parrot [20,21] indicated that the

water absorption rate was very sensitive to the moisture content of the concrete, particularly at relative humidities above 60% which were common for field exposure. Water leaves the largest accessible pores first. It can be seen from Fig. 1b that capillary pores occupy the range of humidity from approximately 80% to 100% RH. As such, initially upon drying water leaves the capillary pores. The lower the relative humidity, the greater the total volume of pores that are empty and available to be filled with water during the sorption test. Further, the lower humidity will empty smaller pores, creating a higher suction force in the materials and resulting in a greater sorption rate and a larger overall total absorption.

According to ASTM C1585, the standardized test conditioning will generally provide an internal relative humidity similar to relative humidities found near the surface in some field concrete structures [1,22,23]. This range of relative humidities can represent what is found in samples in the field; however, it is wide enough to considerably affect the test results.

Castro et al. [24] shows that the relative humidity of samples that were kept in the field under different exposure conditions was in the range of 80–100% depending on the type of exposure, which is somewhat higher than what is mentioned in ASTM C1585.

1.3. Research objectives

The objectives of this research are threefold. First, this research will examine the influence of conditioning relative humidity (oven dry, 50%, 65% and 80% RH) on the results of sorption tests performed on mortars with different w/c , containing a fixed volume of aggregate. Second, this research will examine the influence of the volume of aggregate (or equivalently the paste content) on the results of sorption testing. Third, this research will examine the effect of the conditioning method specified in ASTM C1585-04.

2. Materials

An ASTM C150 Type 1 ordinary portland cement (OPC) was used in this study, with a Blaine fineness of $370 \text{ m}^2/\text{kg}$ and an estimated Bogue composition of 56% C_3S , 16% C_2S , 12% C_3A , 7% C_4AF and a Na_2O equivalent of 0.68% by mass.

A polycarboxylate-based high-range water-reducing admixture (HRWRA) was added in varying rates as indicated in Table 1, depending on the mixture proportions, to maintain similar consistencies (i.e., workability). The sand used was natural river sand with a fineness modulus of 2.71, an apparent specific gravity of 2.58, and a water absorption of 1.8% by mass.

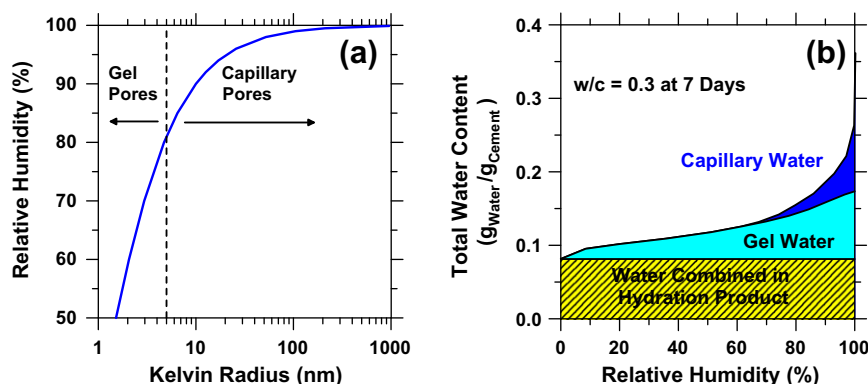


Fig. 1. Relation between relative humidity and partially empty pores in cement paste.

Table 1
Mixture proportions in saturated surface dry (SSD) conditions.

Material	55/0.35	55/0.40	55/0.45	55/0.50	45/0.50	35/0.50
Volume fraction of aggregate	55%	55%	55%	55%	45%	35%
w/c	0.35	0.40	0.45	0.50	0.50	0.50
Cement (kg/m ³)	673	626	585	549	671	793
Water (kg/m ³)	235	250	263	275	336	397
Fine aggregate (kg/m ³), SSD	1442	1442	1442	1442	1180	918
HRWRA (g/100 g cement)	0.60	0.40	0.20	0.00	0.00	0.00

2.1. Mixture proportioning

Six different mixtures were prepared in total. Four of the mixtures were mortars with a single volume fraction of fine aggregate (55% of the total volume) and different w/c (0.35, 0.40, 0.45, and 0.50). These mixtures were designated as 55/0.35, 55/0.40, 55/0.45 and 55/0.50, with the number on the left representing the volume fraction of fine aggregate and the number on the right representing w/c. Additionally, two other mortars were prepared with w/c of 0.50, but with different volume fractions of fine aggregate (35% and 45% of the total volume). They were designated as 35/0.50, 45/0.50. A list of the mixture proportions can be found in Table 1.

2.2. Mixing procedure

The mixing procedure used for the mortar was in accordance with ASTM C192-06 [25]. The aggregate was oven dried and cooled for 24 h before mixing. The volume of water was corrected by the absorption of the aggregate. The water and cement were conditioned for 24 h at room temperature prior to mixing.

3. Experimental method

Six 100 mm × 200 mm cylinders were cast for each mixture. After 1 day of curing, the samples were demolded and then sealed in double plastic bags for sealed curing. Bags were stored in a room at 23 ± 1 °C until samples reached an age of 28 d. After that, cylinders were removed from bags and three 50 mm ± 2 mm thick samples were cut from the central portion of each cylinder with a wet saw using water as the cooling fluid.

After cutting, samples were conditioned by placing them in environmental chambers at 23 ± 0.5 °C. Specimens from mixtures 55/0.35, 55/0.40, 55/0.45 and 55/0.50 were placed in environmental chambers at three different relative humidities (50 ± 1%, 65 ± 1% and 80 ± 1%). Specimens from mixtures 35/0.50 and 45/0.50 were placed in an environmental chamber at 50 ± 1% relative humidity. Samples were kept in the environmental chamber until they reached mass equilibrium, defined as a mass change of less than 0.02% over a 15 day period. Mixture 55/0.35 placed at 50 ± 1% relative humidity required the longest period of time (14 months) to reach mass equilibrium. However, all samples were maintained in the chambers for 14 months to test them all at the same age.

Additional specimens from mixtures 55/0.35, 55/0.40, 55/0.45 and 55/0.50 were placed at 50 ± 1% RH. After the 14 months, these specimens were dried in an oven at 105 ± 2 °C until they reached mass equilibrium.

Once the samples were removed from the chambers or from the oven, the side surface (i.e. outer circumference) was sealed with epoxy. A section of plastic is clamped to the surfaces during the application of epoxy to keep the surfaces clean. This also helped to limit drying during the curing process. After the epoxy was dry, the top surface was covered with plastic to avoid evaporation from the sample during testing. After the samples were prepared, testing occurred in accordance with ASTM C1585-04 [1].

Specimens from mixtures 55/0.35, 55/0.40, 55/0.45 and 55/0.50 were tested over a period of 90 days. Specimens from mixtures 35/0.50 and 45/0.50 were tested over a period of 8 days.

Two additional 100 mm × 200 mm cylinders were cast for each mortar mixture. After 1 day of curing, the samples were demolded and then sealed in double plastic bags for sealed curing. Bags were stored in a room at 23 ± 1 °C until samples reached an age of 28 d. After that, cylinders were removed from bags and 10 mm ± 2 mm thick samples were cut from the central portion of each cylinder with a wet saw. After cutting, mortar samples were vacuum saturated for 24 h. After that, specimens were placed in environmental chambers at six different relative humidities (93 ± 1%, 87 ± 1%, 80 ± 1%, 75 ± 1%, 65 ± 1% and 50 ± 1%) to determine their desorption isotherms.

4. Experimental results and discussion

4.1. Desorption isotherms

Fig. 2 shows the desorption isotherm curves measured using 10 mm thick samples. Mass change was monitored at regular intervals until it reached equilibrium, defined as a mass change of less than 0.02% over a 15 day period. At the end, all samples were oven dried to express water absorption in terms of the dry mass of the sample.

It can be noticed that while the values of the moisture content are similar at 50% and lower RH (lower RH results not shown in Fig. 2), as it refers to the small gel pore system [19], the capillary pores at high RH are strongly influenced by the w/c.

4.2. Effect of initial conditioning on water absorption tests

4.2.1. Effects of relative humidity on sorption test

Fig. 3 shows the absorbed water during the 90 days of testing performed on mortars conditioned at different relative humidities

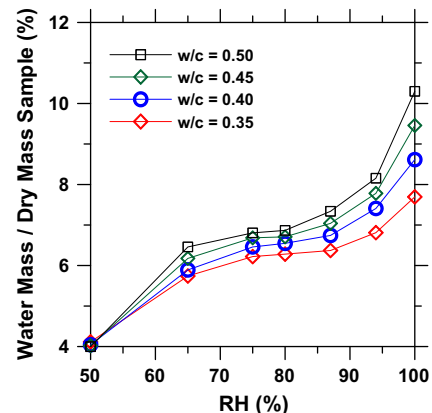


Fig. 2. Desorption curves for 14 months mortar samples (typical standard deviation in the average of three samples is lower than 0.2%).

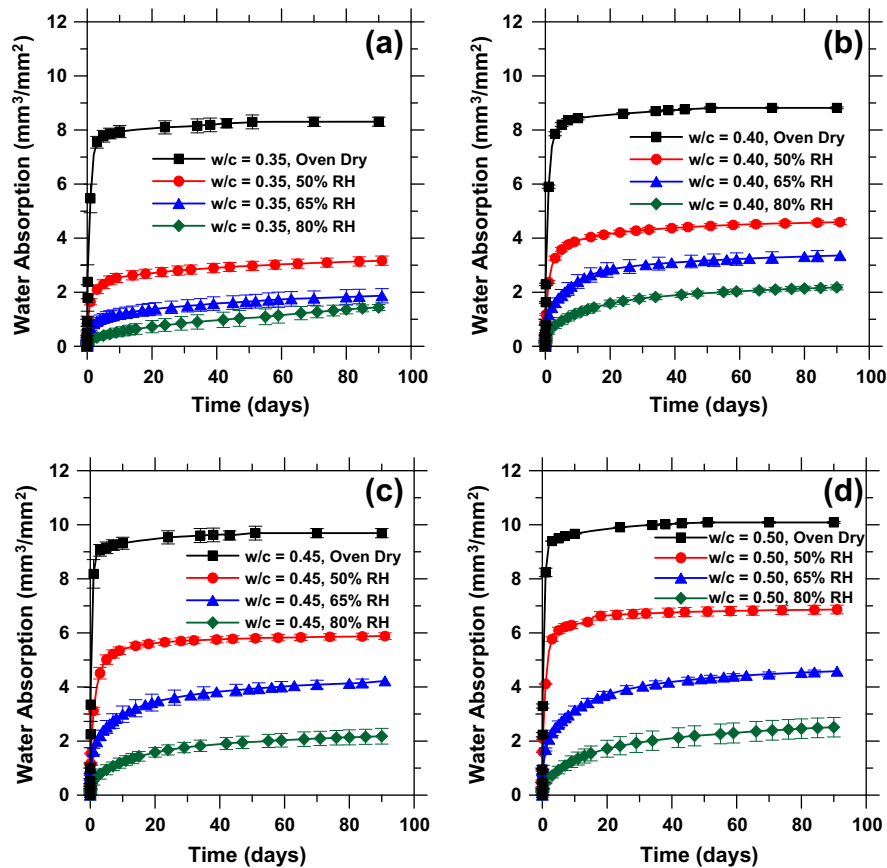


Fig. 3. Absorbed water in mortars as a function of relative humidity (a) mixture 55/0.35, (b) mixture 55/0.40, (c) mixture 55/0.45, (d) mixture 55/0.50. Error bars represent the standard deviation for the average of three samples.

(mixtures 55/0.35, 55/0.40, 55/0.45 and 55/0.50). It can be noticed that the water absorption is very sensitive to the relative humidity at which the specimens were pre-conditioned before testing. In each case, as the conditioning relative humidity increases, more water is retained in the pore system and thus the absorption decreases.

These results can be viewed in a slightly different manner if they include the initial amount of water held in the pores before the test. In order to do this, samples were oven dried at the end of the sorption test to calculate the amount of water they held before starting the test. Additional specimens that were kept at $50 \pm 1\%$ RH during the 14 months were oven dried and then saturated by the procedure described in ASTM C642-07 [26] to measure the total amount of interconnected porosity in the systems. Results from Fig. 3 were then normalized by the total amount of pores in the system, which can be viewed as the degree of saturation of the sample as a function of time. This is presented in Fig. 4. Fig. 5 shows the total degree of saturation for the samples after 90 days.

Figs. 4 and 5 show that samples prepared at different relative humidities with a low w/c (e.g. $w/c = 0.35$) do not reach values near to saturation even after 90 days of being in contact with water. It may be attributed to the refined pore network of this low w/c system which makes it difficult for water to move through the sample to fill all the pores. This is commonly referred to as depercolation, which occurs after different hydration times for different w/c [27].

In contrast after 90 days, samples prepared with a higher w/c (e.g. $w/c = 0.50$) reach much higher levels of saturation. It can be noted from Fig. 4 that samples conditioned at 50% RH reach values near saturation after about 40 days of testing, similar to what is obtained with oven dry samples. Again this may be attributed to the

connectivity of the pore network and the size of these pores. In this case, a more interconnected pore network will facilitate the movement of water to the interior of the specimens and the diffusion of water vapor out of the sample. However, when these samples were conditioned at higher relative humidities (65 and 80% RH), the amount of initially retained water is high enough to reduce the diffusion of vapor out of the sample. As a result, this may explain why the level of saturation of these specimens is lower.

4.2.2. Effects of relative humidity on the amount of absorbed water after 8 days

Fig. 6 shows the cumulative water that was absorbed after 8 days of testing performed on mortars conditioned at different relative humidities, expressed as a function of w/c (Fig. 6a) and as a function of the relative humidity (Fig. 6b).

Fig. 6a shows that mixture 55/0.50 can exhibit six times higher absorption when the samples are conditioned at 50% RH compared with similar samples conditioned at 80% RH.

Fig. 7 shows a normalization of the data presented in Fig. 6. In Fig. 7a the normalization is made with respect to the absorption of samples with $w/c = 0.35$ (mixture 55/0.35). In Fig. 7b the normalization is made with respect to the absorption of samples conditioned at 50% relative humidity. It can be seen that the values follow a consistent trend in each case, except for the oven dry samples. This is in general agreement with the parallel nature of the desorption isotherms for the mortars provided in Fig. 2.

4.2.3. Effects of relative humidity on initial sorptivity

Fig. 8 shows the initial sorptivity calculated as the slope of the absorption vs. the square root of time during the first 6 h of test [1].

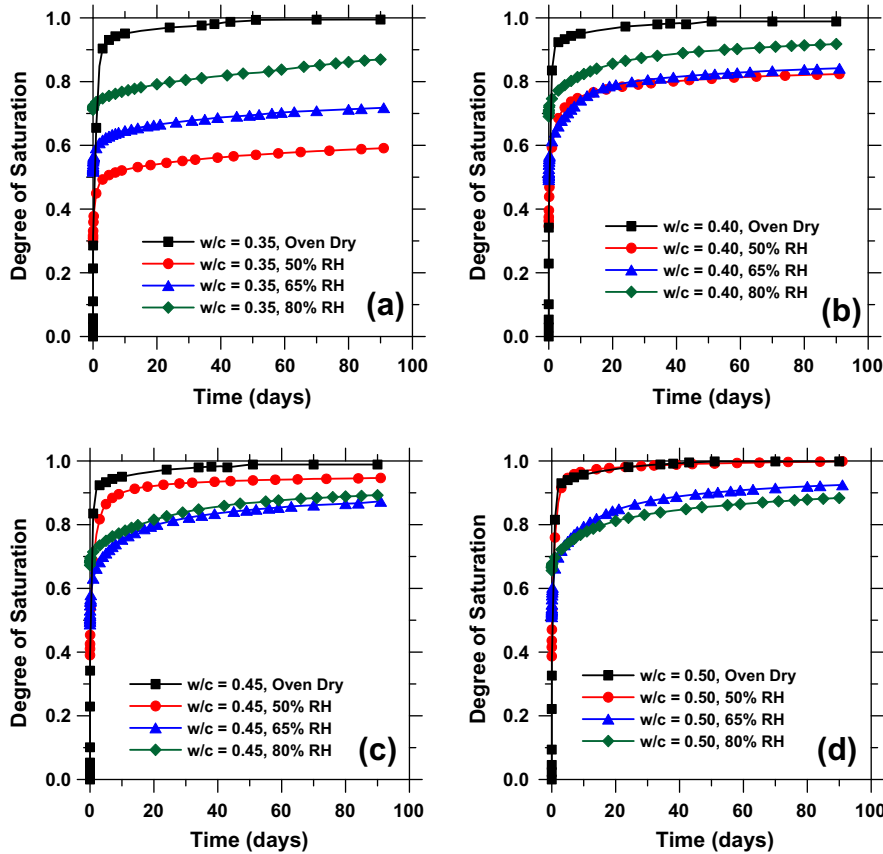


Fig. 4. Degree of saturation as a function of time during the water absorption test: (a) mixture 55/0.35, (b) mixture 55/0.40, (c) mixture 55/0.45, (d) mixture 55/0.50. Typical standard deviation of the average of three samples is lower than 0.02 points in the degree of saturation.

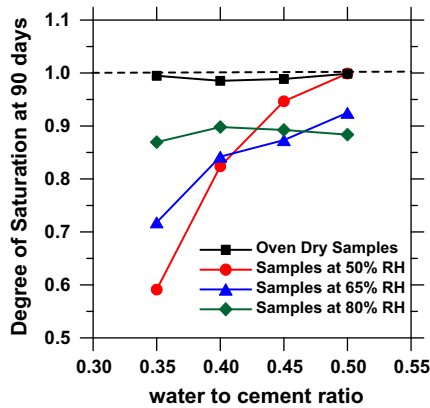


Fig. 5. Degree of saturation after 90 d in contact with water as a function of the w/c.

Fig. 8a shows that mixture 55/0.50 can exhibit a ten times higher initial sorptivity when the samples are conditioned at 50% RH compared with similar samples conditioned at 80% RH.

It needs to be noted that the oven dry samples show a much higher initial sorptivity, due to the fact that the gel’s capillary pores are empty. It is also possible that the samples exhibit microcracking around the aggregates due to differential thermal expansion and contraction which may result in the aggregate restraining paste movement. This would be in addition to any microcracking caused by moisture gradients that may occur in the samples that

have dried. During drying, the paste may contract much more than the aggregates that do not really lose moisture or at least not as much moisture loss. Even with some moisture loss from the aggregate, they would likely shrink much less than the surrounding paste due to their higher modulus. While the increase in sorptivity is observed to be linear for the specimens conditioned at 50%, 65% and 80% relative humidity, this trend appears to break down for the oven dry samples which may be attributed to increased micro-cracking generated during the sample preparation [28–32].

4.2.4. Effects of relative humidity on secondary sorptivity

Fig. 9 shows the secondary sorptivity calculated as the slope of the absorption vs. the square root of time between 1 d and 8 d of testing. Trends are similar to those observed for the initial sorptivity. However, it needs to be noted that samples that were oven dry prior to the test present a considerably lower secondary absorption with respect to the samples conditioned in environmental chambers. This may be explained by the high initial absorption of the oven dry samples shown in Fig. 8. During this initial absorption it can be noticed that since a majority of the water was already absorbed in the first hours of the test, the secondary rate of absorption will be much lower. It can also be expected that microcracking enabled a more rapid ingress of water [33].

Fig. 9 shows a similar trend to what was noted in the case of total absorption and initial sorptivity, namely that the secondary sorptivity of samples conditioned in chambers exhibits a consistent trend when the results are plotted against the w/c or the relative humidity at which samples were conditioned. However, samples that are conditioned by drying them in an oven at 105 °C do not follow the same tendency.

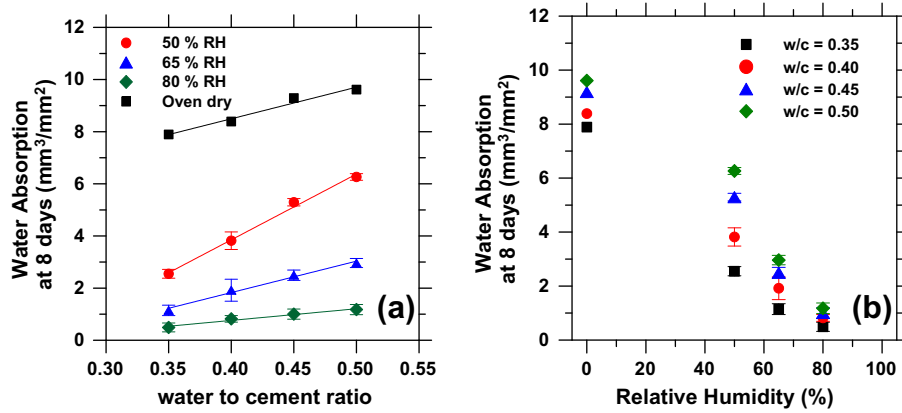


Fig. 6. Cumulative absorption at 8 d for mortars with 55% aggregates versus: (a) w/c, (b) relative humidity. Solid lines are provided only to show a general tendency in the data. Error bars represent the standard deviation on the average of three samples.

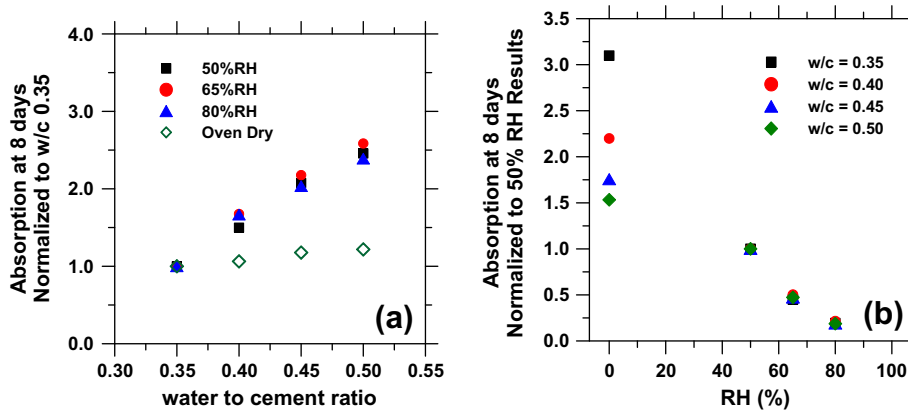


Fig. 7. Cumulative absorption at 8 days versus w/c and relative humidity: (a) normalized to absorption of mixture 55/0.35, (b) normalized to absorption at 50%RH.

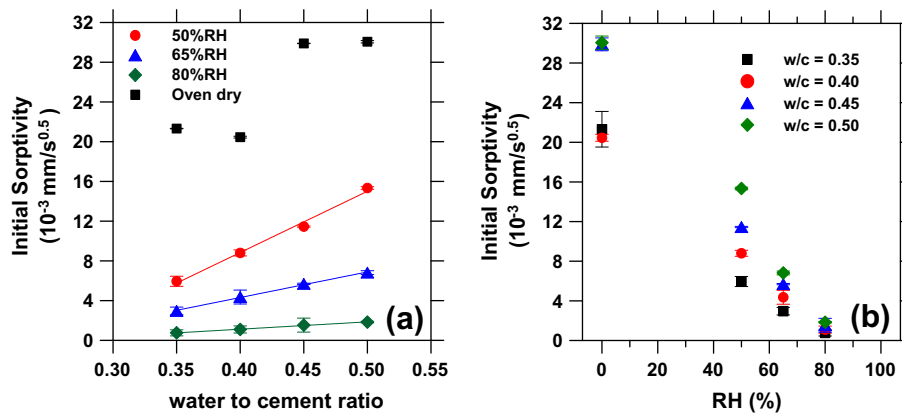


Fig. 8. Initial absorption of the 55% aggregate mortars conditioned at different RH as a function of: (a) w/c, (b) relative humidity. Solid lines are provided to show a general tendency in the data. Error bars represent the standard deviation on the average of three samples.

4.3. Effects of initial moisture of samples on ASTM C1585 conditioning method

At the age of 24 months, samples from each mixture conditioned at the three different relative humidities were removed from the chambers. The side surface was sealed with epoxy to be then “re-conditioned” using the 18 day procedure described in ASTM C1585. In addition, three other samples from each mixture

were saturated following the procedure described in ASTM C642 [26], to then be “re-conditioned” following the same 18 day procedure. While such a resaturation procedure was employed in the initial sorption testing upon which the ASTM C1585 standard was based [34], it was subsequently omitted from the standard. After samples were fully prepared, testing was performed in accordance with ASTM C1585 over a period of 8 days, with results provided in Fig. 10. In addition, Fig. 11 shows the calculated initial and

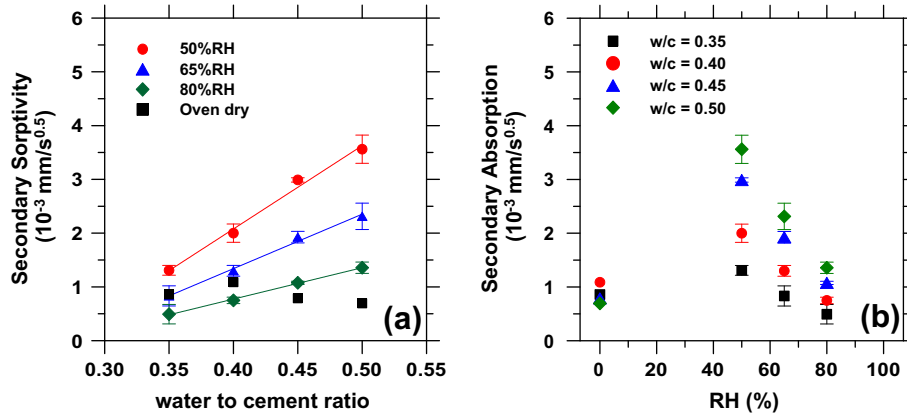


Fig. 9. Secondary absorption on mortars with 55% aggregates conditioned at different RH as a function of: (a) w/c, (b) relative humidity. Solid lines are provided to show a general tendency in the data. Error bars represent the standard deviation on the average of three samples.

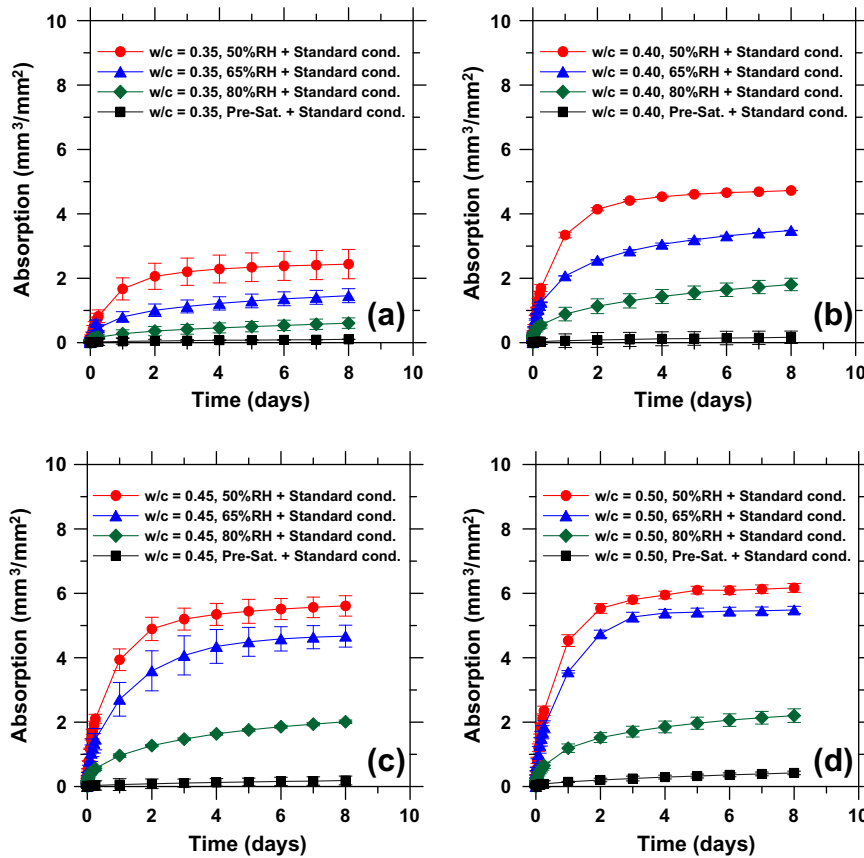


Fig. 10. Effect of initial moisture on the conditioning procedure established in ASTM C1585-04 (a) mixture 55/0.35, (b) mixture 55/0.40, (c) mixture 55/0.45, (d) mixture 55/0.50. Error bars represent the standard deviation for the average of three samples.

secondary sorptivities from these tests. Secondary sorptivity values are not reported when the correlation coefficient is lower than 0.98.

Figs. 10 and 11 show that the 3 days of controlled drying at $50 \pm 2 \text{ }^\circ\text{C}$ and 80% RH followed by the 15 days for internal moisture equilibration is not capable of eliminating the effects of the “moisture history”. These results suggest that the ASTM C1585 preparation method does not prepare all the samples to the same water content before a water absorption test. As such this accelerated method can make a substantial difference in how the data is interpreted. This may be due to a moisture hysteresis effect [35]. It

should be noted that this can be a concern for field samples evaluated using this method, as their as-received relative humidities may easily vary between the extremes examined in this study.

4.4. Effects of volume of aggregate on sorption test

Fig. 12 shows the absorbed water during 8 days of testing performed on mortars containing different volumes of aggregate (mixtures 55/0.50, 45/0.50 and 35/0.50) conditioned at 50% relative humidity. In Fig. 12a the effect of a higher volume of paste is observed as the mixture containing the lower volume of aggregate

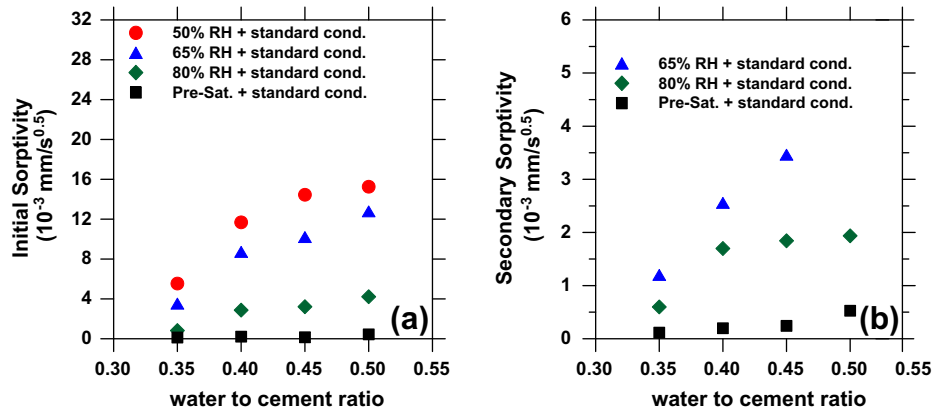


Fig. 11. Initial and secondary sorptivities on mortars with different initial moisture contents, conditioned with the procedure established in ASTM C1585-04.

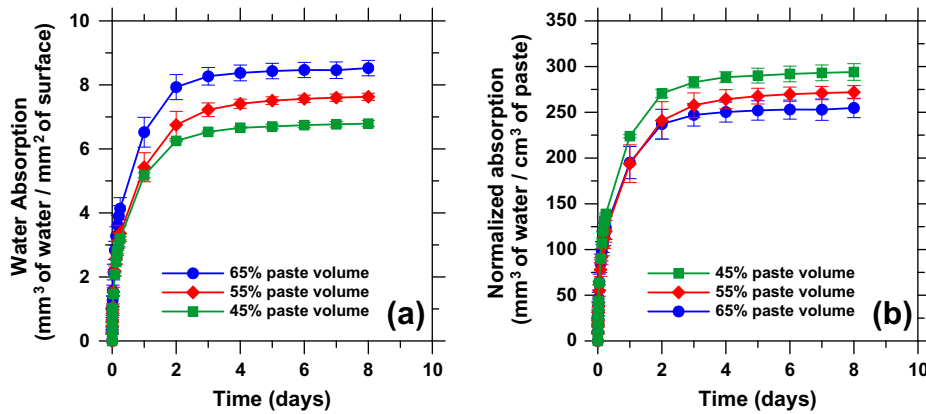


Fig. 12. Water absorption in mortars containing different volume of aggregates: (a) normalized by surface in contact with water, (b) normalized by volume of paste.

has the higher absorption. However, when the results are normalized by the volume of paste (volume of the main absorbent material), a reversal in the order of the samples is observed (Fig. 12b). The samples with the higher volume of aggregates have a higher absorption.

Water absorption is typically reported without considering the effect of the absorption of the aggregate in the samples. To better understand its effect, Fig. 13 was calculated assuming five different sand absorptions (0.0%, 0.6%, 1.2%, 1.8%, and 2.4%) to then subtract

these values from the absorption in Fig. 12b. When the sand absorption is assumed to be 0.0%, the resulting absorption at 8 days will be the same as the absorption presented in Fig. 12b. From Fig. 13, it can be noticed that for the assumed 1.8% sand absorption, the normalized water absorbed for the sample is the same after 8 days, independent of the amount of aggregate in the sample.

Fig. 14 shows a desorption isotherm for the sand used in these mixtures. It can be noted that at 50% RH (humidity at which the samples were conditioned), the amount of water on the sand is

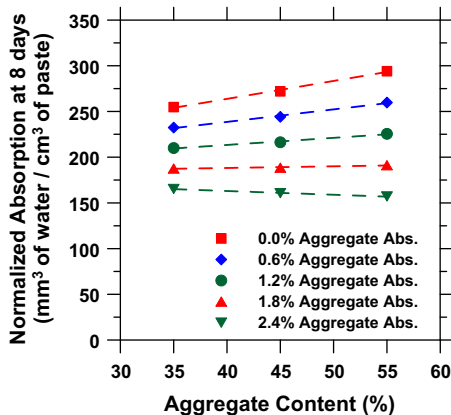


Fig. 13. Water absorption at 8 d normalized by volume of paste, corrected by different values of aggregate absorption.

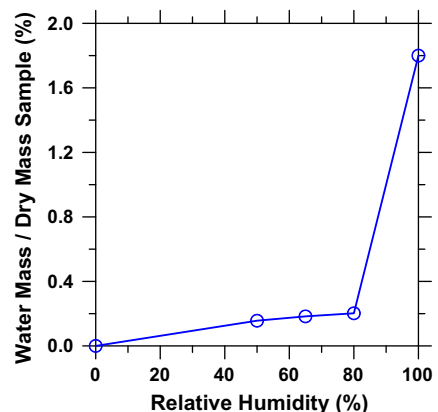


Fig. 14. Desorption isotherm for the sand used in this research.

about 0.2%. Considering that the aggregate used in this study has a 24 h absorption of 1.8%, this would imply that an effective aggregate desorption of 1.6% would have occurred in the samples at 50% relative humidity. This is reasonably consistent with the difference in water absorption of samples containing different amounts of aggregate and their absorption can be explained mainly by the amount of water absorbed by the aggregates.

5. Conclusions

This paper has described the absorption behavior of mortars conditioned at different relative humidities. As was shown in previous works by Hall [12], Hooton et al. [4,7] and Martys and Ferraris [16,34], the water absorption test is considerably affected by the relative humidity of the samples before starting the test, which if not properly accounted for can lead to a misunderstanding of the actual absorption behavior. Samples conditioned at a 50% relative humidity can show a total absorption that is approximately six times greater than similar samples conditioned at 80% relative humidity. This is consistent with expectations based on the mortars' desorption curves.

Initial sorptivity, secondary sorptivity and total absorption at 8 days for samples conditioned in chambers show a linear trend related to the w/c and the relative humidity at which samples were conditioned. Samples that are conditioned by drying in an oven at 105 °C do not follow the same trend as samples conditioned in other approaches. This is attributed to two factors: (1) emptying of a wider range of pores, and (2) the potential for microcracking. The conditioning procedure described in ASTM C1585-04 is not able to eliminate the "moisture history" of the samples, and thus can lead to a misunderstanding of the water absorption test results, especially in field samples which have obtained a lower relative humidity. It is recommended that field samples be pre-saturated prior to being exposed to the conditioning regimen of ASTM C1585.

Comparing samples containing different volumes of aggregate can also lead to a misunderstanding of the actual absorption behavior. Samples containing higher volumes of cement paste will absorb more water. When the results are normalized by the volume of cement paste, the sample containing lower volumes of cement paste will absorb more water. However, for the materials examined in this study, this difference can be mainly explained by the amount of water absorbed by the aggregates in the sample.

Acknowledgments

This work was supported in part by the Joint Transportation Research Program administered by the Indiana Department of Transportation and Purdue University (Project SPR 3093). The contents of this paper reflect the views of the authors, who are responsible for the facts and the accuracy of the data presented herein, and do not necessarily reflect the official views or policies of the Federal Highway Administration and the Indiana Department of Transportation, nor do the contents constitute a standard, specification, or regulation. The authors gratefully acknowledge support received from the Center for Advanced Cement Based Materials.

References

- [1] ASTM International, ASTM C1585. Standard test method for measurement of rate of absorption of water by hydraulic-cement concretes; 2004.
- [2] Sabir B, Wild S, O'Farrell M. A water sorptivity test for mortar and concrete. *Mater Struct* 1998;31(8):568–74.
- [3] Maltais Y, Samson E, Marchand J. Predicting the durability of Portland cement systems in aggressive environments – laboratory validation. *Cement Concrete Res* 2004;34(9):1579–89.
- [4] Hooton RD, Mesisc T, Beal DL. Sorptivity testing of concrete as an indicator of concrete durability and curing efficiency. In: Proceedings of the third Canadian symposium on cement and concrete, Ottawa, Ontario; 1993. p. 264–75.
- [5] Parrot LJ. Water absorption in cover concrete. *Mater Struct* 1992;25(5):284–92.
- [6] Fagerlund G. Predicting the service-life of concrete exposed to frost action through a modeling of the water absorption process in the air pore system. In: Jennings H, Kropp J, Scrivener K, editors. The modeling of microstructure and its potential for studying transport properties and durability. The Netherlands; 1996. p. 503–39.
- [7] Hearn N, Hooton D, Mills R. Pore structure and permeability. In: Klieger P, Lamond J, editors. Significance of tests and properties of concrete and concrete-making materials. ASTM STP 169C; 1994. p. 240–62.
- [8] Henskensiefken R, Castro J, Bentz D, Nantung T, Weiss J. Water absorption in internally cured mortar made with water-filled lightweight aggregate. *Cem Concr Res* 2009;39(10):883–92.
- [9] Neithalath N. Analysis of moisture transport in mortars and concrete using sorption-diffusion approach. *ACI Mater J* 2006;103(3):209–18.
- [10] Yang Z. Assessing cumulative damage in concrete and quantifying its influence on life cycle performance modeling. PhD thesis, Purdue University; 2004.
- [11] Bentz DP, Ehlen MA, Ferraris CF, Garboczi EJ. Sorptivity-based service life predictions for concrete pavements. In: Proceedings 7th international conference on concrete pavements, Orlando FL; 2001. p. 181–93.
- [12] Hall C. Water sorptivity of mortars and concretes: a review. *Mag Concr Res* 1989;41(146):51–61.
- [13] Spragg R, Castro J, Li W, Pour-Ghaz M, Huang P, Weiss J. Wetting and drying of concrete using aqueous solution containing deicing salt. *Cem Concr Compos* 2011;33(5):535–42.
- [14] Yang Z, Weiss J, Olek J. Water absorption in partially saturated fracture concrete. RILEM workshop: transport mechanism in cracked concrete. Ghent; 2007.
- [15] Martys NS. Diffusion in partially saturated porous materials. *Mater Struct* 1999;32(8):991–1004.
- [16] Martys N, Ferraris CF. Capillary transport in mortar and concrete. *Cem Concr Res* 1997;27(5):747–60.
- [17] Lockington D, Parlange JY, Dux P. Sorptivity and the estimation of water penetration into unsaturated concrete. *Mater Struct* 1999;32(5):342–7.
- [18] Hall C. Anomalous diffusion in unsaturated flow: fact or fiction? *Cem Concr Res* 2007;37(3):378–85.
- [19] Powers TC, Brownyard TL. Studies of the physical properties of hardened Portland cement paste. *Am Concr Inst Proc* 1946;43:469–82.
- [20] Parrott LJ. Moisture conditioning and transport properties of concrete test specimens. *Mater Struct* 1994;27(8):460–8.
- [21] Parrott LJ. Factor influencing relative humidity in concrete. *Mag Concr Res* 1991;43(154):45–52.
- [22] DeSouza SJ, Hooton RD, Bickley JA. Evaluation of laboratory drying procedures relevant to field conditions for concrete sorptivity measurements. *Cem Concr Agg* 1997;19(2):59–63.
- [23] DeSouza SJ, Hooton RD, Bickley JA. A field test for evaluating high performance concrete covercrete quality. *Can J Civil Eng* 1998;25(3):551–6.
- [24] Castro J, Kompare P, Poursaee P, Nantung T, Weiss J. JTRP Report SPR-3093, Portland cement concrete pavement performance relative to permeability. Indiana Department of Transportation; 2010.
- [25] ASTM International, ASTM C305. Standard practice for mechanical mixing of hydraulic cement pastes and mortars of plastic consistency; 2006.
- [26] ASTM International ASTM C642. Standard test method for density, absorption, and voids in hardened concrete; 2006.
- [27] Powers TC, Copeland LI, Mann HM. Capillary continuity or discontinuity in cement pastes. *J. PCA Res. Dev. Lab* 1959;1(2):38–48.
- [28] Hwang C, Young J. Drying shrinkage of portland cement pastes. Microcracking during drying. *Cem Concr Res* 1984;14(4):585–94.
- [29] Chatterji S. Drying shrinkage of cement paste and concrete: a reappraisal of the measurement technique and its significance. *Cem Concr Res* 1976;6(1):145–8.
- [30] Van Bisschop J, Mier J. How to study drying shrinkage microcracking in cement-based materials using optical and scanning electron microscopy? *Cem Concr Res* 2002;32(2):279–87.
- [31] Samaha H, Hover K. Influence of microcracking on the mass transport properties of concrete. *ACI Mater J* 1992;89(4):416–24.
- [32] Yang Z, Weiss J, Olek J. Water transport on concrete damaged by tensile loading and freeze-thaw cycling. *J Mater Civil Eng* 2006;18(3):424–34.
- [33] Yang Z. Assessing cumulative damage in concrete and quantifying its influence on life cycle performance modeling. PhD thesis, Purdue University, West Lafayette, Indiana; 2004.
- [34] Bentz DP, Ehlen CF, Ferraris CF, Winpiger JA. Service life prediction based on sorptivity for highway concrete exposed to sulfate attack and freeze-thaw conditions, FHWA-RD-01-162, US Department of Transportation; 2002. p. 62.
- [35] Nilsson LO. Hygroscopic moisture in concrete – drying, measurements and related material properties. PhD thesis. Lund University; 1980.

Water Absorption and Critical Degree of Saturation Relating to Freeze-Thaw Damage in Concrete Pavement Joints

Wenting Li¹; Mohammad Pour-Ghaz, M.ASCE²; Javier Castro³; and Jason Weiss, M.ASCE⁴

Abstract: Fluid ingress is a primary factor that influences freeze-thaw damage in concrete. This paper discusses the influence of fluid ingress on freeze-thaw damage development. Specifically, this paper examines the influence of entrained air content on the rate of water absorption, the degree of saturation, and the relationship between the saturation level and freeze-thaw damage. The results indicate that whereas air content delays the time it takes for concrete to reach a critical degree of saturation it will not prevent the freeze-thaw damage from occurring. The results of the experiments show that when the degree of saturation exceeds 86–88%, freeze-thaw damage is inevitable with or without entrained air even with very few freeze-thaw cycles. DOI: 10.1061/(ASCE)MT.1943-5533.0000383. © 2012 American Society of Civil Engineers.

CE Database subject headings: Absorption; Emissions; Concrete pavements; Deterioration; Freeze and thaw; Joints.

Author keywords: Absorption; Acoustic emission; Air content; Concrete; Concrete pavement; Degree of saturation; Deterioration; Freeze-thaw; Pavement joint; Water absorption.

Background on the Problem of Joint Deterioration in Concrete Pavements

Concrete pavements represent a large portion of the transportation infrastructure. Whereas many of these pavements provide excellent long-term performance, a portion of these pavements have recently shown premature joint deterioration throughout the Midwestern states (Weiss et al. 2007; Sutter et al. 2006; Leech et al. 2008; Rangaraju et al. 2006). This joint deterioration is problematic because it compromises the performance and potential service life of an otherwise healthy pavement. Fig. 1 is photographs of a typical damaged pavement joint. This type of damage is frequently seen as either the development of cracking parallel to the joint or spalling and cracking at the joint from the bottom of the saw cut to the surface of pavement approximately 4–6 in. from the joint. Unfortunately, damage is not frequently observed at the surface of the pavement until a significant amount of damage has occurred

inside the joint. During field inspections it has been observed that where the joints are damaged the sealant is damaged and the joint contained standing water. Research is needed to better understand how this standing water may lead to freeze-thaw damage. Further, this damage occurs in both poorly air entrained and properly air entrained concrete. As a result, the role of air content needed to be quantified which is the reason for this study.

Background on Water Absorption and the Critical Degree of Saturation

Concrete is susceptible to freeze-thaw damage when it is saturated (Sutter et al. 2006; Leech et al. 2008; Fagerlund 1972, 1975, 1977, 1979, 1981, 2004; Bentz et al. 2001; Litvan 1988; Litvan and Sereda 1980; Shimada et al. 1991; Beaudoin and Cameron 1972; Feldman 1987; Scherer 1993; Scherer and Valenza 2005; Sun et al. 2007). Whereas the water content in concrete can be quantified in several different ways, this paper defines the degree of saturation (S) as the ratio of the absolute volume of absorbed water to the total volume of pores (i.e., the total volume of water that can be absorbed by concrete).

It has been suggested that there is a critical degree of saturation (S_{cr}) beyond which freeze-thaw damage can begin to initiate (Fagerlund 1972, 1975, 1977, 1979, 1981, 2004; Bentz et al. 2001; Litvan 1988; Litvan and Sereda 1980; Shimada et al. 1991; Beaudoin and Cameron 1972). For degrees of saturation below the critical degree of saturation freeze-thaw damage is not observed to occur even after a large number of freeze-thaw cycles (Fagerlund 1972, 1975, 1977, 1979, 1981, 2004; Bentz et al. 2001; Litvan 1988; Litvan and Sereda 1980; Shimada et al. 1991; Beaudoin and Cameron 1972).

Fig. 2 schematically illustrates the concept of water absorption and the critical degree of saturation (Fagerlund 2004; Barde et al. 2009). We can begin by assuming that the representative volume element shown in Fig. 2 is filled with pores with different sizes at a given spacing. It is assumed that there are two critical values

¹Graduate Research Assistant, School of Materials Science, Southeast Univ., Nanjing 211189, China, and Graduate Research Assistant, School of Civil Engineering, Purdue Univ., West Lafayette, IN. E-mail: li448@purdue.edu

²Assistant Professor, Dept. of Civil, Construction, and Environmental Engineering, North Carolina State Univ., Campus Box 7908, 431C Mann Hall, Raleigh, NC 27695; formerly, Graduate Research Assistant, School of Civil Engineering, Purdue Univ., West Lafayette, IN. E-mail: mpourghaz@ncsu.edu

³Assistant Professor, School of Engineering, Pontificia Universidad Católica de Chile, Casilla 306, Correo 22, Santiago, Chile. E-mail: jecastro@ing.puc.cl

⁴Professor, Director of Pankow Materials Laboratory, Purdue Univ., West Lafayette, IN (corresponding author). E-mail: wjweiss@ecn.purdue.edu

Note. This manuscript was submitted on February 17, 2011; approved on August 29, 2011; published online on August 29, 2011. Discussion period open until August 1, 2012; separate discussions must be submitted for individual papers. This paper is part of the *Journal of Materials in Civil Engineering*, Vol. 24, No. 3, March 1, 2012. ©ASCE, ISSN 0899-1561/2012/3-299-307/\$25.00.



Fig. 1. Field observation showing damage in pavement joints

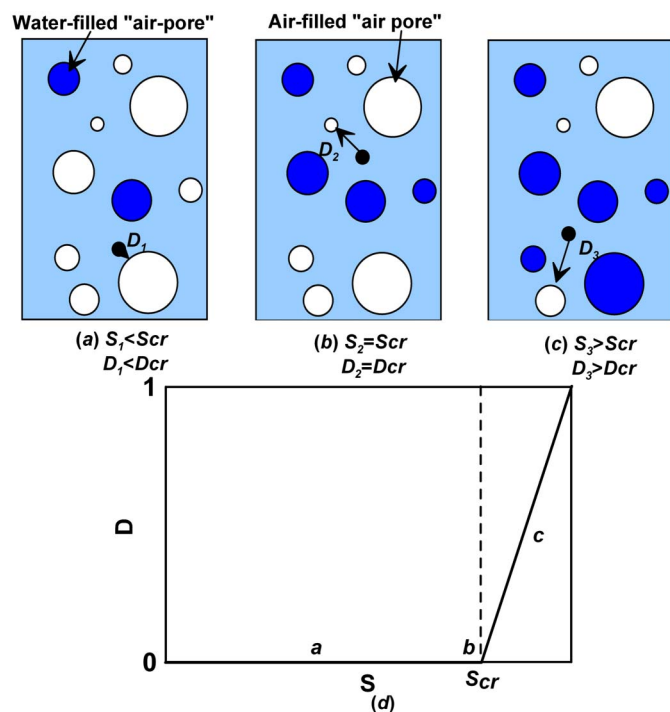


Fig. 2. Schematic of relation between degree of saturation with freeze-thaw damage (10, 19)

that describe the freeze-thaw performance. The first parameter is related to the degree of saturation as described previously. The second parameter is related to a “critical flow distance” (i.e., D_{cr}), which is the maximum distance that water can flow from freezing site to the surrounding nearest air-filled space. Damage doesn’t occur when the flow distance (D) is below the critical distance (D_{cr}) and the degree of saturation (S) is less than the critical degree of saturation (S_{cr}), as shown in Fig. 2(a). However, the flow distance increases with the amount of absorbed water (or poor quality air void system) as does the degree of saturation. If either the critical flow distance or the critical degree of saturation is exceeded, frost damage initiates upon the next freezing cycle [Fig. 2(c)]. The degree of damage can be quantified by the reduction in the dynamic elastic modulus of concrete, as shown schematically in Fig. 2(d).

In Fig. 2(d) for all the values of degree of saturation below the critical degree of saturation the amount of damage (reduction is the elastic modulus) is very small. As soon as the degree of saturation exceeds the critical degree of saturation, damage initiates in the material (Fagerlund 1972, 1975, 1977, 2004; Bentz et al. 2001).

The quality of air distribution and the volume of the air are two important parameters affecting the freeze-thaw resistance of the system. The quality of the air system is related to the critical flow distance whereas the quantity of the air voids (volume of air) is related to the critical degree of saturation. A fully saturated system, however, regardless of the quantity and quality of the air cannot even sustain a single freezing cycle without accumulating a significant amount of damage (Litvan 1988).

Background on Use of Acoustic Emission to Quantify Freeze-Thaw Damage

Acoustic emission (AE) is a nondestructive test method that is on the basis of measuring the release of energy in concrete (e.g., the release of energy that occurs at the time of cracking). However, AE can be performed in either a passive (i.e., capturing the acoustic wave generated because of the formation of permanent defect such as crack) or active (i.e., using one transducer to generate a pulse and another transducer to capture the same pulse (in the simplest arrangement)). Classically, AE is typically performed in passive mode in cement/concrete studies (Ohtsu 1999, Ohtsu and Shigeishi 1993; Bentz et al. 2008; Hossain et al. 2003; Shah and Weiss 2006; Kim and Weiss 2003; Moon and Weiss 2006; Ouyang et al. 1991a, 1991b; Suaris and Van Mier 1995, 1993; Pour-Ghaz et al. 2010; Puri and Weiss 2006; Yang et al. 2006; Yoon et al. 1999). The AE has been used in concrete to assess damage attributable to restrained shrinkage (Bentz et al. 2008; Hossain et al. 2003; Shah and Weiss 2006; Kim and Weiss 2003; Moon and Weiss 2006) and mechanical loading (Ouyang et al. 1991a, 1991b; Suaris and Van Mier 1995, 1993; Pour-Ghaz et al. 2010; Puri and Weiss 2006; Yang et al. 2006; Yoon et al. 1999). The AE has also been used to monitor freezing and thawing of mortar and it was observed that activity during both freezing and thawing (Shimada et al. 1991; Krishnan 2002).

In the present work the evolution of damage in concrete during freeze-thaw cycles was monitored using both active and passive AE. The reduced relative dynamic elastic modulus was calculated for each cycle according to the transmitting time of waves using active AE. Passive AE was recorded to better understand the damage that develops during the freeze-thaw cycle.

Hypothesis and Outline for Experimental Investigation

There has been a great deal of debate on possible causes of joint deterioration in concrete pavements. It is the hypothesis of this

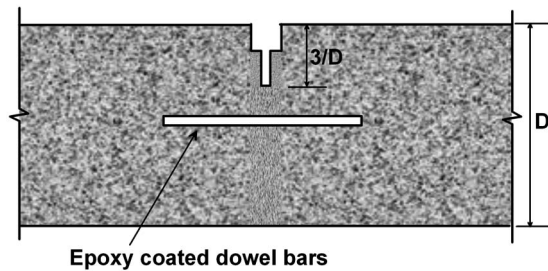


Fig. 3. Cross section of the joints in pavement

work that the presence of water (or solution containing deicing salt solutions) in the joints plays a significant role in the deterioration of concrete pavement joints. First, it is hypothesized that joints can hold water or deicing fluids substantially longer than other parts of the pavement because of the specific geometry of the joint as shown in Fig. 3 (especially if the joint does not crack). This would enable the concrete at the joint to become preferentially saturated. The potential for a joint to hold water increases when the joint sealant is damaged or missing, at low spots in the pavement, and when the joint does not crack and open as designed (as has been noticed in the field). It is hypothesized that this propensity for saturation could make the concrete more susceptible to local freeze-thaw damage. Second, it is hypothesized that the use of air entrainment can increase the resistance to joint deterioration, however, it is also believed that the use of air entrainment will not eliminate the potential for damage to occur. The addition of air entrainment is believed to extend the time required for the concrete to reach to the critical degree of saturation.

Whereas other factors can contribute to joint deterioration (e.g., the use of specific deicers, curing conditions, mixture proportions, construction details), they are not specifically considered in this paper. The scope of this paper is to examine the role of air entrainment on the rate of water ingress and degree of saturation increase in concrete. Second, this paper provides data to relate the degree of saturation to freeze-thaw damage in air entrained and nonair entrained concrete.

Experimental Plan

This section describes mixture proportioning, specimen conditioning, and the procedures of the testing in detail.

Mixture Proportions

Three mortar mixtures were prepared with different air contents (6, 10, 14% air by volume as measured in mortar). The air volume was calculated for an equivalent paste and concrete system, respectively, with the assumptions shown in Table 1. All specimens were made with ordinary Portland cement (Type I) and had a water to

Table 1. Mixture Proportions and Constituent Materials

Air content of paste (% by volume of mortar ^a /concrete ^b)	Cement (Type I) (kg/m ³)	Water (kg/m ³)	Sand (kg/m ³)
13 (6/4)	573.3	240.8	1,333.3
22 (10/7)	548.9	230.6	1,276.5
31 (14/9)	524.5	220.3	1,219.8

^aIn calculating the equivalent air content in mortar it was assumed 45% paste by volume of the mortar.

^bIn calculating the equivalent air content in concrete it was assumed 30% paste by volume of the concrete.

cement ratio (w/c) of 0.42 which is typical of concrete pavements in the state of Indiana. Table 1 presents the proportions of the materials that were used.

Mixing was performed in accordance with ASTM C192-06 (ASTM 2006). Two specimen geometries were used in this study: cylinders (25 mm height × 100 mm diameter) and prisms (25 mm × 25 mm × 125 mm). Cylindrical specimens were used for the water absorption test. The prism specimens were used to evaluate the freeze-thaw damage development using AE. These specimens were cut from larger specimens.

Specimen Conditioning

The method of the specimen conditioning prior to water absorption testing can substantially influence the results of the test (Castro et al. 2011, 2010; Spragg et al. 2011). If the specimen is not properly conditioned, it can lead to a misunderstanding of the actual absorption behavior (Castro et al. 2011, 2010; Spragg et al. 2011). Because of the significance of conditioning and necessity for the specimens to reach equilibrium, the standard curing procedures were not used (Scherer and Valenza 2005). The procedure that was used in this study allowed the specimens to equilibrate for a longer period.

The cylindrical specimens were cut 24 h after casting from a larger cylindrical sample and sealed in two layers of plastic. The specimens were stored at 23 ± 1°C for 28 days. After 28 days the specimens were removed from the plastic bag and placed in 50 ± 1, 65 ± 1, and 80 ± 1% relative humidity (RH) environments in which they were kept for more than a year to equilibrate. Table 2 lists the air content and RH of each specimen.

Water Absorption

A procedure similar to ASTM C1585-04 (ASTM 2004) was used, however, the specimens were not conditioned following the accelerated ASTM testing procedure (described previously). After conditioning, the outer circumference of the specimen was sealed with two layers of epoxy resin. After the epoxy hardened, the specimens were placed under water. Two small spacers were placed under the sample to provide a small gap between the bottom of the container and the lower surface of the sample. This allowed water absorption from both circular surfaces (Fig. 4).

Freeze-Thaw Testing

This section describes specimen preparation and procedures used in freeze-thaw testing.

Table 2. Initial Condition, Air Content, and Namely Scheme for Specimens Used in the Present Study

Specimen name	Air content of the paste (%)	RH (%)
50-13 ^a	13	50
65-13	13	65
80-13	13	80
50-22	22	50
65-22	22	65
80-22	22	80
50-31	31	50
65-31	31	65
80-31	31	80

^aThe first number shows the initial humidity of the specimen (e.g., 50-13 is 50% RH); the second number shows the air content of mortar of the specimen (e.g., 50-13 is 13% air by volume of paste).

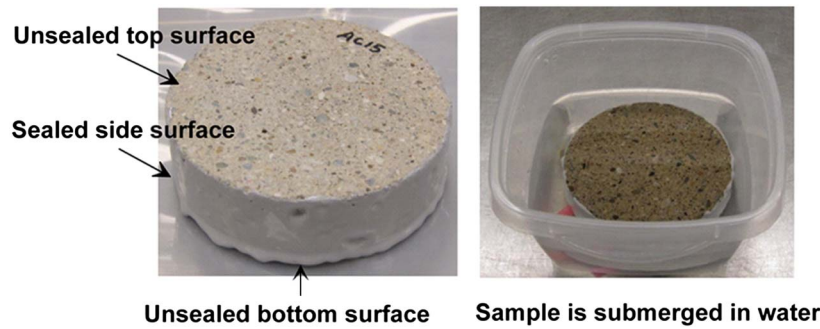


Fig. 4. Double-sided sorption test of specimen with 1-in. thickness

Specimen Saturation

The prismatic specimens were prepared to have different degrees of saturation before freeze-thaw testing was performed. The specimens were oven dried in steps to 105°C where they were maintained for 2 days. The specimens were then placed in a desiccator and evacuated to a residual pressure of 30 mm Hg (4,000 Pa) for 3 h. After evacuation and while still under vacuum, water was introduced into the desiccators to cover the specimens. The specimens were left in the desiccators for 24 h. This condition was considered as saturated (i.e., 100% degree of saturation). The degree of saturation was reduced for some specimens (i.e., 0.96, 0.92, 0.90, 0.86, 0.82, and 0.78) by short periods of drying at 23°C and 50% RH. During the drying period, the mass of the specimens was closely monitored. After drying, all the specimens were sealed in plastic bags for a minimum of 3 days to allow moisture to redistribute before freezing and thawing testing.

Preparation of the Specimen for Freezing and Thawing

Fig. 5 shows the procedure used for preparing the specimens for AE testing during freeze-thaw cycles. The specimens were first

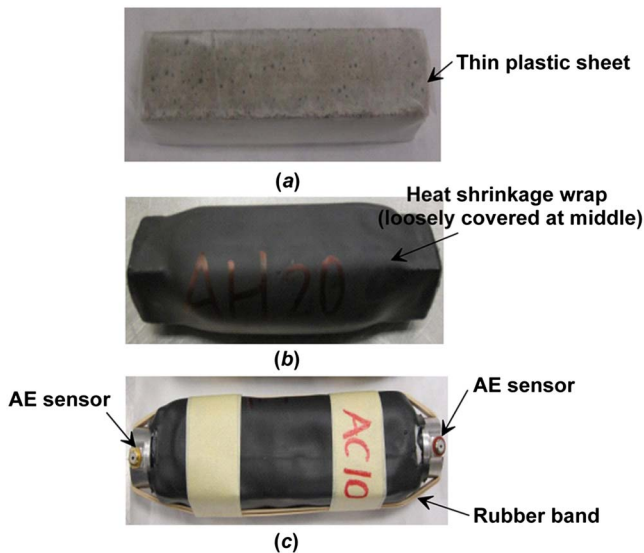
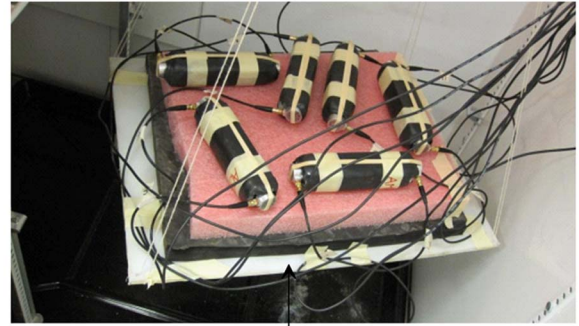


Fig. 5. Specimens prepared for AE testing during freeze-thaw cycle: (a) thin plastic sheet to avoid evaporation during specimen preparation and handling; (b) specimen covered by heat shrinkable wrap to avoid evaporation during specimen preparation and handling; (c) acoustic emission sensors installed at the both ends of the specimens



Suspended plate to eliminate vibration and noise from environment

Fig. 6. Specimens placed on a suspended base to eliminate vibration and noise from surrounding environment (inside of freeze-thaw chamber)

preconditioned to different degrees of saturation as described previously. After preconditioning, the specimens were wrapped with a thin plastic sheet as shown in Fig. 5(a). The thin plastic sheet was used to protect the sample from further drying during the handling. The specimens were then sealed with a “heat shrink wrap” to further protect the specimens against moisture exchange with surroundings (prevent them from absorbing or releasing water during the freeze-thaw process) as shown in Fig. 5(b). It is important to note that the “heat shrink wrap” was in loose contact with sample (with the exception of the specimen ends) so that the specimen can expand freely during the test whereas minimizing any restraint.

The AE sensors (transducers) were attached on the two ends with a thin layer of vacuum grease as shown in Fig. 5(c). Fig. 6 shows that all the specimens were placed on a suspended base in testing to minimize noise/vibration transmission from surrounding environment. The threshold was set at 60 dB and 34 dB for active and passive AE, respectively. Testing was also performed on dry specimens to ensure that sounds were not being recorded from the environment, freezing unit, or coupling agent (Pour-Ghaz and Weiss 2010).

Temperature Cycle used for Freeze-Thaw Testing

Fig. 7 shows the temperature cycle (in air) which allows one cycle per day. Temperature was controlled to vary from $10 \pm 1^\circ\text{C}$ to $-18 \pm 1^\circ\text{C}$. The rate of the temperature change was $14^\circ\text{C}/\text{h}$ resulting in a 2-h transition period and two 10-h periods at $10 \pm 1^\circ\text{C}$ and $-18 \pm 1^\circ\text{C}$, respectively.

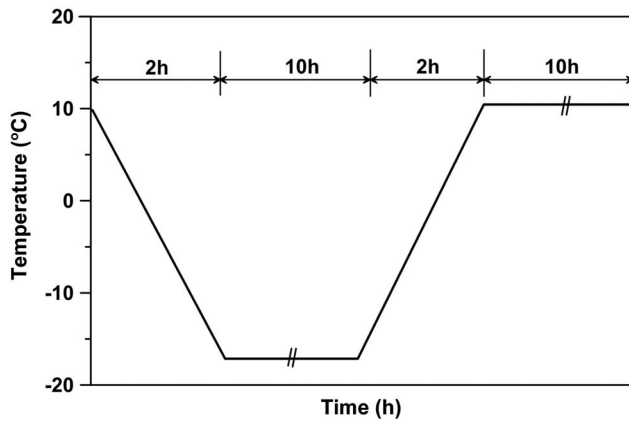


Fig. 7. Temperature cycle used in freeze-thaw experiment (air temperature)

Experimental Results and Discussion

Water Absorption

Sorptivity

The amount of absorbed water (I) is normalized by the cross-sectional area exposed to water as outlined in ASTM C1585 (ASTM 2004)

$$I = m_t / (a \cdot d) \quad (1)$$

where m_t = change in specimen mass at time t in grams; a = area of the both sides exposed to water in mm^2 ; and d = density of water in g/mm^3 .

Sorptivity is defined as the slope of the water absorption versus square root of time curve (ASTM 2004). The initial sorptivity is the slope of this curve within the first 6 h, whereas the secondary sorptivity is the slope of the curve between 1 and 8 days.

Fig. 8(a) illustrates the sorption results for the specimens conditioned at 50% RH with 13 and 31% air contents by volume of paste. The specimens show a similar sorptivity (slope of the curves) and amount of absorbed water initially; however, over time the specimens with higher volumes of air absorb more water. This occurs because the air voids provide space for water (Helmuth 1961; Warris 1964), however, the diffusion of air and the overpressure in the air bubbles delays water absorption which corresponds for the long time to saturation (Fagerlund 1993, 1995, 2004). Although the secondary sorptivity for sample with higher air content is higher, this sample requires to absorb more water to reach to the critical degree of saturation.

Fig. 8(b) shows the water absorption results for specimens conditioned at 65% RH. Comparing this result with Fig. 8(a) suggests that the amount of absorbed water for the specimens conditioned at 65% RH is lower than that of specimens conditioned at 50% RH with the same air content. Fig. 8(c) shows the absorption for specimens conditioned at 80% RH. The specimens at 65% RH and 50% RH show a nick point at the end of the 6 h on a water absorption square root of time curve, however, the nick point can not be seen on the results of 80% RH and a more graduate rate of absorption can be seen.

The RH in which the specimens were conditioned in has a significant impact on the results (Castro et al. 2011, 2010; Spragg et al. 2011). The driving force of unsaturated fluid transport is the capillary suction (Hall and Hoff 2002; Martys and Ferraris 1997; Hanžič et al. 2010). When samples are in equilibrium with a lower RH, a larger volume of pores are empty and available to be filled with water during the water sorption. Furthermore, at lower humidity,

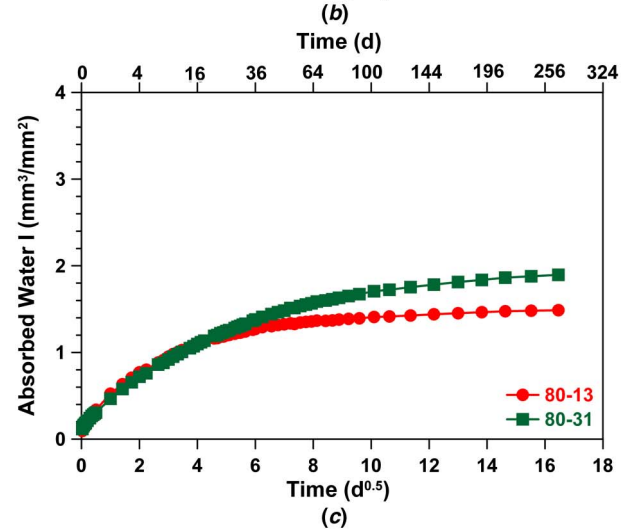
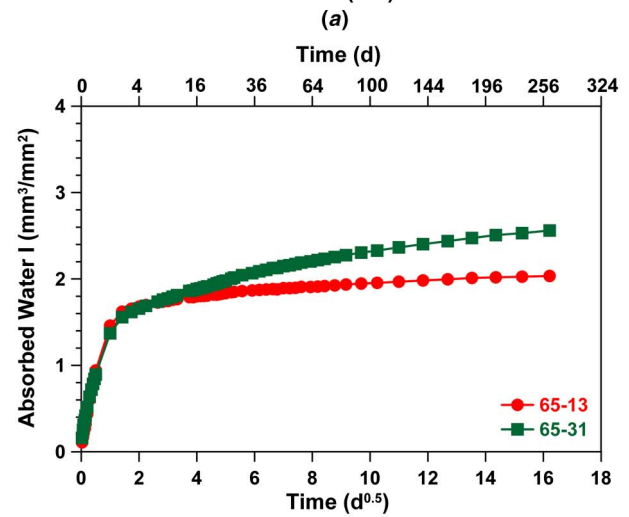
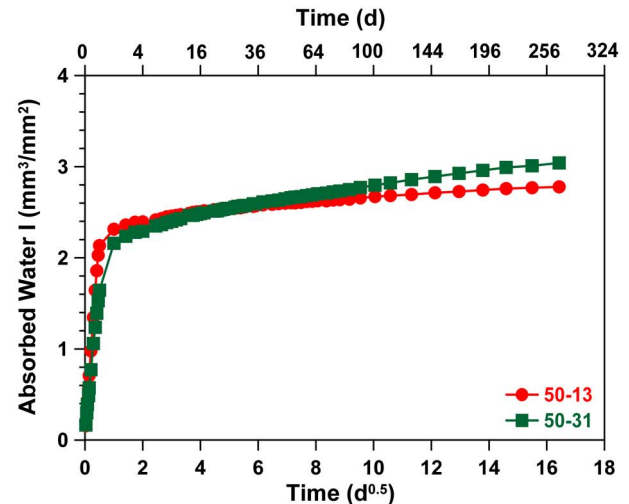


Fig. 8. Effect of air content and initial moisture on water absorbed: (a) 50% RH; (b) 65% RH; (c) 80% RH

the maximum size of the pores that is filled with water is smaller, creating a higher suction force. The overall effect will be higher rate of water absorption and high volume of absorbed water.

Degree of Saturation

Fig. 9 shows the degree of saturation (S) of the specimens conditioned at 50, 65, and 80% RH with two air contents (13 and 31% by volume of paste). The degree of saturation is plotted as a function of

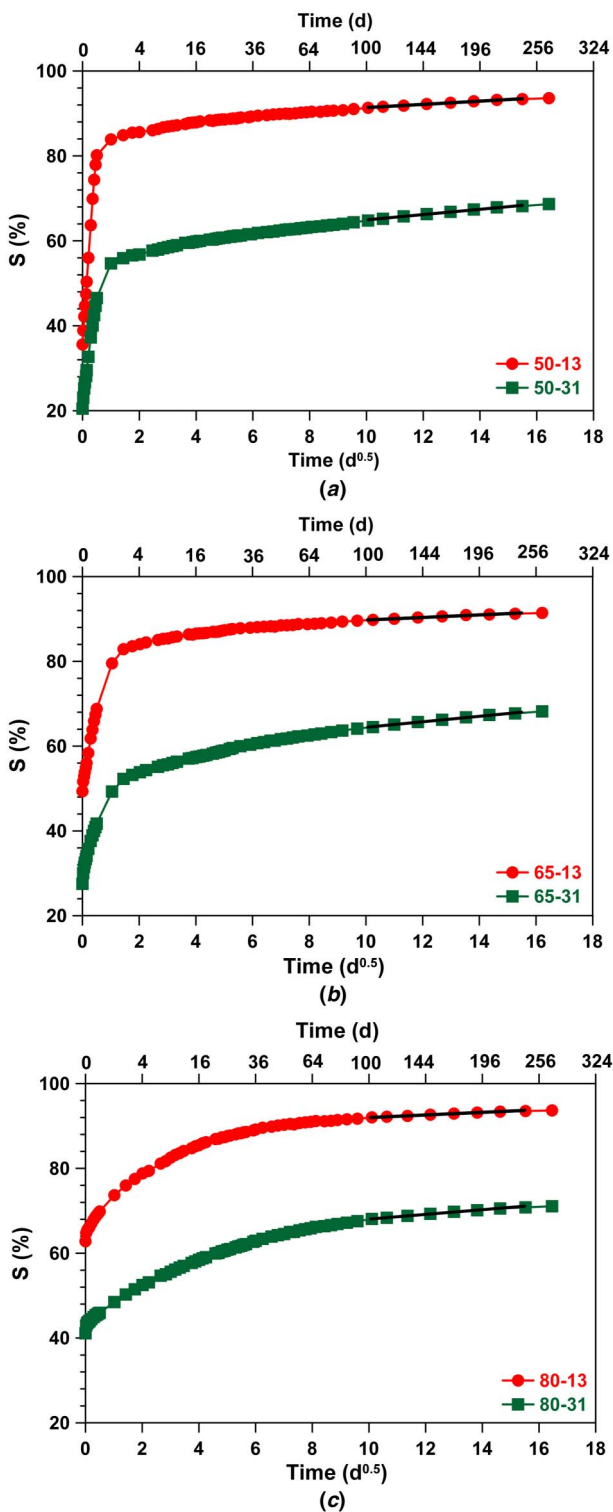


Fig. 9. Results of sorption test provided as increase in the degree of saturation: (a) 50% RH; (b) 65% RH; (c) 80% RH

squareroot of time on the lower x-axis whereas actual time is shown on the upper x-axis.

The most striking feature of the graphs in Fig. 9 is the fact that the degree of saturation decreases with air content. At the end of the initial 6-h sorption period, samples with lower air content show higher degree of saturation. For samples equilibrated at 50% RH, the degree of saturation is 39% less when the air content increases 10%, the decrease in degree of saturation for samples equilibrated at 65% and 80% RH is 23% and 26%, respectively.

Table 3. Time to Reach to the Critical Level of Saturation (88%) for the Specimens with Different Air Content

Initial RH (%)	Air content by volume of paste (%)	Secondary sorptivity ($\text{mm}^3/\text{mm}^2 \cdot \text{d}^{0.5}$)	Time to reach the critical degree of saturation (88%) (S_{cr}) in years ($\pm 1.7\%$)
50	13	0.485	0.011 (4d)
	22	0.691	5.08
	31	0.750	6.10
65	13	0.368	0.016 (6d)
	22	0.513	5.63
	31	0.785	5.90
80	13	0.563	0.015 (5d)
	22	0.606	4.00
	31	1.009	5.82

The secondary rate of absorption (Fig. 8) is different for samples with different air content; however, in Fig. 9 the secondary rate of increase in degree of saturation is approximately the same for materials with different air content. This suggests that for an equal time of exposure to water, the specimen with the higher air content has a lower degree of saturation (Fagerlund 1993, 1995, 2004).

The secondary rate of increase in degree of saturation can be fitted with a linear function to estimate the amount of absorbed water over a long period of time. The linear fit used in Fig. 9 is shown with a solid line. Because the objective here is to estimate the degree of saturation over a long period of time, only the date between 100 and 240 days is used in fitting this straight line. Using this linear function, the time to reach to critical degree of saturation is calculated for each specimen with different air content and initial equilibrium condition and reported in Table 3.

Freeze-Thaw Testing

Monitoring the Damage Development Using Active Acoustic Emission

The relative dynamic elastic modulus is frequently used as an index to evaluate the extent of damage (Fagerlund 1972, 1975, 1977, 1979, 1981, 2004; Bentz et al. 2001; Litvan 1988; Litvan and Sereda 1980; Shimada et al. 1991). Using active AE, the transmission time of a single pulse was measured along the sample. The transmission time along the length of the sample was measured in both directions (i.e., from Sensor 1 to 2 and from Sensor 2 to 1). The transmission time was measured three times in each direction and the average transmission time is reported here (average of 6 values). The transmitting time was measured after each cycle when the temperature was stable at 10°C for a minimum of 2 h.

The relative elastic modulus, i.e., E_t/E_o , is square proportional to the velocity of wave transmitting through materials, which is inversely square proportional to the ratio of the wave transmission times (ASTM 2008), as shown in Eq. (2). Damage parameter (D) can also be estimated using Eq. (2).

$$D = 1 - E_t/E_o = 1 - (T_o/T_t)^2 \quad (2)$$

where E_o , T_o = dynamic elastic modulus before freeze-thaw testing began and corresponding transmitting time; and E_t , T_t = dynamic elastic modulus during testing at any time t and corresponding transmitting time.

The main cracks were along the direction of wave propagation and as such the wave is least sensitive to these cracks, however, the damage was still easily recorded.

Fig. 10 illustrates the damage index [Eq. (2)] with increasing cycles of freezing and thawing. The damage initiates during the first cycle when the degree of saturation is above 86~88%. The specimens with lower degree of saturation do not show damage whereas specimens with a higher degree of saturation show a rapid deterioration. The saturated specimens ($S = 100\%$) can not sustain more than three cycles before complete failure occurs.

Fig. 11 shows the rate of damage (dD) development per freeze-thaw cycle (dN) (as determined by the slope of Fig. 10) for specimens with different degrees of saturation. A critical degree of saturation appears to occur at approximately 86–88%. The critical degree of saturation appears to be independent of the air content.

Acoustic Energy Measured Using Passive Acoustic Emission

Fig. 12 shows the amplitude of the acoustic events as a function time for a specimen with 96% degree of saturation and 13% air content during freezing cycle. The temperature is the temperature measured in the center of the mortar specimen. Fig. 12(a) illustrates the amplitude distribution for the first freeze-thaw cycle and Fig. 12(b) illustrates the amplitude distribution during the second freeze-thaw cycle for the same specimen.

In Fig. 12(a) the acoustic events begin to occur as the temperature of the specimen decreases. A cluster of acoustic event is shown in Fig. 12(a) as highlighted by the ellipsoid. This cluster

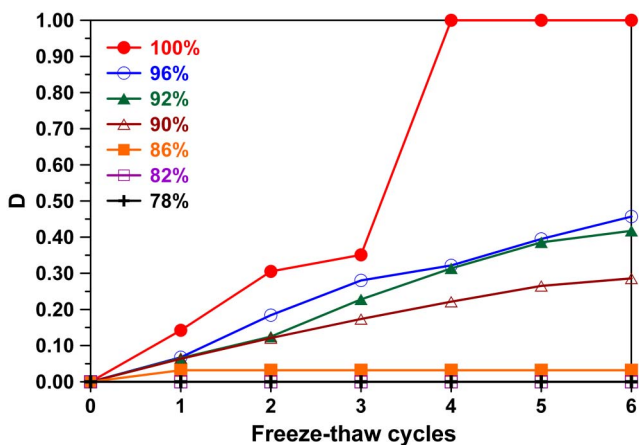


Fig. 10. Decrease of the relative dynamic elastic modulus with freeze-thaw cycles of the specimen with 13% air content by volume of the paste

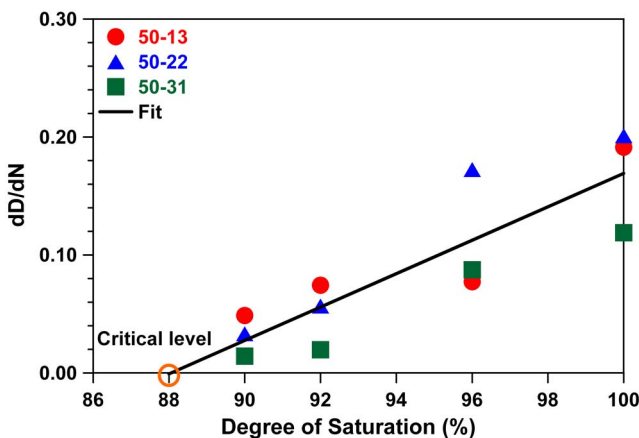


Fig. 11. Rate of decrease of relative dynamic elastic modulus with degree of saturation

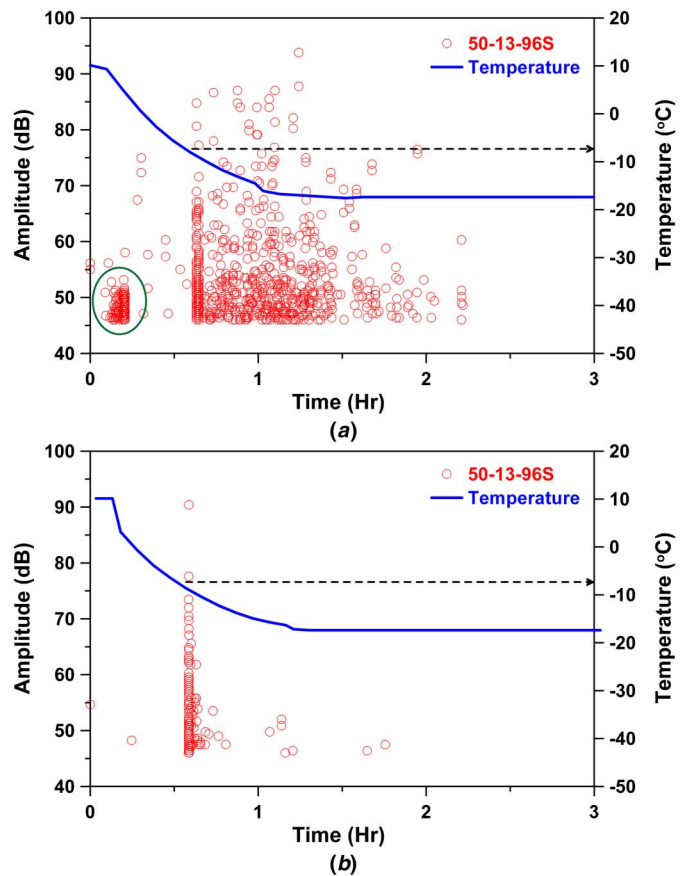


Fig. 12. Amplitude in the transition time of freezing (96S): (a) first cycle; (b) second cycle

of data is not seen in Fig. 12(b). These events can be attributed to microcracking of the specimen because of the thermal loading, which may be a result of temperature gradient or a result of thermal expansion coefficient mismatch between the paste and aggregate. Because the thermal loading is not changed during the second cycle, the damage attributed to thermal loading does not exceed the previous level of damage in materials and additional cracking would not be expected (Kaiser 1950; Kline and Egle 1987).

In Fig. 12 the acoustic events begin to increase dramatically after the temperature drops below -8°C in both cycles. The number of events is higher in the first cycle compared to the second cycle as more cracking would be expected in the first freeze-thaw cycle whereas these cracks would be expected to extend in the following cycles. The damage at the point (below -8°C) is likely attributed to formation of ice and cracking inside the specimen. This is consistent with the observation that pore solution freezes below 0°C because of pore confinement and dissolved ions in pore solution (Fagerlund 1973; Helmuth 1960).

Desorption Isotherm

Fig. 13 shows the desorption isotherm for the specimens with 13 and 31% air content by volume of paste. The desorption curve demonstrates the mass of water lost from the specimen at each RH step (i.e., different pore sizes begin to empty out at different RHs starting with large pores at high RHs and smaller pores at lower humidities). The profile of the desorption curve is similar for both specimens until high RHs, i.e., 97.5% RH. At RHs higher than 97.5%, a larger difference of the porosity can be seen. This difference corresponds to the air entrained porosity.

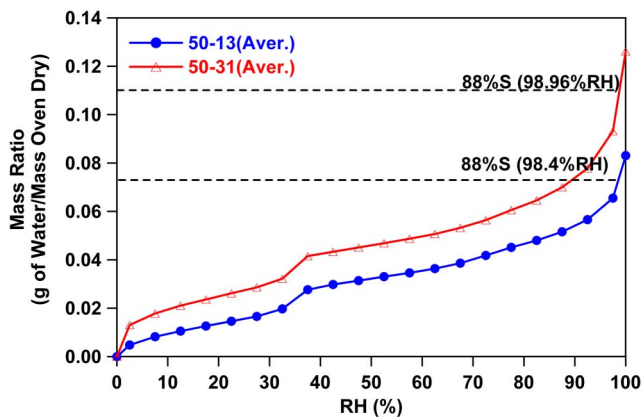


Fig. 13. Mass change at decreasing RH containing deionized water

The critical degree of saturation (88%) corresponds to RH of 98.4% for specimen with 13% air content and 98.96% RH for specimen with 31% air content, respectively. This implies that some of the air entrained pores are water filled when the specimen is at or above critical degree of saturation. The difference in mass loss between the 13 and 31% air content at 2.5% RH is currently unknown, however, this is repeatable between specimens.

Calculated Time to Reach the Critical Degree of Saturation

The rate of absorption of water and its relation to the degree of saturation was discussed previously and the influence of the degree of saturation on freeze-thaw damage was discussed after that. To better understand how these findings can be related to one another to predict the time to freeze-thaw damage, a linear function was fit to the plot of degree of saturation versus squareroot of time data (using the secondary absorption).

Table 3 shows the time required for each specimen equilibrated at different initial conditions to reach the critical degree of saturation (i.e., 88% in this study). Specimens without air entrainment can reach to the critical degree of saturation within days (4 ~ 6 days). The use of air entrainment raised the air content and decreases the degree of saturation. This increases the time to reach a critical degree of saturation to 3 ~ 6 years. The rate of water absorption is substantially different in the systems with entrained air compared to nonair entrained systems.

Conclusions

The water absorption of mortar containing different volumes of entrained air was examined in this study, whereas tests like ASTM C 1585-04 (ASTM 2004) can be used to provide an index of water absorption, the differences between nonair entrained and air entrained systems were small when only mass gain was investigated. Whereas the absorption rates in plain and air entrained systems were similar, initially the air entrained system showed a higher rate of ingress at later ages. By normalizing the results of water absorption in terms of the degree of saturation, a clear distinction between the nonair entrained and air entrained mixtures can be made. Whereas the nonair entrained system took 4–6 days to reach 88% saturation, the air entrained system is estimated to require approximately 3–6 years. This shows that entrained air will substantially increase the time to failure.

The damage attributable to freeze-thaw was monitored using both passive and active AE. A critical degree of saturation was observed with specimens that have a degree of saturation greater than the 86–88% exhibiting damage during the few freeze-thaw cycles.

The critical degree of saturation appears to be independent of the air content as materials with a degree of saturation above the critical degree undergoing damage after a few of freeze-thaw cycles irrespective of the air content. The volume of air and quality of the air void system however likely has a strong relation to the critical flow distance.

Increasing the air content resulted in a longer time for the mortar to reach to the critical degree of saturation. Whereas increasing the air content can delay the time freeze-thaw damage initiates in practice, it appears that increasing of the air content can not eliminate the potential for freeze-thaw damage. To solve this problem, the benefits of sealers as well as improving the understanding of the correlation between the critical spacing and the degree of saturation and the freezing rate are being investigated.

Acknowledgments

The experiments reported in this paper were conducted in the Pankow Materials Laboratories at Purdue University. This work was supported in part by Compass Minerals and the Joint Transportation Research Program administered by the Indiana Department of Transportation and Purdue University. The contents of this paper reflect the views of the authors, who are responsible for the facts and the accuracy of the data presented in this paper, and do not necessarily reflect the official views or policies of the Indiana Department of Transportation, nor do the contents constitute a standard, specification, or regulation. The authors appreciate the assistance of Gaurav Sant for his work in casting/cutting the specimens while he was a graduate assistant funded on this project. The authors also acknowledge many useful discussions with Dick Newell, John Poncher, Mike Byers, Tommy Nantung, Dave Andrews, and Jan Olek.

References

- ASTM. (2004). "Standard test method for measurement of rate of absorption of water by hydraulic-cement concretes." *Standard C1585-04*, ASTM International, West Conshohocken, PA.
- ASTM. (2006). "Standard practice for making and curing concrete test specimens in the laboratory." *Standard C192*, ASTM International, West Conshohocken, PA.
- ASTM. (2008). "Test method for resistance of concrete to rapid freezing and thawing." *Standard C666*, ASTM International, West Conshohocken, PA.
- Barde, V., Radlinska, A., Cohen, M., and Weiss, W. J. (2009). "Relating material properties to exposure conditions for predicting service life in concrete bridge decks in Indiana." *The Joint Transportation Research Program of the Indiana Department of Transportation*, Purdue Univ., West Lafayette, IN.
- Beaudoin, J. J., and Cameron, M. (1972). "Dimensional changes of hydrated Portland cement paste during slow cooling and warming." *Cement and Concrete Research*, 2(2), 225–240.
- Bentz, D. P., Ehlen, M. A., Ferraris, C. F., and Garboczi, E. J. (2001). "Sorptivity-based service life predictions for concrete pavements." *7th Int. Conf. on Concrete Pavements*, NIST, Orlando, FL, 181–193.
- Bentz, D. P., Sant, G., and Weiss, J. (2008). "Early-age properties of cement-based materials I: Influence of cement fineness." *J. Mater. Civ. Eng.*, 20(7), 502–508.
- Castro, J., Bentz, D., and Weiss, J. (2011). "Effect of sample conditioning on the water absorption of concrete." *Cement and Concrete Compos.*, 33(8), 805–813.
- Castro, J., Kompare, P., Poursaeed, P., Nantung, T., and Weiss, J. (2010). "Portland cement concrete pavement performance relative to permeability." *JTRP Rep. SPR-3093*, Indiana Department of Transportation, West Lafayette, IN.
- Fagerlund, G. (1972). "Critical degrees of saturation at freezing of porous and brittle materials." *Rep. 34*, Div. of Building Technology, Lund Institute of Technology, Lund, Sweden, 408.

- Fagerlund, G. (1973). "Determination of pore-size distribution from freezing-point depression." *Mater. Struct.*, 6(3), 215–225.
- Fagerlund, G. (1975). "The significance of critical degrees of saturation at freezing of porous and brittle materials." *Conf. on Durability of Concrete, ACI STP, Atlantic*, Vol. 47, New Jersey and Ottawa, Ontario, 13–65.
- Fagerlund, G. (1977). "The international cooperative test of the critical degree of saturation method of assessing the freeze/thaw resistance of concrete." *Mater. Struct.*, 10(4), 231–253.
- Fagerlund, G. (1979). "Prediction of the service life of concrete exposed to frost action, studies on concrete technology." *Studies on Concrete Technology*, Swedish Cement and Concrete Research Institute, Stockholm, 249–276.
- Fagerlund, G. (1981). "The principles of frost resistance of concrete." *Nordisk Betong*, (2), 5–13 (in Swedish).
- Fagerlund, G. (1993). "The long-time water absorption in the air-pore structure of concrete." *Rep. TVBM-3051*, Div. of Building Technology, Lund Institute of Technology, Lund, Sweden.
- Fagerlund, G. (1995). "The required air content of concrete." *Proc., Int. Workshop on Mass-Energy Transfer and Determination of Building Components*, BRI-Japan and CSTB-France, Paris, 591–609.
- Fagerlund, G. (2004). "A service life model for international frost damage in concrete." *Rep. TVBM-3119*, Div. of Building Technology, Lund Institute of Technology, Lund, Sweden.
- Feldman, R. F. (1987). "Diffusion measurements in cement paste by water replacement using propan-2-OL." *Cement and Concrete Research*, 17(4), 602–612.
- Hall, C., and Hoff, W. D. (2002). "Water in porous materials." *Water-Transport in Brick, Stone and Concrete*, Taylor & Francis, Abingdon, Oxon, 29–41.
- Hanžič, L., Kosec, L., and Anžel, I. (2010). "Capillary absorption in concrete and the Lucas–Washburn equation." *Cement and Concrete Compos.*, 32(1), 84–91.
- Helmuth, R. A. (1960). "Capillary size restrictions on ice formation in hardened Portland cement pastes." *Proc., 4th Int. Symp. on Chemistry of Cement*, Paper VI-S2, Portland Cement Association, Research and Development Laboratories, Skokie, IL, 855–869.
- Helmuth, R. A. (1961). "Dimensional changes of hardened Portland cement pastes caused by temperature changes." *Proc., Highway Research Board*, Vol. 40, Portland Cement Association, Research and Development Laboratories, Skokie, IL, 315–336.
- Hossain, A. B., Pease, B., and Weiss, J. (2003). "Quantifying early-age stress development and cracking in low water-to-cement concrete—restrained-ring test with acoustic emission." *Transportation Research Record*, 1834(1), 24–32.
- Kaiser, J. (1950). "A study of acoustic phenomena in tensile tests." Ph.D. dissertation, Technical University of Munich, Bayern, Germany.
- Kim, B., and Weiss, J. (2003). "Using acoustic emission to quantify damage in restrained fiber-reinforced cement mortars." *Cement and Concrete Compos.*, 33(2), 207–214.
- Kline, R. A., and Egle, D. M. (1987). "A brief note on the Kaiser and Felicity effects." *J. Acoustic Emission*, 6(3), 205–206.
- Krishnan, A. (2002). "Durability of concrete containing fly ash or slag exposed to low temperatures at early ages." M.S. thesis, Purdue Univ., West Lafayette, IN.
- Leech, C., Lockington, D., Hooton, R. D., Galloway, G., Cowin, G., and Dux, P. (2008). "Validation of Mualem's conductivity model and prediction of saturated permeability from sorptivity." *ACI Mater. J.*, 105(1), 44–51.
- Litvan, G. G. (1988). "The mechanism of frost action in concrete—theory and practical implications." *Proc. of Workshop on Low Temperature Effects on Concrete*, National Research Council of Canada, Montreal, Canada, 115–134.
- Litvan, G. G., and Sereda, P. J. (1980). "Freeze-thaw durability of porous building materials." *Durability of Building Materials and Components, ASTM STP 691*, P. J. Sereda and G. G. Litvan, eds., ASTM International, West Conshohocken, PA, 455–463.
- Martys, N. S., and Ferraris, C. E. (1997). "Capillary transport in mortars and concrete." *Cement and Concrete Research*, 27(5), 747–760.
- Moon, J. H., and Weiss, J. (2006). "Estimating residual stress in the restrained ring test under circumferential drying." *Cement and Concrete Compos.*, 28(5), 486–496.
- Ohtsu, M. (1999). "Estimation of crack and damage progression in concrete by quantitative acoustic emission analysis." *Mater. Evaluation*, 57(5), 521–525.
- Ohtsu, M., and Shigeishi, M. (1993). "Experimental crack identification of mixed mode by acoustic emission." *Int. Conf. on Fracture and Damage of Concrete and Rock (FDCR-2)*, H. P. Rossmannith, ed., E&FN Spon, London, 186–195.
- Ouyang, C., Landis, E., and Shah, S. P. (1991a). "Damage assessment in concrete using quantitative acoustic emission." *J. Eng. Mech.*, 117(11), 2681–2698.
- Ouyang, C., Landis, E., and Shah, S. P. (1991b). "Detection of microcracking in concrete by acoustic emission." *Experimental Techniques*, 15(3), 24–28.
- Pour-Ghaz, M., et al. (2010). "Using electrical, magnetic and acoustic sensors to detect damage in segmental concrete pipes subjected to permanent ground deformation." School of Civil Engineering, Purdue Univ., West Lafayette, IN.
- Pour-Ghaz, M., and Weiss, J. (2010). "Quantifying damage due to aggregate expansion in cement matrix." *Advances in the Material Science of Concrete, ACI SP-270-9*, 101–113.
- Puri, S., and Weiss, J. (2006). "Assessment of localized damage in concrete under compression using acoustic emission." *ASCE J. Mater. Civ. Eng.*, 18(3), 325–333.
- Rangaraju, P. R., Sompura, K. R., and Olek, J. (2006). "Investigation into potential of alkali-acetate-based deicers to cause alkali-silica reaction in concrete." *Transportation Research Record*, 1979, 69–78.
- Scherer, G. W. (1993). "Freezing gels." *J. Non-Crystalline Solids*, 155(1), 1–25.
- Scherer, G. W., and Valenza, J. J. (2005). "Mechanisms of frost damage." *Mater. Science of Concrete*, 7, 209–246.
- Shah, H. R., and Weiss, J. (2006). "Quantifying shrinkage cracking in fiber reinforced concrete using the ring test." *Mater. Struct.*, 39(9), 887–899.
- Shimada, H., Sakai, K., and Litvan, G. G. (1991). "Acoustic emissions of mortar subjected to freezing and thawing." *Durability of Concrete: Second Int. Conf.*, V. M. Malhotra, ed., American Concrete Institute, Detroit, 263–278.
- Spragg, R., Castro, J., Li, W., Pour-Ghaz, M., Huang, P., and Weiss, J. (2011). "Wetting and drying of concrete in the presence of deicing salt solutions." *Cement and Concrete Compos.*, 33(5), 535–542.
- Suaris, W., and Van Mier, J. G. M. (1993). "Acoustic emission and source location in concrete subjected to mixed mode loading." *Int. Conf. on Fracture and Damage of Concrete and Rock (FDCR-2)*, H. P. Rossmannith, ed., E&FN Spon, London, 157–165.
- Suaris, W., and Van Mier, J. G. M. (1995). "Acoustic emission source characterization in concrete under biaxial loading." *Mater. Struct.*, 28(8), 444–449.
- Sun, Z., Kumpf, D., and Scherer, G. W. (2007). "Kinetics of ice growth in concrete." *Proc., 12th Int. Congress Cement Chemistry*, J. J. Beaudoin, J. M. Makar, and L. Raki, eds., National Research Council of Canada, Montreal, W4–07.1.
- Sutter, L., Van Dam, T., Peterson, K. R., and Johnston, D. P. (2006). "Long-term effects of magnesium chloride and other concentrated salt solutions on pavement and structural Portland cement concrete phase I results." *Transp. Res. Rec.*, 1979, 60–68.
- Warris, B. (1964). "The influence of air-entrainment on the frost-resistance of concrete, part B, hypothesis and freezing experiments." *Proc., No. 36 Swedish Cement and Concrete Research Institute, Svenska Forskningsinstitutet för Cement och Betong*, Stockholm, 130.
- Weiss, W. J., Abraham, D., and Nantung, T. (2007). "SPR3200—A proposal for a research study on saw-cutting and curing of concrete pavements." *The Joint Transportation Research Program of the Indiana Department of Transportation*, Purdue Univ., West Lafayette, IN.
- Yang, Z. F., Weiss, W. J., and Olek, J. (2006). "Water transport in concrete damaged by tensile loading and freeze-thaw cycling." *J. Mater. Civ. Eng.*, 18(3), 424–434.
- Yoon, D. J., Weiss, W. J., Prine, D. W., and Shah, S. P. (1999). "Assessing corrosion damage in reinforced concrete beams using acoustic emission." *Non-Destr. Eval. Bridg. Highw.*, 3587, 254–263.

MOISTURE PROFILES AND DIFFUSION COEFFICIENTS IN MORTARS CONTAINING SHRINKAGE REDUCING ADMIXTURES

Mohammad Pour-Ghaz⁽¹⁾, Robert Spragg⁽¹⁾ and Jason Weiss⁽¹⁾

(1) Purdue University, School of Civil Engineering, West Lafayette, Indiana, USA

Abstract

Shrinkage reducing admixtures (SRAs) have been used over the last three decades to reduce the volume change (i.e., shrinkage) that occurs in cement paste, mortar, and concrete during drying. The goal of reducing shrinkage is to reduce the risk of shrinkage cracking in concrete elements. SRAs alter the properties of the pore solution, such as surface tension and viscosity, which result in a reduction in the magnitude of drying shrinkage, especially at humidities below 80-85%. In addition to altering the magnitude of shrinkage, SRAs appear to alter the rate of drying and diffusivity coefficient. This paper examines the role of SRAs in two ways. First, desorption spectra are measured to obtain the moisture diffusivity of plain mortar and mortar containing SRA. Second, the paper measures relative humidity in slabs to obtain moisture profiles. The relative humidity profile predicted from the non-linear diffusion coefficient is compared with the measured humidity profile.

1. Background

Shrinkage Reducing Admixtures (SRAs) were introduced to the concrete industry in the 1980's [1, 2]. Recent reviews have summarized three decades of research on SRA on concrete properties [3-6]. SRA's are generally observed to reduce shrinkage which can substantially reduce the propensity for restrained shrinkage cracking.

The majority of shrinkage measurements on concrete containing SRA are performed on concrete samples with a relatively large cross section, like those that one may use in standard shrinkage tests like ASTM C-157 [7]. While this type of test can provide information on the benefits of SRA, it has two primary limitations. First, it generally only describes the shrinkage of the concrete at one relative humidity (50% for example for ASTM C-157 [7]). Second, it measures the average length change of the prism and does not explicitly account for moisture gradients.

To overcome the limitation of measuring shrinkage at one relative humidity, a series of tests were performed measuring small paste and mortar samples with and without SRA at different relative humidities [8]. This response can be used to describe the shrinkage that may be expected over a wide range of relative humidities [9-11]. This does however indicate, not surprisingly, that shrinkage is not linearly related to relative humidity [8]. The shrinkage of the paste can be extended to mortar or concrete using the Pickett [12] or Hobbs [13] approaches.

Previous work has been performed to measure relative humidity profiles in concrete. This includes the work of Monfore [14] and Grasley et al. [15] who used resistance based gages to measure humidity in vapor filled cavities in concrete, the work of Molina [16] who measured relative humidity using chilled mirror technology, and work of Schießl et al. [17] using electrical resistance measurements of concrete to assess the moisture distribution.

Relative humidity measurements in slabs can be complicated by the size of the probe that is used to measure the humidity. Measurements in small cavities with limited vapor volume can make it difficult to use techniques that require a substantial air flow rate like chilled mirrors. Previous measures of electrical resistance of concrete require two assumptions. First, that there are no hysteretic effects [18, 19] and second, that the resistance is measured at the depth of the electrodes. It can be noted that the first assumption is required since electrical measurements measure water content and not relative humidity directly and hysteretic effects due to drying and wetting can complicate the interpretation [19]. The second assumption is more nebulous as the shape of the electrical field that develops between the two electrodes is not symmetric at the plane of the electrodes since more charge will pass through the side containing more liquid [19]. As such it may be beneficial to measure the moisture diffusion coefficient directly rather than measuring relative humidity profiles and back calculating the diffusion coefficient.

One advantage of using desorption measurements to obtain a non-linear diffusion coefficient is the fact that the testing can be performed over a much shorter duration than drying of thick concrete slabs. For example, the non-linear diffusion coefficient measured in this paper took approximately 5 days to measure after casting and curing which is substantially shorter than allowing a concrete slab to dry and back-fitting the diffusion coefficient (which can take many many months). Second, this approach is not subjected so some of the issues that arise in attempting to ascertain the correct depth of the relative humidity measurement or the influence of a relatively large size cavity on the measured value.

2. Research Objective

This paper describes research that is attempting to measure a non-linear moisture diffusion coefficient in a mortar. Mortar was preferred to cement paste to minimize the potential impact of different pore size distributions that may occur between pastes and mortars. In addition the mortar was preferred to minimize potential issues that may occur with inconsistent mixing action that can be encountered in paste samples. This paper has three main objectives:

- First, the paper describes tests on mortar that is dried in a controlled fashion to evaluate the non-linear diffusion coefficient following the approach used by Anderberg and Wadso [20] and Garbalinska [21],
- Second, the paper provides data that illustrates the influence of shrinkage reducing admixture on the non-linear diffusion coefficient, and
- Third, the paper will provide a comparison of the relative humidity profile predicted using the non-linear diffusion coefficient with a measured relative humidity profile in a slab.

3. Relative Humidity Gradient and Cracking Potential

Previous work [9, 10, 22-24] has suggested that the humidity gradient in a slab can be used to predict the free shrinkage, stress development, slab cracking, and curling in a thick concrete element. The background for this type of approach can be found in [10, 25]. Figure 1 schematically illustrates the approach can be taken to utilize the relative humidity profile to compute the stress distribution and gradient. Strong dependence of diffusion coefficient on the shape and magnitude of the relative humidity profile can result in higher stress gradient and increase in cracking potential.

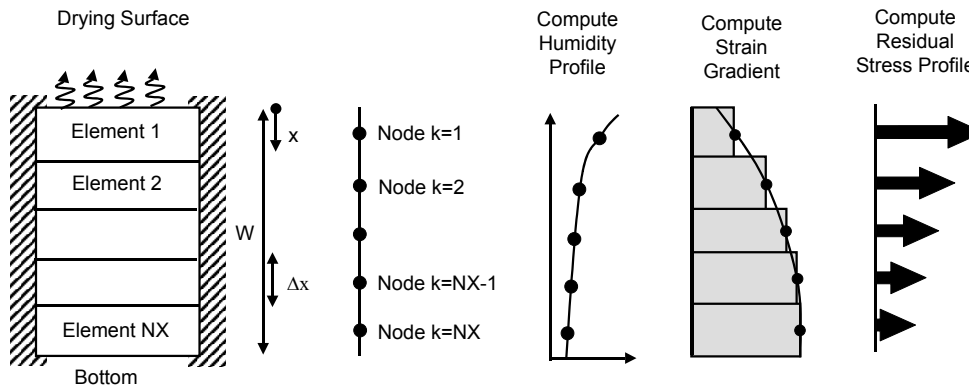


Figure 1: Schematically illustrates the approach can be taken to utilize the relative humidity and moisture content (W) profile to compute the stress distribution [10].

4. Materials and Methods

Three mortar mixtures were prepared for this study. The plain mortar had a water to cement ratio (w/c) of 0.50 and consisted of 55% aggregate by volume. The mortars containing shrinkage reducing admixture (SRA) had 1% and 5% of the mix water replaced with a SRA (denoted as 1% SRA and 5% SRA respectively). ASTM C150 [7] Type I ordinary portland cement (OPC) was used with a Blaine fineness of 370 m^2/kg and an estimated Bogue phase composition of 56 % C_3S , 16 % C_2S , 12 % C_3A , 7 % C_4AF and a Na_2O equivalent of 0.68 % by mass. The normal weight aggregate (NWA) was natural river sand with a fineness modulus of 2.71, an apparent specific gravity of 2.58, and an absorption of 1.8 % by mass.

The SRA was commercially available Tetragaurd AS20. All of the NWA was oven-dried and air-cooled for 24 hr before mixing. The mixing procedure used for the mortar was in accordance with ASTM C192-06 [7]. The samples were all tested in a sealed condition unless otherwise noted.

The experiments that were performed consist primarily of two specimen geometries. The first sample geometry was used for the diffusivity tests. This sample consisted of a 0.8 mm thick by 6 mm diameter mortar disk that was taken from a larger cylinder that was sealed from the time of casting before being exposed to progressive drying at an age of 7 days for determination of the moisture diffusivity. The second sample geometry consisted of slab specimens (177.8 mm x 254.0 mm x 508.0 mm) with relative humidity sensors embedded at four depths (12.7, 25.4, 38.1 and 92 mm) measured from the drying surface. The slabs were exposed to drying at $50 \pm 1\%$ at an age of 7 days. The slab geometry is shown in Figure 2.



Figure 2: Slab geometry with one-sided drying

5. Measurements of a Non-Linear Diffusion Coefficient

The samples used for determining the diffusion coefficient were cut from a small cylinder of mortar using a high precision wet saw. The test started approximately 5 minutes after cutting the sample. The samples were kept in water. At the start of the test the sample was removed from the water and was placed in a clean towel for a few seconds to remove the surface water. The sample was then placed in the desorption analyzer. The diffusivity test was performed in an automated absorption/desorption analyzer [26, 27] at 23°C in which samples were subjected to isothermal desorption at different relative humidities. The first step in the isothermal desorption was isothermal conditioning at 97.5 % relative humidity. The samples were allowed to equilibrate to 97.5%. After isothermal conditioning at 97.5% the relative humidity was decreased in 5% relative humidity increments. Samples at each step of the desorption were considered to be at equilibrium when the mass change was smaller than 0.001 mg for 15 minutes [26].

For a slab geometry with double-sided drying (where the contribution of mass transfer from the edges of the sample is negligible compared to mass transfer from the surface of the slab [20, 21, 28]) the mass change due to drying (M_t), at any time (t), can be related to the moisture diffusivity, (D), using Equation 1 [20, 21, 28]

$$\frac{M_t}{M_\infty} = \frac{4}{\pi} \left(\frac{Dt}{L^2} \right)^{1/2} \quad (1)$$

where M_∞ is the mass change at equilibrium and L is the thickness of the sample.

The diffusivity over each relative humidity step can be obtained from the linear portion of a plot of $(M_t/M_\infty)^2$ against $(16t/\pi^2L^2)$. Generally the mortar samples tested exhibited the linear portion of their curve between 20 and 80% of the equilibrium mass. For materials for which the diffusivity is a function of relative humidity, Equation 1 can be used provided that the diffusivity can be assumed constant during each isothermal desorption step. In the present work since the samples were subjected to 5% change of relative humidity, the diffusivity can be assumed constant during each step of desorption. Better results can be obtained by decreasing the size of the steps, however the duration of the testing would increase but a sensitivity analysis would need to be determined.

Figure 3 illustrates the calculated diffusivity of the 0.8 mm thick specimens (exposed to 2 sided drying) of plain mortar, and mortar samples with 1 and 5% SRA. Note that the diffusivity at each step is expressed as diffusivity at average relative humidity of that step (e.g., the diffusivity of the samples that is equilibrated at 97.5% relative humidity and exposed to 92.5% relative humidity is reported as diffusivity at 95%). The samples with SRA demonstrate a lower diffusivity than the plain system at higher relative humidity. This lower relative humidity in the SRA system corresponds with a reduced rate of drying (at high relative humidity). This would suggest that plain mortar has a more non-linear moisture diffusivity while samples with SRA are more linear with respect to the diffusivity over a large range of moisture contents. This can have substantial implications on the moisture profile, shrinkage profile, reduction in curling, drying rate, and microcracking at the surface of the slab [29].

6. Relative Humidity Measurements in Slabs

The internal relative humidity and temperature of the slab was measured at four depths (12.7, 25.4, 38.1 and 92 mm) in a series of 250 mm hollow shafts (parallel to the surface) that contain I-button sensors [30] that measure temperature and relative humidity. The depth of the hollow shaft reported is measured from the exposed surface of the slab to the center of the shaft. Slabs were exposed to drying from the top surface.

The I-button data loggers measure the relative humidity with $\pm 1.0\%$ and temperature $\pm 0.1^\circ\text{C}$ accuracy respectively. The advantage of this type of relative humidity sensor is the fact that it measures the relative humidity of the air inside the hollow shaft directly which is in equilibrium with surrounding materials. To ensure accuracy of the measurements all the sensors were compared to two salt solutions with 87 and 78% relative humidities. The sensors were within $\pm 1.0\%$ of the expected relative humidity. In addition to calibration, data were corrected for saturation drift [30].

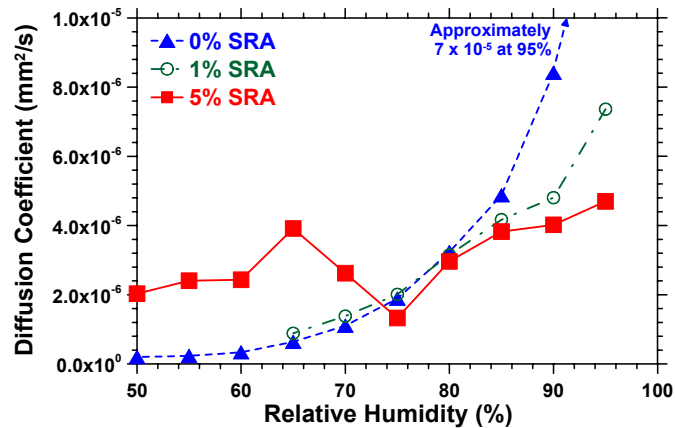


Figure 3: Moisture diffusivity of mortar samples with different loadings of shrinkage reducing admixture (SRA)

At the time of casting the slabs, cylindrical samples (with 2.54 cm diameter and 5.1 cm height) were cast from the same materials used to make the slabs and was kept sealed. These samples were used to measure the internal relative humidity at 7, 28 and 63 days (two samples at each age). The measurements were performed by crushing the samples and placing them in an air-tight container against a temperature and relative humidity sensor [26]. These measurements were performed to account for the self-desiccation effect which is needed in Equation 2.

Figure 4 illustrates the relative humidity of the slabs that have been exposed to drying at an age of 7 days (results are based on the average independent measurement in two slabs). It can be noticed that the relative humidity appears to remain higher in the samples containing SRA. The depth of the sensors is the distance to the center of the hollow shaft (in which sensor is placed in) from the surface of the slab. It is expected that the measured relative humidity with sensor may be more representative of the top of the hollow shaft.

7. Comparing Slab Measurements with Predictions Using the Diffusion Coefficient

Equation 2 describes the relative humidity as a function of time and position [31-35]

$$\frac{\partial H}{\partial t} = \text{div}(D_H \text{grad } H) - \frac{\partial H_s}{\partial t} \quad (2)$$

where H is the relative humidity, D_H is the moisture diffusivity as a function of relative humidity and H_s is the variation of relative humidity due to self-desiccation.

Equation 2 assumes that the contribution of thermal gradients and aging are negligible [33]. The second term on the right-hand-side of Equation 2 is the contribution of self-desiccation [33]. The self-desiccation term in the present work is measured independently from crushed samples as described above. The boundary conditions at the sealed (bottom) surface of the

slab and top (exposed to drying) surface of the slab can be expressed by $\partial H / \partial x = 0$ and $H = 0.50$ respectively. The initial condition of the slab at drying (i.e., humidity at 7 days) is obtained by measuring the internal relative humidity of the crushed samples.

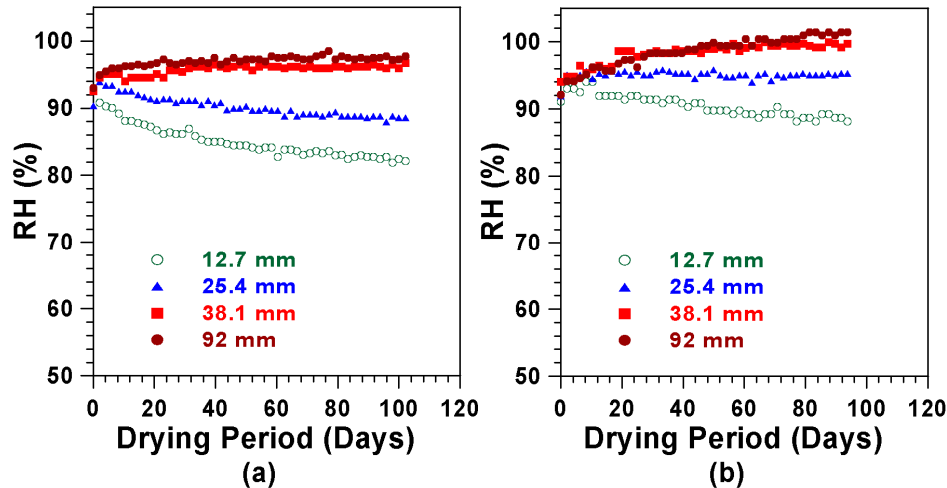


Figure 4: Change of internal relative humidity of slabs at different depth measured from exposed surface of the slab, (a) plain mortar, (b) mortar containing 5% shrinkage reducing admixture (SRA)

A non-linear finite difference scheme [33, 36, 37] was used. To effectively capture the non-linearity caused by the diffusivity, Crank-Nicolson (central difference) scheme was used. Crank-Nicolson scheme is stable [33, 36, 37] and effective in capturing non-linearities caused by strong dependence of diffusivity on relative humidity. In using this scheme any oscillations around the exact solution can be avoided by decreasing the time increments. In each time step the first solution was obtained by time lagging the diffusivity one time step and then improving the solution by subsequent iterations. In subsequent iterations, a weighted average diffusivity of the last two iterations was used. This method of averaging is known as modified Picard iterations [38] and requires less number of iterations in each time step.

Figure 5 illustrates the comparison of the experimentally obtained relative humidity at different locations and the numerically obtained profiles using the non-linear diffusivity coefficients.

8. Implications of Differences in Relative Humidity Profiles

Results of the non-linear diffusion coefficient can be used to describe moisture distribution at early ages and its potential impact on microcracking, curling and through cracking. The SRA's, especially at 5% show a reduced rate of drying. This is confirmed with less mass loss. This work may also provide insight on microcracking and damage localization that ultimately leads to through cracking in restrained elements. Acoustic emission has shown that the inclusion of SRA substantially reduces the acoustic activity due to microcracking in the specimens that contain 5% SRA as compared with the plain mixture.

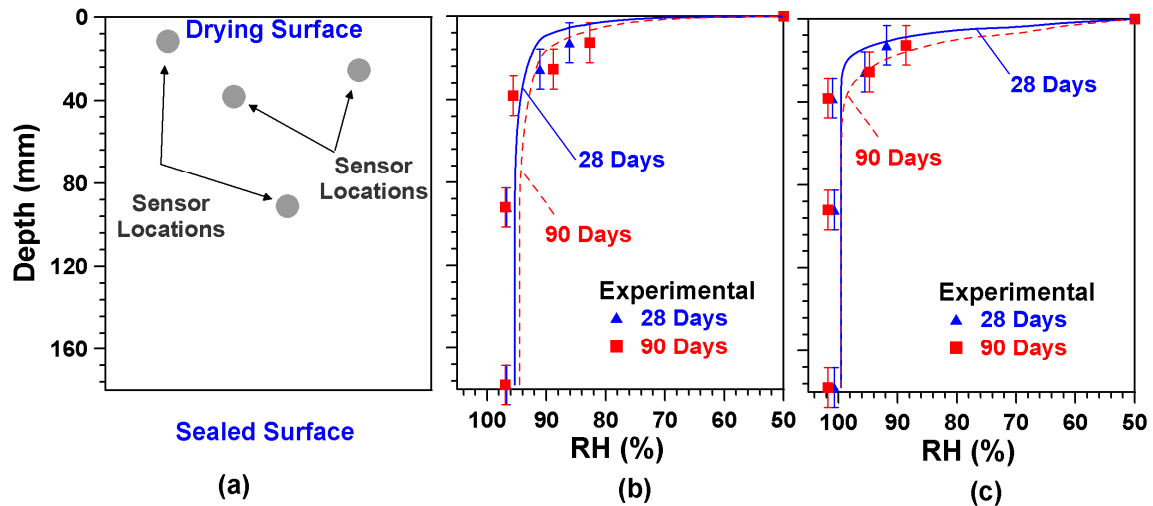


Figure 5: Comparison of the experimentally measured relative humidity and numerically obtained relative humidity profile, (a) illustration of location of the sensors and boundary conditions of the slab, (b) plain mortar, (c) mortar with 5% shrinkage reducing admixture (SRA)

9. Conclusions

This paper examined the role of SRAs on the relative humidity profile that develops in a drying mortar. The paper begins by describing the measurement of desorption spectra to obtain the moisture diffusivity of plain mortar and mortar containing SRA. The paper uses these non-linear diffusion coefficients to predict the moisture profiles that would be expected to occur in drying slabs. The results indicate that SRA dries more slowly at high relative humidities (liquid diffusion) however this trend may be reduced for lower relative humidities when the vapor diffusion prevails. The relative humidity profiles computed using the non-linear diffusion coefficient were directly compared with independently measured relative humidity in slabs. A reasonable comparison was observed given the issues associated with errors in relative humidity depth location and the shortcomings of using a non-aging coefficient. The implications of this approach could be more rapid indications of relative humidity profiles in concrete as well as explanations of shrinkage, stress and cracking distributions throughout the sample cross section.

10. Acknowledgements

The authors gratefully acknowledge the support of BASF, the Construction Chemical Company. This work was conducted in the Charles Pankow Concrete Materials Laboratory at Purdue University. As such, the authors gratefully acknowledge the support which has made this laboratory and its operation possible.

8. References

- [1] Sato, T., Goto, T., and Sakai, K., 'Mechanism for Reducing Drying Shrinkage of Hardened Cement by Organic Additives,' *CAJ Review*, (1983) 52-54.
- [2] Tomita, R., Simoyama, Y., and Inoue, K., 'Properties of hardened concrete impregnated with cement shrinkage reducing agent,' *CAJ Review*, (1986) 314-317.
- [3] ACI.Committee.231, 'Report on Early-Age Cracking: Causes, Measurement, and Mitigation,' American Concrete Institute ACI 231R-10, 2010.
- [4] Nmai, C., Tomita, R., Hondo, F., and Buffenbarger, J., 'Shrinkage reducing admixtures,' *Concr. Int.*, **20** (4)(1998) 31-37.
- [5] Shah, S.P., Weiss, W.J., and Yang, W., 'Shrinkage cracking – can it be prevented?,' *Concr. Int.*, **20** (4)(1998) 51-55.
- [6] Weiss, J. and Berke, N.S., 'Shrinkage reducing admixtures,' in *Early age cracking in cementitious systems, RILEM state-of-the-art report—Report 25*, A. Bentur, Ed., ed Bagnaux, France: RILEM, 2002.
- [7] *Annual Book of ASTM Standards*. West Conshohocken, PA: American Society for Testing and Materials, ASTM International, 2009.
- [8] Weiss, J., Lura, P., Rajabipour, F., and Sant, G., 'Performance of shrinkage-reducing admixtures at different humidities and at early ages,' *ACI Mater. J.*, **105** (5) Sep-Oct (2008) 478-486.
- [9] Bazant, Z.P., Ed., *Fourth RILEM International symposium on Creep and Shrinkage of Concrete: Mathematical Modeling* Northwestern University, 1986.
- [10] Weiss, W.J., 'Prediction of early-age shrinkage cracking in concrete,' Ph.D., Civil Engineering, Northwestern University, Evanston, IL, 1999.
- [11] Moon, J.H., 'Shrinkage, Residual Stress, and Cracking in Heterogeneous Materials,' Ph.D., Civil Engineering, Purdue University, West Lafayette, IN, 2006.
- [12] Pickett, G., 'Shrinkage stresses in concrete,' *Mater. Struct.*, **42** (8)(1946) 165-204.
- [13] Hobbs, D.W., 'Influence of aggregate restraint on the shrinkage of concrete,' *ACI Journal*, **71-30** (1974) 445-450.
- [14] Monfore, G.E., 'A small probe-type gauge for measuring relative humidity,' *Journal of the PCA Research and Development Laboratories*, **5** (2)(1962).
- [15] Grasley, Z.C., Lange, D.A., and D'Ambrosia, M.D., 'Internal relative humidity and drying stress gradients in concrete,' *Mater. Struct.*, **39** (9) Nov (2006) 901-909.
- [16] Molina, L., 'Measurement of high humidity in cementitious material at an early age,' Swedish Cement and Concrete Research Institute, Stockholm, Sweden 1990.
- [17] Schielßl, A., Weiss, W.J., Shane, J.D., Berke, N.S., Mason, T.O., and Shah, S.P., 'Assessing the moisture profile of drying concrete using impedance spectroscopy,' *Concr. Sci. Eng.*, **2** (2000) 106-116.
- [18] Elkey, W. and Sellevold, E.J., 'Electrical resistivity of concrete,' Norwegian Road Research Laboratory 1995.
- [19] Rajabipour, F., 'Insitu electrical sensing and materials health monitoring in concrete structures,' Ph.D., Civil Engineering, Purdue University, West Lafayette, IN, 2006.
- [20] Anderberg, A. and Wadso, L., 'Method for simultaneous determination of sorption isotherms and diffusivity of cement-based materials,' *Cem. Concr. Res.*, **38** (1) Jan (2008) 89-94.

- [21] Garbalinska, H., 'Application of root t-type, logarithmic and half-time methods in desorptive measurements of diffusivity in narrow humidity ranges,' *Cem. Concr. Res.*, **36** (7) Jul (2006) 1294-1303.
- [22] Moon, J.H. and Weiss, J., 'Estimating residual stress in the restrained ring test under circumferential drying,' *Cem. Concr. Compos.*, **28** (5) May (2006) 486-496.
- [23] Weiss, W.J., Yang, W., and Shah, S.P., 'Shrinkage cracking of restrained concrete slabs,' *J. Eng. Mech.*, **124** (7) Jul (1998) 765-774.
- [24] Weiss, W.J., Yang, W., and Shah, S.P., 'Influence of specimen size/geometry on shrinkage cracking of rings,' *J. Eng. Mech.*, **126** (1) Jan (2000) 93-101.
- [25] Bazant, Z.P., 'Material Models for Structural Creep Analysis,' in *Mathematical Modeling of Creep and Shrinkage of Concrete*, Z. P. Bazant, Ed., ed New York: John Wiley and Son Ltd, 1988.
- [26] Castro, J., Lura, P., Rajabipour, F., and Weiss, J., 'Internal curing: discussion on the role of pore solution on relative humidity measurements and desorption of lightweight aggregate (LWA)' in *Advances in the Material Science of Concrete*. vol. SP-270, J. H. Ideker and A. Radlinska, Eds., ed Chicago, IL: American Concrete Institute, 2010.
- [27] Instruments, T., 'Dynamic Vapor Sorption Analysis: Q5000 SA,' <http://www.tainstruments.com2010>.
- [28] Crank, J., *The Mathematics of Diffusion*, 2nd ed. New York: Oxford University Press, 1980.
- [29] Neithalath, N., Pease, B.J., Moon, J.H., Rajabipour, F., Weiss, J., and Attiogbe, E., 'Considering moisture gradients and time-dependent crack growth in restrained concrete elements subjected to drying,' in *High Performance Cement Based Concrete Composites*, J. J. Bernacki, et al., Eds., ed Chennai, India: American Ceramics Society, 2005, pp. 279-290.
- [30] Maxim, 'Data Logger, Temperature/Humidity Loggers, and Sensors,' Sunnyvale, CA, 2010.
- [31] Bazant, Z.P. and Kim, J.K., 'Consequences of Diffusion-Theory for Shrinkage of Concrete,' *Mater. Struct.*, **24** (143) Sep (1991) 323-326.
- [32] Bazant, Z.P., Kim, J.K., and Panula, L., 'Improved Prediction Model for Time-Dependent Deformations of Concrete .1. Shrinkage,' *Mater. Struct.*, **24** (143) Sep (1991) 327-345.
- [33] Bazant, Z.P. and Najjar, L.J., 'Nonlinear water diffusion in nonsaturated concrete,' *Mater. Struct.*, **5** (25)(1972) 3-20.
- [34] Xi, Y.P., Bazant, Z.P., and Jennings, H.M., 'Moisture Diffusion in Cementitious Materials - Adsorption-Isotherms,' *Adv. Cem. Based Mater*, **1** (6) Nov (1994) 248-257.
- [35] Xi, Y.P., Bazant, Z.P., Molina, L., and Jennings, H.M., 'Moisture Diffusion in Cementitious Materials - Moisture Capacity and Diffusivity,' *Adv. Cem. Based Mater*, **1** (6) Nov (1994) 258-266.
- [36] Crank, J. and Nicolson, P., 'A Practical Method for Numerical Evaluation of Solutions of Partial Differential Equations of the Heat-Conduction Type,' *Proceedings of the Cambridge Philosophical Society*, **43** (1)(1947) 50-67.
- [37] Ozisik, M.N., *Finite Difference in Heat Transfer*. London: CRC Press, 1994.
- [38] Pour-Ghaz, M., 'A novel approach for practical modelling of steel corrosion in concrete,' M.A.Sc, Civil Engineering, Carleton University, Ottawa, Canada, 2007.



An automated electrical monitoring system (AEMS) to assess property development in concrete

A. Poursaei*, W.J. Weiss

School of Civil Engineering, Purdue University, West Lafayette, IN, 47907, United States

ARTICLE INFO

Article history:

Accepted 29 December 2009

Keywords:

Electrical impedance
Automation
Concrete
Electrical properties
Imaging
LabVIEW

ABSTRACT

Electrical impedance measurement techniques are being increasingly used to measure material property development and permeability of concrete and other cement based materials. This paper describes the development of an automated electrical measurement system (AEMS) for measuring the properties of cementitious materials. The components of this system are an electrical impedance spectrometer, a digital multi-meter, a switching unit, and a customized software (AEMS) which communicates between different components of the system to control the testing and to collect data. This system enables electrical properties of multiple specimens to be measured in an automated fashion thereby making this approach very amenable for use in quality control applications. Further, an extension of this system is proposed which would enable its use to detect flaws in concrete using electrical imaging.

© 2010 Elsevier B.V. All rights reserved.

1. Introduction

Electrical impedance measurement techniques have been shown to provide useful information that can be used to characterize cementitious systems [1–3]. This technique studies the system response to the application of a small amplitude alternating potential signal at different frequencies. AC electrical impedance measurements have the advantages of being non-invasive and non-destructive, require little in term of preparation of the sample, and offer the possibility of continual measurements to describe the effect of hydration [4,5] drying [6], or permeability [7].

Electrical impedance techniques have been used in different research projects in concrete to study a wide range of concrete properties specifically this included studies on the microstructural development of cementitious materials [8,9], precipitation of calcium hydroxide on the surface of steel after the setting of the mortar [10], long-term effectiveness of concrete inhibitors for steel in concrete [11–15], the chloride diffusivity in concrete [16], chloride permeability of high performance concrete [17], detection of damage during tensile loading of cement composites [18], freezing of water in Portland cement paste [19], water penetration in concrete [20–22], setting time of concrete [23,24], measuring the concrete internal moisture content [25], and assessing the change in microstructure due to rapid chloride permeability test [26,27].

While numerous applications exist, they are frequently limited to the measurement of one sample at a time. It is regularly necessary to

conduct experimental measurements at multiple locations in a sample or on multiple specimens. For example, Schmit [28] described the use of multiple sensors and quantified the influence of sensor position and number in uncertainty of the results. The ability to perform multiple measurements is very valuable for monitoring the hydration process, monitoring multiple specimens, or imaging the crack by electrical impedance measurements [29]. In addition, a single measurement cannot properly represent the behavior of a material. To improve measurements accuracy multiple measurements are needed. This paper describes the development of a user friendly Automatic Electrical Monitoring System (AEMS). By using this system, multiple electrical measurements can be performed on specimens and different properties of concrete materials can be monitored. The developed system is discussed and some applications of the AEMS were shown in this paper.

2. Objective

This paper describes the development of an Automated Electrical Monitoring System (AEMS). The data acquisition system consists of a computer, a Keithley digital multi-meter and switching unit [30], and Solartron 1260 impedance spectrometer¹ [31]. The role of the software is to communicate between all components of the system and to control data collection. This paper shows that the system is reliable for both short and long-term monitoring. Further, this paper points out that while in the past the use of electrical impedance

¹ Certain commercial products are identified in this paper to specify the materials used and procedures employed. In no case does such identification imply endorsement by the authors, nor does it indicate that the products are necessarily the best available for the purpose.

* Corresponding author.

E-mail address: poursaei@purdue.edu (A. Poursaei).

measurement techniques has been time consuming, automation enables these measurements to be performed efficiently. This enables new applications, like electrical imaging, to be performed effectively and enables EIS to be extended for use in daily quality control processes such as permeability measurements. Since electrical impedance requires less preparation and time, it can be a good replacement for the tests like rapid chloride permeability which is time consuming and can alter the microstructure of the concrete.

3. Component of the measurement system

The system developed for this investigation can be used to measure the AC electrical impedance response of the material. The components in the system consist of an impedance spectrometer, digital multi-meter, and a switching unit.

The electrical impedance spectrometer used in this study is capable of performing only one measurement at a time. There are multi-channel spectrometer units on the commercial market. However, in addition to their high cost most of the units are limited to only a few measurements (up to 16) at a time which also may be a limiting factor.

The digital multi-meter and switching unit chosen for this project included a Keithley model 2750 mainframe which has five slots and a model 2700 which has two slots for inserting the plug-in switch/control modules. Each slot can support a series of multiplexer, matrix, or control modules. For example the Module 7708 which was used in this project has 40 channels. The general features of this module are described in [32]. The role of the mainframe is to communicate between channels. Temperature can also be measured using this system as this is needed for temperature corrections [33].

For each impedance measurement (each sample), 2 channels are required, (i.e., the Keithley model 2750 mainframe with five 7708 modules can be used for 100 impedance measurements). If more than 100 measurements are necessary, several mainframes can be joined together to provide the appropriate number of channels.

To combine the mentioned components, the software (named AEMS) was developed, using LabVIEW. This software selects the sample that will be tested and then runs the impedance spectrometer on that sample. After the measurements are completed, the AEMS, stops the spectrometer, switches the sample and runs the test again. The measurements are performed one by one not simultaneously. In all the graphs shown in the paper, this time is considered. This time for AC measurements is a function of selected frequency and in all examples in this paper it was about 40 s. However, when the concrete is hardened, this time difference is not considerable. If some interval time is necessary between measurements, the AEMS can be programmed to place the necessary time interval between measurements. In addition, the AEMS can communicate with the mainframe to

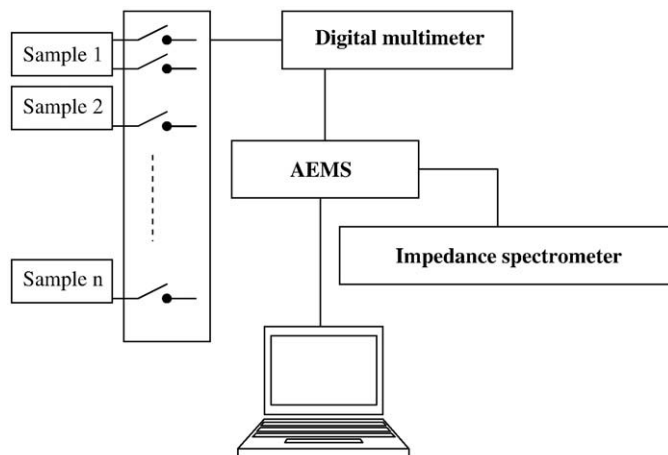


Fig. 1. Schematic relationship between the components of the system.



Fig. 2. Components of the system.

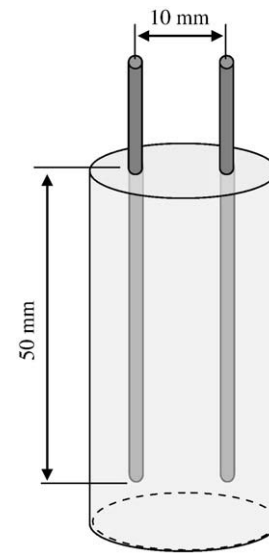


Fig. 3. Schematic view of the cylindrical paste specimens, used to measure variability in cement paste.

measure voltage, DC resistance and temperature independent from the spectrometer. Fig. 1 schematically shows the component of the system and the actual parts are shown in Fig. 2.

While an RS-232 serial port was used to control the multi-meter and switching system in this study, faster data transfer can be performed using a GPIB² [34] card. The role of the AEMS software is to control and switch the channels for each measurement, to control and run the spectrometer and save data to the computer for later analysis.

² The General Purpose Interface Bus (GPIB) is an industry standard published by the Institute of Electrical and Electronic Engineers (IEEE) as ANSI/IEEE Standard 488. GPIB defines the electrical, mechanical, functional, and software specifications of an interfacing system to connect PCs to programmable instrument.

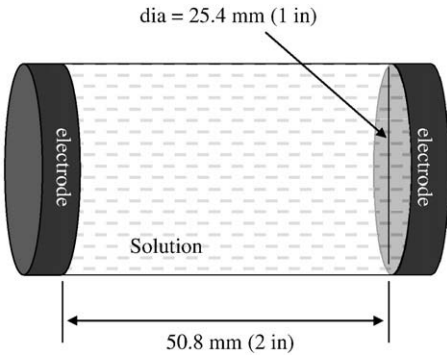


Fig. 4. Schematic view of the container with known geometry, to measure the conductivity of the solutions.

The software contains options which enable the user to set the number of samples, measurement frequency, and the time between each set of measurements. The saved data can be opened and analyzed in Excel[®]. Based on the number of measurements, one may end up with thousands of data files. Therefore, a macro was developed to automatically analyze individual data and place the summarized results in a worksheet.

4. Experimental results

To verify the performance of the switching units, two simple experiments were conducted. In the first test, a known resistor (10 Ω) was connected to all available channels and the resistance was measured. In the second test, a known potential was measured, using

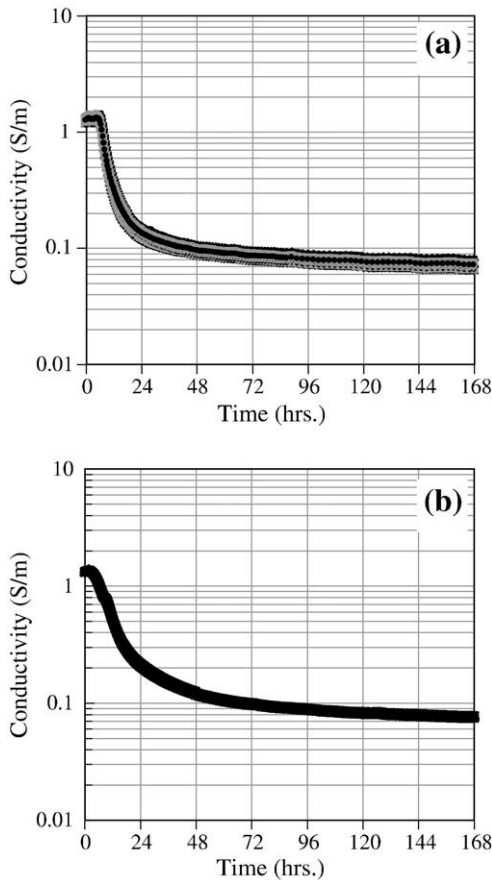


Fig. 5. Development of the conductivity of (a) 15 cement paste samples with w/c = 0.45 and, (b) 5 cement paste samples with w/c = 0.50.

all channels. Results show that there is no significant difference between measured values with each channels and the relative standard deviation was less than 0.005%.

4.1. Electrical conductivity of cement paste sample during hydration

Electrical measurements can provide information about the change in pore structure due to hydration process [23,35]. It is important to use multiple specimens for these measurements due to the inhomogeneity and corresponding variability of cementitious materials. To determine the variation between different samples the electrical conductivity of cement paste samples was measured using cylindrical paste specimens as described in Fig. 3. Type I ordinary Portland cement was used with a Blaine fineness of 360 m²/kg and a Bogue phase composition of 60% C₃S, 12% C₂S, 12% C₃A, 7% C₄AF and Na₂O equivalent of 0.72%. Fifteen samples were prepared with a w/c of 0.45 and 5 samples were prepared with a w/c of 0.50. The measurement frequency range that was used for the tests ranged from 1 MHz to 10 Hz with ten measurements per decade using the 500 mV AC stimulus. To determine the conductivity of the material, the bulk resistance (R_b) obtained from the impedance response normalized for the effects of specimen and electrode geometries, using the following equation:

$$\sigma_t = k / R_b \tag{1}$$

where, σ_t is the conductivity (S/m) of the paste, R_b is the measured bulk resistance (Ω) and k is a geometry factor. The geometry factor

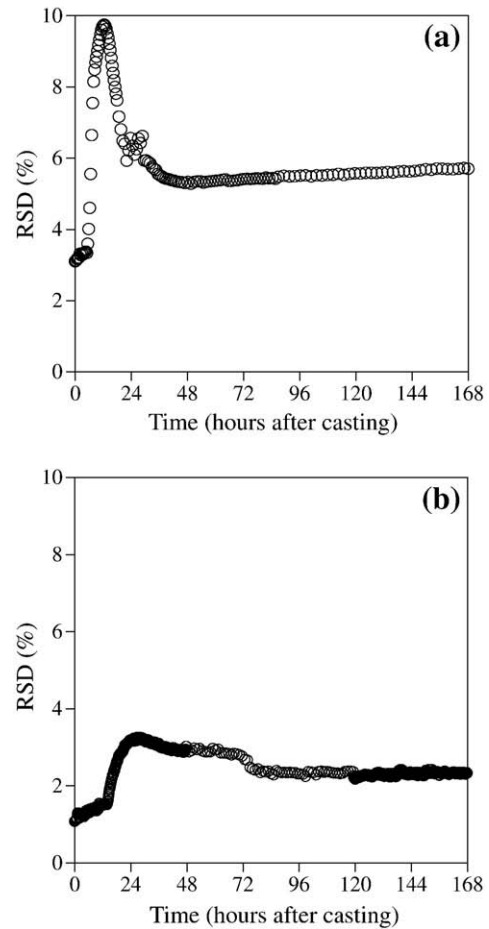


Fig. 6. Relative standard deviation between (a) 15 cement paste samples, with w/c = 0.45, at different ages and, (b) between 5 cement paste samples, with w/c = 0.50, at different ages.

was determined by filling the molds with solutions of known conductivity and measuring the bulk resistance between the electrodes. In this experiment two sodium chloride solutions were prepared with two different concentrations (0.1 M and 1 M). The conductivity of the two solutions was measured (7.72 and 1.01 S/m for 1 M and 0.1 M solutions, respectively), using a container with known geometry as shown in Fig. 4. By using this information, the value of the geometry factor, k , was calculated to be 15.5/m for the geometry shown in Fig. 3.

The electrical impedance of the samples was measured for 7 days, starting 30 min after casting. Fig. 5 shows the conductivity of the samples with w/c of 0.45 and 0.50, respectively. At the end of the test, all samples were inspected to ascertain the uniformity of specimen.

It can be seen that the conductivity of all samples follows the same pattern. As expected, the conductivity decreases as the system hydrates [36–38].

To better assess the variation, the relative standard deviation (RSD) can be used. The RSD is useful for comparing the uncertainty between different measurements of varying absolute magnitude. The

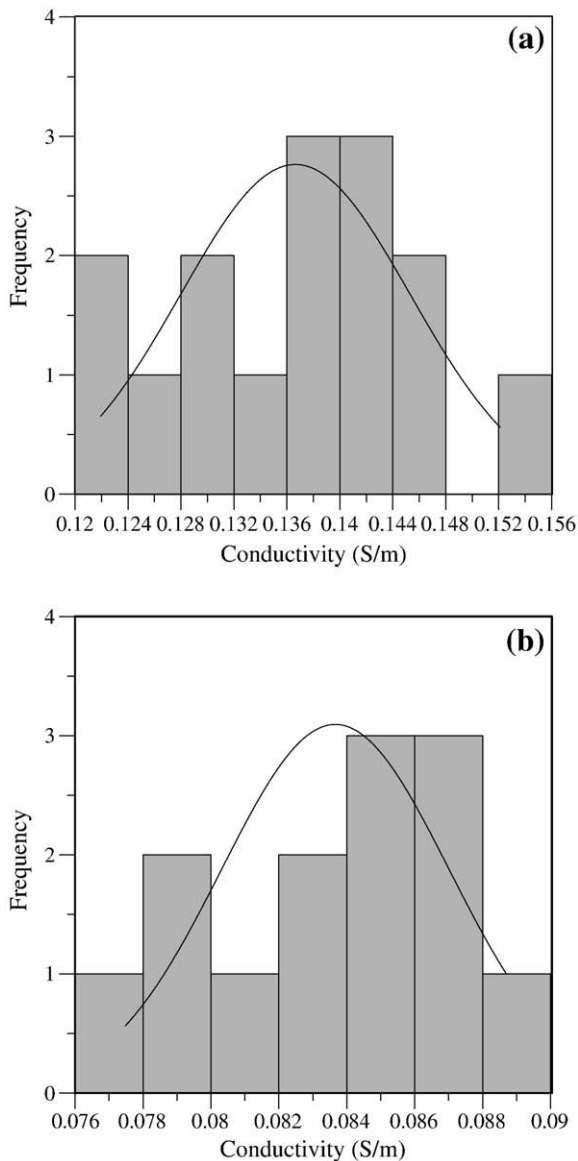


Fig. 7. Histogram of conductivity of paste samples with $w/c=0.45$ (a) 24 h after casting, (b) 72 h after casting.

Table 1
Mixture proportions of concrete samples.

Materials	Batch proportion for 100 kg (kg)		
	$w/c=0.48$, no WR	$w/c=0.53$, no WR	$w/c=0.48$ with WR
Cement (Type I)	8.0	8.0	8.0
Water	3.9	4.3	3.9
Coarse aggregate	68.9	68.6	68.7
Fine aggregate	19.1	19.0	19.0
Water reducer (WR)	0.0	0.0	0.3

RSD is the absolute value of the coefficient of variation calculated using Eq. (2):

$$\text{RSD} = \frac{(\text{Standard deviation of conductivity})}{\text{Average of conductivity}} \times 100 \quad (2)$$

Fig. 6 shows the RSD of the samples at different ages. Results show that, even when the samples are made from one mixture there is variability in the conductivity of the samples, especially at early ages when the properties change most dramatically. However, the RSD decreases over time as the measurements stabilize. This is shown in Fig. 7, which gives the histograms of conductivities for $w/c=0.45$ (15 samples) at two different ages. The maximum difference is less than 10% for $w/c=0.45$ and 3.5% for $w/c=0.50$ at all ages.

4.2. Electrical conductivity of concrete sample

To show the capability of the AEMS, the conductivity of concrete cylinders was measured with different mixture proportions (shown in Table 1). For this purpose, 200 mm (diameter) \times 400 mm (length) concrete cylinders were prepared with two (1.9 mm diameter) stainless steel rods as the electrodes. The electrodes were spaced 100 mm apart from each other and fixed in the mold. For each mixture, five cylinders were cast and impedance tests were performed every 15 min. The impedance measurements began 30 min after casting and continued for 7 days. Results show that the conductivities of all five samples of each mixture have very similar results with the RSD between 1 and 2.5% as can be seen in Fig. 9. As can be seen in Fig. 8, at about 10 h, the conductivity of concrete samples is similar. It is obvious from the results that impedance spectroscopy technique is capable to evaluate and compare different samples with different mixture proportions.

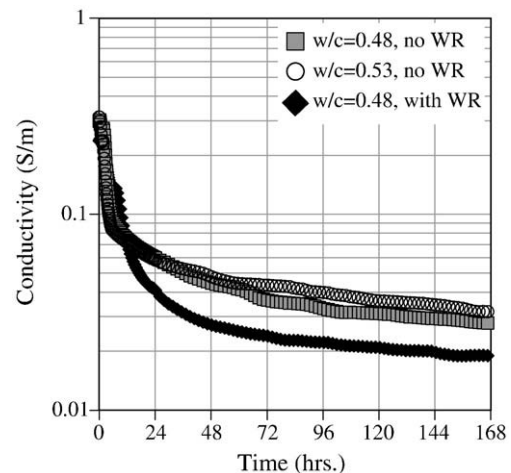


Fig. 8. Conductivity of concrete with three different mixture proportions, shown in Table 1.

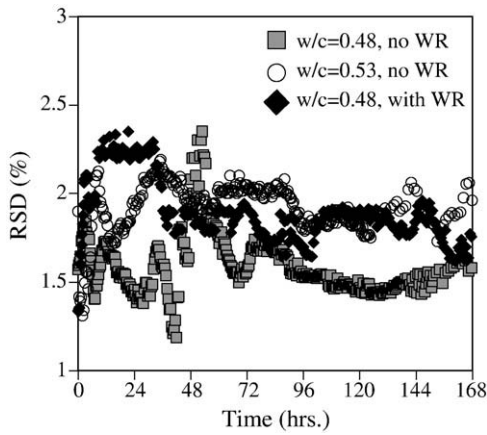


Fig. 9. Relative standard deviation between concrete samples with three different mixture proportions, shown in Table 1, at different ages.

4.3. Crack imaging in cement paste and concrete, using impedance spectroscopy

Electrical impedance imaging has been used by many researchers in the medical field to monitor various physiological variables [39–41]. Previous studies indicated that this technique can also be used in imaging the defects in cementitious materials [29,42]; however, studies in cement are somewhat limited. The approach consists of measuring the impedance at different locations on the surface of the concrete and constructing electrical conductivity (or resistivity) contour plot from the measured impedances. Since the presence of damage (e.g., a crack) changes the path of electrical flow in the concrete, any damage will appear on the plot. Electrical contour plots can be used to locate visible and invisible damage. In order to investigate this technique a small test unit developed consisting of twenty electrodes, as shown in Fig. 10. The impedance was measured between each pin, in X and Y directions. Then the measured values were used to construct electrical resistance contour plots. For this experiment, two concrete samples were prepared with water: cement:coarse aggregates:fine aggregates ratio of 0.4:1:3:2.85:2.37. The measurement frequency range was 1 MHz to 10 Hz, with the 500 mV AC stimulus. After performing the measurements, the resistances measured between each pin were normalized based on the maximum measured value in each case and then the normalized values were mapped. Fig. 11 shows the constructed image. The location of the saw cut is clearly visible in this image. A similar setup

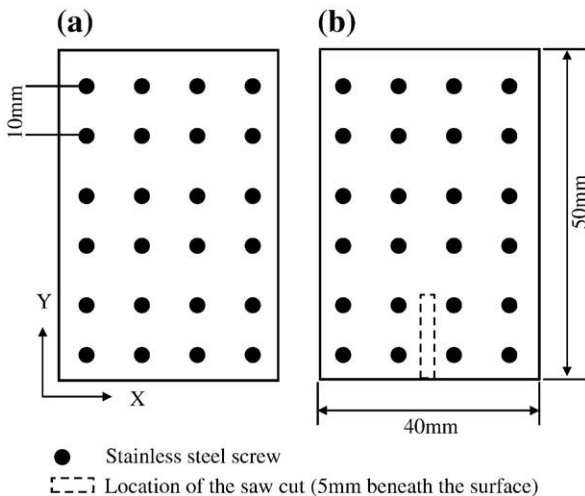


Fig. 10. The dimensions of the concrete samples and the measurement setup, used for imaging: (a) concrete sample with no cut, and (b) concrete sample with the saw cut.

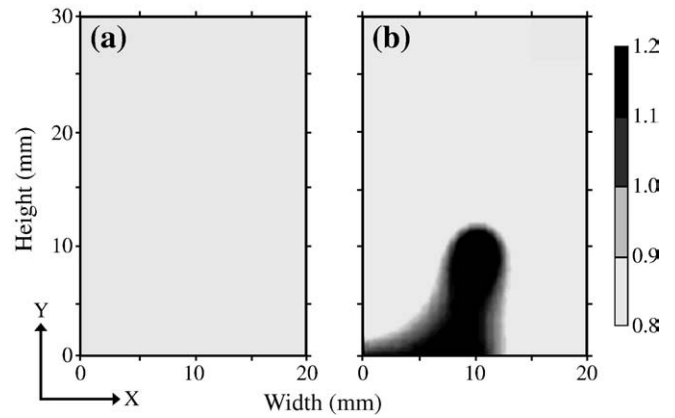


Fig. 11. Image of the concrete sample (a) without and (b) with saw cut, created by electrical impedance measurements.

(with different size and spacing between electrodes) can be used to determine the location of the damaged area beneath the sealed saw cut or joints which is currently under investigation.

5. Conclusion

This paper described an approach to automate electrical impedance measurements with an automated electrical monitoring system (AEMS) that enable multiple measurements to be made.

This switching system enables measurements to be performed on multiple specimens or where multiple locations are needed. This enables the aging processes be better quantified, allows variability to be qualified for quality control, and enables electrical imaging to be performed.

The system described in this paper was successfully used to investigate the behavior of concrete sample with different mixture proportions by continuously monitoring their conductivity. In addition, variability among different samples was studied and the results show that there is variability between samples even cast from one batch which needs to be considered, specifically in statistical analysis. Constructed electrical image maps can be used to locate the cracked and damaged area, even if it is beneath the surface.

Acknowledgements

This work was supported in part by the Joint Transportation Research Program administered by the Indiana Department of Transportation and Purdue University (study no. TPF-5(179)). The contents of this paper reflect the views of the authors, who are responsible for the facts and the accuracy of the data presented herein, and do not necessarily reflect the official views or policies of the Indiana Department of Transportation, nor do the contents constitute a standard, specification, or regulation.

References

- [1] W.J. McCarter, et al., Characterization and monitoring of cement-based systems using intrinsic electrical property measurements, *Cement and Concrete Research* 33 (2003) 197–206.
- [2] B.J. Christensen, et al., Impedance spectroscopy of hydrating cement-based materials: measurement, interpretation, and application, *Journal of the American Ceramic Society* 77 (1) (1994) 2789–2801.
- [3] P. Gu, P. Xie, J.J. Beaudoin, Some applications of AC impedance spectroscopy in cement research, *Cement, Concrete and Aggregates* 17 (2) (1995) 113–118.
- [4] F. Rajabipour, W.J. Weiss, Electrical conductivity of drying cement paste, *Materials and Structures* 40 (2007) 1143–1160.
- [5] W.J. Weiss, J.D. Shane, A. Mieses, T.O. Mason, S.P. Shah. Aspects of monitoring moisture changes using electrical impedance spectroscopy. In 2nd Symposium on Self-Dessication and Its Importance in Concrete Technology. 1999. Lund, Sweden: Lund Institute of Technology, Division of Building Materials.

- [6] A. Schiessl, et al., Assessing the moisture profile of drying concrete using impedance spectroscopy, *Concrete Science and Engineering* 2 (2) (2000) 106–116.
- [7] Z. Liu, J.J. Beaudoin, An assessment of the relative permeability of cement systems using A.C. impedance techniques, *Cement and Concrete Research* 29 (7) (1999) 1085–1090.
- [8] P. Gu, P. Xie, J.J. Beaudoin, Microstructural characterization of the transition zone in cement systems by means of A. C. impedance spectroscopy, *Cement and Concrete Research* 23 (1993) 581–591.
- [9] R.A. Olson, et al., 1995. Microstructure-electrical property relationships in cement-based materials. in *Materials Research Society Symposium*. Boston, MA, USA: Materials Research Society, Pittsburgh, PA, United States.
- [10] L. Lemoine, F. Wenger, J. Galland, Study of the corrosion of concrete reinforcement by electrochemical impedance measurement. *Corrosion Rates of Steel in Concrete ASTM STP 1065*, American Society for Testing and Materials, 1990.
- [11] L. Dhouibi, E. Triki, A. Raharinaivo, The application of electrochemical impedance spectroscopy to determine the long-term effectiveness of corrosion inhibitors for steel in concrete, *Cement & Concrete Composites* 24 (2002) 35–43.
- [12] C. Monticelli, A. Frignani, G. TrabANELLI, A study on corrosion inhibitors for concrete application, *Cement and Concrete Research* 30 (2000) 635–642.
- [13] G. TrabANELLI, et al., Electrochemical study on inhibitors of rebar corrosion in carbonated concrete, *Cement and Concrete Research* 35 (2005) 1804–1813.
- [14] P. Gu, et al., A study of corrosion inhibitor performance in chloride contaminated concrete by electrochemical impedance spectroscopy, *ACI Materials Journal* 94 (5) (1997) 385–395.
- [15] B.B. Hope, A.K.C. Ip, Corrosion inhibitors for use in concrete, *ACI Materials Journal* 86 (6) (1989) 602–608.
- [16] M. Shi, Z. Chen, J. Sun, Determination of chloride diffusivity in concrete by AC impedance spectroscopy, *Cement and Concrete Research* 29 (7) (1999) 1111–1115.
- [17] M.R. Hansen, et al., 1993. Chloride permeability and AC impedance of high performance concrete. *ACI-SP140-06*. 140: p. 121–146.
- [18] A. Peled, et al., Electrical impedance spectra to monitor damage during tensile loading of cement composites, *ACI Materials Journal* 98 (4) (2001) 313–322.
- [19] S. Perron, J.J. Beaudoin, Freezing of water in Portland cement paste—an AC impedance spectroscopy study, *Cement & Concrete Composites* 24 (5) (2002).
- [20] W.J. McCarter, H. Ezirim, M. Emerson, Properties of concrete in the cover zone: water penetration, sorptivity, and ionic ingress, *Magazine of Concrete Research* 48 (1996) 149–156.
- [21] A. Schießl, et al., Assessing the moisture profile of drying concrete using impedance spectroscopy, *Concrete Science and Engineering* 2 (2) (2000) 106–116.
- [22] F. Rajabipour, et al., Procedure to interpret electrical conductivity measurements in cover concrete during rewetting, *ASCE Journal of Materials in Civil Engineering* 17 (5) (2005) 586–594.
- [23] Z. Li, L. Xiao, X. Wei, Determination of concrete setting time using electrical resistivity measurement, *Journal of Materials Science in Civil Engineering* 19 (5) (2007) 423–427.
- [24] G. Sant, F. Rajabipour, P. Fishman, P. Lura, W.J. Weiss. Electrical conductivity measurements in cement paste at early ages. in *International RILEM Workshop on Advanced Testing of Fresh Cementitious Materials*, 2006, Stuttgart, Germany: RILEM.
- [25] G.D. Davis, M.J. Rich, L.T. Drzal, Monitoring moisture uptake and delamination in CFRP-reinforced concrete structures with electrochemical impedance sensors, *Journal of Nondestructive Evaluation* 23 (1) (2004) 1–9.
- [26] J.D. Shane, et al., Microstructural and pore solution changes induced by rapid chloride permeability test measured by impedance spectroscopy, *Concrete Science and Engineering* 1 (2) (1999) 110–119.
- [27] C. Shi, Effect of mixing proportions of concrete on its electrical conductivity and the rapid chloride permeability test (ASTM C1202 or ASSHTO T277) results, *Cement and Concrete Research* 34 (2004) 537–545.
- [28] T.J. Schmit, A fundamental investigation on utilizing error propagation, Monte Carlo simulation, and measurement interpretation technique to design efficient in situ concrete sensing systems MS thesis in Civil Engineering, Purdue University, 2005.
- [29] M. Niemuth, Using Impedance Spectroscopy to Detect Flaws in Concrete, Purdue University, MS thesis in Civil Engineering, 2004.
- [30] Keithley Instruments Inc., 2700, 2701 and 2750 Multimeter/Data Acquisition/Switch Systems, Keithley Instruments Inc., 2009 <http://www.keithley.com/products/dmm/integrasystems/?path=2700/Documents#4>.
- [31] Solartron Group, 2009. www.solartronanalytical.com/downloads/datasheets/1260.pdf.
- [32] Keithley Instruments Inc., Integra Series Technical Data Sheet, 2003.
- [33] G. Sant, F. Rajabipour, W.J. Weiss, The influence of temperature on electrical conductivity measurements and maturity predictions in cementitious materials during hydration, *The Indian Concrete Journal* (April 2008) 1–10.
- [34] National Instruments, What is NI GPIB?, 2009.
- [35] P. Gu, et al., Study of the hydration and setting behavior of OPC-HAC pastes, *Cement and Concrete Research* 24 (4) (1994) 682–694.
- [36] C.A. Scuderi, T.O. Mason, H.M. Jennings, Impedance spectra of hydrating cement pastes, *Journal of Materials Science* 26 (1991) 349–353.
- [37] J.M. Torrents, R. Pallas-Areny, 1997. Measurement of cement setting by impedance monitoring. in *IEEE Instrumentation and Measurement, Technology Conference*. May 19–21. Ottawa, Canada.
- [38] A. Poursae, C.M. Hansson, Reinforcing steel passivation in mortar and pore solution, *Cement and Concrete Research* 37 (2007) 1127–1133.
- [39] D. Murphy, et al., Impedance imaging in the newborn, *Clinical Physics and Physiological Measurement* 8 (Suppl. A) (1987) 131–140.
- [40] M. Weindling, et al., Electrical impedance to study cerebral haemodynamics in the newborn: which index is best? *Biology of the Neonate* 45 (1984) 300.
- [41] L. Tarassenko, P. Rolfe, Imaging spatial distribution of resistivity—an alternative approach, *Electronics Letters* 20 (1984) 574–576.
- [42] T. Hou, J.P. Lynch, Electrical impedance tomographic methods for sensing strain fields and crack damage in cementitious structures, *Journal of Intelligent Material Systems and Structures*, 2008, pp. 1–18.

The influence of temperature on electrical conductivity measurements and maturity predictions in cementitious materials during hydration

Gaurav Sant, Farshad Rajabipour and Jason Weiss

Electrical property measurements are being increasingly used to assess the transport properties of building materials. While conductivity measurements have been extensively used, the combined dependence of electrical conductivity on measurement temperature and microstructural development (cement hydration) is often overlooked. In this paper the influence of temperature and microstructural development (i.e. hydration) are separated. Two cement paste mixtures are assessed at 283K, 296K, and 309K, and the conductivity response is analysed to differentiate the contribution of maturity (pore structure refinement due to hydration) and temperature (due to changing ionic mobility). The conductivity measurements are used to determine the activation energy of electrical conduction (i.e. temperature dependence of ion mobility) and hydration (i.e. temperature dependence of reaction rates). This work provides an improved understanding of how temperature influences electrical measurements in cementitious systems at early ages, and can provide for an accurate interpretation of the electrical properties of the system. This information will enable improvements in the use of electrical measurements for quality control and quality assurance (QC/QA) testing.

Keywords: *Electrical conductivity, hydration, maturity, temperature, quality control.*

Electrical measurements are powerful non-destructive testing techniques that are capable of providing information about hydration reactions, microstructural features and the transport properties of cement based materials. However, electrical measurements (e.g., conductivity or resistivity) exhibit temperature dependence due to changing ionic mobility with temperature. In an electrolyte, electrical conduction occurs due to the migration of ions through the solution under an applied potential gradient¹. Consequently, conduction in aqueous electrolytes is dependent on ionic mobility and the solution's concentration. In cementitious materials, temperature change influences ionic mobility and salt solubility resulting in a change in the electrical conduction response as a function of temperature². These considerations highlight the need to account for the temperature dependent conductivity response of cementitious materials. Further, chemical reactions (such as cement hydration) are influenced by temperature³. This topic has received significant treatment in the literature with the objective of determining how temperature influences the rate of material property development^{4,5,6,7}. Maturity transformations have been extensively used to correlate material properties to the extent of reaction that occurs in the system^{8,9}.

Due to the influence of temperature on the rate of hydration and ionic mobility it would be reasonable to consider that the electrical properties (conductivity or

resistivity) of cement systems are a function of maturity and temperature effects as shown in Equation 1.

$$\sigma(t, T) = f(M) \bullet f(T) \quad \dots\dots(1)$$

where, $\sigma(t, T)$ is the time and temperature dependent electrical property (in this case the conductivity (S/m)) of the sample, $f(M)$ is a function which defines the influence of time and temperature on the sample maturity (microstructure development), and $f(T)$ is a function that defines the influence of sample temperature and accounts for effects such as the ionic mobility and solution concentration.

The temperature dependence of electrical properties in cement based systems was studied several decades ago by Hammond and Robson who used the Hinrichson-Rasch law to describe the conductivity of concrete over a range of temperatures (Equation 2).^{10,11}

$$\ln\left(\frac{\sigma(T)}{\sigma(T_{REF})}\right) = A\left(\frac{1}{T} - \frac{1}{T_{REF}}\right) \quad \dots\dots(2)$$

where, $\sigma(T)$ is the concrete conductivity (S/m) at temperature T (K), $\sigma(T_{REF})$ is the conductivity (S/m) at a reference temperature T_{REF} (296K for this work) and 'A' is an empirical constant (K). Hammond and Robson indicated 'A' to be equal to 5500K based on work by Spencer^{10,12}. Later, Elkey and Sellevold extended the scope of this investigation and determined 'A' to vary between 2000 and 5000K depending on the mixture composition¹³.

Whittington et al. used a similar approach to investigate concrete using electrical resistivity¹⁴. Using a slightly different form of relationship (Equation 3) described by Hammond and Robson they determined concrete to have a negative temperature coefficient of resistivity, equal to 0.022/°C.

$$\frac{\rho(T)}{\rho(T_{REF})} = \frac{1}{1 + \alpha(T - T_{REF})} \quad \dots\dots(3)$$

where, $\rho(T) = 1/\sigma(T)$ is the resistivity (ohms.m) at temperature T (K), $\rho(T_{REF})$ is the resistivity (ohms.m) at a reference temperature T_{REF} (K) and α is temperature coefficient of resistivity of the material. The work of Whittington et al translates to an empirical constant 'A' of 2130 K for the concretes tested.

In the 1990s, McCarter determined the temperature coefficient of resistivity of concrete as 0.026/°C.¹⁵ More recently, McCarter proposed a formulation to determine the activation energy of electrical conduction based on the Arrhenius Law (Equation 4)^{16,17}.

$$\sigma_{Bulk} = A \bullet \exp\left[\frac{-E_{aC}}{R \bullet T}\right] \quad \dots\dots(4)$$

where, σ_{Bulk} is the bulk sample conductivity (S/m) at an absolute temperature T (K), R is the universal gas constant (8.314 J/K mol), E_{aC} is the activation energy for the conduction process (J/mol) and A (S/m) is a material constant (theoretically equivalent to the conductivity at infinite temperature; $\sigma(T = \infty)$). The activation energies of electrical conduction were determined to be in the range of 16-30 KJ/mole for the mixtures evaluated in this project.

Research objective

This paper proposes an approach to simultaneously assess the influence of temperature and microstructural changes (i.e. maturity) on the measured electrical conductivity in cementitious systems. The results of this work are aimed at understanding the influence of temperature on early-age conductivity measurements. This understanding would permit the reliable use of electrical measurements in early-age quality control and quality assurance (QC/QA) testing and for specification compliance of cement-based materials.

Materials and mixing procedures

Two different cement paste mixtures were prepared according to the mixture proportions shown in Table 1. Type I ordinary portland cement was used with a Blaine fineness of 360 m²/kg and a Bogue phase composition of 60% C₃S, 12% C₂S, 12% C₃A, 7% C₄AF and a Na₂O equivalent of 0.72%. To enhance the workability of the mixtures, a high range water reducing admixture was added. A commercially available shrinkage reducing admixture (SRA) was added at a 5% concentration of the initial water content by replacement (by mass) of the initial mixing water. For the measurement of electrical conductivity de-aired, neat cement pastes were prepared using de-ionised water. The water was de-aired by boiling then cooled to room temperature before mixing. The dry constituent materials were placed inside a special mixing chamber¹⁸. The chamber was then sealed, air was evacuated from the chamber using a vacuum pump, and the solution of water and the chemical admixtures was introduced into the chamber

under the same evacuated condition. The chamber was then placed in a commercial paint shaker and shaken for five minutes to uniformly mix the constituents and obtain a consistent cement paste mixture. After mixing, the chamber was opened and the cement paste slurry was placed in the moulds using external vibration.

Table 1. Mixture proportions (mass)

	W/C = 0.30	W/C = 0.30 + 5% SRA
Water	0.300	0.285
Cement	1.000	1.000
HRWRA	0.005	0.005
SRA	~	0.015

Experimental procedures

Electrical conductivity of fresh and mature cement pastes

The electrical conductivity of cement paste samples was measured using cylindrical paste specimens (22 mm diameter, 50 mm height). The specimens were cast and stored in an airtight plastic vial. Two stainless steel

electrodes (2.5 mm diameter rods spaced 10 mm centre to centre) were embedded longitudinally inside each vial (Figure 1b). An impedance gain-phase analyser measured the impedance response of each specimen. The measurements were made over a wide frequency range; i.e. 10 MHz to 1 Hz (10 steps/frequency decade) using a 100 mV AC stimulus. The bulk resistance (R_b) obtained from the impedance response was used to determine the material's conductivity after normalising for the effects of specimen and electrode geometry (Equation 5).

$$\sigma_t = \frac{k}{R_b} \quad \dots(5)$$

where, σ_t is the paste conductivity (S/m), R_b is the bulk resistance (ohms; Ω) and k is a geometry factor (15.76/m) that was determined experimentally for this specific geometry¹⁹. During measurements, the specimens remained sealed inside plastic vials. Electrical impedance measurements were performed for a duration of 7 days (at a reference temperature of 296K) after casting on

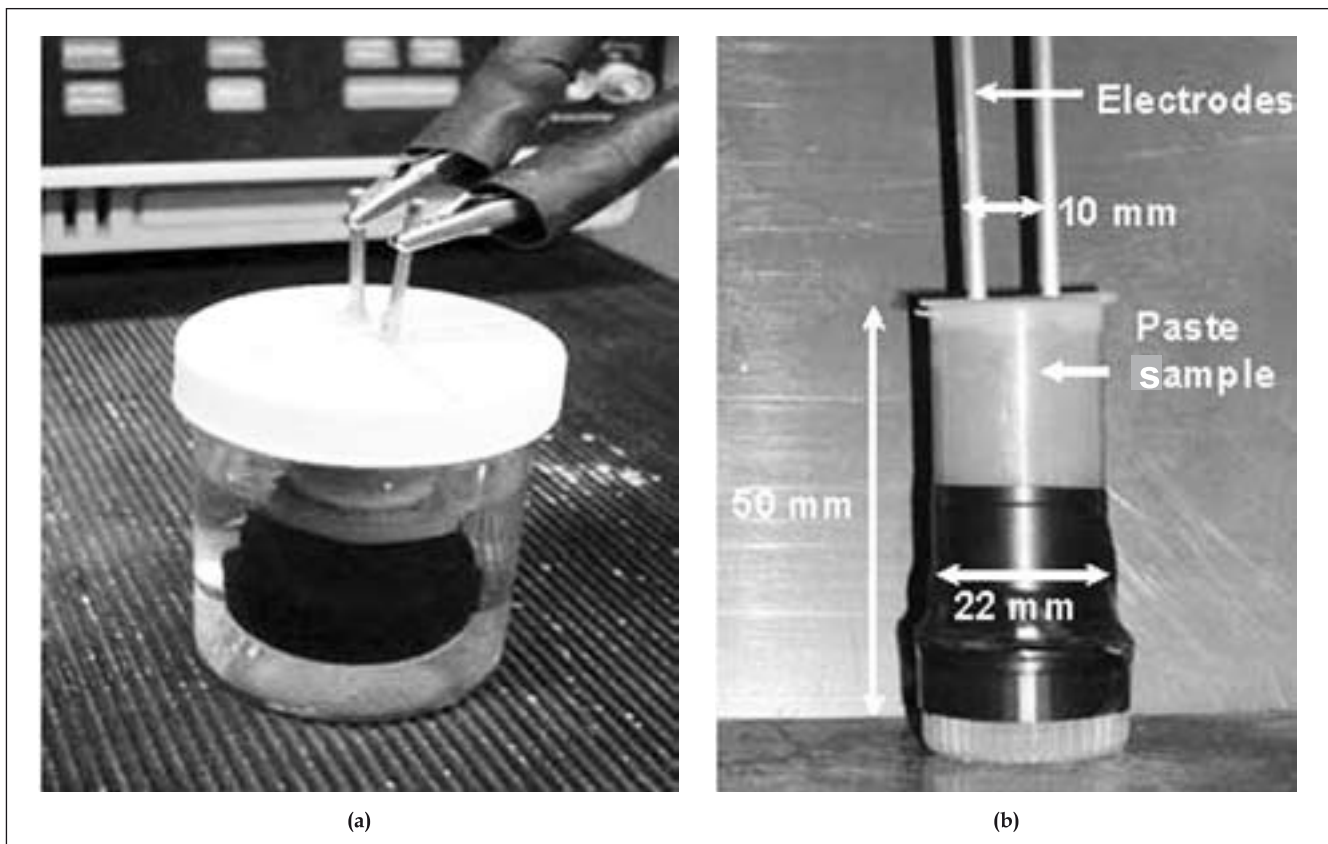


Figure 1. An illustration of the apparatus used for the measurement of electrical conductivity of cement pastes (a) The conductivity cell for cement pastes immersed in a water bath (b) The vial with embedded electrodes for paste and pore solution conductivity assessment

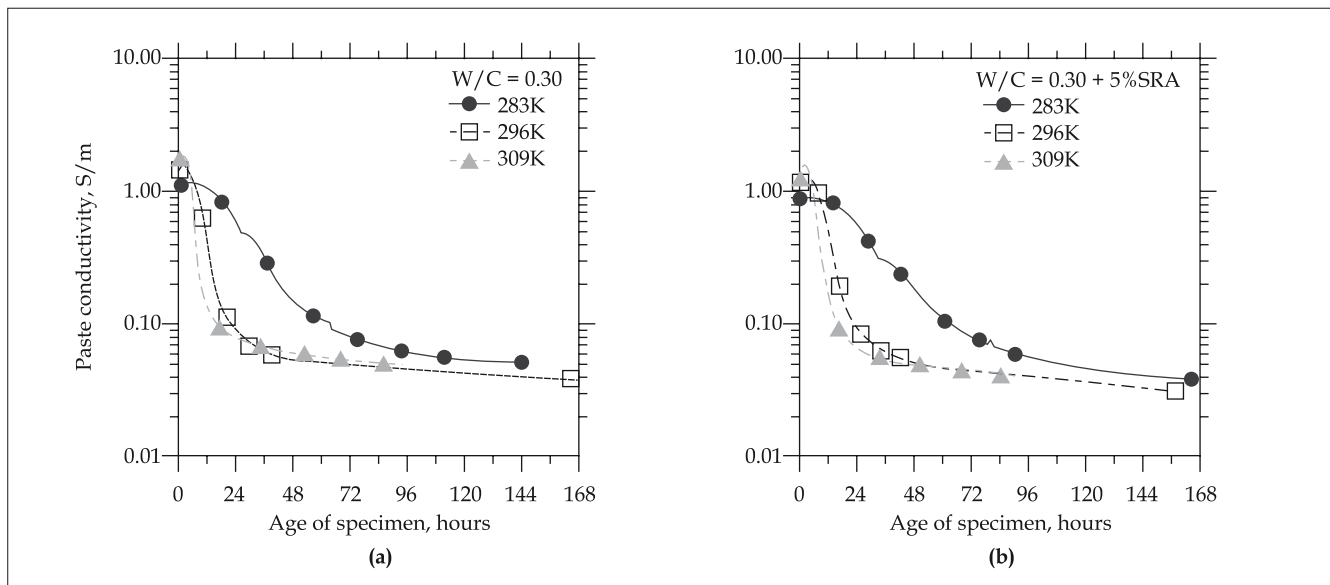


Figure 2. The electrical conductivity of the cement pastes as function of specimen age (a) $W/C = 0.30$ and (b) $W/C = 0.30 + 5\% \text{ SRA}$

specimens which were kept in a water bath to minimise temperature variations (Figure 1a). Measurements were performed on samples cured at 283K (14 days), 296K (7 days) and 309K (4 days). Prior to mixing, the raw materials were temperature conditioned to ensure an appropriate mixture temperature (equivalent to the measuring temperature) at the end of the mixing cycle. For consistency, conductivity measurements until an age of 168 hours (real and equivalent age) are presented in this paper. The measurements were used to determine the activation energy of cement hydration, after a correction to account for the influence of temperature (ionic mobility) on electrical conductivity.

To determine the influence of temperature on the conductivity of the pore solution (i.e. activation energy of electrical conduction; E_{aC} (J/mol)) in cement pastes, conductivity measurements were performed on cement paste samples (cured for 7 days at 296K; $\sim 70\%$ hydration – which corresponds to the maximum degree of hydration for the mixture as computed using Powers model²⁰ that were conditioned to 283K, 296K and 309K ($\pm 0.5K$) in an environmental chamber. Further, companion specimens were cast with thermocouples embedded to monitor the temperature profile of the cement paste mixtures.

Electrical conductivity of synthetic pore solutions

To determine the activation energy of electrical conduction in an electrolyte, synthetic pore solutions

of varying concentrations were prepared (0.35 KOH + 0.05 NaOH, 0.70 KOH + 0.10 NaOH, 1.40 KOH + 0.20 NaOH). The solutions were then conditioned to 283K, 296K and 309K ($\pm 0.5K$) in an environmental chamber. When the solutions had achieved an equilibrium temperature (measured using thermocouples immersed in the solution), the conductivity of the solutions was measured using a conductivity cell (Figure 1b) connected to a impedance gain-phase analyser²⁰.

Experimental results

Influence of the rate of reaction on the electrical conductivity

Figure 2 shows the electrical conductivity of cement paste mixtures cured at temperatures of 283K, 296K and 309K. An initial increase in the conductivity is noted for ~ 1.5 hours for all the cement paste mixtures. This may be explained by the rapid initial dissolution of alkalis and sulphates into the mixing water. After this time (1.5 hours), a reduction in conductivity is noted for all mixtures. A significantly different trend is observed in the rate of measured conductivity (Figure 2) for specimens cured at different temperatures. The samples cured at low temperatures show a gradual decrease in the conductivity, while mixtures cured at higher temperatures exhibit a more rapid decrease. This observation may be explained by the temperature dependence of the rate of hydration in these cement paste mixtures (i.e. the rate of pore structure refinement as a function of the reaction temperature).

Influence of temperature on the electrical conductivity of cement pastes

Figure 3 shows the measured electrical conductivity of two cement paste specimens (cured for 7 days), which have been subjected to thermal cycles. After being cured for 7 days at 296K, the samples were placed at temperatures of 283K and 309K (alternate heating and cooling was performed for 12 hours to ensure equivalent maturity). The results are shown in Figure 3(b). As expected, the measured conductivity is lower at lower temperatures. The lower conductivity of the SRA mixture as compared to the plain mixture is attributed to the non-conductive nature of the SRA in cement paste and pore solution^{20,21}. The measured value of conductivity was then used to determine the activation energy of the conduction process in cement pastes. This is further discussed later.

Influence of temperature on the electrical conductivity of pore solution

Figure 4 shows the measured electrical conductivity of synthetic pore solutions (0.35 KOH + 0.05 NaOH, 0.70 KOH + 0.10 NaOH, 1.40 KOH + 0.20 NaOH) conditioned to temperatures of 283K, 296K and 309K. The electrical conductivity is observed to increase linearly over the temperature range from 283K to 309K. This is consistent with the increase in ionic mobility and the extent of dissociation of the dissolved ionic species as a function of temperature. The measured value of conductivity was then used to determine the activation

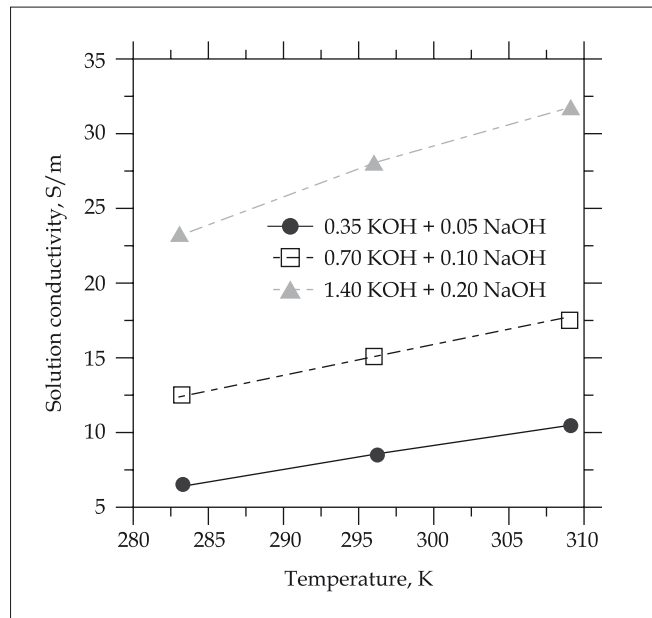


Figure 4. The temperature dependent response of electrical conductivity of synthetic pore solutions investigated in this project

energy of the conduction process in the electrolytes. This is further discussed later.

Discussion of experimental results

The electrical conductivity of cementitious materials has been described extensively using a modified parallel

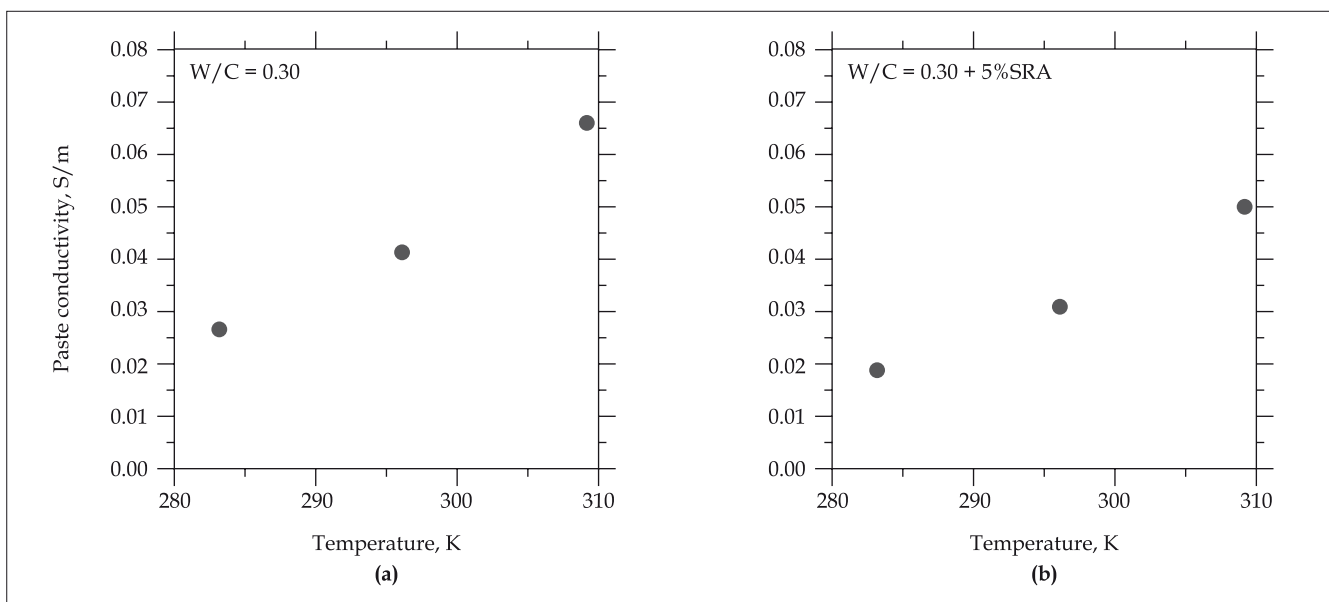


Figure 3. The temperature dependent electrical conductivity of the cement pastes (a) W/C = 0.30 and (b) W/C = 0.30 + 5% SRA

law^{22,23,24}. This relationship can be described using Equation 6.

$$\sigma_t = \sigma_0 \phi \beta \quad \dots(6)$$

where, σ_t is the bulk cement paste conductivity (S/m), σ_0 is the pore solution conductivity (S/m), ϕ is the volume fraction of the solution contained in the pores and β is the pore connectivity. The modified parallel law can be used to determine which parameters are impacted by a change in temperature. The first component which would contribute to the bulk conductivity would be the pore solution conductivity. Considering hydrated products and cement particles to be non-conductive (their conductivity is several orders of magnitude lower than the ionic pore solution), electrical conduction in cementitious materials can be modelled to occur primarily through the ionic pore fluid (in the gel and capillary porosity)^{20,23}. This is significant, as temperature influences chemical equilibrium states; impacting ionic mobility (primary effect) and solubility (secondary effect)^{25,26}. Ionic mobility (or equivalent conductivity) is noted to increase with increasing temperature due to the decreasing viscosity of the fluid (water), and an increase in the extent of dissociation of the dissolved ionic species, which increases the conductivity of the

system¹. An inverse effect (decreasing conductivity) would be noted with decreasing temperature.

The second component which contributes to the overall conductivity would be the pore fluid volume. For a sealed system, at a given degree of hydration ignoring changes in fluid volume due to changes in density with temperature, the pore fluid volume would be fixed; as solution is not removed from or added to the system. This should however be distinguished from a change in the pore fluid volume due to the consumption of water during hydration.

The third component is the pore fluid connectivity (equivalent to the inverse tortuosity), which decreases due to pore structure refinement with increasing maturity; a function of time and the reaction temperature.

Activation energy of electrical conduction in cement paste and pore solution

Cement paste specimens subjected to thermal cycling were used to determine the influence of temperature on the cement paste conductivity, Figure 3. The results were used to determine the activation energy of electrical conduction (E_{aC}) in cement pastes, Figure 5. The activation energy of conduction was determined to be 25.6 kJ/mol for the plain mixture and 27.6 kJ/mol for the SRA mixture. A higher activation energy of conduction

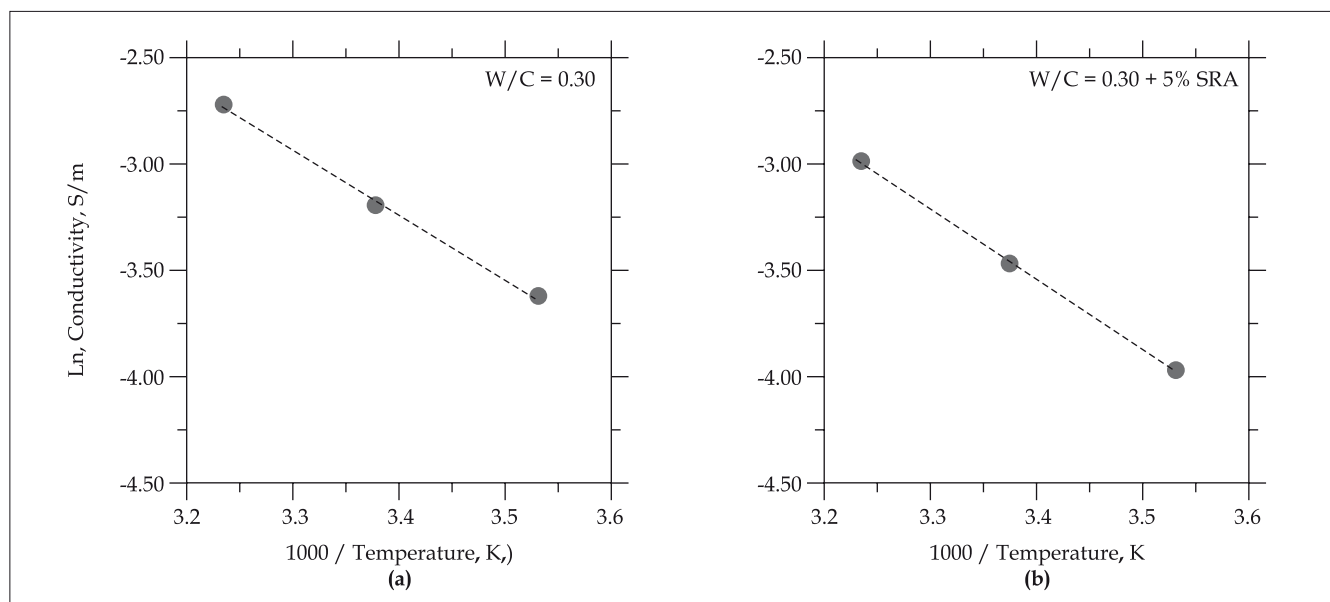


Figure 5. The activation energy of electrical conduction for cement pastes investigate (a) W/C = 0.30 and (b) W/C = 0.30 + 5% SRA

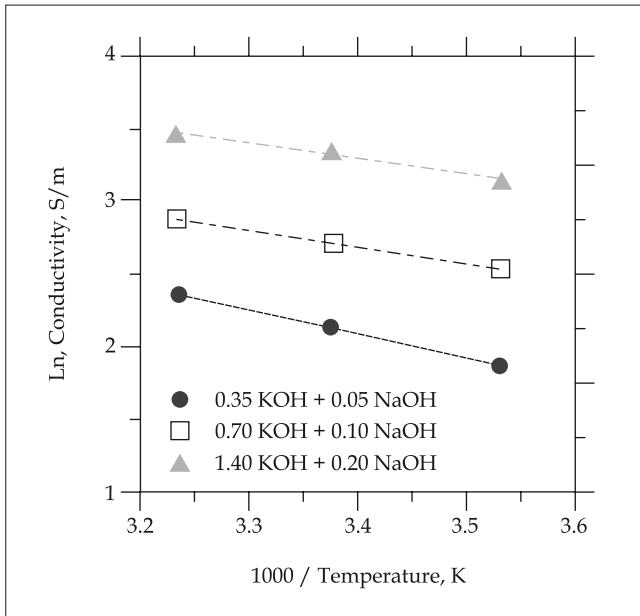


Figure 6. The activation energy of the conduction process for synthetic pore solutions

in mixtures containing a SRA may be explained by the non-conductive nature of the SRA which impedes ion migration in the system. Further, the SRA may bind ions reducing electrical conduction in the system²¹.

To fully understand the influence of temperature on the conductivity of an aqueous electrolyte a brief background on electrolytic conductivity is needed. The conductivity of an aqueous electrolyte can be expressed using Equation 7 where, z is the species valence (unitless), c is the molar concentration of the electrolyte (mol/L) and λ is the equivalent conductivity ($\text{cm}^2 \text{S/mole}$) of each species at infinite dilution (which is a function of temperature) and is proportional to the ionic mobility²⁶. At low concentrations ($< 0.01 \text{ mol/l}$), that is, in dilute solutions the equivalent conductivity is a constant for a specific species. However, at high concentrations the equivalent conductivity is observed to decrease inversely (but non-linearly), due to ion-ion interactions in the solution^{19,27}.

$$\sigma_{\text{Solution}} = \sum z_i c_i \lambda_i \quad \text{.....(7)}$$

Conductivity measurements were performed on synthetic pore solutions subjected to thermal cycling. The solutions were selected to correspond to the concentration of the pore fluid of an early-age cement paste (~ 2 hours), a

later age cement paste (48 hours), and a pore fluid with a very high molar (ionic) strength. The results of these tests were used to determine the activation energy of the conduction process (E_{ac}) (Figure 6; 13.55 kJ/mole, 9.65 kJ/mole and 8.98 kJ/mole, respectively, in order of increasing solution concentration) in the ionic solutions. It is noticed that the activation energy decreases with increasing concentration, indicating concentrated solutions are less sensitive to temperature change as compared to dilute solutions. This observation can be explained by the large degree of inter-ionic interactions in concentrated solutions, which significantly alter the conductivity behaviour²⁷.

Temperature correction for electrical conductivity

The activation energy of conduction in an electrolyte can be used to correct the influence of temperature, by transforming the conductivity at any temperature (in this case 283K or 309K) to a reference temperature (in this case 296K) using the expression shown in Equation 8.

$$\sigma(T_{REF}) = \frac{\sigma(T)}{\exp\left(-\frac{E_{ac}}{R} \left(\frac{1}{T} - \frac{1}{T_{REF}}\right)\right)} \quad \text{.....(8)}$$

where, $\sigma(T)$ is the sample conductivity (S/m) at any temperature T (K), $\sigma(T_{REF})$ is the conductivity (S/m) at a reference temperature, T_{REF} (296K), E_{ac} is the activation energy of electrical conduction in an electrolyte (or cement paste) (J/mole) and R is the universal gas constant (J/K.mole). The temperature correction is performed using the activation energy of conduction of the pore solution, having the lowest concentration (conductivity). This solution was selected as it is noted to correspond to the pore solution chemistry (conductivity) of a 2 hour old cement paste (0.35 KOH + 0.05 NaOH), which contains a large fluid volume; whose electrical conductivity behaviour is most sensitive to changes in temperature (Figure 6 – highest E_{ac}).

Determination of the activation energy of the hydration reaction

Electrical conductivity can be corrected to account for the influence of temperature on the rate of hydration and, consequently microstructural development (pore structure refinement). This component may be accounted for using a temperature transformation such as an equivalent age (i.e. maturity) function proposed by Hansen and Pedersen²⁸; Equation 9. In this paper, the equivalent age function (Equation 9) is used to

determine the activation energy of cement hydration (E_{aR}), after normalising conductivity at any temperature to a reference temperature $T(K)$; using Equation 8.

$$M(t, T) = \int_0^t \exp\left(-\frac{E_{aR}}{R} \left(\frac{1}{T} - \frac{1}{T_{REF}}\right)\right) \cdot dt \quad \dots\dots(9)$$

where, M (hours) is the maturity (or equivalent age) of the specimen at a reference temperature T_{REF} (K), E_{aR} (KJ/mol) is the apparent activation energy of the hydration reaction, R (J/(mol · K)) is the gas constant (8.314 J/mol·K), T (K) is the average temperature of the concrete, and dt (hours) is the time interval²⁸. The apparent activation energy determined from 10% to 35% hydration; (39.50 kJ/mol) is similar to values determined by other methods (e.g. chemical shrinkage) for the cement systems investigated²⁰.

Correction for the influence of temperature on hydration and electrical conductivity

As illustrated in Equation 1, the conductivity behaviour of a cementitious material can be expressed as a function of maturity and the measurement temperature. This section will describe a procedure which can be used to simultaneously account for the influence of temperature on cement hydration and electrical conductivity. Due to space considerations, this paper will describe

the procedure only for the plain cement mixture ($W/C = 0.30$).

A function can be fit to describe the experimental conductivity measurement ($W/C = 0.30$) at the reference temperature (in this case 296K). This function is shown in Equation 10 ($R^2 = 0.9996$).

$$\sigma(t, 296K) = \frac{1.38 - 0.82t + 0.19t^2 - 0.01t^3 + 0.0002t^4}{1.00 - 0.66t + 0.19t^2 - 0.02t^3 + 0.001t^4 + 0.00002t^5} \quad \dots\dots(10)$$

where, $\sigma(t, 296K)$ is the measured conductivity at time t (hours) at a measurement temperature of 296K (the reference temperature). The type of fit used to describe the conductivity response is not important. To extend the applicability of this function to describe the electrical conductivity behaviour at any temperature requires the incorporation of a reaction rate constant k_R (unitless) which accounts for the influence of temperature on the rate of cement hydration and an electrical conduction constant k_T (unitless) which accounts for the influence of temperature on electrical conductivity. This approach is described in Equations 11, 12 and 13.

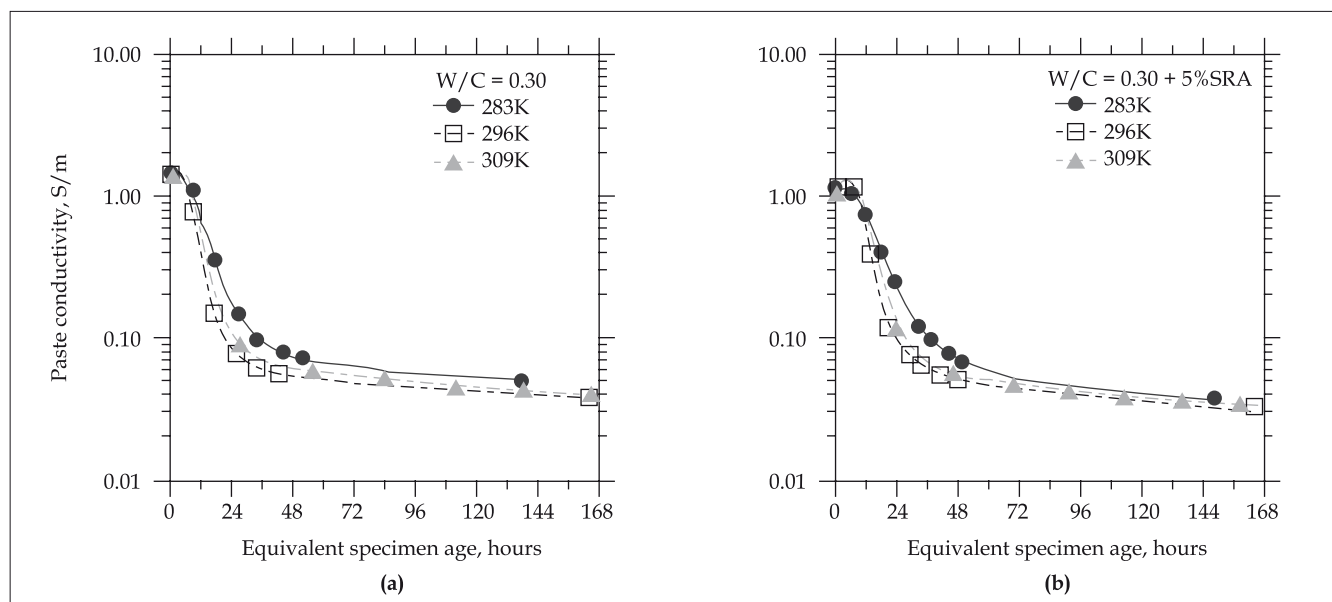


Figure 7. The reaction and solution temperature corrected electrical conductivity of the cement pastes as a function of equivalent specimen age (a) $W/C = 0.30$ and (b) $W/C = 0.30 + 5\% \text{ SRA}$

$\sigma(t, T) =$

$$\left(\frac{1.38 - 0.82(t \cdot k_R) + 0.19(t \cdot k_R)^2 - 0.01(t \cdot k_R)^3 + 0.0002(t \cdot k_R)^4}{1.00 - 0.66(t \cdot k_R) + 0.19(t \cdot k_R)^2 - 0.02(t \cdot k_R)^3 + 0.001(t \cdot k_R)^4 + 0.00002(t \cdot k_R)^5} \right) \cdot (k_T) \quad \dots\dots(11)$$

where,

$$k_R = \exp \left[-\frac{E_{aR}}{R} \left(\frac{1}{T} - \frac{1}{T_{REF}} \right) \right] \quad \dots\dots(12)$$

$$k_T = \exp \left[-\frac{E_{aC}}{R} \left(\frac{1}{T} - \frac{1}{T_{REF}} \right) \right] \quad \dots\dots(13)$$

where, k_R (unitless) is the reaction rate constant which accounts for the influence of temperature on the rate of cement hydration, k_T (unitless) is the electrical conduction constant which accounts for the influence of temperature on electrical conductivity and T (K) is the average temperature of the concrete.

Figure 7 shows the electrical conductivity response of the two cement paste mixtures evaluated using the approach described above, to account for the influence of temperature on cement hydration and electrical conductivity; using the activation energy of cement hydration ($E_{aR} = 39.50$ kJ/mole) and electrical conduction for the electrical conductivity response of an early pore fluid (0.35 KOH + 0.05 NaOH; $E_{aC} = 13.55$ kJ/mole). It can be seen that (Figure 7), using the approach described in Equation 11, the influence of temperature on hydration and electrical conductivity can be comprehensively described for mixtures cured at any temperature.

An improved approach is proposed to perform the temperature correction for electrical conductivity if the pore solution chemistry (conductivity) at early-ages is well known. This would involve determining the activation energy of electrical conduction in electrolytes (pore fluids) having an age-dependent concentration (and conductivity). This information can be used to perform a comprehensive temperature correction for electrical conductivity. An example of such an approach is illustrated in Figure 8 which shows the activation energy of electrical conduction as a function of the solution's conductivity at the reference temperature (296K)^{20,29}.

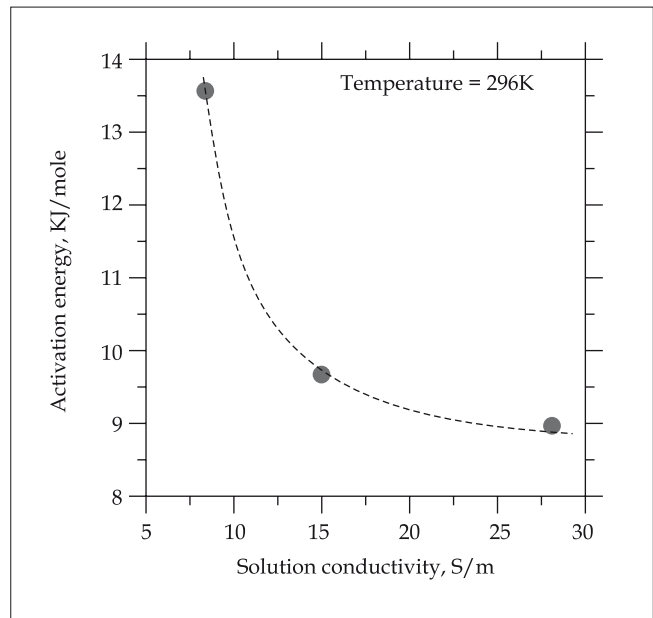


Figure 8. The non-linear relationship between the activation energy of electrical conduction (E_{ac}) and the solution conductivity at 296K

Conclusions

Measurements of electrical conductivity performed on paste, mortar and concrete require a two-part correction to accurately describe early-age behaviour. The first part of this approach accounts for the influence of temperature on cement hydration (pore refinement), and the second part accounts for the influence of temperature on electrical conductivity. This paper demonstrates the successful application of this correction for electrical conductivity measurements using the activation energy of electrical conduction and cement hydration. In this context, the activation energy of electrical conduction has been determined for electrolytes of varying concentrations and for cement pastes. In addition, the activation energy of cement hydration has been determined to be 39.50 kJ/mol (independent of w/c) and is noted to be similar to values determined using other techniques (e.g. chemical shrinkage or heat of hydration). The approach demonstrated in this paper would be crucial for forecasting the long-term durability performance of field concretes, based on the early-age electrical properties of the material using an approach similar to that presented by Lane³⁰. An approach of this nature would provide fundamental information needed for quality control and quality assurance (QC/QA) applications and for ensuring the specification compliance of field concretes. This information would have an immense impact in determining how field concrete is specified, evaluated or purchased.

Acknowledgement

The authors gratefully acknowledge the support from the Center for Advanced Cement Based Materials (ACBM) and the National Science Foundation (NSF). This material is based in part on work supported by NSF Grant No. 0134272: a 'CAREER AWARD' granted to the last author. This work was conducted in the Material Characterisation and Sensing Laboratory at Purdue University and as such, the authors gratefully acknowledge the support that has made this laboratory and its operation possible. The contents of this paper reflect the views of the authors, who are responsible for the accuracy of the data presented herein.

References

1. Adamson, A.W., *A Text-book of Physical Chemistry*, Academic Press, USA, 1973.
2. Binder, R.C., *Fluid Mechanics*, Prentice-Hall Inc., Englewood Cliffs, NJ, 1973.
3. Activation Energy, *Encyclopedia Britannica*, 2007.
4. Carino, N.J., The maturity method, *CRC handbook on nondestructive testing of concrete*, Edited by V.M. Malhotra and N.J. Carino, CRC Press, Boca Rotan, Florida, 1991, pp. 101-146.
5. Weiss, W.J., Experimental determination of the 'Time-Zero', *Early age cracking in cementitious systems - RILEM report TC-EAS*, Edited by Arnon Bentur, 2002.
6. Pinto, R.C.A. and Hover, K.C., Application of maturity approach to setting time, *ACI Materials Journal*, 1999, Vol. 96, No. 6, pp. 686-691.
7. Roy, D.M., Scheetz, B.E., Sabol, S., Brown, P.W., Shi, D., Licastro, P.H., Idorn, G.M., Andersen, P.J., and Johanson, V., Maturity model and curing technology, Strategic Highway Research Program, SHRP-C-625, (1993)
8. Nurse, R.W., Steam curing of concrete, *Magazine of Concrete Research*, 1949, Vol. 1, No. 2, pp. 79-88.
9. Saul, A.G.A., Principles underlying the steam curing of concrete at atmospheric pressure, *Magazine of Concrete Research*, 1951, pp. 127-140.
10. Hammond, E., and Robson, T.D., Comparison of Electrical Properties of Various Cements and Concretes, *The Engineer*, 1955, Vol. 199, pp. 78-80.
11. Rasch, E. and Hinrichsen, F.W., Uber eine beziehung zwischen elektrischer leitfähigkeit und Temperatur, *Zeitschrift fur electrochemie*, 1908, Vol. 14, No. 41, pp. 41- 48.
12. Spencer, R.W., Measurement of the Moisture content of concrete, *Journal of the American Concrete Institute*, 1937, Vol. 9, No. 1, pp. 45-61.
13. Elkey, W. and Sellevold, E.J., *Electrical resistivity of concrete*, Norwegian Road Research Laboratory, Publication No. 80, 1995, Oslo.
14. Whittington, H.W., McCarter, W.J. and Forde, M.C., The conduction of electricity through concrete, *Magazine of Concrete Research*, 1981, Vol. 33, No. 114, pp. 48-60.
15. McCarter, W.J., Effects of temperature on conduction and polarization in portland cement mortar, *Journal of the American Ceramic Society*, 1995, Vol. 78, No. 2, pp. 411-415.
16. McCarter, W.J., Starrs, G. and Chrisp, T.M., Electrical conductivity, diffusion, and permeability of portland cement-based mortars, *Cement and Concrete Research*, 2000, Vol. 30, No. 9, pp. 1395-1400.
17. Arrhenius, S., On the reaction velocity of the inversion of cane sugar by acids, *Zeitschrift für physikalische Chemie*, 4, 226, (1889).
18. Sant, G., Lura, P. and Weiss, W.J., Measurement of volume change in cementitious materials at early ages: Review of testing protocols and interpretation of results, *The Transportation Research Record*, 2006, 1979.
19. Rajabipour, F., Weiss, W.J. and Abraham, D., Insitu electrical conductivity measurements to assess moisture and ionic transport in concrete, *Advances in concrete through science and engineering, Proceedings of the International RILEM Symposium*, Evanston, Illinois, 2004.
20. Sant, G., *Examining volume changes, stress development and cracking in cement-based systems*, MSCE Thesis, Purdue University, West Lafayette, Indiana, USA, 2007.
21. Rajabipour, F., Sant, G. and Weiss, W.J., Interactions between shrinkage reducing admixtures and cement paste's pore solution, *Cement and Concrete Research*, 2008, Vol. 38, pp. 606-615.
22. Garboczi, E.J., Permeability, diffusivity, and microstructural parameters : A critical review, *Cement and Concrete Research*, Vol. 20, No. 4, pp. 591-601.
23. Rajabipour, F., *Insitu electrical sensing and material health monitoring in concrete structures*, PhD Dissertation, Purdue University, West Lafayette, Indiana, USA, 2006.
24. Christensen, B.J., Coverdale, R.T., Olson, R.A., Ford, S.J., Garboczi, E.J., Jennings, H.M. and Mason, T.O., Impedance spectroscopy of hydrating cement-based materials: Measurement, interpretation, and application, *The American Ceramic Society*, 1994, Vol. 77, No. 11, pp. 2789-2802.
25. Taylor, H.F.W., *Cement Chemistry*, Academic Press, London, (1990)
26. Bockris, J.O.M., and Reddy, A.K.N., *Modern electrochemistry*, Vol. 1, Section 4.4, 1970, Plenum, New York City, NY, USA.
27. Snyder, K.A., Feng, X., Keen, B.D. and Mason, T.O., Estimating the electrical conductivity of cement paste pore solutions from OH-, K+ and Na+ concentrations, *Cement and Concrete Research*, 2003, Vol. 33, No. 6, pp. 793-798.
28. Hansen, F., and Pedersen, E. J., Maturity computer for controlled curing and hardening of concrete, *Nordisk Betong*, 1977, No. 1, pp. 21-25 (in Danish).
29. _____. *Standard practice for estimating concrete strength by the maturity method*, ASTM C1074-04, ASTM International, West Conshohocken, Pennsylvania, USA, 2004.
30. Lane, D.S., Supplanting the rapid chloride permeability test with a quick measurement of concrete conductivity, Virginia Transportation Research Council, Charlottesville, Virginia, USA, 2005.



Mr. Gaurav Sant received his bachelor's (BSCE) and master's degrees (MSCE) in civil engineering from Purdue University with an emphasis in construction materials. Currently, he is pursuing his PhD at the School of Civil Engineering at Purdue University. His research interests include early-age shrinkage and cracking, non-destructive testing and moisture transport in cementitious materials.



Dr. Farshad Rajabipour received his BSc from Sharif University of Technology (Tehran) and his MS and PhD from Purdue University. Currently, he is an assistant professor of civil and environmental engineering at the University of Hawaii, Mānoa. His research interests include materials science of concrete, construction sustainability and use of recycled materials, and non-destructive testing and health monitoring.



Prof. Jason Weiss is associate head in the School of Civil Engineering at Purdue University and the associate director of the National Science Foundation, Center for Advanced Cement Based Materials at Northwestern University. His research interests include early-age shrinkage, cracking and its influence on durability, durability of environmentally friendly binders, moisture transport and service-life predictions of civil infrastructure.

R. P. Spragg,¹ J. Castro,² T. Nantung,³ M. Paredes,⁴ and J. Weiss⁵

Variability Analysis of the Bulk Resistivity Measured Using Concrete Cylinders

REFERENCE: Spragg, R. P., Castro, J., Nantung, T., Paredes, M., and Weiss, J., "Variability Analysis of the Bulk Resistivity Measured Using Concrete Cylinders," *Advances in Civil Engineering Materials*, Vol. 1, Issue 1, 2012, pp. 1–17, doi:10.1520/ACEM104596. ISSN 2165-3984.

ABSTRACT: Many agencies are interested in using a rapid test method for measuring the electrical properties of concrete (i.e., the resistivity or conductivity) because the electrical properties can be related to fluid transport (e.g., ion diffusion). The advantage of electrical testing is that it is relatively easy to perform, and the test method is relatively fast (it takes less than a minute). Over the past century, many studies have investigated different approaches for measuring electrical properties. This paper describes the variability associated with measuring the bulk resistivity along the longitudinal axis of a cylinder after placing electrodes on either end. A multi-laboratory evaluation was performed at ten laboratories. Data from this evaluation provided variability data for 12 concrete mixtures at testing ages of 28, 56, and 91 days. Information on the variability is important in the development of precision and bias statements for standard test methods. In addition, this work discusses how the resistivity results obtained from this test can be correlated with surface resistivity measurements made using a Wenner probe. Linear agreement was noticed between the Wenner test and the measurement through the cylinder, but with a factor confirmed by previous research by Morris et al. ("Practical Evaluation of Resistivity of Concrete in Test Cylinders Using a Wenner Array Probe," *Cem. Concr. Res.*, Vol. 26, 1996, pp. 1779–1787). Additionally, the effect of electrode resistance is discussed, and for high resistivity concrete such as that used in much transportation infrastructure, this effect appears to be negligible; however, it can be accounted for easily.

KEYWORDS: concrete, resistivity, surface resistivity, bulk resistivity, RCPT, electrical properties, electrode resistance, variability, precision statements, standard development, inter-laboratory test, round-robin test

Introduction

Over the past century, tests have been proposed for measuring the electrical properties of concrete [1–7]. These methods have the advantage of being relatively fast, and the principle behind these tests is relatively straightforward. Concrete is a composite consisting of a vapor phase (vapor filled porosity or "air"), a solid phase (aggregate and cementitious solids), and a fluid phase (the pore solution), and the resistivity of each of these individual phases is very different. The resistivities of the solid and vapor phases are extremely low, approximated as 10^9 and 10^{15} Ohm-meter, respectively, whereas the resistivity of the liquid phase is several orders of magnitude lower, ranging from 1×10^{-2} to 5×10^{-2} Ohm-meter [8,9]. As such, it can be assumed that the majority of conduction occurs through the pore fluid. A number of composite models have been developed in which this

Manuscript received December 2, 2011; accepted for publication April 3, 2012; published online July 2012.

¹Graduate Research Assistant, Purdue Univ., School of Civil Engineering, 550 Stadium Mall Dr., West Lafayette, IN 47907, e-mail: rspragg@purdue.edu

²Assistant Professor, Pontificia Universidad Catolica de Chile, School of Civil Engineering, Casilla 306, Correo 22, Santiago, Chile 6904411, e-mail: jecastro@ing.puc.cl

³Manager for Pavement Materials and Construction Research, Indiana Dept. of Transportation, Division of Research and Development, P.O. Box 2279, West Lafayette, IN 47906, e-mail: tnantung@indot.in.gov

⁴State Corrosion Engineer, Florida Dept. of Transportation State Materials Office, Corrosion Research and Durability Laboratory, 6007 NE 39th Ave., Gainesville, FL 32609, e-mail: mario.paredes@dot.state.fl.us

⁵Professor of Civil Engineering, Director of Pankow Materials Laboratory, Purdue Univ., School of Civil Engineering, 550 Stadium Mall Dr., West Lafayette, IN 47907, e-mail: wjweiss@purdue.edu

concept is used [10–13]. Two of the more popular equations that are used in the cement and concrete literature are Archie's expression and the modified parallel expression [11,14]. Several documents have reviewed these methods previously; the goal of this section is to describe how the overall resistivity is dependent on three factors (the resistivity of the fluid in the pores, the degree of saturation of the concrete, and the volume and connectivity of the pore network), as illustrated in Eq 1.

$$\rho = \rho_0 \cdot F \cdot \frac{1}{f(S)} \quad (1)$$

where:

ρ = bulk resistivity,

ρ_0 = resistivity of the fluid phase,

F = formation factor that is the product of the pore volume and a tortuosity coefficient, and

$f(s)$ = function that describes the degree of saturation, which is taken as 1 for a saturated system.

This implies that the resistivity decreases with a higher water content (i.e., pore volume) and a more open pore network (i.e., a lower tortuosity coefficient). This expression can also be written in terms of electrical conductivity, as it is simply the inverse of the electrical resistivity.

One of the more popular test methods that is currently performed based on electrical concepts is the rapid chloride permeability (RCP) test [15,16]. This test method involves placing a saturated concrete specimen, typically 102 mm in diameter and 51 mm thick, between electrodes in different solutions and integrating the charge that is passed over a 6 h testing period [15]. Although this test has come into wide use, a few drawbacks have been highlighted out [17–19]. First, this test is performed using high voltages and a direct current, which limits each sample to providing a single measurement at a single age. Second, saturating the specimen can require a relatively long preparation time. Third, there is potential for heating effects due to the large voltage and possible modification of the microstructure [20,21]. Research has been conducted regarding temperature correction for the RCP test [22,23], and many changes to this test have been proposed, including extrapolating the charge passed after a test duration of 30 min to the 6 h value [24], increasing the size of the reservoirs to reduce the heating effects [25], reducing the large voltages in the test [26], and using a single resistance reading measured at an early age, often 1 min or 5 min [18,19].

Alternative testing methods have been proposed that require little to no sample preparation and which allow the sample to be tested at different ages. One rapid test for the electrical resistivity of concrete is the Wenner probe. As with any test, there are certain considerations that can impact the results. For example, the probe spacing, the geometry of the sample, the aggregate size, and surface moisture conditions can all influence the measured electrical response [27]. Because the moisture conditions at the surface of the test specimen are quite important, care should be taken to protect against drying or using surface treated concretes [28–30]. Additionally, some work has suggested the need for an additional non-linear geometry factor for this method that occurs from the constricted geometry, such as that of a standard test cylinder [27]. Further, when this method is used on real structures, the location and proximity of the rebar need to be considered [31,32].

Several of these concerns can be addressed if a standard testing protocol is adopted. A draft test method has been developed that uses a four-probe Wenner configuration on a 102 mm × 204 mm

standard test cylinder with a probe tip spacing of 38 mm. Temperature monitoring can be difficult and is frequently not done [33]. This surface resistivity (SR) test method places the probes directly on the surface of the test specimen. This test method has recently been accepted for use by the Louisiana Department of Transportation and the Florida Department of Transportation on select projects, and preliminary work has been done to expand its use for quality control [28,34]. Work has also been done to correlate RCP testing and diffusion testing with SR [28,35,36]. This method has a distinct advantage in that it can be performed rapidly and is easy to perform on the surface of a cylinder.

The resistance of a concrete cylinder can alternatively be evaluated by using plate electrodes that can be placed on the end of the sample [32,37]. The resistance value obtained can be normalized by means of specimen geometry—simply, the ratio of the sample cross-sectional area to the length—in order to obtain the sample resistivity, termed the bulk resistivity (BR). For this test, good electrical contact must be ensured between the plate electrodes and the test specimen [27,37]. This can be assisted through the use of a conductive medium, but the surface finish of the cylinder ends should be flat. Some work has previously been performed with regard to evaluating the contact pressure between the plate and the specimen [37]. Like other electrical tests, this method is subject to the influence of the specimen's moisture content and temperature. This test, however, has the distinct advantages of rapid testing and a simple geometry factor. To the best of the authors' knowledge, a multi-laboratory evaluation of variability has not been performed on this geometry, though some studies have reported exchanges of samples between two laboratories [37].

Three major factors that should be considered in any electrical resistivity testing are (1) the influence of geometry, (2) the influence of temperature, and (3) the influence of moisture. First, whereas the normalized BR of concrete can be considered a material property, the tests that are performed provide a measure of electrical resistance. The resistance measurements need to be corrected for the geometry of the test. Geometry factors can be determined experimentally [8,38] or numerically [27] and are largely dependent on the current flow through the material. A uniform current flow through the bulk of the geometry provides an easy geometry factor, the ratio of the cross-sectional area to the length. Other tests do not have this uniform current path, so the geometry factor is different. Temperature is another important factor in the testing of concrete resistivity. As the primary conduction path is through the ionic pore solution, an increase in the temperature increases the mobility of the ions, decreasing the resistivity. There has been work that has investigated the possibility of a temperature correction for resistivity tests [6,39–43]. In this work, the samples are all tested in laboratory conditions; as such, the sample temperature should be $23^{\circ}\text{C} \pm 2^{\circ}\text{C}$. Lastly, the degree of saturation is a major component in resistivity testing of concrete. As a result, knowledge of the moisture history and moisture content at testing are important considerations in the evaluation of resistivity data [44].

The main objectives of this evaluation are fourfold. First, it provides some background on electrical property measurements for concrete and provides some of the physical principles behind these tests. Second, it presents the results of an inter-laboratory evaluation of the variation in the electrical BR of concrete. This information can be used in the development of precision and bias statements. Third, it demonstrates the relationship between surface resistance test methods (e.g., Wenner) and measurements performed on a bulk cylindrical geometry. Fourth, it highlights important considerations in the development of testing standards and policies for the use of electrical methods as quality control/quality assurance tests.

Experimental Details

Materials

A round-robin testing program was proposed in 2009 for the evaluation of the repeatability of Wenner and bulk resistance tests on concrete cylinders. A series of 12 concrete mixtures were prepared at the laboratories that participated in this evaluation (Table 1). The mixtures are structural/bridge deck concretes used by state departments of transportation from around the United States. A final report detailing a parallel series of Wenner and BR tests conducted by the American Association of State Highway and Transportation Officials Technology Implementation Group is available [45]. It should be noted that a wide range of cements, supplementary materials, and aggregates were used in this investigation.

Sample Conditioning

The samples were demolded at an age of 48 h and placed into a saturated lime-water bath that was kept at a constant room temperature until the age of testing ($23^{\circ}\text{C} \pm 2^{\circ}\text{C}$). At an age of 14 days, the respective laboratories removed the samples and wrapped them in paper towels soaked in saturated lime-water. The samples were then double-bagged and prepared for two-day shipping to the other participating laboratories. The goal was to ensure that the samples remained wet during testing.

After the samples were received by the other testing laboratories, they were removed from the bag and placed into saturated lime-water baths kept at room temperature ($23^{\circ}\text{C} \pm 2^{\circ}\text{C}$). At ages of 28, 56, and 91 days, the samples were removed from the saturated lime bath, the surface was wiped dry, and the samples were tested for SR and BR. After this testing, the samples were placed back in the saturated lime-water.

Testing Procedure

It should be noted that the test described herein (with the plates placed on the end of the cylinder) was a part of a larger evaluation of variation conducted by the AASTHO TIG [45,46]. Not all of the laboratories chose to participate in this portion of the evaluation, and the nonparticipating

TABLE 1—Summary of mixture proportions used in this evaluation (for Saturated Surface Dry conditions).

Mixture Number	Water, w/cm	Cement, kg/m ³	Fly Ash, kg/m ³	Micron Fly Ash, kg/m ³	Slag, kg/m ³	Silica Fume, kg/m ³	Meta-kaolin, kg/m ³	Coarse Aggregate 1, kg/m ³	Coarse Aggregate 2, kg/m ³	Fine Aggregate, kg/m ³
1	0.34	163	237	119	...	119	...	1059	...	717
2	0.40	144	285	71	282	854	824
3	0.39	199	392	119	785	...	724
4	0.35	158	279	178	940	...	793
5	0.40	164	308	103	909	...	879
6	0.37	145	390	1068	...	712
7	0.40	160	297	80	24	532	528	686
8	0.39	131	251	84	555	...	1295
9	0.41	151	291	65	15	1032	...	697
10	0.30	151	297	153	44	1009	...	638
11	0.30	157	430	95	1033	...	577
12	0.35	156	402	44	1009	...	624

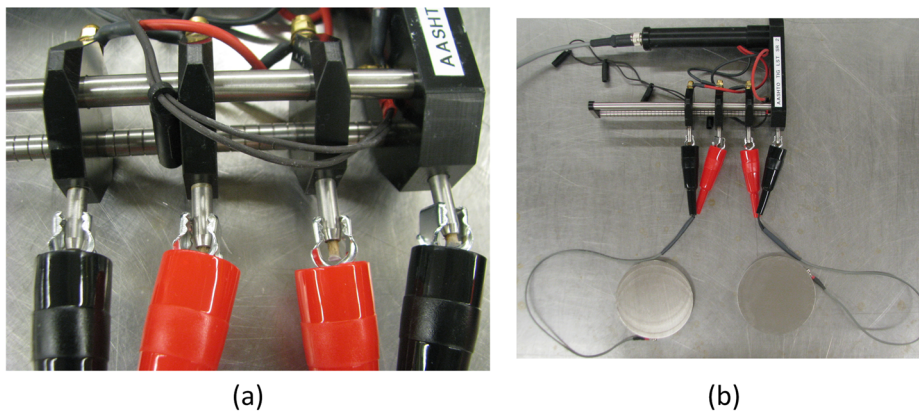


FIG. 1—Attachment of the alligator clips to the Wenner probe tips: (a) close-up; (b) at a distance. The steel plates have a diameter of 102 mm, and the probe tip spacing is 38 mm.

laboratories have been excluded from the following data; however, in order to avoid confusion, the original laboratory numbers were retained.

Equipment

The equipment involved in this test consisted of a CNS Farnell Mk II U95 SR meter using an alternating current at a frequency of 13 Hz, a set of 102 mm diameter stainless steel plate electrodes, and 16 AWG two-conductor wire used to connect the probe tips of the SR meter to the plate electrodes.

The cable was outfitted with alligator clips on one end to allow easy access to the probe tips of the resistivity meter. The other end of the cable was outfitted with a ring terminal to connect to the plate electrode. The plate electrode was drilled and tapped to allow easy and consistent attachment.

It is important to ensure proper electrical contact between the cylinder and the plate electrodes [27,37]. For this evaluation, this was done using thin lime-water-saturated sponges.

Testing Procedure

The plate electrodes should be connected to the pins of the SR meter. The first two pins that generate the current and measure the potential were connected to one of the steel plate electrodes, and likewise for the second set of pins, as shown in Fig. 1.

The resistances of the top and bottom sponges were then measured, as shown in Fig. 2. The resistance of each individual sponge is largely dependent on its moisture content. The moisture content of the sponge is dependent on the weight placed on top of it (e.g., large weights push more water from the sponge). In order to ensure that the moisture contents remain the same, the weight it carries during the test was used. For the top sponge, only the top plate was used as a weight. For the bottom cylinder, the top plate and the cylinder were used to provide the weight, but the cylinder was placed above the top plate, so its resistance was not measured. The goal of this was to provide a correction for sponge resistance, as discussed below. The concrete cylinder was then placed between the plate electrodes, with sponges being placed between the plates and the concrete cylinder, as shown in Fig. 3.

Calculations

The resistances of the top and bottom sponge are termed $R_{\text{top sponge}}$ and $R_{\text{bottom sponge}}$, respectively. The measured resistance of the system (two sponges and a specimen), as depicted in Fig. 3, is

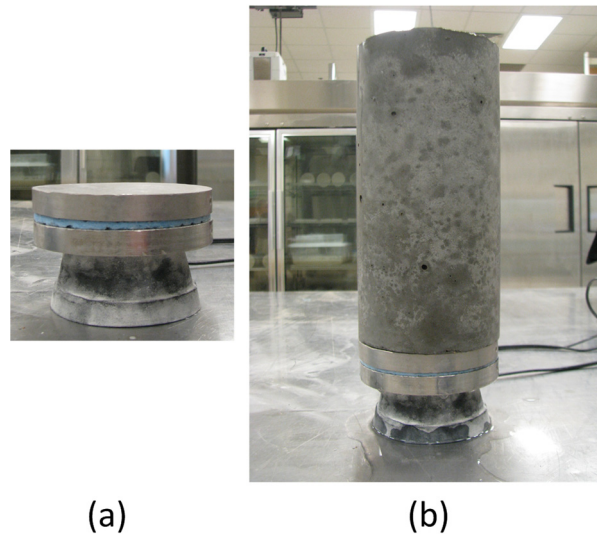


FIG. 2—Measuring the sponge resistance for (a) the top and (b) the bottom sponges. The steel plates have a diameter of 102 mm, and the test cylinder is a standard 102 mm × 204 mm.

termed R_{measured} . The measured resistance was corrected for the resistance of the sponges by treating the system as resistors in series, as shown in Fig. 2 [37]. It was noticed for the sponges used in this evaluation that the resistance values in each lab tended to remain relatively constant. Thus, for sponges that show this constant resistance, it is proposed that they be measured only periodically, and their resistances can be assumed to remain unchanged between measurements.

$$R_{\text{cylinder}} = R_{\text{measured}} - R_{\text{top sponge}} - R_{\text{bottom sponge}} \quad (2)$$

The BR, denoted as ρ , can be determined using Equation 3. The geometry factor K for the current flow through the bulk material is given by Equation 4. This can be extended to other sample geometries through experimental testing [8].

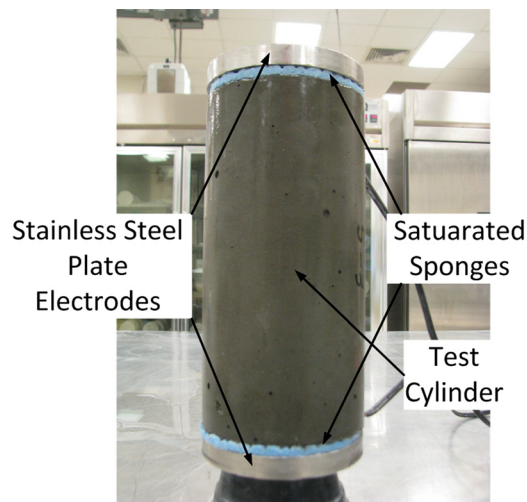


FIG. 3—Measuring the resistance of the system. The test cylinder is a standard 102 mm × 204 mm.

$$\rho = KR_{\text{cylinder}} \tag{3}$$

$$K = \frac{A}{L} \tag{4}$$

where:

R_{cylinder} = calculated resistance of the concrete test cylinder from Eq 1,

A = cross-sectional area, and

L = length of the test specimen.

Results and Discussion

Bulk Resistivity Data

The samples were tested at three ages: 28, 56, and 91 days. The average BR (Avg.) and variance (Var.) of three test cylinders measured at each testing age for each mixture by each testing laboratory are presented in Tables 2–4. Cells marked with “n/a” signify that no data were reported. The last row in each table represents the pooled statistics, calculated according to ASTM C802 [47].

Data measured at an age of 28 days are presented in Table 2. Mixtures 1 through 5 were not tested for 28 day BR, as the equipment was being distributed. Data measured at an age of 56 days are presented in Table 3. Mixture 1 was not tested for 56 day BR because the equipment had still not been received. Data measured at an age of 91 days are presented in Table 4.

TABLE 2—Average BR and variance obtained at a testing age of 28 days, kohm-cm.

Laboratory		Mixture											
		1	2	3	4	5	6	7	8	9	10	11	12
1	Avg.	n/a	n/a	n/a	n/a	n/a	5.29	13.41	14.97	8.84	12.67	6.46	14.89
	Var.	n/a	n/a	n/a	n/a	n/a	0.03	0.15	1.28	0.16	0.06	0.03	0.82
2	Avg.	n/a	n/a	n/a	n/a	n/a	5.27	14.12	16.98	8.36	13.49	6.73	18.84
	Var.	n/a	n/a	n/a	n/a	n/a	0.01	0.21	0.18	0.02	0.30	0.64	0.61
3	Avg.	n/a	n/a	n/a	n/a	n/a	5.19	13.54	14.03	7.69	11.53	5.43	16.04
	Var.	n/a	n/a	n/a	n/a	n/a	0.03	0.12	0.24	0.14	0.17	0.05	1.71
5	Avg.	n/a	n/a	n/a	n/a	n/a	5.65	15.19	16.73	8.31	16.93	7.36	n/a
	Var.	n/a	n/a	n/a	n/a	n/a	0.05	0.10	0.47	0.13	0.16	0.10	n/a
6	Avg.	n/a	n/a	n/a	n/a	n/a	5.55	15.24	15.69	9.60	13.72	6.68	20.24
	Var.	n/a	n/a	n/a	n/a	n/a	0.10	0.17	0.09	0.08	0.43	0.05	0.01
7	Avg.	n/a	n/a	n/a	n/a	n/a	5.03	13.59	15.01	8.91	12.87	6.88	16.90
	Var.	n/a	n/a	n/a	n/a	n/a	0.04	0.12	0.16	0.01	0.14	0.07	0.07
8	Avg.	n/a	n/a	n/a	n/a	n/a	5.84	14.36	16.58	8.63	14.59	6.81	18.21
	Var.	n/a	n/a	n/a	n/a	n/a	0.03	0.36	0.14	0.10	0.45	0.13	0.15
9	Avg.	n/a	n/a	n/a	n/a	n/a	5.31	14.39	16.37	8.91	13.15	7.00	16.48
	Var.	n/a	n/a	n/a	n/a	n/a	0.00	0.01	0.11	0.05	0.40	0.04	0.84
10	Avg.	n/a	n/a	n/a	n/a	n/a	5.12	14.20	15.60	8.62	14.22	6.77	18.55
	Var.	n/a	n/a	n/a	n/a	n/a	0.00	0.05	0.02	0.39	0.13	0.01	0.12
12	Avg.	n/a	n/a	n/a	n/a	n/a	5.68	14.02	15.11	8.30	12.30	6.40	16.76
	Var.	n/a	n/a	n/a	n/a	n/a	0.01	0.20	0.04	0.21	0.26	0.13	0.11
All labs	Mean	n/a	n/a	n/a	n/a	n/a	5.39	14.21	15.71	8.62	13.55	6.65	17.43
	Pooled variance	n/a	n/a	n/a	n/a	n/a	0.03	0.15	0.27	0.13	0.25	0.13	0.49
	Variance	n/a	n/a	n/a	n/a	n/a	0.07	0.40	0.90	0.26	2.22	0.26	2.72

TABLE 3—Average BR and variance obtained at a testing age of 56 days, kohm-cm.

Laboratory		Mixture											
		1	2	3	4	5	6	7	8	9	10	11	12
1	Avg.	n/a	6.73	8.76	12.63	8.07	6.56	24.34	29.99	14.78	22.20	11.98	18.14
	Var.	n/a	0.07	0.08	0.18	0.01	0.03	0.04	0.05	0.15	0.34	0.09	0.03
2	Avg.	n/a	8.64	9.10	12.05	10.83	7.22	24.52	27.25	13.14	22.53	12.69	20.12
	Var.	n/a	0.38	0.05	0.10	0.65	0.09	1.28	0.11	0.05	0.79	0.64	0.42
3	Avg.	n/a	6.18	7.81	12.26	7.71	5.81	23.13	21.61	12.17	17.26	n/a	17.71
	Var.	n/a	0.23	0.05	0.01	0.00	0.00	0.73	0.39	0.11	0.19	n/a	1.48
5	Avg.	n/a	7.98	9.26	11.41	7.26	7.08	24.10	29.12	14.92	22.48	10.91	n/a
	Var.	n/a	0.00	0.48	0.03	0.12	0.02	0.39	0.24	1.12	0.14	0.01	n/a
6	Avg.	n/a	7.70	9.16	12.89	9.99	6.70	n/a	25.02	n/a	19.62	10.09	21.49
	Var.	n/a	0.06	0.46	0.02	0.01	0.21	n/a	0.87	n/a	0.78	0.08	0.12
7	Avg.	n/a	8.38	8.55	12.34	8.33	6.57	24.20	27.18	16.50	21.37	12.16	19.88
	Var.	n/a	0.64	0.09	0.08	0.05	0.04	0.27	1.46	0.06	0.02	1.03	0.62
8	Avg.	n/a	7.18	9.27	13.64	9.31	6.72	25.89	31.29	14.38	24.98	12.55	20.85
	Var.	n/a	0.18	0.12	0.06	0.08	0.03	1.73	0.68	0.25	0.36	0.10	0.46
9	Avg.	n/a	n/a	9.20	13.50	8.59	6.52	26.09	30.28	15.13	23.23	13.43	20.27
	Var.	n/a	n/a	0.11	0.72	0.01	0.05	0.07	0.81	0.10	0.93	0.22	0.25
10	Avg.	n/a	7.98	8.92	14.85	7.94	6.26	26.58	26.03	14.20	22.24	11.22	21.46
	Var.	n/a	0.00	0.23	0.61	0.13	0.01	0.34	0.08	0.81	0.17	0.03	0.25
12	Avg.	n/a	6.10	8.34	11.94	7.90	6.52	22.21	23.65	13.06	18.67	9.95	15.99
	Var.	n/a	0.03	0.01	0.03	0.16	0.03	1.76	0.68	0.53	0.73	0.05	0.86
All labs	Mean	n/a	7.43	8.84	12.75	8.59	6.59	24.56	27.14	14.25	21.46	11.66	19.55
	Pooled variance	n/a	0.18	0.17	0.18	0.12	0.05	0.73	0.54	0.35	0.44	0.25	0.50
	Variance	n/a	0.86	0.23	1.02	1.25	0.15	2.02	9.74	1.70	5.29	1.44	3.52

The data presented in Tables 2 through 4 were analyzed according to ASTM C802 in order to determine the corresponding components of variance for the variability from within-laboratory and multi-laboratory data. The within-laboratory variability is typically attributed to variability stemming from the operator, as well as variability inherent in the test equipment and in the samples being tested. It should be noted that when using the approach taken for this round-robin testing, variations between samples arising from sample preparation issues could contribute to this component of variability. This is discussed later in this paper.

The data were also analyzed to evaluate the relationship between the variability of each of the mixtures and the properties of that mixture. Specifically, the w/c and the mass fraction of cementitious materials were evaluated. No significant correlation was seen between the variability and these mixture characteristics.

Within-laboratory Variability

The operator variability, the variability of specimens, and the inherent variability in the mixture are all grouped together into the within-laboratory variability. This value is computed using the average within-laboratory coefficient of variation (COV), presented in Table 5 [47]. Previous work evaluating the development of an automated resistivity testing system has reported a similar within-laboratory COV of around 3 % to 4 % for samples older than 24 h [48]. It should be noted that the variation increases over time. It is believed that this might be due to slight variations in

TABLE 4—Average BR and variance obtained at a testing age of 91 days, kohm-cm.

Laboratory		Mixture											
		1	2	3	4	5	6	7	8	9	10	11	12
1	Avg.	10.24	8.07	12.14	18.71	11.36	7.58	38.05	42.08	19.44	34.98	17.90	18.80
	Var.	0.19	0.05	0.23	0.39	0.02	0.06	0.01	7.14	0.37	1.22	0.20	0.79
2	Avg.	12.16	10.43	15.12	18.83	16.81	8.31	32.40	39.19	17.58	29.78	16.17	24.58
	Var.	0.48	0.12	0.94	0.77	0.62	0.04	2.72	0.25	0.04	1.25	0.89	1.08
3	Avg.	10.43	7.85	10.61	16.58	9.46	6.65	28.87	31.78	14.63	22.71	13.10	17.18
	Var.	0.16	0.43	0.68	0.07	0.19	0.26	2.12	2.63	0.32	0.21	0.79	0.36
5	Avg.	11.01	8.36	12.12	16.21	10.20	8.48	33.45	37.14	20.19	28.66	15.45	n/a
	Var.	0.20	0.02	0.47	0.05	0.16	0.02	0.50	1.07	2.72	0.27	0.29	n/a
6	Avg.	13.91	10.11	14.34	23.58	n/a	7.65	30.97	30.81	15.60	29.92	15.80	20.96
	Var.	0.00	0.03	1.04	0.09	n/a	0.40	0.98	0.05	0.35	0.89	0.06	0.01
7	Avg.	10.67	10.05	14.11	19.27	12.58	7.94	35.83	40.06	20.81	29.55	17.18	21.03
	Var.	0.15	0.44	0.83	0.04	0.08	0.03	0.70	2.41	0.05	0.10	0.03	0.48
8	Avg.	12.22	8.92	13.25	20.47	13.29	7.67	38.06	45.59	19.19	35.36	18.49	20.29
	Var.	0.02	0.23	0.18	0.23	0.11	0.05	4.03	1.94	0.43	1.04	0.18	0.51
9	Avg.	11.16	10.09	14.35	19.54	12.06	8.60	37.74	43.37	n/a	34.48	22.41	19.55
	Var.	0.00	0.59	0.05	2.77	0.10	0.42	0.02	9.91	n/a	3.77	4.91	0.79
10	Avg.	12.39	9.75	13.71	22.44	12.65	6.74	37.54	38.41	18.26	30.51	16.50	21.15
	Var.	0.07	0.80	0.34	2.00	1.42	0.00	0.24	0.08	1.21	0.46	0.14	0.23
12	Avg.	10.07	7.82	11.12	15.96	10.40	7.26	31.21	33.11	14.93	22.67	12.69	18.01
	Var.	0.23	0.02	0.00	0.04	0.15	0.04	3.08	1.92	0.52	0.78	0.01	0.02
All labs	Mean	11.43	9.15	13.09	19.16	12.09	7.69	34.41	38.15	17.85	29.86	16.57	20.17
	Pooled variance	0.15	0.27	0.47	0.65	0.32	0.13	1.44	2.74	0.67	1.00	0.75	0.47
	Variance	1.48	1.10	2.29	6.45	4.77	0.45	11.91	24.83	5.35	20.28	7.67	4.70

curing conditions that might have occurred at each lab, which could have amplified differences over time.

Multi-laboratory Variability

The multi-laboratory variability can be described by the average COV computed from the multi-laboratory component of variance [47]. The average values of the multi-laboratory COV are shown in Table 6. It should be noted that the variation increases over time. Again, slight variations in curing conditions that might have occurred at each lab could have amplified differences over time.

Precision Statements

Precision estimates were calculated [49]. For this experiment, the fundamental statistic was determined to be the COV, represented as 1s% in ASTM C670. Therefore, the calculated precision

TABLE 5—Average within-laboratory coefficient of variation.

Testing Age, days	Within-laboratory Coefficient of Variation, %
28	3.34
56	3.87
91	4.36

TABLE 6—Average multi-laboratory coefficient of variation.

Testing Age, days	Multi-laboratory Coefficient of Variation, %
28	7.75
56	9.83
91	13.22

indices correspond to d_{2s} as described in ASTM C670, determined by multiplying the average COV by the factor $2\sqrt{2}$ [49]. This index represents the maximum difference between two individual test results, expressed as a percentage of their average. The precision indices for different testing ages are shown in Table 7. The maximum precision index for within-laboratory and multi-laboratory variability is used to form the precision statements, which correspond to a testing age of 91 days.

The maximum pooled single-operator COV was found to be 4.36 %. Therefore, the results of two tests properly conducted by the same operator on the same concrete material at the same age are not expected to differ by more than 12.34 % of their average. The maximum pooled multi-laboratory COV was found to be 13.22 %. Therefore, the results of two tests properly conducted by different laboratories on the same concrete material at the same age are not expected to differ by more than 37.38 % of their average.

The precision statements for BR presented in this paper can be compared with the precision statements for other electrical test methods, namely, the RCP test and a corresponding SR test. The variability of the RCP test was obtained from the corresponding ASTM standard [15], and SR data were obtained from a report detailing the resistivity round robin [45]. For consistency, the SR data from Ref 45 were analyzed according to the same procedure described in this paper. Two tests done by the same operator on material from the same concrete mixture should not differ from their average by more than 42 % for the RCP test, 13.28 % for the SR test (with each test consisting of eight average measurements), and 12.34 % for the BR test (with each test consisting of one measurement). For tests conducted in separate laboratories, results should not differ from their average by more than 51 % for the RCP test, 34.55 % for the SR test, and 37.38 % for the BR test. It should be noted that because the SR test is sensitive to the specific location in which measurements is taken, an average of eight measurements is taken for each sample, which contributes to smaller variability in the pooled statistics. However, this means that more time is needed in order to perform the test. Conversely, the bulk measurement described herein is a single measurement.

Correlation with Other Electrical Test Methods

SR measurements were conducted as a part of this evaluation [45]. Figure 4 compares the measured SR and the calculated BR.

TABLE 7—Precision indices for bulk resistivity.

Testing Age, days	Within-laboratory	Multi-laboratory
28	9.44	21.93
56	10.94	27.82
91	12.34	37.38

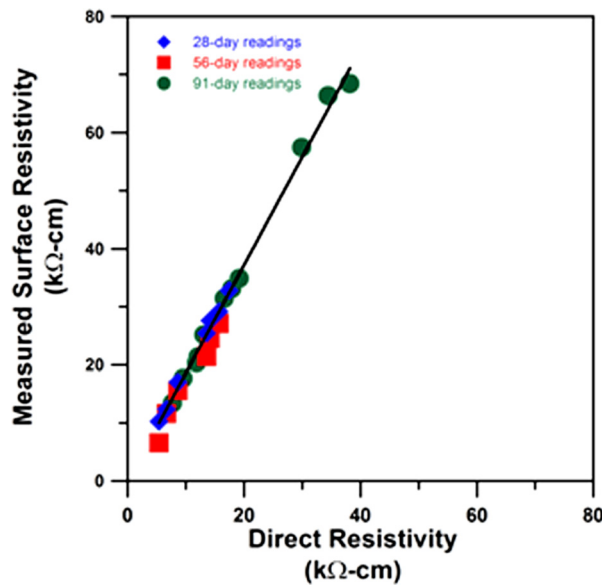


FIG. 4—Correlation of measured SR and BR of samples of differing ages; each data point represents the average of three samples.

A linear correlation was noticed, with $R^2 = 0.9986$, and with SR measurements tending to be 1.86 times higher than the BR. The large data in the experimental results support previous work using finite element methods that showed that additional geometry factors must be used in order to account for aspects of the test geometry, such as probe spacing, cylinder length, and cylinder diameter [27]. The factor of 1.86 is in good agreement with the geometric correction proposed by Morris et al. [27] for a cylinder with a length of 205 mm, a diameter of 102 mm, a probe spacing of 38.1 mm, and a maximum aggregate size of 19 mm, which was approximately 1.9.

As the RCP test is a widely used test for mixture characterization, Table 8 has been prepared to relate concrete resistivity to values obtained from RCP and SR testing. Previous empirical studies have also shown that RCP values can be related to concrete resistivity, termed the Berke empirical, and to the apparent SR, termed the Paredes empirical [28,36]. The total charge passed during the RCP test is used with Ohm’s law, an assumed testing period of 6 h, and a voltage of 60 V to

TABLE 8—Relationships between values obtained via different electrical test methods.

ASTM C1202 Classification ^a	Charge Passed, Coulombs ^a	Direct Resistivity, kohm-cm ^b	Berke Empirical, kohm-cm	Paredes Empirical, kohm-cm ^c	Apparent Surface Resistivity (102 mm × 205 mm), kohm-cm ^d
High	>4000	<5.2	<4.9	<6.5	<9.7
Moderate	2000–4000	5.2–10.4	4.9–8.76	6.5–11.3	9.7–19.3
Low	1000–2000	10.4–20.8	8.8–15.6	11.3–19.9	19.3–38.6
Very low	100–1000	20.8–207	15.6–105.9	19.9–136.6	38.6–386
Negligible	<100	>207	>105.9	>136.6	>386

^aFrom ASTM C1202 [15].

^bCalculated using Ohm’s law and geometry.

^cCorrected for geometry from Kessler et al. [28].

^dBulk resistivity multiplied by geometry factor.

determine the resistance. The standard test specimen (i.e., a 102 mm × 51 mm disc) can be normalized by the geometry using the factor described in Eq 4 to determine the BR [15]. This is a direct computation that does not consider the temperature effects or possible damage previously discussed. The values for the BR or apparent SR can then be ranked as classified by the RCP test method [15].

Effects of Electrode Resistance

Previous work has shown that electrode resistance (and other factors involved in ensuring connectivity between the electrode and sample) can influence the results as shown in Equation 2.

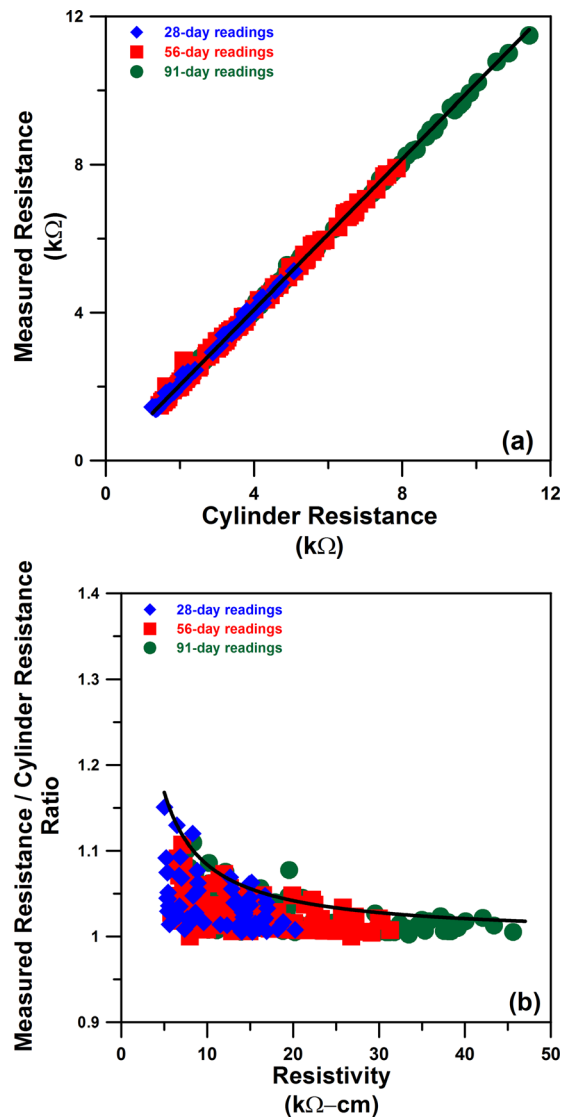


FIG. 5—Influence of electrode resistance on (a) the measured resistance (sample and electrodes) as a function of the cylinder (sample) resistance and (b) the ratio of measured resistance (sample and electrodes) to cylinder (sample) resistance as a function of concrete resistivity.

The major contributor to electrode resistance is poor contact between the plate electrode and the surface of the test cylinder. Some work has suggested the possibility of using flexible electrodes [27]. An alternative solution is to use an aid that allows for good electrical contact. In the laboratory, this can be accomplished through the use of an electrically conductive gel [50,51]. The alternative is to use another soft, conductive medium. Popular solutions have included the use of saturated sponges, chamois cloth, and paper towels [21,37].

An important issue becomes the associated resistance of the sponges. Previously, this associated resistance has been treated as a series of resistors in parallel with the test cylinder, which produces the correction shown and described by Equation 2.

The sponge resistance is largely dependent on the moisture content of the sponges and the conductivity of the solution in which they are saturated. For this evaluation, the solution was saturated lime-water, which was also used as the storage solution for the test cylinders. Furthermore, in order to ensure the proper moisture content, the contact pressure for the sponge was kept constant between the sponge resistivity test and the cylinder test, as shown in Figs. 2 and 3.

Although this correction provides the truest value of the BR, the results of this evaluation show that this correction might not always be very large. For the sponges used in this evaluation, the resistances of the two sponges were much less than the resistance of the cylinder. Figure 5(a) shows the measured resistance (i.e., sample, sponges, and electrodes) as a function of the cylinder resistance (i.e., the sample alone), as defined in Equation 2. The best fit line, given by Eq 5a with an R^2 of 0.9997, shows an average difference of less than 2 % between the measured resistance and the cylinder resistance.

Additionally, the ratio of the measured resistance to the actual cylinder resistance, as defined in the preceding paragraph, can be shown against the concrete resistivity, depicted in Fig. 5(b). This ratio represents the correction from the cylinder resistance. Figure 5(b) shows an upper bound of this ratio, given by Eq 5b. We can see that for lower concrete resistivities, the ratio can be significant. However, for better concrete (i.e., higher resistivity concrete), this ratio approaches 1.

$$\text{Measured Resistance} = 1.019 \times \text{Cylinder Resistance} \quad (5a)$$

$$\frac{\text{Measured Resistance}}{\text{Cylinder Resistance}} = 1.0 + 0.84 \times \frac{1}{\text{Concrete Resistivity}} \quad (5b)$$

Summary and Conclusions

This paper reports results from a multi-laboratory investigation of the variability associated with testing the electrical BR of concrete cylinders by placing plate electrodes on the ends of the cylinder. An analysis of the data is presented. It should be noted that the samples used in this evaluation were conditioned by storing the samples in lime-saturated water between test measurements. The following observations can be made regarding the variability of the resistivity test method: First, resistivity testing is a rapid test that drastically reduces the amount of time a technician needs to spend conditioning the sample and conducting the test. Therefore, this test is well suited for quality control testing. Second, resistivity testing can be considered a non-destructive test. This means that for each mixture being evaluated using resistivity, only a small number of samples need be prepared, and these samples can be measured at several different ages. This can be contrasted with other destructive electrical tests that require a larger series of samples for proper mixture evaluation. In fact, this testing can be performed on cylindrical samples before they are tested for

compressive or splitting tensile strength. Third, the operator and multi-laboratory precision of this test method have been quantified using data from the average COV obtained from an inter-laboratory evaluation consisting of ten laboratories and twelve different mixtures. For the BR test method, the within-laboratory COV is 4.36 %, and the multi-laboratory COV is 13.22 %. Fourth, the specimen geometry can greatly influence the results of an electrical test, and the use of a geometry correction factor is often required. For the BR test, this geometry factor is simply the ratio of the sample cross-sectional area to the sample length. Finally, the effects of electrode resistance were addressed using a series model. Whereas previous work described corrections for end plate resistance, the variability data from this investigation show that for the materials used in this evaluation, the correction that is needed is quite small. It is suggested that a standard resistivity test be developed that could allow samples to be tested using a variety of sample geometries, including (1) the Wenner probe geometry, (2) the bulk resistance described herein, and (3) alternative geometries, provided the geometry factor can be quantified. This could enable the use of all the different methods to obtain the material property known as BR.

Acknowledgments

The experiments reported in this paper were conducted as part of a larger evaluation sponsored by the Pooled Fund Program and the American Association of American Highway and Transportation Official's Technology Implementation Group and organized by the Florida Department of Transportation. The contents of this report reflect the views of the authors, who are responsible for the facts and the accuracy of the data presented herein. The contents do not necessarily reflect the official views or policies of the Indiana Department of Transportation or the Federal Highway Administration at the time of publication. This report does not constitute a standard, specification, or regulation. The writers would like to thank the participating laboratories and testing personnel for their time and efforts in collecting data. This includes, but is not limited to: Rob Reis, Cipriano Manansala, and Joe Shanabrook, California Department of Transportation; Jagan Gudimettla, FHWA Mobile Concrete Laboratory; Celik Ozyildirim and Bill Ordell, Virginia Department of Transportation; Wilfredo Malpica and Javier Molinari, Grupo-Carmelo; Ed McGaffin and Dan Dennis, New York State Department of Transportation; Lieska Halsey, Jeremy Weigel, and Tim Krason, Nebraska Department of Transportation; Eric Prieve and Azis Khan, Colorado Department of Transportation; John Kern and Wayne DeMarco, CEMEX; Thomas Frank and Ronald Simmons, Florida Department of Transportation; and Jeremiah Hersey and Professor Mike Jackson, University of North Florida. The writers also appreciate useful discussions with Ken Snyder and Dale Bentz of the National Institute of Standards and Technology and Kyle Bemis and Professor Bruce Craig of the Statistics Consulting Service at Purdue University

References

- [1] Hammond, E. and Robson, T. D., "Comparison of Electrical Properties of Various Cements and Concretes. I-II," *The Engineer*, Vol. 199, 1955, pp. 78–80.
- [2] Shimizu, Y., "An Electrical Method for Measuring the Setting Time of Portland Cement," *Concrete*, Vol. 32, 1928, pp. 111–113.
- [3] Calleja, J., "Effect of Current Frequency on Measurement of Electrical Resistance of Cement Pastes," *J. Am. Concr. Inst.*, Vol. 24, 1952, pp. 329–332.

- [4] Weiss, W. J., Shane, J. D., Miseses, A., Mason, T. O., and Shah, S. P., "Aspects of Monitoring Moisture Changes Using Electrical Impedance Spectroscopy," *Second Symposium on the Importance of Self Desiccation in Concrete Technology*, June 18, 1999 Lund, Sweden: Lund Institute of Technology, Division of Building Materials.
- [5] Monfore, G. E., *The Electrical Resistivity of Concrete*, Portland Cement Association, Research and Development Laboratories, Skokie, IL, 1968.
- [6] Whittington, H. W., McCarter, J., and Forde, M. C., "The Conduction of Electricity through Concrete," *Mag. Concrete Res.*, Vol. 33, 1981, pp. 48–60.
- [7] Christensen, B. J., Coverdale, R. T., Olson, R. A., Ford, S. J., Garboczi, E. J., Jennings, H. M., and Mason, T. O., "Impedance Spectroscopy of Hydrating Cement-based Materials: Measurement, Interpretation, and Application," *J. Am. Ceram. Soc.*, Vol. 77, 1994, pp. 2789–2804.
- [8] Rajabipour, F., 2006, "In Situ Electrical Sensing and Material Health Monitoring in Concrete Structures," Ph.D. dissertation, Purdue University, West Lafayette, IN.
- [9] Rajabipour, F. and Weiss, J., "Linking Health Monitoring in Concrete Structures with Durability Performance Simulations," *ASCE Structures Congress*, B. Cross and J. Finke, Eds., ASCE, St. Louis, MO, 2006.
- [10] Torquato, S., *Random Heterogeneous Materials: Microstructure and Macroscopic Properties*, Springer, New York, 2002.
- [11] Archie, G. E., "The Electrical Resistivity Log as an Aid in Determining Some Reservoir Characteristics," *Society of Petroleum Engineers Reprint Series*, 2003, pp. 9–16.
- [12] Aplin, K. L., "Aspirated Capacitor Measurements of Air Conductivity and Ion Mobility Spectra," *Rev. Sci. Instrum.*, Vol. 76, 2005, 104501.
- [13] McLachlan, D. S., Blaszkiewicz, M., and Newnham, R. E., "Electrical Resistivity of Composites," *J. Am. Ceram. Soc.*, Vol. 73, 1990, pp. 2187–2203.
- [14] Garboczi, E. J., "Permeability, Diffusivity, and Microstructural Parameters: A Critical Review," *Cem. Concr. Res.*, Vol. 20, 1990, pp. 591–601.
- [15] ASTM C1202, 2010, "Standard Test Method for Electrical Indication of Concrete's Ability to Resist Chloride Ion Penetration," ASTM International, West Conshohocken, PA.
- [16] AASHTO T277, 2007, "Standard Method of Test for Electrical Indication of Concrete's Ability to Resist Chloride Ion Penetration," American Association of State Highway and Transportation Officials, Washington, D.C.
- [17] Shane, J. D., Aldea, C. D., Bouxsein, N. F., Mason, T. O., Jennings, H. M., and Shah, S. P., "Microstructural and Pore Solution Changes Induced by the Rapid Chloride Permeability Test Measured by Impedance Spectroscopy," *Concr. Sci. Eng.*, Vol. 1, 1999, pp. 110–119.
- [18] Riding, K. A., Poole, J. L., Schindler, A. K., Juenger, M. C. G., and Folliard, K. J., "Simplified Concrete Resistivity and Rapid Chloride Permeability Test Method," *ACI Mater. J.*, Vol. 105, 2008, pp. 390–394.
- [19] Snyder, K. A., Ferraris, C., Martys, N. S., and Garboczi, E. J., "Using Impedance Spectroscopy to Assess the Viability of the Rapid Chloride Test for Determining Concrete Conductivity," *J. Res. Natl. Inst. Stand. Technol.*, Vol. 105, 2000, pp. 497–509.
- [20] Sohn, D. and Mason, T. O., "Electrically Induced Microstructural Changes in Portland Cement Pastes," *Adv. Cem. Based Mater.*, Vol. 7, 1998, pp. 81–88.
- [21] Shane, J. D., 2000, "Electrical Conductivity and Transport Properties of Cement-based Materials Measured by Impedance Spectroscopy," Ph.D. dissertation, Northwestern University, Evanston, IL.

- [22] Julio-Betancourt, G. A. and Hooton, R. D., "Study of the Joule Effect on Rapid Chloride Permeability Values and Evaluation of Related Electrical Properties of Concretes," *Cem. Concr. Res.*, Vol. 34, 2004, pp. 1007–1015.
- [23] Bentz, D. P., "A Virtual Rapid Chloride Permeability Test," *Cem. Concr. Compos.*, Vol. 29, 2007, pp. 723–731.
- [24] McGrath, P. F. and Hooton, R. D., "Re-evaluation of the AASHTO T259 90-day Salt Ponding Test," *Cem. Concr. Res.*, Vol. 29, 1999, pp. 1239–1248.
- [25] Yang, C. C., Cho, S. W., and Huang, R., "The Relationship between Charge Passed and the Chloride-ion Concentration in Concrete Using Steady-state Chloride Migration Test," *Cem. Concr. Res.*, Vol. 32, 2002, pp. 217–222.
- [26] Nokken, M. R. and Hooton, R. D., "Electrical Conductivity Testing," *Concr. Int.*, Vol. 28, 2006 pp. 58–63.
- [27] Morris, W., Moreno, E. I., and Sagues, A. A., "Practical Evaluation of Resistivity of Concrete in Test Cylinders Using a Wenner Array Probe," *Cem. Concr. Res.*, Vol. 26, 1996, pp. 1779–1787.
- [28] Kessler, R. J., Powers, R. G., and Paredes, M. A., "Resistivity Measurements of Water Saturated Concrete as an Indicator of Permeability," *Corrosion*, NACE International, Houston, TX, 2005.
- [29] Millard, S. G., "Reinforced Concrete Resistivity Measurement Techniques," *Proc. Inst. Civ. Eng., Part 2. Res. Theory*, Vol. 91, 1991, pp. 71–88.
- [30] Rajabipour, F., Weiss, J., Shane, J. D., Mason, T. O., and Shah, S. P., "Procedure to Interpret Electrical Conductivity Measurements in Cover Concrete during Rewetting," *J. Mater. Civ. Eng.*, Vol. 17, 2005, pp. 586–594.
- [31] Presuel-Moreno, F., Liu, Y., and Paredes, M., "Concrete Resistivity on the Apparent Surface Resistivity Measured via the Four-point Wenner Method," *Corrosion*, NACE International, Atlanta, GA, 2009.
- [32] Polder, R. B., "Test Methods for On Site Measurement of Resistivity of Concrete—A RILEM TC-154 Technical Recommendation," *Constr. Build. Mater.*, Vol. 15, 2001, pp. 125–131.
- [33] FM 5-578, 2004, "Florida Method of Test for Concrete Resistivity as an Electrical Indicator of Its Permeability," Florida Department of Transportation, Tallahassee, FL.
- [34] Rupnow, T. D. and Icenogle, P., *Evaluation of Surface Resistivity Measurements as an Alternative to the Rapid Chloride Permeability Test for Quality Assurance and Acceptance*, Louisiana Department of Transportation, Baton Rouge, LA, 2011, p. 68.
- [35] Vivas, E., Hamilton, H. R. I., and Boyd, A. J., *Permeability of Concrete—Comparison of Conductivity and Diffusion Methods*, Department of Civil and Coastal Engineering, University of Florida, Gainesville, FL, 2007, p. 238.
- [37] Berke, N. S. and Hicks, M. C., "Estimating the Life Cycle of Reinforced Concrete Decks and Marine Piles Using Laboratory Diffusion and Corrosion Data," *Corrosion Forms and Control for Infrastructure*, ASTM STP 1137, V. Chaker, Ed., ASTM International, West Conshohocken, PA, 1992, pp. 207–231.
- [37] Newlands, M. D., Jones, M. R., Kandasami, S., and Harrison, T. A., "Sensitivity of Electrode Contact Solutions and Contact Pressure in Assessing Electrical Resistivity of Concrete," *Mater. Struct.*, Vol. 41, 2008, pp. 621–632.
- [38] Castro, J., Spragg, R., Kompare, P., and Weiss, W. J., "Portland Cement Concrete Pavement Permeability Performance," Joint Transportation Research Program, Indiana Department of Transportation and Purdue University, West Lafayette, IN, 2010.

- [39] Nokken, M., Boddy, A., Wu, X., and Hooton, R. D., "Effects of Temperature, Chemical, and Mineral Admixtures on the Electrical Conductivity of Concrete," *J. ASTM Int.*, Vol. 5:5, 2008.
- [40] Castellote, M., Andrade, C., and Alonso, C., "Temperature Correction, from 3 to 25C of the Electrical Resistivity of Mortars and Concretes," *Industria Italiana del Cemento*, Vol. 71, 2001, pp. 850–851, 916–923.
- [41] Sant, G., Rajabipour, F., and Weiss, J., "The Influence of Temperature on Electrical Conductivity Measurements and Maturity Predictions in Cementitious Materials during Hydration," *Indian Concr. J.*, Vol. 82, 2008, pp. 7–16.
- [42] Villagran Zaccardi, Y. A., Fullea Garcia, J., Huelamo, P., and Di Maio, A. A., "Influence of Temperature and Humidity on Portland Cement Mortar Resistivity Monitored with Inner Sensors," *Mater. Corros.*, Vol. 60, 2009, pp. 294–299.
- [43] McCarter, W. J., Forde, M. C., and Whittington, H. W., "Resistivity Characteristics of Concrete," *Proc. Inst. Civ. Eng. (UK)*, Vol. 71, 1981, pp. 107–117.
- [44] Castro, J., Spragg, R., and Weiss, J., "Water Absorption and Electrical Conductivity for Internally Cured Mortars with a w/c between 0.30 and 0.45," *J. Mater. Civ. Engr.*, Vol 24:2, 2012, pp. 223–231.
- [45] Jackson, N. M., *Results of Round-robin Testing for the Development of Precision Statements for the Surface Resistivity of Water Saturated Concrete*, Report Number: FL/DOT/SMO/11-549, Jackson Research Engineers, Ponte Vedra Beach, FL, 2011.
- [46] AASHTO TP95, 2011, "Draft Standard Method of Test for Surface Resistivity Indication of Concrete's Ability to Resist Chloride Ion Penetration," American Association of State Highway and Transportation Officials, Washington, D.C.
- [47] ASTM C802, 2009, "Standard Practice for Conducting an Interlaboratory Test Program to Determine the Precision of Test Methods for Construction Materials," ASTM International, West Conshohocken, PA.
- [48] Poursaee, A. and Weiss, W. J., "An Automated Electrical Monitoring System (AEMS) to Assess Property Development in Concrete," *Autom. Constr.*, Vol. 19, 2010, pp. 485–490.
- [49] ASTM C670, 2010, "Standard Practice for Preparing Precision and Bias Statements for Test Methods for Construction Materials," ASTM International, West Conshohocken, PA.
- [50] Henkensiefken, R., Castro, J., Bentz, D. P., Nantung, T., and Weiss, J., "Water Absorption in Internally Cured Mortar Made with Water-filled Lightweight Aggregate," *Cem. Concr. Res.*, Vol. 39, 2009, pp. 883–892.
- [51] Thomas, M. D. A., "The Use of Conductive Gel," personal communication, W. J. Weiss, 2008.

1 **Wetting and Drying of Concrete Using Aqueous Solutions Containing Deicing Salts**

2
3
4 Robert P. Spragg
5 Undergraduate Research Assistant
6 School of Civil Engineering
7 Purdue University
8 West Lafayette, IN 47907-2051
9 E-mail: rspragg@purdue.edu
10 Phone: 765.494.0358

11
12 Javier Castro
13 Graduate Research Assistant and Ph.D. Candidate
14 School of Civil Engineering
15 Purdue University
16 West Lafayette, IN 47907-2051
17 E-mail: jcastro@purdue.edu
18 Phone: 765.494.0358

19
20 Wenting Li
21 Graduate Research Assistant
22 School of Civil Engineering
23 Purdue University and Southeast University
24 West Lafayette, IN 47907-2051
25 Nanjing, China 211189
26 E-mail: li448@purdue.edu
27 Phone: 765.494.0358

28
29 Mohammad Pour-Ghaz
30 Graduate Research Assistant
31 School of Civil Engineering
32 Purdue University
33 West Lafayette, IN 47907-2051
34 E-mail: mpourghaz@purdue.edu
35 Phone: 765.494.0358

36
37 Pao-Tsung Huang
38 Graduate Research Assistant
39 School of Civil Engineering
40 Purdue University
41 West Lafayette, IN 47907-2051
42 E-mail: huang69@purdue.edu
43 Phone: 765.494.6242

44
45 Jason Weiss (Corresponding Author)
46 Professor and Director of Pankow Materials Laboratory
47 Associate Director of the Center for Advanced Cement Based Materials
48 School of Civil Engineering
49 Purdue University
50 West Lafayette, IN 47907-2051
51 E-mail: wjweiss@purdue.edu
52 Phone: 765.494.2215

1 **Abstract**

2

3 A series of wetting and drying tests were performed on concrete using different aqueous
4 solutions containing deicing salts. The rate of fluid absorption was generally lower for aqueous
5 solutions containing deicing salts than it was for water. In addition, less fluid was absorbed for
6 samples exposed to aqueous solutions containing deicing salts than for samples exposed to water.
7 The change in the rate of aqueous fluid absorption was proportional to the square root of the ratio
8 of surface tension and viscosity of the absorbed fluid. Concrete that has been exposed to
9 solutions containing deicing salts showed less mass loss during drying. Measures of equilibrium
10 relative humidity over the salt solutions are used to interpret drying behavior. Experimental data
11 indicates that concretes that had previously been exposed to deicing solutions can also exhibit
12 reduced rate of absorption, even if water is the fluid being absorbed.

13

14

15 **1. Research Need and Significance**

16

17 Some jointed plain portland cement concrete pavements in freezing prone climates have shown
18 premature deterioration at the longitudinal and transverse joints. While some have attributed this
19 damage to a chemical attack, inadequate air entrainment, poor mixture design, inadequate
20 constituent materials, or poor construction practices; it is the hypothesis of the authors of this
21 paper that this joint deterioration may be attributed, at least in part, to preferential absorption of
22 fluid at joints. This hypothesis was developed based on observations from the field that show
23 these deteriorated locations frequently occurred at low spots in the pavement, where joint sealers
24 were damaged, where water has collected, or where the joint does not appear to have opened
25 thereby trapping water [1]. Preferential fluid ingress at joints could increase a variety of damage
26 mechanisms including deleterious chemical reactions, crystallization pressure, or freeze thaw
27 damage that may degrade the concrete. To fully evaluate fluid ingress at the joints it is essential
28 that the wetting and drying behavior of concrete is evaluated using aqueous solutions containing
29 deicing salts.

30

1 This work is limited in scope as it considers only the ingress of aqueous solutions over short time
2 periods and does not explicitly consider any chemical reaction that occurs between the aqueous
3 solution and the concrete. This information is intended to provide reference for those developing
4 tests to evaluate potential deicer-concrete interactions [2], for developing tests on fluid
5 absorption, for evaluating fluid absorption in concrete [3], for input parameters in computer
6 simulation of fluid ingress at joints [4], and for potential approaches to limit joint deterioration
7 like penetrating sealers for possible use in concrete pavements [5].

10 **2. Fluid Absorption in Porous Materials**

12 Fluid absorption is a frequently used test to provide an indication of the durability of concrete
13 systems since it is simple to perform. Several standard tests exist for measuring water absorption
14 including ASTM C 1585-04 [6], BS 1881-99 [7], and ASTM D6489-99 [8]. While the concept
15 behind these tests is very similar, there are differences in how the samples are conditioned,
16 treated, and tested. In each of these tests water is typically used as the fluid that is being
17 absorbed. Hall [9] discusses that water can interact with the cement matrix adding complexity to
18 the interpretation of results. To overcome some of these limitations or to indicate how
19 absorption can be reduced by fluid composition other solutions have been tested [9-13].

21 MacInnis and Nathawad [14] assessed the absorption of an aqueous solution consisting of a NaCl
22 deicing salt and reported a decrease in absorption. Sutter et al. [15] reported that sorptivity
23 decreased from highest to lowest in the order of water, NaCl, CaCl₂ and MgCl₂. Similar data has
24 recently been observed by Janusz [16]. As a result, it can be observed that concrete exposed to
25 deicing salt solutions absorb fluid at a slower rate than they would absorb water; however the
26 previous work has not related this behavior to the fluid properties or described the influence of
27 salt concentration or properties of the aqueous solution.

29 The results of one-dimensional fluid absorption tests (assuming negligible gravitational effects)
30 are typically reported as the cumulative water absorbed per surface area (surface from which
31 water is absorbed) versus the square root of wetting time. Equation 1 is frequently used to

1 describe the water absorption (total volume of fluid absorbed) and the sorptivity (related to the
2 rate of absorption) [17].

3

$$i = S\tau^{1/2} \quad \text{Eq. 1}$$

4

5 where i [mm³/mm²] is the cumulative water absorption, S [mm/s^{1/2}] is the sorptivity, and τ [s] is
6 the elapsed time. It should be noted that additional equation have been proposed to account for
7 time dependent properties [18].

8

9 Hall [9] proposed that the diffusion would scale proportionately with the ratio of surface tension
10 (γ) and viscosity (η) of the fluid. Hall further related this to sorptivity since sorptivity is related
11 to the square root of diffusion. Kelham [19] derived an expression for fluid absorption (Equation
12 2) that shows the relationship between depth of penetration and the square root of the ratio of
13 surface tension and viscosity.

14

$$x(\tau) = \sqrt{\frac{4k\gamma\cos(\theta)\tau}{p\eta r}} \quad \text{Eq. 2}$$

15

16 where $x(\tau)$ [mm] is the penetration depth, γ [N/mm] is the surface tension, θ [rad] is the liquid-
17 solid contact angle, p [Dimensionless] dis the porosity of the medium, r [mm] is the pore radius,
18 k [mm²] is the intrinsic permeability of the material, and η [Pa.s] is the viscosity of fluid. An
19 expression similar to equation 2 was derived by Scherer and Wheeler [20] for stone consolidates.

20

21 Previous research using organic fluids has shown an absorption rate that scales proportionally
22 with the square root of the ratio of surface tension and viscosity of the fluid ($(\gamma/\eta)^{1/2}$). This work
23 will use this approach to attempt to interpret results from absorption tests that used aqueous
24 solutions containing deicing salts.

25

26

27 **3. Properties of Deicing Salt Solutions**

28

1 Physical properties of pure solutions were gathered from literature and compared with measured
2 values for the industrially available deicing solutions tested in this research, and they are
3 provided here for convenience in one location. The properties of the deicing solutions will be
4 used in interpreting the wetting and drying results, discussed later in this paper. This section is
5 divided into four sections. The first three sections describe the influence of the deicing solutions
6 in terms of surface tension, viscosity, and equilibrium relative humidity over the aqueous
7 solution. The fourth section describes the specific gravity of the solution as a function of
8 concentration as this is used to determine the volume of solution absorbed during the absorption
9 test.

12 **3.1 Surface Tension of Deicing Salt Solutions**

14 [Figure 1 \(a\)](#) shows surface tension measurements at different concentrations for the three
15 solutions used in this research: NaCl, CaCl₂, MgCl₂. The surface tension for NaCl was obtained
16 from [10], CaCl₂ from [21] and MgCl₂ from [22]. A Du Noüy Ring Tensiometer KRÜSS was
17 used with a resolution of 0.1 mN/m for the industrial deicers tested in this study. The
18 tensiometer was cleaned between measurements following ASTM D971-04 [24]. The
19 tensiometer was first calibrated using de-ionized water, which provided a value of 71.0×10^{-6}
20 N/mm. A series of three measurements were performed for each solution, with the average
21 reported.

23 The closed points in [Figure 1 \(a\)](#) are the values measured for the industrially available solutions.
24 The lines represent values taken from literature for pure salt solutions at different mass
25 concentrations. While the general trends are consistent, differences between the solutions
26 containing industrial deicing salts and literature values may be due to impurities or other additives
27 however further work is needed to examine this in greater detail.

30 **3.2 Viscosity of Deicing Salt Solutions**

1 [Figure 1 \(b\)](#) shows a comparison of the viscosities for the solutions used in this research between
2 pure solutions taken from literature and measurements of the deicing solutions. Viscosity
3 measurements for the industrial deicers were performed on the salt solutions using an Anton-Parr
4 rheometer, model Physica MCR 301. The rheometer kept the solution being tested at 23.0 ± 0.02
5 °C and from the torque applied to the fluid that causes a shear from which the viscosity can be
6 found. Calibration of the device was performed using a reference standard.

7
8 The dashed lines presented are viscosities at different concentrations and are taken from
9 literature [[10, 21-23](#)], while the points represent measured viscosities of the industrially available
10 solutions. Again, differences between literature values and those of the solutions measured can
11 be explained by differences in possible additions or chemistries of the industrial deicers.

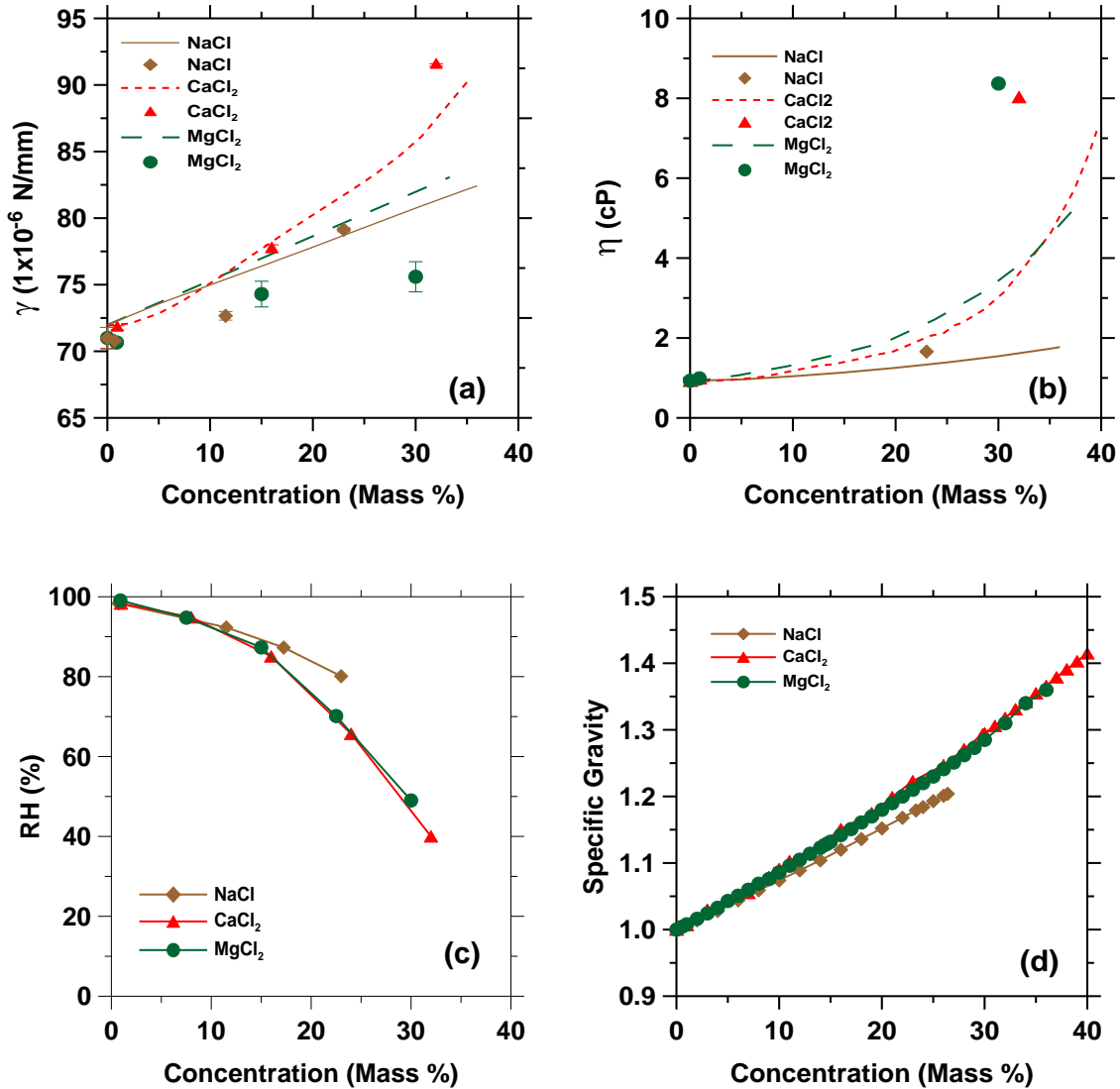
14 **3.3 Relative Humidity of Deicing Salt Solutions**

15
16 Relative humidity measurements were performed on the salt solutions using Rotronic
17 HygrClip2S sensors (± 0.8 % RH at 23 ± 0.1 °C). The relative humidity probes were mounted in
18 a 75 mm x 68 mm stainless steel cylinder that was placed over a water jacketed sample cup
19 holder. The water jacket was connected with a water bath at a constant temperature of 23.0 ± 0.1
20 °C.

21
22 [Figure 1 \(c\)](#) shows the relative humidity measured over salt solutions for a wide range of solution
23 concentrations. As the concentration increased the relative humidity over the solution decreased.
24 The measured relative humidities of these unsaturated salt solutions are higher than that of the
25 saturated solution of these salts which are 75.4 % RH for NaCl [[25](#)], 33.0 % RH for MgCl₂ [[25](#)]
26 and 22 % for CaCl₂ [[21](#)].

29 **3.4 Specific Gravity of Deicing Salt Solutions**

1 Figure 1 (d) shows the specific gravity of different deicing solutions as a function of
 2 concentration. The specific gravity of the solution increases with concentration. The CaCl₂ and
 3 MgCl₂ increase at very similar rates with an increase in concentration, while the NaCl increases
 4 slightly less than the CaCl₂ and MgCl₂ (i.e., 25 % less increase with concentration). This may be
 5 attributed to the colligative properties of solutions.



6
7

8
9

10 **Fig .1.** Properties of Deicing Salts at 23-25 °C: (a) Surface Tension (b) Viscosity (c) Relative
 11 Humidity (d) Specific Gravity (Rosenburgh 2010, unpublished data)

12
13
14

4. Wetting and Drying for Concrete with Deicing Solutions

4.1 Experimental Program of Wetting and Drying of Concrete with Deicing Solutions

The concrete mixture that was used for these tests was a typical INDOT class C bridge deck concrete. The mixture proportions of this concrete are shown in Table 1. The fresh air content was 5.7 %, which was measured according to ASTM C231-09 [26]. The hardened air content of the concrete was 4.4 % as assessed using an automated optical scanning approach [18] based on the method proposed by Peterson et al. [28].

Table 1. Mixture Proportions of Concrete Assuming Saturated Surface Dry (SSD) Conditions

Material	Mass
Cement (kg/m ³)	316
Class C Fly Ash (kg/m ³)	60
Water (kg/m ³)	150
Fine Aggregate (kg/m ³)	736
Coarse Aggregate (kg/m ³)	1049
Air Entraining Admix. (ml/100 kg of cem. materials)	20
High Range Water Reducer Admix. (ml/100 kg of cem. materials)	456
Retarder Admixture (ml/100 kg of cem. materials)	98

The concrete was produced in a central mix plant and discharged from a ready mix concrete truck. A series of 100 mm × 200 mm cylinders were cast. After one day of curing, the cylinders were demolded and sealed in double plastic bags at 23 ± 0.5 °C until the samples reached an age of 28 d. After 28 days of curing the cylinders were removed from bags and three 50 mm ± 2 mm thick samples were cut from the central portion of each cylinder using a wet saw.

Two different sets of samples were used in this study. The first set of samples were used to evaluate the effect of sample conditioning on water absorption. In each condition, three samples were used. A total of five conditions were considered: ASTM C1585-04, oven-dry, 50 % RH, 65 % RH and 80 % RH. To ensure that these samples that were conditioned at 50 %, 65 %, and 80 % RH, reached equilibrium, a 12-month conditioning was period was considered. The second set of

1 samples that were used for aqueous salt solution absorption, drying, and de-ionized water re-
2 absorption were conditioned at 50 ± 2 % RH, 23 ± 0.5 °C for 36 months and two samples were
3 tested for each salt solution.

4
5 To prepare the specimens for fluid absorption testing, the sides of the samples were sealed with
6 epoxy. After the epoxy had hardened, the top surface was covered with plastic to avoid
7 evaporation from the sample during testing.

8
9 The absorption test involves recording incremental mass change measurements during the first
10 six hours after the sample comes in contact with the fluid and subsequently taking one
11 measurement every day for the next eight days. The amount of absorbed fluid is normalized by
12 the cross-section area of the specimen exposed to the fluid using Equation 3.

$$i = \frac{m_t}{(a \cdot \rho)} \quad \text{Eq. 3}$$

14
15 where: i (mm^3/mm^2) is the normalized absorbed fluid, m_t (g) is the change in specimen mass at
16 time t ; a (mm^2) is the area of the specimen exposed to the fluid (i.e., that of the bottom face), and
17 ρ (g/mm^3) is the density of the absorbed fluid (this is provided in greater detail in 3.1). These
18 absorption measurements are then plotted as a function of the square root of time, as provided by
19 Equation 1. The sorptivity is the slope of this graph.

20
21 The second series of samples were tested using seven different fluids. Their composition was
22 primarily based on one of three different industrially available deicing products, either NaCl,
23 MgCl_2 or CaCl_2 . A low concentration was used for each salt solution as well as a higher
24 concentration that was selected to be near the eutectic composition for each salt. De-ionized
25 water was also used as a reference fluid.

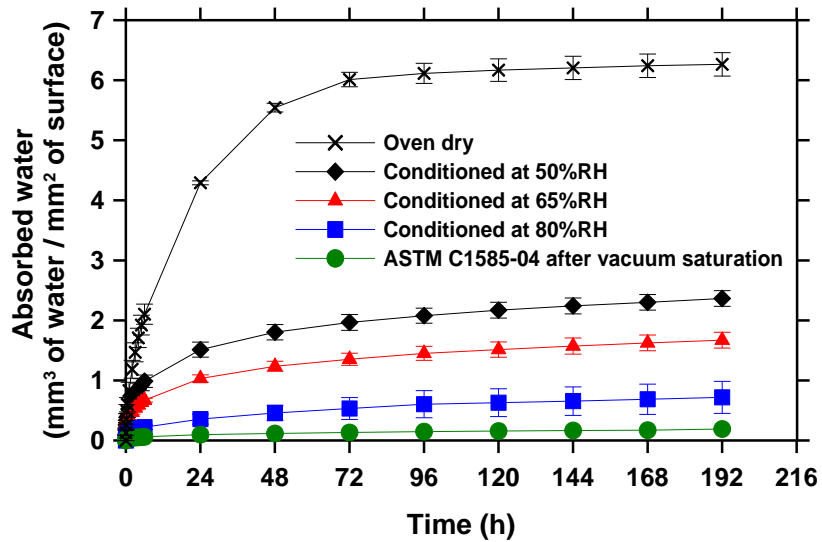
26
27

28 **4.2 Experimental Results from Wetting with Water for Different Conditioning Methods**

29

1 [Figure 2](#) shows the results from water absorption tests performed on the first series of samples
 2 that were conditioned with different environmental conditions as mentioned earlier (ASTM
 3 C1585-04 accelerated conditioning, 80 % RH, 65 % RH, 50 % RH and oven drying). It should
 4 be remembered that these samples were conditioned for 12 months while the remainder of the
 5 samples discussed in this paper were conditioned at 50 % RH for a much longer time. Sample
 6 preparation has an enormous impact on the water absorption results as more severe drying
 7 enables a greater volume of water to be absorbed during the test.

8



9

10

11 **Fig. 2.** Water absorption on samples subjected to different conditioning procedures.

12

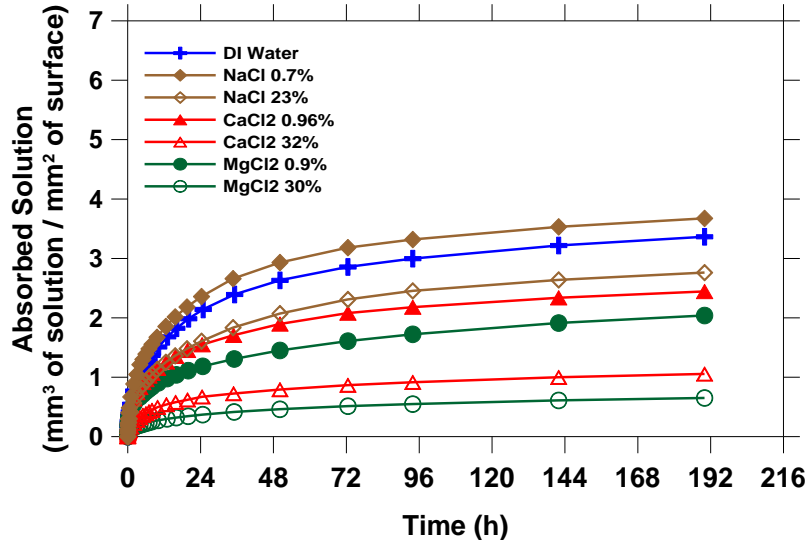
13

14 **4.3 Experimental Results from Wetting and Drying with Deicing Solutions**

15

16 [Figure 3](#) illustrates the results of the fluid absorption test as a function of time (for concrete at 50 %
 17 RH for a longer conditioning time than the samples in [Figure 2](#)). It can be seen that even though
 18 the concrete that is used for all the tests in [Figure 3](#) has the same conditioning and exposure
 19 conditions, the volume of solution absorbed by each material is dependent on the deicing salt
 20 solution and the concentration of the deicing salt solution that was absorbed. The sample with
 21 the low concentration of NaCl showed a slight increase in the rate of absorption (as compared
 22 with water) as well as the amount of fluid absorbed. This is consistent with the data reported by

1 MacInnis and Nathawad [14]. The absorption of all the other fluids was reduced when compared
2 with water. As a result, it can be concluded that in general as the salt concentration increased the
3 rate of absorption reduced and and the total absorption was reduced. Further work is needed to
4 examine lower concentrations for NaCl to ascertain why a slight increase is typically reported.
5

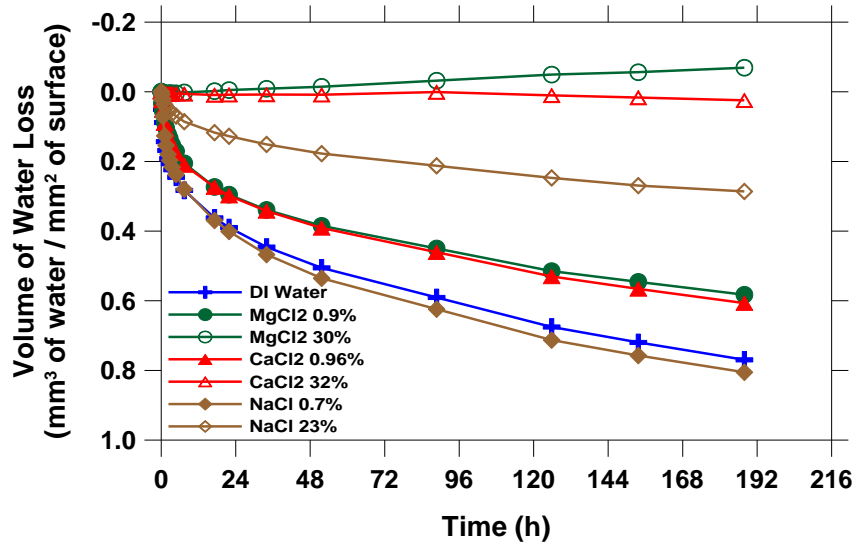


6
7
8 **Fig. 3.** Volume of deicing solutions absorbed by concrete as a function of time (typical standard
9 deviation less than $0.1 \text{ mm}^3/\text{mm}^2$).

10
11 After the fluid absorption test was performed for 8 days the samples were dried at $50 \pm 2 \%$ RH,
12 $23 \pm 0.5 \text{ }^\circ\text{C}$ for seven days. The samples were kept in the same one-faced exposed condition for
13 the drying test; however, the exposed surface that was facing down in the absorption testing was
14 placed facing up to simulate drying from the top. During the drying test the mass of the samples
15 was recorded at regular intervals.

16
17 **Figure 4** shows the volume of water loss during the drying period. It is important to note that the
18 drying test will result in only the water portion of the solution being evaporated from the system
19 leaving the salt to become more concentrated in the solution before it eventually precipitates out.
20 It can be noticed that as the concentration of deicing solution was increased the mass loss during
21 drying decreased. This was particularly evident in the high concentration solutions, which
22 showed nearly no mass loss or even a slight gain during drying.

1



2

3

4 **Fig. 4.** Drying of concrete prewetted with different salt solutions as a function of time (typical
 5 standard deviation less than $0.03 \text{ mm}^3 \text{ water/mm}^2$).

6

7

8 **4.4 Experimental Results from Wetting Previously Exposed to Deicing Solutions**

9

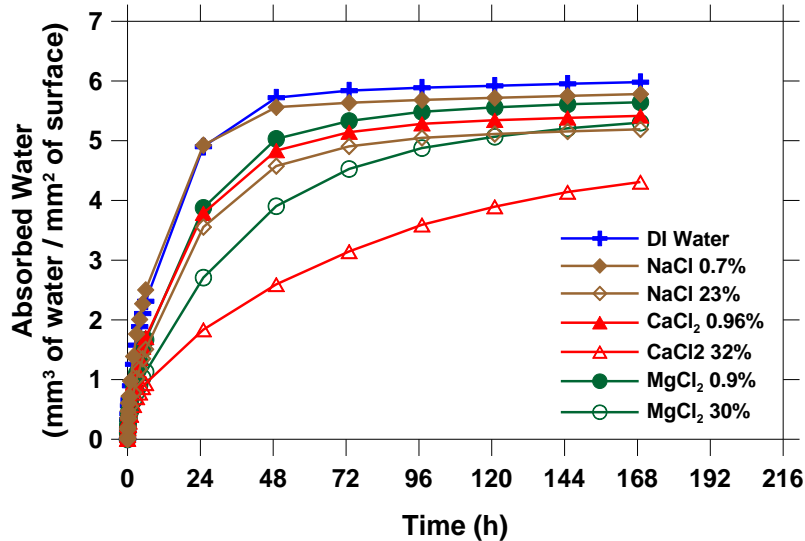
10 The same set of samples that were previously tested for absorption and drying were oven dried to
 11 be tested for second absorption test using de-ionized water. This was done to investigate the
 12 effects of previously absorbed salts on re-absorption of de-ionized water. However, in the case of
 13 the oven-dried samples, higher water absorption is expected. This can be due to the empty
 14 capillary pores and possibly to microcracking generated during oven drying [29-33].

15

16 To prepare the samples for the de-ionized water re-absorption test, the samples were placed in an
 17 oven at $105 \pm 2 \text{ }^\circ\text{C}$ until they reached to equilibrium. The equilibrium condition was defined as a
 18 difference less than 0.5 % between two successive mass measurements (24 hours apart). It is
 19 important to note that this drying process will evaporate only the water portion of the solution
 20 pre-absorbed, leaving salt in the pores. Since these samples were oven dried, their absorption
 21 rates and absorbed water are not comparable with any previous tests.

22

1 **Figure 5** shows the results for this second absorption test. It can be seen by comparing the results
 2 to the results in **Figure 3** that the behavior of the samples was dependent on the deicing solutions
 3 and the concentrations of deicing solutions used in the first wetting test. These results are a clear
 4 indication that the history of the samples affects the results of fluid absorption. This suggests
 5 when sorption testing is performed on field concretes, some understanding of the admixtures or
 6 salts that remain in the pore system is needed to fully interpret the results.



8
 9
 10 **Fig 5.** Volume of de-ionized water absorbed by concrete as a function of time in the second fluid
 11 absorption test (Fluid from the original test is shown in the caption).

12
 13
 14 **4.5 Drying of Mortars Saturated with Different Deicing Salts**

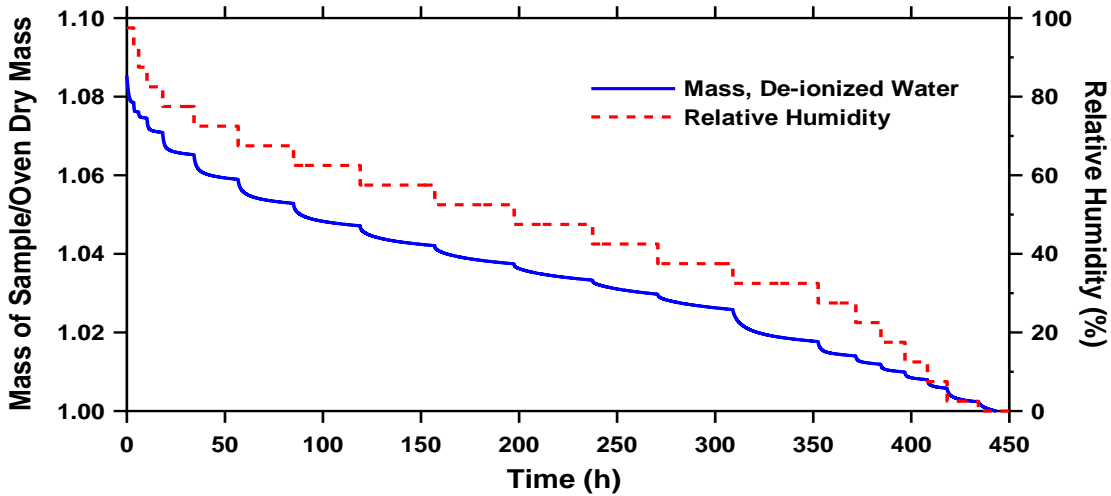
15
 16 Moisture desorption is an established technique for evaluating the effect of moisture loss at a
 17 given humidity for a material. A TA Q5000 SA moisture sorption analyzer was used to carefully
 18 control temperature and humidity. Mortar samples were prepared ($w/c = 0.42$ and 55 %
 19 aggregate by volume) and cast in a cylindrical mold with a 34 mm diameter and 50 mm height.
 20 At an age of 28 days the specimens were demolded and 34 mm diameter 0.8 ± 0.05 mm thick
 21 slices were taken from the middle of the samples. The samples were dried under controlled
 22 conditions (at 23 ± 0.1 °C and 50 ± 1 % RH) in a CO₂ free chamber until they reach mass

1 equilibrium. Then, samples were submerged for a minimum of 5 days in aqueous solutions with
2 23 % NaCl, 32 % CaCl₂, and 30 % MgCl₂ by mass.

3
4 For the samples submerged in NaCl, CaCl₂, and MgCl₂ solutions a 50 mg to 70 mg piece of
5 sample was placed in a tared quartz pan after a minimum of 5 days of submersion. The pan
6 containing the sample was then suspended from the balance (± 0.001 mg accuracy) and placed in
7 the relative humidity chamber to equilibrate at 23.0 ± 0.1 °C and 97.5 ± 0.1 % RH for up to 96 h
8 or until the sample had achieved a stable mass (less than an 0.001 % mass change/15 minutes).
9 Then, the relative humidity was reduced to reach 95 %. After the sample mass equilibrated, the
10 relative humidity in the chamber was changed in 10 % RH steps to 55 % RH, allowing the
11 sample to attempt to equilibrate (12 h or 0.01% change in mass over 15 minutes) at each new
12 humidity. After equilibrating at 55 % RH the samples were dried to 0 % RH. For the sample
13 submerged in de-ionized water the procedure was similar, but the relative humidity was reduced
14 in 5 % steps from 97.5 % to 2.5 %, and then reduced to 0 % RH.

15
16 **Figure 6** shows the plot of mass change as a function of time for the mortar saturated in de-
17 ionized water. The sample soaked in water can be seen to lose mass with the decrease of RH.
18 For this system, when the environment is below 100 % RH, water will move from the pores to
19 outside of the sample and classical drying behavior is observed. The maximum mass of the
20 sample is 8.5 % higher than the mass of the oven dry sample.

21



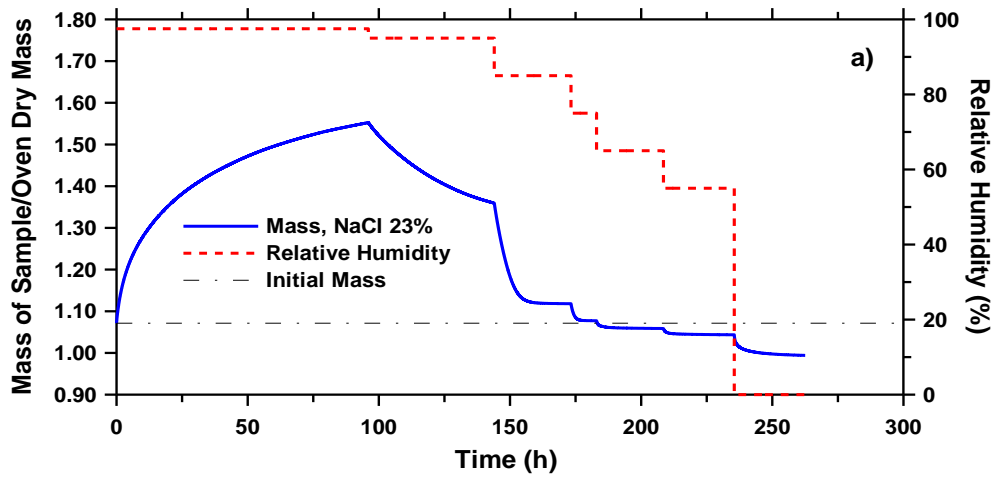
22

23

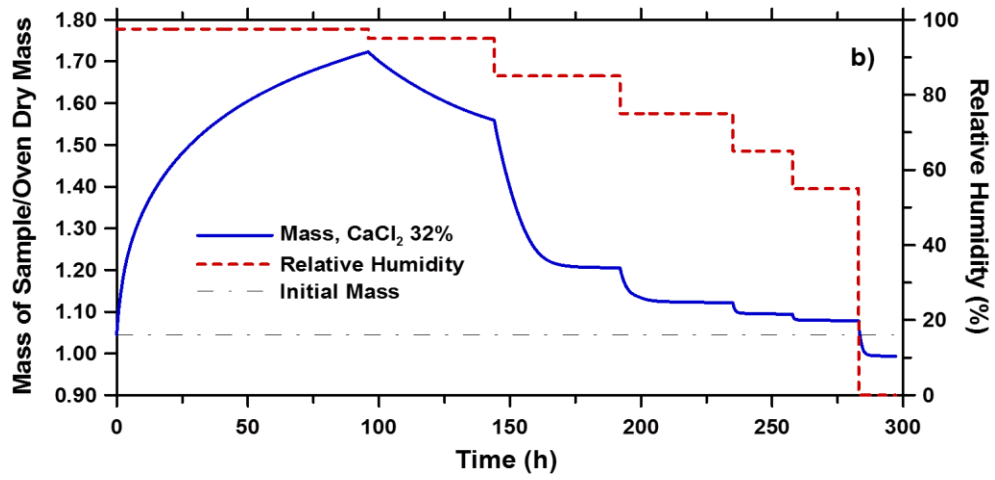
1 **Fig. 6.** Mass change at decreasing RH for samples containing de-ionized water

2
3 Figure 7 shows a plot of mass change for the mortar samples submerged in aqueous solutions of
4 23 % NaCl, 32 % CaCl₂, and 30 % MgCl₂. It can be observed that initially upon placement in
5 the testing chamber at 97.5 % relative humidity the mass of the sample increases for the first 96
6 h until the relative humidity of the chamber is changed. The samples absorb water during this
7 time of preconditioning, with values much higher than the 8.5 % increase in mass of the sample
8 with de-ionized water as compared with the oven dry sample.

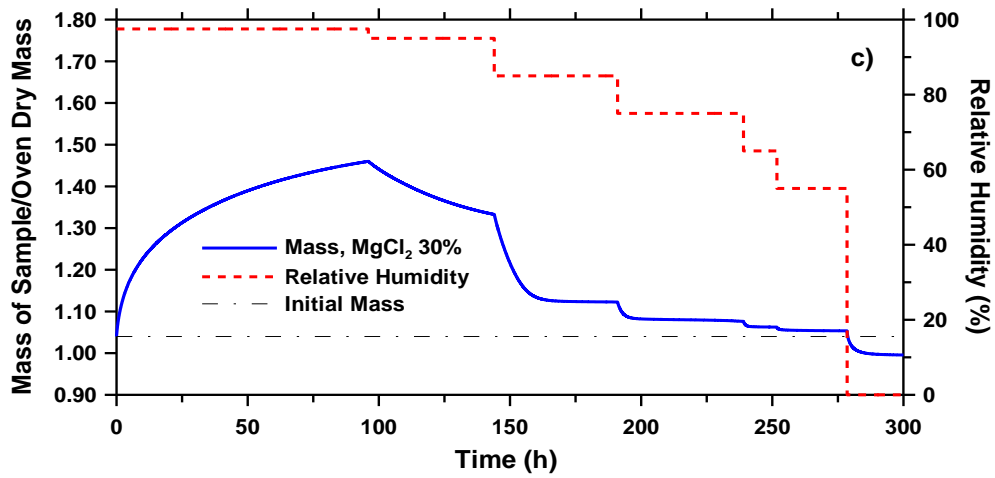
9
10 The sample loses weight as the relative humidity is decreased however it should be noted that the
11 sample mass does not decrease to below the initial mass obtained from soaking the sample in the
12 deicing solution until relative humidity was decreased below 85 %, 55 % and 55 % for NaCl,
13 CaCl₂ and MgCl₂ respectively. This will be compared with the equilibrium relative humidity of
14 the salt solution later in the paper.



1
2



3
4



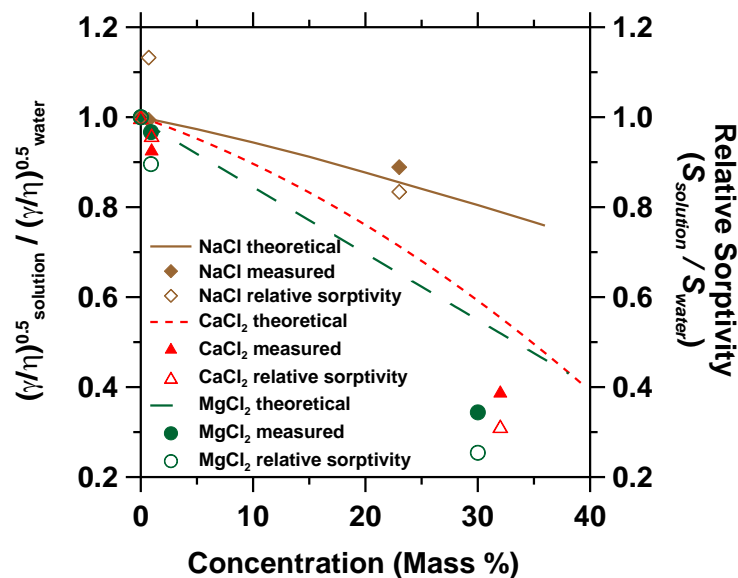
5
6
7

Fig. 7. Mass change for samples submerged in aqueous solutions containing deicing salts: (a) NaCl 23% (b) CaCl₂ 32 % and (c) MgCl₂ 30%.

5. Discussion of Results

5.1 Aqueous Solution Absorption Behavior as a Function of Surface Tension and Viscosity

Equation 3 showed that the rate of absorption was related to the square root of surface tension and viscosity. Figure 8 plots the square root of the ratio of surface tension and viscosity versus mass concentration of salt. Pure salt solutions are shown as lines while industrial deicing solutions are presented as solid points, and the open points represent the measured sorption response of concrete (i.e., salt sorptivity/water sorptivity) from Figure 3. Figure 8 confirms that as the solution concentration increases, the rate of fluid absorption (i.e., sorptivity) decreases. Further, while the properties of pure solutions may not exactly represent the response of industrially available deicing solutions they do provide a comparable trend. Reasonable agreement is seen between the measured sorption and square root of the ratio of surface tension and viscosity the measured properties. Additional work is currently being performed to extend these results to a wide range of temperatures.



21
22

1 **Fig 8.** Relative sorptivity for deicing solutions.
2
3

4 **5.2 Drying Time Versus Wetting Time** 5

6 Comparing [Figures 3](#) and [4](#) indicates that wetting happens much faster than drying. When de-
7 ionized water was used as the absorbed fluid, the amount of fluid that was evaporated from the
8 sample after eight days was $0.8 \text{ mm}^3/\text{mm}^2$. In contrast, it took just two hours for samples to
9 absorb the same amount of fluid. These differences are even larger when salt solutions were
10 used as the absorbed fluid. When MgCl_2 solution was used as the absorbed fluid, the amount of
11 fluid that was evaporated from the sample after eight days was $0.07 \text{ mm}^3/\text{mm}^2$, but it took just
12 ten minutes for the samples to absorb the same amount of fluid.

13
14 This is important as it suggests that field concrete may be more susceptible to increasing its level
15 of saturation over time rather than drying out. Further, it shows that laboratory tests that use
16 equal times for drying and wetting increase the saturation level of the concrete over time.
17 Researchers [\[34\]](#) observed an increase in sample mass during wetting and drying cycling with
18 deicers which was attributed to microcracking; however an increase in mass would be consistent
19 with the wetting and behavior observed in this paper.

20 21 22 **5.3 Reduced Drying with Salt Solutions – The Role of Solution Equilibrium Humidity** 23

24 The relative humidity of different salt solutions presented in [Figure 1 \(b\)](#) help to understand the
25 results from the drying tests. The equilibrium relative humidity for the 23% NaCl , 32% CaCl_2
26 and 30% MgCl_2 solutions are 80 %, 40 % and 50 % respectively. When the samples are placed
27 in an environment with a relative humidity that is greater than or equivalent to the approximate
28 equilibrium relative humidity over the aqueous solution in the pores water will not be lost to then
29 environment. ([Figure 4](#)) and the sample can actually gain mass ([Figure 4 and 7](#)), most likely due
30 to the water absorption on the surface of the sample. This can be seen by the thinner (dashed
31 lines in [Figure 7](#)), which show the initial mass of the sample after it has been submerged in a

1 aqueous solution for over 5 days. At relative humidity higher than the equilibrium of the aqueous
2 salt solution the samples will increase in mass. At relative humidities where the environment is
3 less than the equilibrium humidity over the salt solution, the samples will be expected to
4 decrease in mass. The drying behavior of systems containing concentrated aqueous solutions of
5 deicing salts is complex and requires additional research.

6 7 8 **5.4 Effect of Solution on Rewetting**

9
10 When samples of concrete that were previously exposed to deicing solutions were rewet with
11 water they had an absorption and rate of absorption that depended on the history of the
12 specimens (Figure 5). The absorption of water can be 30 % to 50 % less in specimens that were
13 exposed to deicing solutions at some point in their lives. This is an important, yet subtle, factor
14 to understand. This is important since absorption tests of field concrete may be mistakenly
15 interpreted by relating the reduction in sorption to pore filling or delayed sorption. Both of these
16 observations (lower sorptivity and delayed sorption) are consistent with data here for samples
17 that did not have reduced porosity or differences in sample damage.

18 19 20 **6. Summary and Conclusions**

21
22 This paper has reported experimental results of fluid absorption measurements and drying of
23 concrete in the presence of deicing solutions. The following observations can be made. First,
24 the absorption of fluid in concrete depends on the drying environment used to condition the
25 samples. Samples stored at a lower RH absorbed a greater volume of fluid. Second, it was
26 observed that the deicing solutions reduce the rate of fluid absorption. This reduction can be
27 related to the square root of the ratio of surface tension and viscosity [10]. Third, the time scale
28 between drying and wetting is different and concrete is more likely to become preferentially
29 increasingly wet over time. Fourth, the drying of concrete containing aqueous solutions with
30 deicers differs from that of water. The equilibrium relative humidity of the aqueous solution
31 plays an important role on limiting drying. Finally, the presence of deicing salts in field samples

1 impacts the absorption when field samples are tested in the lab using water. This suggests that
2 care must be taken in analyzing field concrete exposed to deicing salt solutions.

3 4 5 **7. Acknowledgments**

6
7 The experiments reported in this paper were conducted in the Pankow Materials Laboratories at
8 Purdue University. This work was supported in part by the Joint Transportation Research
9 Program administered by the Indiana Department of Transportation and Purdue University (SPR
10 3093 and 3200). The contents of this paper reflect the views of the authors, who are responsible
11 for the facts and the accuracy of the data presented herein, and do not necessarily reflect the
12 official views or policies of the Indiana Department of Transportation, nor do the contents
13 constitute a standard, specification, or regulation.

14 15 **8. References**

- 16
17 1. Weiss J, Nantung T. INDOT Proposal on the Permeability of Concrete Pavement
18 Performance Relative to Permeability, 2006.
- 19 2. Shi X, Fay L, Peterson MM, Yang Z. Freeze-Thaw damage and chemical change of a
20 Portland cement concrete in the presence of diluted deicers. *Mater Struct*, 2010; 43(7): 933-
21 946.
- 22 3. Hong K, Hooton RD. Effect of cyclic chloride exposure on penetration of concrete cover.
23 *Cement Concrete Res* 1999, 29(9): 1379-1386.
- 24 4. Pour-Ghaz M, Rajabipour F, Couch J, Weiss J. Numerical and experimental assessment of
25 unsaturated fluid transport in saw-cut (notched) concrete elements. SP-266 American
26 Concrete Institute: Modeling as a solution to concrete problems, 2009.
- 27 5. Coates K, Mohtar S, Tao B, Weiss J. Can soy methyl esters reduce fluid transport and
28 improve the durability of concrete? *Transport Res Rec*, 2009; 2113:22-30.
- 29 6. ASTM International, ASTM C1585. Standard test method for measurement of rate of
30 absorption of water by hydraulic cement concretes; 2004.

- 1 7. British Standard Institution, BS 1881. Methods of testing concrete part 5: Methods of testing
2 hardened concrete for other than strength; 1990.
- 3 8. ASTM International, ASTM D6489. Standard test method for determining the water
4 absorption of hardened concrete treated with a water repellent coating; 2006.
- 5 9. Hall C, Marchand J, Gerard G, Sosoro M. Chapter 2: Transport of fluids in homogenous
6 isotropic cementitious composites. In: Reinhardt HW, editor. Penetration and permeability of
7 concrete, RILEM report 16, 1997; pp. 5-79.
- 8 10. Hall C, Hoff WD. Water-transport in brick, stone and concrete. London: Spon Press, 2002.
- 9 11. Weiss WJ. Prediction of early-age shrinkage cracking in concrete. Ph.D. thesis. Evanston, IL
10 Northwestern University, 1999.
- 11 12. Bentz DP, Peltz MA, Snyder KA, Davis JM. VERDiCT: Viscosity enhancers reducing
12 diffusion in concrete technology. Concrete International, 2009; 31(1): 31-36.
- 13 13. Sant G, Eberhardt A, Bentz DP, Weiss J. Influence of shrinkage-reducing admixtures on
14 moisture absorption in cementitious materials at early ages. J Mater Civil Eng, 2010; 22(3):
15 277-286.
- 16 14. MacInnis C, Nathawad YR. The effects of a deicing agent on the absorption and permeability
17 of various concretes. In: Litvan GG, Sereda PJ, editors. Proceedings of the first international
18 conference on durability of building materials and components, ASTM Special Technical
19 Publication STP-691, 1980. pp 485-496.
- 20 15. Sutter L, Peterson K, Julio-Betancourt G, Hooton D, Van Dam T, Smith K. The deleterious
21 chemical effects of concentrated deicing solutions on Portland cement concrete. South
22 Dakota Department of Transportation, Final Report, 2008.
- 23 16. Janusz A. Investigation of Deicing Chemicals and Their Interactions with Concrete Materials.
24 Master Thesis. West Lafayette, IN Purdue University, 2010.
- 25 17. Martys, NS. (1995). Survey of concrete transport properties and their measurements. NISTIR
26 5592, U.S. Department of Commerce
- 27 18. Martys N, Ferraris CF. Capillary transport in mortar and concrete. Cement Concrete Res
28 1997; 27(5): 747-760
- 29 19. Kelham M. A Water absorption test for concrete. Mag Concrete Res, 1988; 40(143): 106-
30 110.

- 1 20. Scherer G, Wheeler GS. Silicate consolidants for stone. *Key Engineering Materials*, 2009;
2 391: 1-25.
- 3 21. Conde M. Aqueous solutions of lithium and calcium chlorides: Property formulations for use
4 in air conditioning equipment design. *International Journal of Material Sciences*, 2004; 43(4):
5 367-382.
- 6 22. Phang S, Stokes RH. Density, Viscosity, Conductance and transference numbers of
7 concentrated aqueous magnesium chloride at 25C. *J Solution Chem*, 1980; 9(7): 497-505.
- 8 23. Afzai M, Saleem M, Mahmood MT. Temperature and concentration dependence of viscosity
9 of aqueous electrolytes from 20 to 50C. Chlorides of Na⁺, K⁺, Mg²⁺, Ca²⁺, Ba²⁺, Sr²⁺,
10 Co²⁺, Ni²⁺, Cu²⁺, and Cr³⁺. *Journal of Chemical Engineering Data*, 1989; 34(3): 339-346.
- 11 24. ASTM International, ASTM D971. Standard test method for interfacial of oil against water
12 by the ring method; 2004.
- 13 25. Greenspan L. Humidity fixed points of binary saturated aqueous solutions. *Journal of*
14 *Research of the National Bureau of Standards – A, Physics and Chemistry*, 1977; 81A(1): 89-
15 96.
- 16 26. ASTM International, ASTM C231. Standard test method for air content of freshly mixed
17 concrete by the pressure method; 2009.
- 18 27. Castro J, Kompare P, Poursaee A, Nantung T, Weiss J. JTRP Report SPR-3093, Portland
19 cement concrete pavement performance relative to permeability. Indiana Department of
20 Transportation, 2010.
- 21 28. Peterson KW, Swartz RA, Sutter LL, Van Dam TJ. Hardened concrete air void analysis with
22 a flatbed scanner. *Transport Res Rec* 2001; 1775: 36-43.
- 23 29. Hwang C, Young J. Drying shrinkage of portland cement pastes. microcracking during
24 drying. *Cement Concrete Res* 1984; 14(4): 585-594.
- 25 30. Chatterji S. (1976). Drying shrinkage of cement paste and concrete: a reappraisal of the
26 measurement technique and its significance. *Cement Concrete Res* 1976; 6(1): 145-148.
- 27 31. Bisschop J, Van Mier J. How to study drying shrinkage microcracking in cement-based
28 materials using optical and scanning electron microscopy? *Cement Concrete Res* 2002;
29 32(2): 279-287.
- 30 32. Samaha H, Hover K. Influence of microcracking on the mass transport properties of concrete.
31 *ACI Mater J* 1992; 89(4): 416-424.

- 1 33. Yang Z, Weiss J, Olek J. Water transport on concrete damaged by tensile loading and freeze-
2 thaw cycling. *J Mater Civil Eng* 2006; 18(3): 424-434.
- 3 34. Wang K, Nelsen D, Nixon W. Damaging effects of deicing chemicals on concrete materials.
4 *Cement and Concrete Composite*, 2006; 28(2): 173-188.

R. P. Spragg,¹ J. Castro,² T. Nantung,³ M. Paredes,⁴ and J. Weiss⁵

Variability Analysis of the Bulk Resistivity Measured Using Concrete Cylinders

REFERENCE: Spragg, R. P., Castro, J., Nantung, T., Paredes, M., and Weiss, J., "Variability Analysis of the Bulk Resistivity Measured Using Concrete Cylinders," *Advances in Civil Engineering Materials*, Vol. 1, Issue 1, 2012, pp. 1–17, doi:10.1520/ACEM104596. ISSN 2165-3984.

ABSTRACT: Many agencies are interested in using a rapid test method for measuring the electrical properties of concrete (i.e., the resistivity or conductivity) because the electrical properties can be related to fluid transport (e.g., ion diffusion). The advantage of electrical testing is that it is relatively easy to perform, and the test method is relatively fast (it takes less than a minute). Over the past century, many studies have investigated different approaches for measuring electrical properties. This paper describes the variability associated with measuring the bulk resistivity along the longitudinal axis of a cylinder after placing electrodes on either end. A multi-laboratory evaluation was performed at ten laboratories. Data from this evaluation provided variability data for 12 concrete mixtures at testing ages of 28, 56, and 91 days. Information on the variability is important in the development of precision and bias statements for standard test methods. In addition, this work discusses how the resistivity results obtained from this test can be correlated with surface resistivity measurements made using a Wenner probe. Linear agreement was noticed between the Wenner test and the measurement through the cylinder, but with a factor confirmed by previous research by Morris et al. ("Practical Evaluation of Resistivity of Concrete in Test Cylinders Using a Wenner Array Probe," *Cem. Concr. Res.*, Vol. 26, 1996, pp. 1779–1787). Additionally, the effect of electrode resistance is discussed, and for high resistivity concrete such as that used in much transportation infrastructure, this effect appears to be negligible; however, it can be accounted for easily.

KEYWORDS: concrete, resistivity, surface resistivity, bulk resistivity, RCPT, electrical properties, electrode resistance, variability, precision statements, standard development, inter-laboratory test, round-robin test

Introduction

Over the past century, tests have been proposed for measuring the electrical properties of concrete [1–7]. These methods have the advantage of being relatively fast, and the principle behind these tests is relatively straightforward. Concrete is a composite consisting of a vapor phase (vapor filled porosity or "air"), a solid phase (aggregate and cementitious solids), and a fluid phase (the pore solution), and the resistivity of each of these individual phases is very different. The resistivities of the solid and vapor phases are extremely low, approximated as 10^9 and 10^{15} Ohm-meter, respectively, whereas the resistivity of the liquid phase is several orders of magnitude lower, ranging from 1×10^{-2} to 5×10^{-2} Ohm-meter [8,9]. As such, it can be assumed that the majority of conduction occurs through the pore fluid. A number of composite models have been developed in which this

Manuscript received December 2, 2011; accepted for publication April 3, 2012; published online July 2012.

¹Graduate Research Assistant, Purdue Univ., School of Civil Engineering, 550 Stadium Mall Dr., West Lafayette, IN 47907, e-mail: rspragg@purdue.edu

²Assistant Professor, Pontificia Universidad Catolica de Chile, School of Civil Engineering, Casilla 306, Correo 22, Santiago, Chile 6904411, e-mail: jecastro@ing.puc.cl

³Manager for Pavement Materials and Construction Research, Indiana Dept. of Transportation, Division of Research and Development, P.O. Box 2279, West Lafayette, IN 47906, e-mail: tnantung@indot.in.gov

⁴State Corrosion Engineer, Florida Dept. of Transportation State Materials Office, Corrosion Research and Durability Laboratory, 6007 NE 39th Ave., Gainesville, FL 32609, e-mail: mario.paredes@dot.state.fl.us

⁵Professor of Civil Engineering, Director of Pankow Materials Laboratory, Purdue Univ., School of Civil Engineering, 550 Stadium Mall Dr., West Lafayette, IN 47907, e-mail: wjweiss@purdue.edu

concept is used [10–13]. Two of the more popular equations that are used in the cement and concrete literature are Archie's expression and the modified parallel expression [11,14]. Several documents have reviewed these methods previously; the goal of this section is to describe how the overall resistivity is dependent on three factors (the resistivity of the fluid in the pores, the degree of saturation of the concrete, and the volume and connectivity of the pore network), as illustrated in Eq 1.

$$\rho = \rho_0 \cdot F \cdot \frac{1}{f(S)} \quad (1)$$

where:

ρ = bulk resistivity,

ρ_0 = resistivity of the fluid phase,

F = formation factor that is the product of the pore volume and a tortuosity coefficient, and

$f(s)$ = function that describes the degree of saturation, which is taken as 1 for a saturated system.

This implies that the resistivity decreases with a higher water content (i.e., pore volume) and a more open pore network (i.e., a lower tortuosity coefficient). This expression can also be written in terms of electrical conductivity, as it is simply the inverse of the electrical resistivity.

One of the more popular test methods that is currently performed based on electrical concepts is the rapid chloride permeability (RCP) test [15,16]. This test method involves placing a saturated concrete specimen, typically 102 mm in diameter and 51 mm thick, between electrodes in different solutions and integrating the charge that is passed over a 6 h testing period [15]. Although this test has come into wide use, a few drawbacks have been highlighted out [17–19]. First, this test is performed using high voltages and a direct current, which limits each sample to providing a single measurement at a single age. Second, saturating the specimen can require a relatively long preparation time. Third, there is potential for heating effects due to the large voltage and possible modification of the microstructure [20,21]. Research has been conducted regarding temperature correction for the RCP test [22,23], and many changes to this test have been proposed, including extrapolating the charge passed after a test duration of 30 min to the 6 h value [24], increasing the size of the reservoirs to reduce the heating effects [25], reducing the large voltages in the test [26], and using a single resistance reading measured at an early age, often 1 min or 5 min [18,19].

Alternative testing methods have been proposed that require little to no sample preparation and which allow the sample to be tested at different ages. One rapid test for the electrical resistivity of concrete is the Wenner probe. As with any test, there are certain considerations that can impact the results. For example, the probe spacing, the geometry of the sample, the aggregate size, and surface moisture conditions can all influence the measured electrical response [27]. Because the moisture conditions at the surface of the test specimen are quite important, care should be taken to protect against drying or using surface treated concretes [28–30]. Additionally, some work has suggested the need for an additional non-linear geometry factor for this method that occurs from the constricted geometry, such as that of a standard test cylinder [27]. Further, when this method is used on real structures, the location and proximity of the rebar need to be considered [31,32].

Several of these concerns can be addressed if a standard testing protocol is adopted. A draft test method has been developed that uses a four-probe Wenner configuration on a 102 mm × 204 mm

standard test cylinder with a probe tip spacing of 38 mm. Temperature monitoring can be difficult and is frequently not done [33]. This surface resistivity (SR) test method places the probes directly on the surface of the test specimen. This test method has recently been accepted for use by the Louisiana Department of Transportation and the Florida Department of Transportation on select projects, and preliminary work has been done to expand its use for quality control [28,34]. Work has also been done to correlate RCP testing and diffusion testing with SR [28,35,36]. This method has a distinct advantage in that it can be performed rapidly and is easy to perform on the surface of a cylinder.

The resistance of a concrete cylinder can alternatively be evaluated by using plate electrodes that can be placed on the end of the sample [32,37]. The resistance value obtained can be normalized by means of specimen geometry—simply, the ratio of the sample cross-sectional area to the length—in order to obtain the sample resistivity, termed the bulk resistivity (BR). For this test, good electrical contact must be ensured between the plate electrodes and the test specimen [27,37]. This can be assisted through the use of a conductive medium, but the surface finish of the cylinder ends should be flat. Some work has previously been performed with regard to evaluating the contact pressure between the plate and the specimen [37]. Like other electrical tests, this method is subject to the influence of the specimen's moisture content and temperature. This test, however, has the distinct advantages of rapid testing and a simple geometry factor. To the best of the authors' knowledge, a multi-laboratory evaluation of variability has not been performed on this geometry, though some studies have reported exchanges of samples between two laboratories [37].

Three major factors that should be considered in any electrical resistivity testing are (1) the influence of geometry, (2) the influence of temperature, and (3) the influence of moisture. First, whereas the normalized BR of concrete can be considered a material property, the tests that are performed provide a measure of electrical resistance. The resistance measurements need to be corrected for the geometry of the test. Geometry factors can be determined experimentally [8,38] or numerically [27] and are largely dependent on the current flow through the material. A uniform current flow through the bulk of the geometry provides an easy geometry factor, the ratio of the cross-sectional area to the length. Other tests do not have this uniform current path, so the geometry factor is different. Temperature is another important factor in the testing of concrete resistivity. As the primary conduction path is through the ionic pore solution, an increase in the temperature increases the mobility of the ions, decreasing the resistivity. There has been work that has investigated the possibility of a temperature correction for resistivity tests [6,39–43]. In this work, the samples are all tested in laboratory conditions; as such, the sample temperature should be $23^{\circ}\text{C} \pm 2^{\circ}\text{C}$. Lastly, the degree of saturation is a major component in resistivity testing of concrete. As a result, knowledge of the moisture history and moisture content at testing are important considerations in the evaluation of resistivity data [44].

The main objectives of this evaluation are fourfold. First, it provides some background on electrical property measurements for concrete and provides some of the physical principles behind these tests. Second, it presents the results of an inter-laboratory evaluation of the variation in the electrical BR of concrete. This information can be used in the development of precision and bias statements. Third, it demonstrates the relationship between surface resistance test methods (e.g., Wenner) and measurements performed on a bulk cylindrical geometry. Fourth, it highlights important considerations in the development of testing standards and policies for the use of electrical methods as quality control/quality assurance tests.

Experimental Details

Materials

A round-robin testing program was proposed in 2009 for the evaluation of the repeatability of Wenner and bulk resistance tests on concrete cylinders. A series of 12 concrete mixtures were prepared at the laboratories that participated in this evaluation (Table 1). The mixtures are structural/bridge deck concretes used by state departments of transportation from around the United States. A final report detailing a parallel series of Wenner and BR tests conducted by the American Association of State Highway and Transportation Officials Technology Implementation Group is available [45]. It should be noted that a wide range of cements, supplementary materials, and aggregates were used in this investigation.

Sample Conditioning

The samples were demolded at an age of 48 h and placed into a saturated lime-water bath that was kept at a constant room temperature until the age of testing ($23^{\circ}\text{C} \pm 2^{\circ}\text{C}$). At an age of 14 days, the respective laboratories removed the samples and wrapped them in paper towels soaked in saturated lime-water. The samples were then double-bagged and prepared for two-day shipping to the other participating laboratories. The goal was to ensure that the samples remained wet during testing.

After the samples were received by the other testing laboratories, they were removed from the bag and placed into saturated lime-water baths kept at room temperature ($23^{\circ}\text{C} \pm 2^{\circ}\text{C}$). At ages of 28, 56, and 91 days, the samples were removed from the saturated lime bath, the surface was wiped dry, and the samples were tested for SR and BR. After this testing, the samples were placed back in the saturated lime-water.

Testing Procedure

It should be noted that the test described herein (with the plates placed on the end of the cylinder) was a part of a larger evaluation of variation conducted by the AASTHO TIG [45,46]. Not all of the laboratories chose to participate in this portion of the evaluation, and the nonparticipating

TABLE 1—Summary of mixture proportions used in this evaluation (for Saturated Surface Dry conditions).

Mixture Number	Water, w/cm	Cement, kg/m ³	Fly Ash, kg/m ³	Micron Fly Ash, kg/m ³	Slag, kg/m ³	Silica Fume, kg/m ³	Meta-kaolin, kg/m ³	Coarse Aggregate 1, kg/m ³	Coarse Aggregate 2, kg/m ³	Fine Aggregate, kg/m ³
1	0.34	163	237	119	...	119	...	1059	...	717
2	0.40	144	285	71	282	854	824
3	0.39	199	392	119	785	...	724
4	0.35	158	279	178	940	...	793
5	0.40	164	308	103	909	...	879
6	0.37	145	390	1068	...	712
7	0.40	160	297	80	24	532	528	686
8	0.39	131	251	84	555	...	1295
9	0.41	151	291	65	15	1032	...	697
10	0.30	151	297	153	44	1009	...	638
11	0.30	157	430	95	1033	...	577
12	0.35	156	402	44	1009	...	624

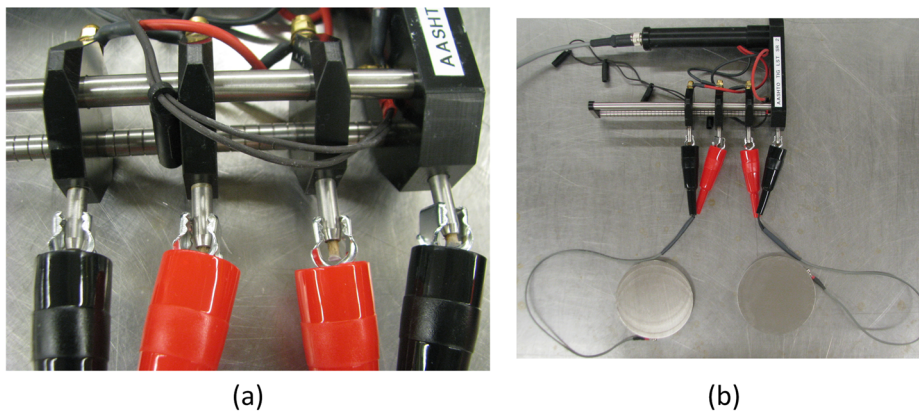


FIG. 1—Attachment of the alligator clips to the Wenner probe tips: (a) close-up; (b) at a distance. The steel plates have a diameter of 102 mm, and the probe tip spacing is 38 mm.

laboratories have been excluded from the following data; however, in order to avoid confusion, the original laboratory numbers were retained.

Equipment

The equipment involved in this test consisted of a CNS Farnell Mk II U95 SR meter using an alternating current at a frequency of 13 Hz, a set of 102 mm diameter stainless steel plate electrodes, and 16 AWG two-conductor wire used to connect the probe tips of the SR meter to the plate electrodes.

The cable was outfitted with alligator clips on one end to allow easy access to the probe tips of the resistivity meter. The other end of the cable was outfitted with a ring terminal to connect to the plate electrode. The plate electrode was drilled and tapped to allow easy and consistent attachment.

It is important to ensure proper electrical contact between the cylinder and the plate electrodes [27,37]. For this evaluation, this was done using thin lime-water-saturated sponges.

Testing Procedure

The plate electrodes should be connected to the pins of the SR meter. The first two pins that generate the current and measure the potential were connected to one of the steel plate electrodes, and likewise for the second set of pins, as shown in Fig. 1.

The resistances of the top and bottom sponges were then measured, as shown in Fig. 2. The resistance of each individual sponge is largely dependent on its moisture content. The moisture content of the sponge is dependent on the weight placed on top of it (e.g., large weights push more water from the sponge). In order to ensure that the moisture contents remain the same, the weight it carries during the test was used. For the top sponge, only the top plate was used as a weight. For the bottom cylinder, the top plate and the cylinder were used to provide the weight, but the cylinder was placed above the top plate, so its resistance was not measured. The goal of this was to provide a correction for sponge resistance, as discussed below. The concrete cylinder was then placed between the plate electrodes, with sponges being placed between the plates and the concrete cylinder, as shown in Fig. 3.

Calculations

The resistances of the top and bottom sponge are termed $R_{\text{top sponge}}$ and $R_{\text{bottom sponge}}$, respectively. The measured resistance of the system (two sponges and a specimen), as depicted in Fig. 3, is

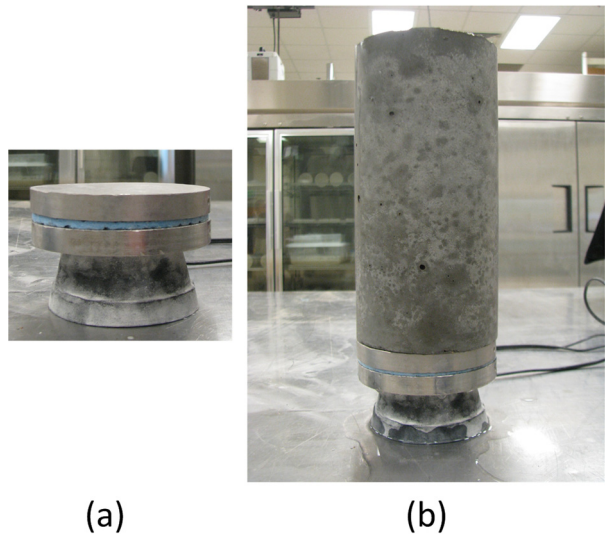


FIG. 2—Measuring the sponge resistance for (a) the top and (b) the bottom sponges. The steel plates have a diameter of 102 mm, and the test cylinder is a standard 102 mm × 204 mm.

termed R_{measured} . The measured resistance was corrected for the resistance of the sponges by treating the system as resistors in series, as shown in Fig. 2 [37]. It was noticed for the sponges used in this evaluation that the resistance values in each lab tended to remain relatively constant. Thus, for sponges that show this constant resistance, it is proposed that they be measured only periodically, and their resistances can be assumed to remain unchanged between measurements.

$$R_{\text{cylinder}} = R_{\text{measured}} - R_{\text{top sponge}} - R_{\text{bottom sponge}} \tag{2}$$

The BR, denoted as ρ , can be determined using Equation 3. The geometry factor K for the current flow through the bulk material is given by Equation 4. This can be extended to other sample geometries through experimental testing [8].

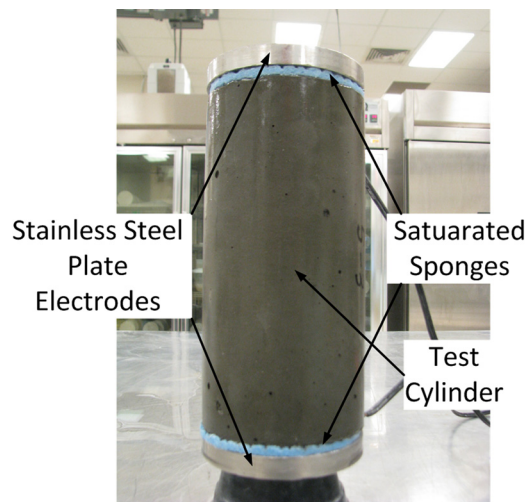


FIG. 3—Measuring the resistance of the system. The test cylinder is a standard 102 mm × 204 mm.

$$\rho = KR_{\text{cylinder}} \tag{3}$$

$$K = \frac{A}{L} \tag{4}$$

where:

R_{cylinder} = calculated resistance of the concrete test cylinder from Eq 1,

A = cross-sectional area, and

L = length of the test specimen.

Results and Discussion

Bulk Resistivity Data

The samples were tested at three ages: 28, 56, and 91 days. The average BR (Avg.) and variance (Var.) of three test cylinders measured at each testing age for each mixture by each testing laboratory are presented in Tables 2–4. Cells marked with “n/a” signify that no data were reported. The last row in each table represents the pooled statistics, calculated according to ASTM C802 [47].

Data measured at an age of 28 days are presented in Table 2. Mixtures 1 through 5 were not tested for 28 day BR, as the equipment was being distributed. Data measured at an age of 56 days are presented in Table 3. Mixture 1 was not tested for 56 day BR because the equipment had still not been received. Data measured at an age of 91 days are presented in Table 4.

TABLE 2—Average BR and variance obtained at a testing age of 28 days, kohm-cm.

Laboratory		Mixture											
		1	2	3	4	5	6	7	8	9	10	11	12
1	Avg.	n/a	n/a	n/a	n/a	n/a	5.29	13.41	14.97	8.84	12.67	6.46	14.89
	Var.	n/a	n/a	n/a	n/a	n/a	0.03	0.15	1.28	0.16	0.06	0.03	0.82
2	Avg.	n/a	n/a	n/a	n/a	n/a	5.27	14.12	16.98	8.36	13.49	6.73	18.84
	Var.	n/a	n/a	n/a	n/a	n/a	0.01	0.21	0.18	0.02	0.30	0.64	0.61
3	Avg.	n/a	n/a	n/a	n/a	n/a	5.19	13.54	14.03	7.69	11.53	5.43	16.04
	Var.	n/a	n/a	n/a	n/a	n/a	0.03	0.12	0.24	0.14	0.17	0.05	1.71
5	Avg.	n/a	n/a	n/a	n/a	n/a	5.65	15.19	16.73	8.31	16.93	7.36	n/a
	Var.	n/a	n/a	n/a	n/a	n/a	0.05	0.10	0.47	0.13	0.16	0.10	n/a
6	Avg.	n/a	n/a	n/a	n/a	n/a	5.55	15.24	15.69	9.60	13.72	6.68	20.24
	Var.	n/a	n/a	n/a	n/a	n/a	0.10	0.17	0.09	0.08	0.43	0.05	0.01
7	Avg.	n/a	n/a	n/a	n/a	n/a	5.03	13.59	15.01	8.91	12.87	6.88	16.90
	Var.	n/a	n/a	n/a	n/a	n/a	0.04	0.12	0.16	0.01	0.14	0.07	0.07
8	Avg.	n/a	n/a	n/a	n/a	n/a	5.84	14.36	16.58	8.63	14.59	6.81	18.21
	Var.	n/a	n/a	n/a	n/a	n/a	0.03	0.36	0.14	0.10	0.45	0.13	0.15
9	Avg.	n/a	n/a	n/a	n/a	n/a	5.31	14.39	16.37	8.91	13.15	7.00	16.48
	Var.	n/a	n/a	n/a	n/a	n/a	0.00	0.01	0.11	0.05	0.40	0.04	0.84
10	Avg.	n/a	n/a	n/a	n/a	n/a	5.12	14.20	15.60	8.62	14.22	6.77	18.55
	Var.	n/a	n/a	n/a	n/a	n/a	0.00	0.05	0.02	0.39	0.13	0.01	0.12
12	Avg.	n/a	n/a	n/a	n/a	n/a	5.68	14.02	15.11	8.30	12.30	6.40	16.76
	Var.	n/a	n/a	n/a	n/a	n/a	0.01	0.20	0.04	0.21	0.26	0.13	0.11
All labs	Mean	n/a	n/a	n/a	n/a	n/a	5.39	14.21	15.71	8.62	13.55	6.65	17.43
	Pooled variance	n/a	n/a	n/a	n/a	n/a	0.03	0.15	0.27	0.13	0.25	0.13	0.49
	Variance	n/a	n/a	n/a	n/a	n/a	0.07	0.40	0.90	0.26	2.22	0.26	2.72

TABLE 3—Average BR and variance obtained at a testing age of 56 days, kohm-cm.

Laboratory		Mixture											
		1	2	3	4	5	6	7	8	9	10	11	12
1	Avg.	n/a	6.73	8.76	12.63	8.07	6.56	24.34	29.99	14.78	22.20	11.98	18.14
	Var.	n/a	0.07	0.08	0.18	0.01	0.03	0.04	0.05	0.15	0.34	0.09	0.03
2	Avg.	n/a	8.64	9.10	12.05	10.83	7.22	24.52	27.25	13.14	22.53	12.69	20.12
	Var.	n/a	0.38	0.05	0.10	0.65	0.09	1.28	0.11	0.05	0.79	0.64	0.42
3	Avg.	n/a	6.18	7.81	12.26	7.71	5.81	23.13	21.61	12.17	17.26	n/a	17.71
	Var.	n/a	0.23	0.05	0.01	0.00	0.00	0.73	0.39	0.11	0.19	n/a	1.48
5	Avg.	n/a	7.98	9.26	11.41	7.26	7.08	24.10	29.12	14.92	22.48	10.91	n/a
	Var.	n/a	0.00	0.48	0.03	0.12	0.02	0.39	0.24	1.12	0.14	0.01	n/a
6	Avg.	n/a	7.70	9.16	12.89	9.99	6.70	n/a	25.02	n/a	19.62	10.09	21.49
	Var.	n/a	0.06	0.46	0.02	0.01	0.21	n/a	0.87	n/a	0.78	0.08	0.12
7	Avg.	n/a	8.38	8.55	12.34	8.33	6.57	24.20	27.18	16.50	21.37	12.16	19.88
	Var.	n/a	0.64	0.09	0.08	0.05	0.04	0.27	1.46	0.06	0.02	1.03	0.62
8	Avg.	n/a	7.18	9.27	13.64	9.31	6.72	25.89	31.29	14.38	24.98	12.55	20.85
	Var.	n/a	0.18	0.12	0.06	0.08	0.03	1.73	0.68	0.25	0.36	0.10	0.46
9	Avg.	n/a	n/a	9.20	13.50	8.59	6.52	26.09	30.28	15.13	23.23	13.43	20.27
	Var.	n/a	n/a	0.11	0.72	0.01	0.05	0.07	0.81	0.10	0.93	0.22	0.25
10	Avg.	n/a	7.98	8.92	14.85	7.94	6.26	26.58	26.03	14.20	22.24	11.22	21.46
	Var.	n/a	0.00	0.23	0.61	0.13	0.01	0.34	0.08	0.81	0.17	0.03	0.25
12	Avg.	n/a	6.10	8.34	11.94	7.90	6.52	22.21	23.65	13.06	18.67	9.95	15.99
	Var.	n/a	0.03	0.01	0.03	0.16	0.03	1.76	0.68	0.53	0.73	0.05	0.86
All labs	Mean	n/a	7.43	8.84	12.75	8.59	6.59	24.56	27.14	14.25	21.46	11.66	19.55
	Pooled variance	n/a	0.18	0.17	0.18	0.12	0.05	0.73	0.54	0.35	0.44	0.25	0.50
	Variance	n/a	0.86	0.23	1.02	1.25	0.15	2.02	9.74	1.70	5.29	1.44	3.52

The data presented in Tables 2 through 4 were analyzed according to ASTM C802 in order to determine the corresponding components of variance for the variability from within-laboratory and multi-laboratory data. The within-laboratory variability is typically attributed to variability stemming from the operator, as well as variability inherent in the test equipment and in the samples being tested. It should be noted that when using the approach taken for this round-robin testing, variations between samples arising from sample preparation issues could contribute to this component of variability. This is discussed later in this paper.

The data were also analyzed to evaluate the relationship between the variability of each of the mixtures and the properties of that mixture. Specifically, the w/c and the mass fraction of cementitious materials were evaluated. No significant correlation was seen between the variability and these mixture characteristics.

Within-laboratory Variability

The operator variability, the variability of specimens, and the inherent variability in the mixture are all grouped together into the within-laboratory variability. This value is computed using the average within-laboratory coefficient of variation (COV), presented in Table 5 [47]. Previous work evaluating the development of an automated resistivity testing system has reported a similar within-laboratory COV of around 3 % to 4 % for samples older than 24 h [48]. It should be noted that the variation increases over time. It is believed that this might be due to slight variations in

TABLE 4—Average BR and variance obtained at a testing age of 91 days, kohm-cm.

Laboratory		Mixture											
		1	2	3	4	5	6	7	8	9	10	11	12
1	Avg.	10.24	8.07	12.14	18.71	11.36	7.58	38.05	42.08	19.44	34.98	17.90	18.80
	Var.	0.19	0.05	0.23	0.39	0.02	0.06	0.01	7.14	0.37	1.22	0.20	0.79
2	Avg.	12.16	10.43	15.12	18.83	16.81	8.31	32.40	39.19	17.58	29.78	16.17	24.58
	Var.	0.48	0.12	0.94	0.77	0.62	0.04	2.72	0.25	0.04	1.25	0.89	1.08
3	Avg.	10.43	7.85	10.61	16.58	9.46	6.65	28.87	31.78	14.63	22.71	13.10	17.18
	Var.	0.16	0.43	0.68	0.07	0.19	0.26	2.12	2.63	0.32	0.21	0.79	0.36
5	Avg.	11.01	8.36	12.12	16.21	10.20	8.48	33.45	37.14	20.19	28.66	15.45	n/a
	Var.	0.20	0.02	0.47	0.05	0.16	0.02	0.50	1.07	2.72	0.27	0.29	n/a
6	Avg.	13.91	10.11	14.34	23.58	n/a	7.65	30.97	30.81	15.60	29.92	15.80	20.96
	Var.	0.00	0.03	1.04	0.09	n/a	0.40	0.98	0.05	0.35	0.89	0.06	0.01
7	Avg.	10.67	10.05	14.11	19.27	12.58	7.94	35.83	40.06	20.81	29.55	17.18	21.03
	Var.	0.15	0.44	0.83	0.04	0.08	0.03	0.70	2.41	0.05	0.10	0.03	0.48
8	Avg.	12.22	8.92	13.25	20.47	13.29	7.67	38.06	45.59	19.19	35.36	18.49	20.29
	Var.	0.02	0.23	0.18	0.23	0.11	0.05	4.03	1.94	0.43	1.04	0.18	0.51
9	Avg.	11.16	10.09	14.35	19.54	12.06	8.60	37.74	43.37	n/a	34.48	22.41	19.55
	Var.	0.00	0.59	0.05	2.77	0.10	0.42	0.02	9.91	n/a	3.77	4.91	0.79
10	Avg.	12.39	9.75	13.71	22.44	12.65	6.74	37.54	38.41	18.26	30.51	16.50	21.15
	Var.	0.07	0.80	0.34	2.00	1.42	0.00	0.24	0.08	1.21	0.46	0.14	0.23
12	Avg.	10.07	7.82	11.12	15.96	10.40	7.26	31.21	33.11	14.93	22.67	12.69	18.01
	Var.	0.23	0.02	0.00	0.04	0.15	0.04	3.08	1.92	0.52	0.78	0.01	0.02
All labs	Mean	11.43	9.15	13.09	19.16	12.09	7.69	34.41	38.15	17.85	29.86	16.57	20.17
	Pooled variance	0.15	0.27	0.47	0.65	0.32	0.13	1.44	2.74	0.67	1.00	0.75	0.47
	Variance	1.48	1.10	2.29	6.45	4.77	0.45	11.91	24.83	5.35	20.28	7.67	4.70

curing conditions that might have occurred at each lab, which could have amplified differences over time.

Multi-laboratory Variability

The multi-laboratory variability can be described by the average COV computed from the multi-laboratory component of variance [47]. The average values of the multi-laboratory COV are shown in Table 6. It should be noted that the variation increases over time. Again, slight variations in curing conditions that might have occurred at each lab could have amplified differences over time.

Precision Statements

Precision estimates were calculated [49]. For this experiment, the fundamental statistic was determined to be the COV, represented as 1s% in ASTM C670. Therefore, the calculated precision

TABLE 5—Average within-laboratory coefficient of variation.

Testing Age, days	Within-laboratory Coefficient of Variation, %
28	3.34
56	3.87
91	4.36

TABLE 6—Average multi-laboratory coefficient of variation.

Testing Age, days	Multi-laboratory Coefficient of Variation, %
28	7.75
56	9.83
91	13.22

indices correspond to d_{2s} as described in ASTM C670, determined by multiplying the average COV by the factor $2\sqrt{2}$ [49]. This index represents the maximum difference between two individual test results, expressed as a percentage of their average. The precision indices for different testing ages are shown in Table 7. The maximum precision index for within-laboratory and multi-laboratory variability is used to form the precision statements, which correspond to a testing age of 91 days.

The maximum pooled single-operator COV was found to be 4.36 %. Therefore, the results of two tests properly conducted by the same operator on the same concrete material at the same age are not expected to differ by more than 12.34 % of their average. The maximum pooled multi-laboratory COV was found to be 13.22 %. Therefore, the results of two tests properly conducted by different laboratories on the same concrete material at the same age are not expected to differ by more than 37.38 % of their average.

The precision statements for BR presented in this paper can be compared with the precision statements for other electrical test methods, namely, the RCP test and a corresponding SR test. The variability of the RCP test was obtained from the corresponding ASTM standard [15], and SR data were obtained from a report detailing the resistivity round robin [45]. For consistency, the SR data from Ref 45 were analyzed according to the same procedure described in this paper. Two tests done by the same operator on material from the same concrete mixture should not differ from their average by more than 42 % for the RCP test, 13.28 % for the SR test (with each test consisting of eight average measurements), and 12.34 % for the BR test (with each test consisting of one measurement). For tests conducted in separate laboratories, results should not differ from their average by more than 51 % for the RCP test, 34.55 % for the SR test, and 37.38 % for the BR test. It should be noted that because the SR test is sensitive to the specific location in which measurements is taken, an average of eight measurements is taken for each sample, which contributes to smaller variability in the pooled statistics. However, this means that more time is needed in order to perform the test. Conversely, the bulk measurement described herein is a single measurement.

Correlation with Other Electrical Test Methods

SR measurements were conducted as a part of this evaluation [45]. Figure 4 compares the measured SR and the calculated BR.

TABLE 7—Precision indices for bulk resistivity.

Testing Age, days	Within-laboratory	Multi-laboratory
28	9.44	21.93
56	10.94	27.82
91	12.34	37.38

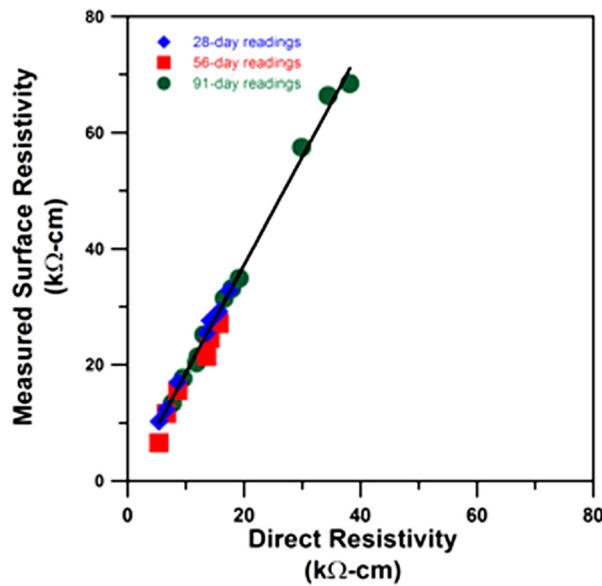


FIG. 4—Correlation of measured SR and BR of samples of differing ages; each data point represents the average of three samples.

A linear correlation was noticed, with $R^2 = 0.9986$, and with SR measurements tending to be 1.86 times higher than the BR. The large data in the experimental results support previous work using finite element methods that showed that additional geometry factors must be used in order to account for aspects of the test geometry, such as probe spacing, cylinder length, and cylinder diameter [27]. The factor of 1.86 is in good agreement with the geometric correction proposed by Morris et al. [27] for a cylinder with a length of 205 mm, a diameter of 102 mm, a probe spacing of 38.1 mm, and a maximum aggregate size of 19 mm, which was approximately 1.9.

As the RCP test is a widely used test for mixture characterization, Table 8 has been prepared to relate concrete resistivity to values obtained from RCP and SR testing. Previous empirical studies have also shown that RCP values can be related to concrete resistivity, termed the Berke empirical, and to the apparent SR, termed the Paredes empirical [28,36]. The total charge passed during the RCP test is used with Ohm’s law, an assumed testing period of 6 h, and a voltage of 60 V to

TABLE 8—Relationships between values obtained via different electrical test methods.

ASTM C1202 Classification ^a	Charge Passed, Coulombs ^a	Direct Resistivity, kohm-cm ^b	Berke Empirical, kohm-cm	Paredes Empirical, kohm-cm ^c	Apparent Surface Resistivity (102 mm × 205 mm), kohm-cm ^d
High	>4000	<5.2	<4.9	<6.5	<9.7
Moderate	2000–4000	5.2–10.4	4.9–8.76	6.5–11.3	9.7–19.3
Low	1000–2000	10.4–20.8	8.8–15.6	11.3–19.9	19.3–38.6
Very low	100–1000	20.8–207	15.6–105.9	19.9–136.6	38.6–386
Negligible	<100	>207	>105.9	>136.6	>386

^aFrom ASTM C1202 [15].

^bCalculated using Ohm’s law and geometry.

^cCorrected for geometry from Kessler et al. [28].

^dBulk resistivity multiplied by geometry factor.

determine the resistance. The standard test specimen (i.e., a 102 mm × 51 mm disc) can be normalized by the geometry using the factor described in Eq 4 to determine the BR [15]. This is a direct computation that does not consider the temperature effects or possible damage previously discussed. The values for the BR or apparent SR can then be ranked as classified by the RCP test method [15].

Effects of Electrode Resistance

Previous work has shown that electrode resistance (and other factors involved in ensuring connectivity between the electrode and sample) can influence the results as shown in Equation 2.

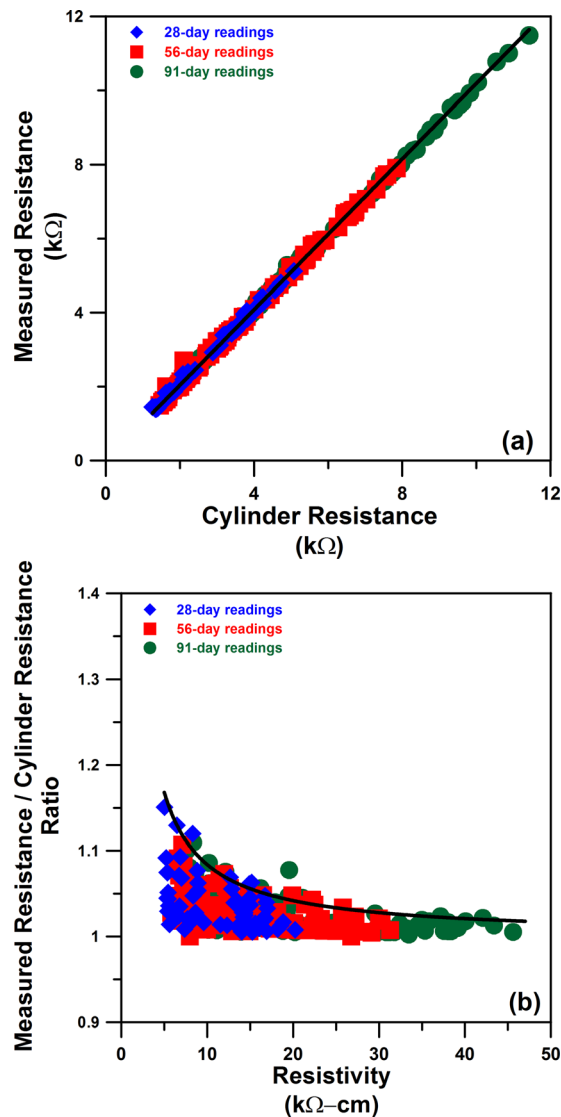


FIG. 5—Influence of electrode resistance on (a) the measured resistance (sample and electrodes) as a function of the cylinder (sample) resistance and (b) the ratio of measured resistance (sample and electrodes) to cylinder (sample) resistance as a function of concrete resistivity.

The major contributor to electrode resistance is poor contact between the plate electrode and the surface of the test cylinder. Some work has suggested the possibility of using flexible electrodes [27]. An alternative solution is to use an aid that allows for good electrical contact. In the laboratory, this can be accomplished through the use of an electrically conductive gel [50,51]. The alternative is to use another soft, conductive medium. Popular solutions have included the use of saturated sponges, chamois cloth, and paper towels [21,37].

An important issue becomes the associated resistance of the sponges. Previously, this associated resistance has been treated as a series of resistors in parallel with the test cylinder, which produces the correction shown and described by Equation 2.

The sponge resistance is largely dependent on the moisture content of the sponges and the conductivity of the solution in which they are saturated. For this evaluation, the solution was saturated lime-water, which was also used as the storage solution for the test cylinders. Furthermore, in order to ensure the proper moisture content, the contact pressure for the sponge was kept constant between the sponge resistivity test and the cylinder test, as shown in Figs. 2 and 3.

Although this correction provides the truest value of the BR, the results of this evaluation show that this correction might not always be very large. For the sponges used in this evaluation, the resistances of the two sponges were much less than the resistance of the cylinder. Figure 5(a) shows the measured resistance (i.e., sample, sponges, and electrodes) as a function of the cylinder resistance (i.e., the sample alone), as defined in Equation 2. The best fit line, given by Eq 5a with an R^2 of 0.9997, shows an average difference of less than 2 % between the measured resistance and the cylinder resistance.

Additionally, the ratio of the measured resistance to the actual cylinder resistance, as defined in the preceding paragraph, can be shown against the concrete resistivity, depicted in Fig. 5(b). This ratio represents the correction from the cylinder resistance. Figure 5(b) shows an upper bound of this ratio, given by Eq 5b. We can see that for lower concrete resistivities, the ratio can be significant. However, for better concrete (i.e., higher resistivity concrete), this ratio approaches 1.

$$\text{Measured Resistance} = 1.019 \times \text{Cylinder Resistance} \quad (5a)$$

$$\frac{\text{Measured Resistance}}{\text{Cylinder Resistance}} = 1.0 + 0.84 \times \frac{1}{\text{Concrete Resistivity}} \quad (5b)$$

Summary and Conclusions

This paper reports results from a multi-laboratory investigation of the variability associated with testing the electrical BR of concrete cylinders by placing plate electrodes on the ends of the cylinder. An analysis of the data is presented. It should be noted that the samples used in this evaluation were conditioned by storing the samples in lime-saturated water between test measurements. The following observations can be made regarding the variability of the resistivity test method: First, resistivity testing is a rapid test that drastically reduces the amount of time a technician needs to spend conditioning the sample and conducting the test. Therefore, this test is well suited for quality control testing. Second, resistivity testing can be considered a non-destructive test. This means that for each mixture being evaluated using resistivity, only a small number of samples need be prepared, and these samples can be measured at several different ages. This can be contrasted with other destructive electrical tests that require a larger series of samples for proper mixture evaluation. In fact, this testing can be performed on cylindrical samples before they are tested for

compressive or splitting tensile strength. Third, the operator and multi-laboratory precision of this test method have been quantified using data from the average COV obtained from an inter-laboratory evaluation consisting of ten laboratories and twelve different mixtures. For the BR test method, the within-laboratory COV is 4.36 %, and the multi-laboratory COV is 13.22 %. Fourth, the specimen geometry can greatly influence the results of an electrical test, and the use of a geometry correction factor is often required. For the BR test, this geometry factor is simply the ratio of the sample cross-sectional area to the sample length. Finally, the effects of electrode resistance were addressed using a series model. Whereas previous work described corrections for end plate resistance, the variability data from this investigation show that for the materials used in this evaluation, the correction that is needed is quite small. It is suggested that a standard resistivity test be developed that could allow samples to be tested using a variety of sample geometries, including (1) the Wenner probe geometry, (2) the bulk resistance described herein, and (3) alternative geometries, provided the geometry factor can be quantified. This could enable the use of all the different methods to obtain the material property known as BR.

Acknowledgments

The experiments reported in this paper were conducted as part of a larger evaluation sponsored by the Pooled Fund Program and the American Association of American Highway and Transportation Official's Technology Implementation Group and organized by the Florida Department of Transportation. The contents of this report reflect the views of the authors, who are responsible for the facts and the accuracy of the data presented herein. The contents do not necessarily reflect the official views or policies of the Indiana Department of Transportation or the Federal Highway Administration at the time of publication. This report does not constitute a standard, specification, or regulation. The writers would like to thank the participating laboratories and testing personnel for their time and efforts in collecting data. This includes, but is not limited to: Rob Reis, Cipriano Manansala, and Joe Shanabrook, California Department of Transportation; Jagan Gudimettla, FHWA Mobile Concrete Laboratory; Celik Ozyildirim and Bill Ordell, Virginia Department of Transportation; Wilfredo Malpica and Javier Molinari, Grupo-Carmelo; Ed McGaffin and Dan Dennis, New York State Department of Transportation; Lieska Halsey, Jeremy Weigel, and Tim Krason, Nebraska Department of Transportation; Eric Prieve and Azis Khan, Colorado Department of Transportation; John Kern and Wayne DeMarco, CEMEX; Thomas Frank and Ronald Simmons, Florida Department of Transportation; and Jeremiah Hersey and Professor Mike Jackson, University of North Florida. The writers also appreciate useful discussions with Ken Snyder and Dale Bentz of the National Institute of Standards and Technology and Kyle Bemis and Professor Bruce Craig of the Statistics Consulting Service at Purdue University

References

- [1] Hammond, E. and Robson, T. D., "Comparison of Electrical Properties of Various Cements and Concretes. I-II," *The Engineer*, Vol. 199, 1955, pp. 78–80.
- [2] Shimizu, Y., "An Electrical Method for Measuring the Setting Time of Portland Cement," *Concrete*, Vol. 32, 1928, pp. 111–113.
- [3] Calleja, J., "Effect of Current Frequency on Measurement of Electrical Resistance of Cement Pastes," *J. Am. Concr. Inst.*, Vol. 24, 1952, pp. 329–332.

- [4] Weiss, W. J., Shane, J. D., Miseses, A., Mason, T. O., and Shah, S. P., "Aspects of Monitoring Moisture Changes Using Electrical Impedance Spectroscopy," *Second Symposium on the Importance of Self Desiccation in Concrete Technology*, June 18, 1999 Lund, Sweden: Lund Institute of Technology, Division of Building Materials.
- [5] Monfore, G. E., *The Electrical Resistivity of Concrete*, Portland Cement Association, Research and Development Laboratories, Skokie, IL, 1968.
- [6] Whittington, H. W., McCarter, J., and Forde, M. C., "The Conduction of Electricity through Concrete," *Mag. Concrete Res.*, Vol. 33, 1981, pp. 48–60.
- [7] Christensen, B. J., Coverdale, R. T., Olson, R. A., Ford, S. J., Garboczi, E. J., Jennings, H. M., and Mason, T. O., "Impedance Spectroscopy of Hydrating Cement-based Materials: Measurement, Interpretation, and Application," *J. Am. Ceram. Soc.*, Vol. 77, 1994, pp. 2789–2804.
- [8] Rajabipour, F., 2006, "In Situ Electrical Sensing and Material Health Monitoring in Concrete Structures," Ph.D. dissertation, Purdue University, West Lafayette, IN.
- [9] Rajabipour, F. and Weiss, J., "Linking Health Monitoring in Concrete Structures with Durability Performance Simulations," *ASCE Structures Congress*, B. Cross and J. Finke, Eds., ASCE, St. Louis, MO, 2006.
- [10] Torquato, S., *Random Heterogeneous Materials: Microstructure and Macroscopic Properties*, Springer, New York, 2002.
- [11] Archie, G. E., "The Electrical Resistivity Log as an Aid in Determining Some Reservoir Characteristics," *Society of Petroleum Engineers Reprint Series*, 2003, pp. 9–16.
- [12] Aplin, K. L., "Aspirated Capacitor Measurements of Air Conductivity and Ion Mobility Spectra," *Rev. Sci. Instrum.*, Vol. 76, 2005, 104501.
- [13] McLachlan, D. S., Blaszkiewicz, M., and Newnham, R. E., "Electrical Resistivity of Composites," *J. Am. Ceram. Soc.*, Vol. 73, 1990, pp. 2187–2203.
- [14] Garboczi, E. J., "Permeability, Diffusivity, and Microstructural Parameters: A Critical Review," *Cem. Concr. Res.*, Vol. 20, 1990, pp. 591–601.
- [15] ASTM C1202, 2010, "Standard Test Method for Electrical Indication of Concrete's Ability to Resist Chloride Ion Penetration," ASTM International, West Conshohocken, PA.
- [16] AASHTO T277, 2007, "Standard Method of Test for Electrical Indication of Concrete's Ability to Resist Chloride Ion Penetration," American Association of State Highway and Transportation Officials, Washington, D.C.
- [17] Shane, J. D., Aldea, C. D., Bouxsein, N. F., Mason, T. O., Jennings, H. M., and Shah, S. P., "Microstructural and Pore Solution Changes Induced by the Rapid Chloride Permeability Test Measured by Impedance Spectroscopy," *Concr. Sci. Eng.*, Vol. 1, 1999, pp. 110–119.
- [18] Riding, K. A., Poole, J. L., Schindler, A. K., Juenger, M. C. G., and Folliard, K. J., "Simplified Concrete Resistivity and Rapid Chloride Permeability Test Method," *ACI Mater. J.*, Vol. 105, 2008, pp. 390–394.
- [19] Snyder, K. A., Ferraris, C., Martys, N. S., and Garboczi, E. J., "Using Impedance Spectroscopy to Assess the Viability of the Rapid Chloride Test for Determining Concrete Conductivity," *J. Res. Natl. Inst. Stand. Technol.*, Vol. 105, 2000, pp. 497–509.
- [20] Sohn, D. and Mason, T. O., "Electrically Induced Microstructural Changes in Portland Cement Pastes," *Adv. Cem. Based Mater.*, Vol. 7, 1998, pp. 81–88.
- [21] Shane, J. D., 2000, "Electrical Conductivity and Transport Properties of Cement-based Materials Measured by Impedance Spectroscopy," Ph.D. dissertation, Northwestern University, Evanston, IL.

- [22] Julio-Betancourt, G. A. and Hooton, R. D., "Study of the Joule Effect on Rapid Chloride Permeability Values and Evaluation of Related Electrical Properties of Concretes," *Cem. Concr. Res.*, Vol. 34, 2004, pp. 1007–1015.
- [23] Bentz, D. P., "A Virtual Rapid Chloride Permeability Test," *Cem. Concr. Compos.*, Vol. 29, 2007, pp. 723–731.
- [24] McGrath, P. F. and Hooton, R. D., "Re-evaluation of the AASHTO T259 90-day Salt Ponding Test," *Cem. Concr. Res.*, Vol. 29, 1999, pp. 1239–1248.
- [25] Yang, C. C., Cho, S. W., and Huang, R., "The Relationship between Charge Passed and the Chloride-ion Concentration in Concrete Using Steady-state Chloride Migration Test," *Cem. Concr. Res.*, Vol. 32, 2002, pp. 217–222.
- [26] Nokken, M. R. and Hooton, R. D., "Electrical Conductivity Testing," *Concr. Int.*, Vol. 28, 2006 pp. 58–63.
- [27] Morris, W., Moreno, E. I., and Sagues, A. A., "Practical Evaluation of Resistivity of Concrete in Test Cylinders Using a Wenner Array Probe," *Cem. Concr. Res.*, Vol. 26, 1996, pp. 1779–1787.
- [28] Kessler, R. J., Powers, R. G., and Paredes, M. A., "Resistivity Measurements of Water Saturated Concrete as an Indicator of Permeability," *Corrosion*, NACE International, Houston, TX, 2005.
- [29] Millard, S. G., "Reinforced Concrete Resistivity Measurement Techniques," *Proc. Inst. Civ. Eng., Part 2. Res. Theory*, Vol. 91, 1991, pp. 71–88.
- [30] Rajabipour, F., Weiss, J., Shane, J. D., Mason, T. O., and Shah, S. P., "Procedure to Interpret Electrical Conductivity Measurements in Cover Concrete during Rewetting," *J. Mater. Civ. Eng.*, Vol. 17, 2005, pp. 586–594.
- [31] Presuel-Moreno, F., Liu, Y., and Paredes, M., "Concrete Resistivity on the Apparent Surface Resistivity Measured via the Four-point Wenner Method," *Corrosion*, NACE International, Atlanta, GA, 2009.
- [32] Polder, R. B., "Test Methods for On Site Measurement of Resistivity of Concrete—A RILEM TC-154 Technical Recommendation," *Constr. Build. Mater.*, Vol. 15, 2001, pp. 125–131.
- [33] FM 5-578, 2004, "Florida Method of Test for Concrete Resistivity as an Electrical Indicator of Its Permeability," Florida Department of Transportation, Tallahassee, FL.
- [34] Rupnow, T. D. and Icenogle, P., *Evaluation of Surface Resistivity Measurements as an Alternative to the Rapid Chloride Permeability Test for Quality Assurance and Acceptance*, Louisiana Department of Transportation, Baton Rouge, LA, 2011, p. 68.
- [35] Vivas, E., Hamilton, H. R. I., and Boyd, A. J., *Permeability of Concrete—Comparison of Conductivity and Diffusion Methods*, Department of Civil and Coastal Engineering, University of Florida, Gainesville, FL, 2007, p. 238.
- [37] Berke, N. S. and Hicks, M. C., "Estimating the Life Cycle of Reinforced Concrete Decks and Marine Piles Using Laboratory Diffusion and Corrosion Data," *Corrosion Forms and Control for Infrastructure*, ASTM STP 1137, V. Chaker, Ed., ASTM International, West Conshohocken, PA, 1992, pp. 207–231.
- [37] Newlands, M. D., Jones, M. R., Kandasami, S., and Harrison, T. A., "Sensitivity of Electrode Contact Solutions and Contact Pressure in Assessing Electrical Resistivity of Concrete," *Mater. Struct.*, Vol. 41, 2008, pp. 621–632.
- [38] Castro, J., Spragg, R., Kompare, P., and Weiss, W. J., "Portland Cement Concrete Pavement Permeability Performance," Joint Transportation Research Program, Indiana Department of Transportation and Purdue University, West Lafayette, IN, 2010.

- [39] Nokken, M., Boddy, A., Wu, X., and Hooton, R. D., "Effects of Temperature, Chemical, and Mineral Admixtures on the Electrical Conductivity of Concrete," *J. ASTM Int.*, Vol. 5:5, 2008.
- [40] Castellote, M., Andrade, C., and Alonso, C., "Temperature Correction, from 3 to 25C of the Electrical Resistivity of Mortars and Concretes," *Industria Italiana del Cemento*, Vol. 71, 2001, pp. 850–851, 916–923.
- [41] Sant, G., Rajabipour, F., and Weiss, J., "The Influence of Temperature on Electrical Conductivity Measurements and Maturity Predictions in Cementitious Materials during Hydration," *Indian Concr. J.*, Vol. 82, 2008, pp. 7–16.
- [42] Villagran Zaccardi, Y. A., Fullea Garcia, J., Huelamo, P., and Di Maio, A. A., "Influence of Temperature and Humidity on Portland Cement Mortar Resistivity Monitored with Inner Sensors," *Mater. Corros.*, Vol. 60, 2009, pp. 294–299.
- [43] McCarter, W. J., Forde, M. C., and Whittington, H. W., "Resistivity Characteristics of Concrete," *Proc. Inst. Civ. Eng. (UK)*, Vol. 71, 1981, pp. 107–117.
- [44] Castro, J., Spragg, R., and Weiss, J., "Water Absorption and Electrical Conductivity for Internally Cured Mortars with a w/c between 0.30 and 0.45," *J. Mater. Civ. Engr.*, Vol 24:2, 2012, pp. 223–231.
- [45] Jackson, N. M., *Results of Round-robin Testing for the Development of Precision Statements for the Surface Resistivity of Water Saturated Concrete*, Report Number: FL/DOT/SMO/11-549, Jackson Research Engineers, Ponte Vedra Beach, FL, 2011.
- [46] AASHTO TP95, 2011, "Draft Standard Method of Test for Surface Resistivity Indication of Concrete's Ability to Resist Chloride Ion Penetration," American Association of State Highway and Transportation Officials, Washington, D.C.
- [47] ASTM C802, 2009, "Standard Practice for Conducting an Interlaboratory Test Program to Determine the Precision of Test Methods for Construction Materials," ASTM International, West Conshohocken, PA.
- [48] Poursaee, A. and Weiss, W. J., "An Automated Electrical Monitoring System (AEMS) to Assess Property Development in Concrete," *Autom. Constr.*, Vol. 19, 2010, pp. 485–490.
- [49] ASTM C670, 2010, "Standard Practice for Preparing Precision and Bias Statements for Test Methods for Construction Materials," ASTM International, West Conshohocken, PA.
- [50] Henkensiefken, R., Castro, J., Bentz, D. P., Nantung, T., and Weiss, J., "Water Absorption in Internally Cured Mortar Made with Water-filled Lightweight Aggregate," *Cem. Concr. Res.*, Vol. 39, 2009, pp. 883–892.
- [51] Thomas, M. D. A., "The Use of Conductive Gel," personal communication, W. J. Weiss, 2008.

1 Using a Saturation Function to Interpret the Electrical Properties of Partially Saturated Concrete

2 Jason Weiss,¹ Ken Snyder,² Jeff Bullard,² and Dale Bentz²

3 1 Purdue University, West Lafayette, IN

4 2 National Institute of Standards and Technology, Gaithersburg, MD

5 Abstract

6 Electrical properties are frequently measured in the concrete construction industry as a part of
7 mixture qualification and quality control testing. While there are several factors that influence the
8 electrical response of concrete, one of the most important factors is its degree of saturation. Although
9 current standard tests rely on the concrete being saturated, this can be difficult to accomplish, is time
10 consuming, and can artificially increase the degree of hydration of the test sample in comparison to that
11 of concrete in field structures (when the test samples are stored in water). While some studies have
12 measured the electrical response of concrete for samples with different moisture content (i.e., stored at
13 different relative humidities), a single expression has not been proposed that predicts how drying
14 changes the electrical response. This paper suggests that a saturation function should be considered as a
15 possible method to account for, and to correct for, less than complete saturation in concrete. This
16 function would provide one term that accounts for changes in pore fluid volume, pore solution
17 concentration, and pore fluid connectivity. While preliminary, this approach has several potential
18 benefits: 1) it could enable testing of partially saturated concrete, thus saving time; 2) it could be used
19 to predict properties under different exposure conditions; 3) it may facilitate more comprehensive
20 service life models; and 4) it may enable a wider use of embedded sensor technology.

21 Background

22 Several test methods exist in the construction industry that use measures of the electrical
23 properties of concrete as an indicator of potential durability performance. The so-called rapid chloride
24 permeability (RCP) test (e.g., AASHTO T277/ASTM C1202) is one example of an electrical test for
25 concrete. For nearly three decades, the concrete profession has qualified concrete mixtures using the
26 RCP testing procedure. While rapid in comparison to long-term ponding tests, the RCP test procedure
27 applies an electrical potential to the test sample for 6 h and requires that the sample be vacuum
28 saturated prior to testing. Several researchers have suggested that the testing time could be
29 dramatically shortened without compromising the quality of the data. Snyder et al. (2000) illustrated
30 that there was no need for the 6 h measurement because values after 1 min or 5 min provide an equally
31 valid indication of the electrical resistivity of the concrete. Other researchers have confirmed that the
32 test can be performed with shorter test times (Shane et al. 1999, Riding et al. 2008). In fact, shortening
33 the test would improve the quality of the results, as it reduces the potential for Joule heating, which
34 artificially increases the measured response of charge passed over time (Julio-Betancourt and Hooton
35 2004). Since the time of the preparation of this paper, ASTM committee C09 has accepted a new test
36 method to implement this more rapid measurement protocol (ASTM C1760). But, even if the
37 measurement time is reduced, the sample preparation time is still inconveniently long. RCP testing (or
38 ASTM C1760) requires saturation of the sample, a task which is time consuming, labor intensive, and
39 difficult to accomplish in many cases. The cost of testing (in terms of time and money) could be
40 significantly reduced if reliable measurements could be made on partially saturated specimens. Such a
41 measurement also has value in that it can provide information on the transport properties under
42 partially saturated conditions.

43 Similarly, time might be saved by using test geometries and methods other than the rapid
44 chloride permeability test. Surface measurements of electrical properties are popular (FM-5-578 2004),
45 and AASHTO has recently developed a provisional standard (TP95-11) based on the Wenner four probe

46 surface resistance test (Morris et al. 1996, Berke and Hicks 1992, Kessler et al. 2005, UNE 2008a, Jackson
47 2011, Rupnow and Icenogle 2011). Although this test procedure can be performed in less than 2 min, it
48 frequently requires the storage of samples in lime-saturated water. While storage in water is intended
49 to ensure that the samples are saturated, low-permeability concretes may not maintain saturation even
50 after long immersion times, due to self-desiccation (internal drying). Likewise, samples stored in air,
51 even humid air, are not fully saturated. Furthermore, storage in water may provide additional curing
52 and/or leaching that are not representative of what may be happening in actual field structures.

53 Other test procedures have also been proposed for rapid electrical testing. Specifically, a test
54 procedure has been proposed that measures a bulk resistivity through cylinders (Whittington et al.
55 1981, Newlands et al. 2008, UNE 2008b, Spragg et al. 2011). Tests could be conducted on samples of
56 other geometries or even between embedded electrodes (Monfore 1968, McCarter et al. 1981, Hansson
57 and Hansson 1983, Christensen et al. 1994, Tumidajski et al. 1996, Gu et al. 1992, Raupach and Scheissl
58 1997, Scheissl et al. 1999, Sellevold et al. 1997, Shane et al. 1999, Weiss et al. 1999, Rajabipour et al.
59 2007, Poursaee et al. 2009, Castro et al. 2010). Each of these methods uses a different electrode
60 configuration and sample size, thereby requiring a separate geometric correction factor; however, the
61 fundamental principles of the tests are similar. Details on many of the geometric correction factors are
62 available in the literature (e.g., Rajabipour 2006).

63 It is interesting to note that, when the appropriate geometric corrections are made and the
64 samples are uniform (i.e., relatively homogenous) and properly conditioned, an intrinsic material
65 property (conductivity or resistivity) is obtained that is independent of sample geometry. Therefore, all
66 of these methods have great promise for moving the field towards qualification and quality control test
67 methods that are simple and related to durability performance, but it should be noted that their results
68 can be dramatically influenced by the degree of saturation of the concrete (Monfore 1968, Scheissl et al.

69 1999, Andrade et al. 2011). This paper will focus on understanding how the moisture content (i.e.,
70 degree of saturation) influences the overall measured electrical response. Specifically, this paper
71 suggests that a universal expression could be used to interpret measurements for partially saturated
72 concrete.

73 **Electrical Conductivity Expression for Saturated Concrete**

74 The electrical conductivity (inverse of resistivity) of concrete depends on five factors: the
75 conductivity of the solution in the pores, the volume of saturated pores (porosity), their connectivity
76 within the microstructure (tortuosity), temperature, and the degree of saturation. Although there are
77 several expressions that could be used to estimate the electrical response of a composite like concrete
78 (Torquato 2002), the two most commonly used are a modified parallel law (i.e., a model of straight non
79 intersecting tubes which is modified to account for tortuosity and connectivity with the term β , Garboczi
80 1990) and Archie's equation (originally developed in 1942 and reprinted in 2003). Of the two, Archie's
81 equation for the electrical conductivity of a rock soaked (saturated) in brine provides a useful starting
82 point:

$$\frac{\sigma_r}{\sigma_b} = a\phi^m \quad [1]$$

83 where a is a parameter that depends upon the rock type, σ_r is the rock conductivity, σ_b is the brine
84 conductivity, and ϕ is the pore volume fraction (porosity). The exponent m is a fitting parameter that is
85 referred to as the cementation factor. It should be noted that the cementation factor refers to how the
86 microstructure is formed, and is not related to the actual cementitious content of the material. Archies
87 law can be related to the modified parallel law as shown by Garboczi (1990).

88 **Electrical Conductivity Expression for Partially Saturated Concrete**

89 Several researchers have developed expressions similar to equation 1 for partially saturated
90 concrete. These modifications consist of reinterpreting the pore volume as only the volume of the pore
91 fluid (Weiss 1999, Andrade et al. 2011). While that simple correction may be expedient, it leads to some
92 confusion between pore volume and fluid-filled pore volume. Further, additional complications arise
93 since several factors in Eq. 1, including the pore solution conductivity and solution connectivity, change
94 as the degree of saturation changes. As such, previous work has accounted for each factor individually
95 (Rajabipour et al. 2007); however this can be very time consuming and does not lend itself to easy use
96 for quality control testing during construction.

97 An alternative approach is to start with the expression that characterizes the pore structure of
98 the concrete called the formation factor (a uniquely defined parameter for a material with a given
99 composition and degree of hydration) and to incorporate an empirical expression for the effects of
100 partial saturation. For a fully saturated concrete, the ratio of the pore solution conductivity at saturation
101 σ_p^o to the concrete conductivity at saturation σ_c^o is the formation factor F (Snyder, 2001):

$$\frac{\sigma_p^o}{\sigma_c^o} = F \quad [2]$$

102 For a partially saturated concrete, the concrete conductivity σ_c decreases as the saturation level of the
103 concrete decreases (assuming the pore solution composition remains constant). This is due, in part, to
104 the reduction in the pore fluid volume but also due to changes in the connectivity of the connected
105 pathways and changes in the pore solution in the system (Rajabipour et al. 2007). For a concrete, the
106 relationship between the concrete conductivity and the saturation could be accounted for using an
107 expression that will be referred to as the saturation factor, $f(S)$:

$$\frac{\sigma_c}{\sigma_p} = \frac{1}{F} f S \quad [3]$$

108 The function $f(S)$ has the property that $f(S=1) = 1$ and $f(S<1) < 1$. Furthermore, if one assumes that the
109 pore solution at saturation (σ_p^o) is known, the pore solution conductivity at values other than saturation
110 (e.g., due to drying) can be, as a first approximation, related to the degree of saturation:

$$\sigma_p = \frac{\sigma_p^o}{S} \quad [4]$$

111 This is an assumption that is not accurate for concentrated solutions, so an additional correction is
112 discussed later in the paper. Combining equations 3 and 4 results in equation 5:

$$\sigma_c = \frac{\sigma_p^o}{S} \frac{1}{F} f S \quad [5]$$

113 It should be remembered that this is not a rigorous algebraic derivation but the development of a trial
114 form for the equation based on fundamental engineering assumptions.

115 While the left hand side of the equation is the conductivity of the concrete as a function of saturation,
116 the right side of the equation has three terms. The first term accounts for the pore solution conductivity
117 (due to the mixture design and subsequent concentration due to water loss), the second term accounts
118 for the total pore space and the third term accounts for the connectivity of the fluid in the pore space.
119 Each term is independent of the others, and all of the parameters are related to well defined properties
120 of the matrix and the solution filling its pores. It should be noted that it is assumed that the
121 sample/solution does not carbonate or precipitate salts in this simplified analysis.

122 The saturation function is used in other transport problems and could be formulated in a number of
123 ways (Millington and Quirk 1961, Martys 1999, Samson and Marchand 2008, Schlumberger (2011)).
124 Within the constraint is that at saturation ($S=1$), the function's value is unity ($f(S=1)=1$), there is flexibility
125 in how the saturation function is approximated. One viable function that has been used to describe the
126 influence of saturation is a power-law relationship:

$$f S = S^n \quad [6]$$

127 where n is a fitting parameter called the saturation coefficient. As described later in this paper, n is
128 typically of the order of 1.5 to 3 for porous rocks, while it may be slightly higher for cement and concrete
129 (i.e., in the range of 3.5 to 5 for the paste and mortar samples or for the computer simulations discussed
130 in this paper).

131 It should also be mentioned that the degree of saturation (S) is frequently determined using the
132 difference in mass before and after drying at 100°C normalized by the equivalent difference in mass for
133 a saturated system. This mass-based form of the degree of saturation is used since it is easy to
134 determine experimentally in the laboratory. But, the mass-based determination is equal to the
135 saturation in terms of fluid volume only if the filling liquid is water. For concentrated electrolytes such as
136 concrete pore solutions, there may be merit in interpreting S as a volumetric degree of saturation
137 (volume of the fluid as compared with the overall volume of fluid that can be held by the pore system of
138 the sample at saturation). For this paper the mass based definition was used.

139 Figure 1 shows a plot of the saturation function S^n along with estimates based on experimental
140 data from Rajabipour et al. (2007), calculated from Eq. 3 using known values for the pore solution
141 conductivity at each step. In figure 1, the degree of saturation was determined on a mass basis. As may
142 be expected, the cement system behaves slightly differently than the siltstone that has larger pores, few
143 if any 'ink bottle pores', and a more open pore network. The saturation coefficient for the siltstone is
144 approximately 2 (which is a value consistent with that reported in the geological literature
145 (Schlumberger Oilfield Glossary 2011)). However, for the cement-based system with a ratio of water
146 mass to cement mass (w/c) of 0.50, the value of the saturation coefficient is approximately 3.5, and the
147 saturation coefficient approaches 5 for the system containing silica fume ($w/c = 0.35 + 5\%$ silica fume).
148 The saturation function shown as the dashed line in Figure 1, using equation 6, assumes $n = 4$. It should

149 be noted that the saturation function shown in Figure 1 is equivalent to the normalized conductivity
150 ratio (the ratio of the conductivity of the concrete to the conductivity of the pore solution, normalized
151 by the value of this ratio at saturation). As such, data like those in Figure 1 are currently quite rare in the
152 concrete literature, as the changes in the pore solution with saturation must be included when
153 developing such data.

154 **Saturation Functions from Simulation (Considering pore fluid volume and connectivity)**

155 The Virtual Cement and Concrete Testing Laboratory software (VCCTL), used to predict degree
156 of hydration, microstructure development, and physical properties of cement paste, mortar, or concrete
157 (Bullard et al., 2008), was adapted in this study to estimate the form of a saturation function. One
158 advantage of the numerical simulations is that they automatically account for the pore solution
159 conductivity, a property which may be difficult to measure experimentally in many partially saturated
160 cementitious samples for three reasons. First, it becomes difficult to extract the pore solution using the
161 pressurized approach like the one proposed by Barneyback and Diamond (1981) in partially saturated
162 conditions, due to the very low volume of available pore fluid. Second, the loss of water by drying can
163 also increase the ionic concentration of the solution, which concurrently increases the pore solution
164 conductivity (Rajabipour et al. 2007). Finally, pore solutions can be susceptible to rapid carbonation,
165 which will also significantly alter their conductivity (Rajabipour 2006).

166 Using the VCCTL, 3D virtual microstructures of cement paste were generated that were
167 chemically and physically representative of the real systems considered in this paper. Hydration and
168 microstructure development, under either saturated or sealed moisture conditions, were simulated out
169 to ages of 1 d, 2 d, 3 d, 7 d, 28 d, 90 d, and 365 d. The 3D microstructures at each age were input into a
170 finite difference model that calculated the net charge flux across the microstructure in response to a
171 fixed applied electric field (Garboczi 1998). The relative conductivity of the microstructure was

172 computed by dividing the charge flux by the electric field (Ohm's law). In addition, the formation factor,
173 F , was calculated by saturating the capillary pore volume (for the sealed curing condition specimens)
174 and repeating the calculation of effective conductivity. Effective conductivities calculated in this way are
175 reproducible to within $\pm 5\%$ for different realizations of a representative volume element of the paste
176 microstructure.

177 Figure 2 shows the simulated cement paste microstructures for a sealed mortar with a w/c of
178 0.42 and an aggregate volume fraction of 55 % at 3 d (Figure 2a) and at 365 d (Figure 2b). Over time, the
179 capillary porosity of the system decreases due to hydration. In addition, since the system is sealed, the
180 vapor-filled space increases due to chemical shrinkage and self-desiccation. To estimate the saturation
181 function, the conductivity of the sealed mortar was compared with the sealed mortar that was
182 'resaturated' by altering the conductivity of the vapor-filled space to be equivalent to that of the pore
183 solution.

184 It should be noted that two types of porosity are generally considered to exist in a hydrated
185 cement paste system. The capillary pores are larger pores (shown in black in Figure 2) which remain
186 from the original space occupied by mix water that has not filled in during hydration. The gel pores are
187 smaller pores that are created within hydration products. In the VCCTL model, microstructure is
188 represented as a 3D digital image where each voxel, a $1\ \mu\text{m}$ cube, is assigned a particular cement phase.
189 Therefore, capillary pores are computed directly from the voxels that represent pores in the simulation,
190 but the gel pores are assumed to occupy 38 % of the volume of any C-S-H voxel. This compares favorably
191 and is consistent with the calculations from a Powers' model type approach (Powers and Brownyard
192 1942). An advantage of the VCCTL model as compared with the Powers' calculations is that it provides a
193 3D spatial distribution of the porosity, including its tortuosity, which can be used in conductivity
194 computations. A disadvantage is that the capillary pores have a lower size limit of $1\ \mu\text{m}$ because of the

195 finite voxel size. This lower limit is relatively coarse compared with the smaller capillary pores in a typical
196 hydrated portland cement, although comparisons of capillary porosity correlation functions determined
197 on model and real microstructures for a $w/c=0.47$ cement paste are quite favorable (Bentz 2006).

198 Figure 3a shows results from the VCCTL simulation of a paste with a w/c of 0.50 and a degree of
199 hydration of 65 % yielding a similar formation factor (24.2) as that from the experimental data shown in
200 Figure 1. The formation factor was selected to match the formation factor that was measured
201 experimentally. A series of simulations were subsequently performed where fluid was systematically
202 removed from the capillary pores to simulate the influence of a change in the degree of saturation
203 caused by drying (after Bentz 1998) . To do so, the pore size surrounding each pore voxel was estimated
204 as the number of pore voxels within a $7 \times 7 \times 7$ box centered on the given voxel, thereby quantifying
205 pore size as an integer between 1 (smallest) and 343 (largest). The pore voxels were ranked in
206 descending order of this size estimate, and water removal was simulated by switching the state of the
207 largest pore voxels from “saturated” to “empty”. While the general trend between the experiment and
208 the simulation is similar, it can be noticed that the simulation shows a more dramatic influence of drying
209 on the saturation function than is observed experimentally ($n = 5$ for the simulations, while $n = 3.5$ for
210 the experiment shown in Figure 1).

211 Figure 3b plots the simulated saturation function for a series of sealed specimens with different
212 w/c ratios. The saturation function was determined by using the conductivity of a sealed mortar and the
213 conductivity of that sealed mortar after being ‘resaturated’, (i.e., by altering the conductivity of the
214 vapor-filled space to be equivalent to that of the pore solution). The results in Figure 3b represent
215 mortars with a wide range of w/c (0.30 to 0.45) and ages of 3 d to 365 d, along with the 0.50 paste that
216 was dried after reaching 65 % hydration (as shown in Figure 3a). The results of these simulations appear
217 to collapse reasonably close to the same line ($n=5$).

218 While these results indicate the potential that a single function may work for cementitious
 219 systems (with n equals approximately 4 from the limited experimental data), it should be noted that an
 220 exhaustive examination of all cement compositions, particle size distributions and degrees of hydration
 221 were not considered, as small changes in n may be observed. It is recommended that experiments be
 222 performed over a wide range of concrete mixture compositions to determine the best choice for this
 223 saturation coefficient.

224 **Correction for High Pore Solution Concentration on Drying**

225 The parameter S appearing in Eq. 4 approximates the influence of the water loss from the pore solution
 226 which increases concentration and conductivity (one example is due to drying). It was mentioned that
 227 equation 4 is a good first approximation for the pore solution conductivity; however, it does not account
 228 for the nonlinear relationship between conductivity and concentration that arises from ionic
 229 interactions. A more thorough expression can be developed based on the work of Snyder (2001). While
 230 the full derivation that is provided in Snyder (2001) was used in the analysis here, a simplified version is
 231 presented that produces nearly identical results where the conductivity of the solution is assumed to be
 232 proportional to the ionic strength I_M (for species with valence z and molar concentration c):

$$233 \quad I_M = \frac{1}{2} \sum_{i=1}^N z_i^2 c_i \quad [7]$$

234 The expression developed by Snyder (2001) for approximating the conductivity of a concentrated
 235 solution required a correction parameter for each species. Here, the assumption is that the composition
 236 of different concrete pore solutions are somewhat similar, so the expression in Snyder (2001) is
 237 modified by using a single parameter for the solution:

$$238 \quad \sigma \propto \frac{I_M}{1+G \frac{I_M}{I_M}} \quad [8]$$

239 where G is the conductivity parameter (assumed to be approximately $0.4 \text{ (mol/L)}^{-1/2}$ for a typical pore
 240 solution). Starting at saturation, as the specimen dries, the ionic strength is inversely proportional to the
 241 saturation (this is the same as increasing the concentration). The ratio of the pore solution conductivity
 242 to the initial pore solution conductivity is given in equation 9. The expression in equation 8 can be
 243 approximated by a power-law relationship where the degree of saturation is raised to a correction
 244 exponent, $\delta-1$ where the value of δ is a function of the pore solution ionic strength as shown in Figure 4.

$$245 \quad \frac{\sigma_p}{\sigma_p^o} \cong \frac{1}{S} \frac{1+G \frac{I_M}{S}}{1+G \frac{1}{S} I_M} = S^{\delta-1} \quad [9]$$

246 The parameter δ represents the degree to which the pore solution conductivity is not inversely
 247 proportional to the water content. It could be determined by experiment or calculation: extract the
 248 pore solution, measure the conductivity, add water, re-measure the conductivity, and fit data to $S^{\delta-1}$;
 249 or determine the ionic strength I_M of the pore solution and use the right two terms in Eq. 9. Combining
 250 equations 2, 3, and 9 yields a result for the ratio of the conductivity of drying concrete to saturated
 251 concrete accounting for the saturation coefficient and the concentration of the pore solution due to
 252 drying, where δ is based on the ionic strength:

$$\frac{\sigma_c}{\sigma_c^o} = S^{n-1+\delta} \quad [10]$$

253 Therefore, once the value of δ has been determined by either direct measurement of the pore fluid ionic
 254 strength (by elemental analysis) or by estimation based on the mixture design using the alkali content
 255 (i.e., the ionic strength), and assuming that n is known for a material or there exists a universal value of
 256 n for concrete, one can use equation 8 to estimate the change in a concrete conductivity due to changes
 257 in its degree of saturation.

258 **Example Application 1 - Comparing Sealed and Saturated Curing Conditions**

259 To illustrate the need for a method that enables electrical conductivity measurements to be
260 corrected based upon the degree of saturation in the concrete, the variation in conductivity was
261 measured from a series of concrete cylinders that were cast along with a bridge deck, made with an
262 ordinary portland cement concrete having a w/c of 0.39. These cylinders were demolded at 24 h and
263 were stored for a year (DiBella et al. 2011). The concrete cylinders were conditioned in one of three
264 ways after demolding. First, some samples were stored in limewater after demolding to simulate water
265 curing. Second, other samples were sealed in a double layer of thermally sealed plastic bags. The
266 samples that were sealed in bags were removed from the bags and tested in the sealed state. The
267 degree of saturation for the concrete sealed in a bag after 1 year was measured to be 0.56, which
268 corresponds to a relative humidity of approximately 85 % to 90 % (Li et al. 2012). Third, after initial
269 testing, the sealed concrete samples were then cut to size for RCP testing and water saturated under
270 vacuum in accordance with the ASTM C1202 procedures. Before conducting the 6 h measurement in
271 ASTM C1202, the resistivity was measured using plates on either side of the concrete disk (52 mm tall by
272 102 mm in diameter). At an age of 365 d, the measured conductivity of the concrete stored in limewater
273 was 0.0143 S/m. In contrast, the sealed concrete conductivity was 0.0037 S/m, and after being
274 resaturated, its conductivity was 0.0296 S/m, which is eight times greater than before resaturation.
275 These values are shown in Figure 5. Therefore, the measured conductivity strongly depends on how the
276 sample was cured and conditioned prior to testing.

277 This sensitive dependence of conductivity on sample storage and preparation implies that there
278 are at least two potential pitfalls when interpreting these kinds of measurements, both of which can
279 cause an underestimation of the conductivity. First, if a conductivity measurement were made on a
280 partially saturated sample, one could mistakenly believe that the material has a conductivity (diffusivity)
281 that is nearly an order of magnitude lower than it actually is when saturated. The second pitfall is to
282 neglect the effect of storage conditions. The concrete stored in lime water has approximately half the

283 conductivity of the concrete that was sealed during curing and saturated at the time of testing.
284 Therefore, a sample stored in lime water in the laboratory would appear to have a lower conductivity
285 than the same concrete that was sealed and saturated at the time of testing due to additional hydration
286 that occurs in the sample stored in water (i.e., a sample in the field can be expected to behave like it is
287 sealed if the curing/sealing compounds were working perfectly and this may differ from the sample
288 tested in the lab due to how the material has been cured)..

289 A mortar similar to that used in the experiments shown in Figure 5 was modeled using the
290 VCCTL ($w/c = 0.39$ and an aggregate volume of 55 %). To do so, the effective conductivity both of the
291 cement paste and of the interfacial transition zone (ITZ) region were first calculated as described earlier.
292 Next, the paste conductivity was used as input to a differential effective medium theory calculation
293 (Garboczi and Berryman (2000)), along with the aggregate volume fraction, grading, and mean ITZ
294 thickness, to calculate the effective conductivity of the mortar. This approach yields effective mortar
295 conductivities that are usually within 10 % of the value predicted by more accurate random walk
296 simulations on the same structure (Garboczi and Berryman (2000)). However, the simulation should not
297 be compared directly to the field concrete since it was performed on mortar and did not include
298 entrained air. The simulation is still helpful, however, since it can provide some useful insights regarding
299 trends and for interpreting the results as a function of their curing conditions and the saturation
300 function. The simulated normalized conductivity obtained using the VCCTL is 0.00047 for the lime water
301 saturated specimen, 0.000266 for the sealed specimen, and 0.00134 for the sealed sample that was
302 resaturated. The conductivity of the pore solution was estimated using an equivalent sodium content of
303 0.67 (<http://concrete.nist.gov/poresolncalc.html>; Bentz (2007)) with a resulting pore solution
304 conductivity between 12.4 S/m and 14.9 S/m. These estimated mortar conductivities are also shown in
305 Figure 5.

306 In comparing the sample that was continuously stored in lime water with the sample that was
307 sealed and saturated at each age, the overall conductivity of the continually saturated sample is lower,
308 presumably due to the differences in the extent of hydration. The experiments also likely show the
309 influence of leaching OH, K and Na ions. Figure 6a shows the simulated degree of hydration as a function
310 of time as obtained from the VCCTL simulations. As one may expect, the system that is saturated has a
311 higher degree of hydration (87 % at one year) than a system that is simply sealed cured (75 % at one
312 year) (Bentz and Stutzman 2006). In this particular experiment, the lime-water cured sample will have a
313 lower porosity (albeit a relatively small decrease from 38 % of the paste volume fraction to 36 % of the
314 paste volume fraction). It should be noted, however, that this small reduction in porosity is actually a
315 relatively large reduction in the fraction of the capillary porosity. For the mixtures being discussed,
316 nearly 65 % of this porosity at this degree of hydration is gel porosity. Figure 6b illustrates the degree of
317 saturation in the simulated mortars. While the saturated sample from the simulation remains at 100 %
318 saturation, the sealed sample has a degree of saturation that progressively decreases to approximately
319 81% at an age of 1 year. It should be noted that the VCCTL simulation did not include entrained air which
320 would comprise approximately 20 % of the *paste volume* for this mixture. If the degree of saturation for
321 the concrete sample is adjusted to account for entrained air (i.e., the air is added to the VCCTL
322 simulation as additional porosity of the system), the degree of saturation of the concrete cylinder is
323 more similar to that of the simulation (approx. 0.76 vs. 0.81).

324 The normalized conductivity for the simulated mortar is plotted as a function of time in Figure
325 7a. This is similar to results previously shown by Bentz (1998). It can be noticed that the samples have a
326 similar conductivity at early ages as one may expect; however over time substantial differences in
327 conductivity begin to develop. To better illustrate the influence of the degree of hydration on the
328 resulting pore structure, the normalized conductivity is plotted in terms of total pore volume in Figure
329 7b. Figure 7b shows that a single curve begins to appear that describes the specimens with water

330 (saturated) curing and the samples with sealed curing when they are tested in a saturated state. This
331 again confirms that the 'formation factor' (a normalized conductivity/pore solution conductivity) is a
332 material property that varies with degree of hydration (or pore volume) for the saturated system. The
333 primary difference between the samples cured under lime water and the samples that were sealed and
334 resaturated is that the samples that are cured under lime water exhibit more hydration, thereby
335 achieving a lower porosity and a lower normalized conductivity than the sealed/resaturated sample at
336 the same age (Figure 7b). Again, this is consistent with the experimental observations.

337 The results from Example Application 1 show that while the electrical conductivity may be a
338 simple property to measure, it can be significantly influenced by curing conditions (sealed versus lime
339 water saturated) and sample preparation (testing the sealed sample versus testing the sealed sample
340 that was resaturated).

341 **Example Application 2 - Measurements Made on Samples Exposed to Drying**

342 In addition to using electrical property measurements on quality control samples, several
343 researchers have measured electrical properties in concrete systems exposed to drying or wetting
344 (Schießl 1999, Weiss et al 1999, 1999b, Sellevold 2000, Andrade et al. 2011). While the drying process
345 takes place over a long time period and may set up moisture gradients inside of the concrete (Weiss et
346 al. 1999 and Rajabipour et al. 2005), moisture gradients are not considered here. The saturation
347 approach may be useful in estimating the response of a concrete equilibrated to different levels of
348 drying.

349 Figure 8 illustrates equation 8 plotted as a function of relative humidity (RH) for a series of
350 concretes with a w/c of 0.4 that were allowed to dry for nearly a year (Weiss et al. 1999). The equation
351 with a saturation coefficient of $n = 4$ provides a reasonable shape response at higher humidities, but this
352 relationship begins to break down for RH less than approximately 60 %. At these lower relative

353 humidities, the saturation function is low (approximately 0.1) and the capillary pore water is likely lost,
354 suggesting that the main conduction pathway likely changes from the large capillary pore network to the
355 gel pores or along the walls of the capillary pores. If this is true, the breakdown of the relation valid at
356 higher RH is not surprising.

357 The data for samples with a w/c of 0.4 and having no chemical admixtures (Schiesl et al. 1999)
358 were compared with equation 8 and a saturation coefficient of 3.9 was obtained for concrete with a w/c
359 of 0.4 for data at relative humidities greater than 60 %. A similar assessment of the data reported by
360 Andrade et al. (2011) would be consistent with saturation coefficients that are approximately 3.5. These
361 coefficients are similar to those observed from the numerical simulations reported in Figures 3 and 4
362 and from the plain pastes in Figure 1. This suggests that this approach may be applicable to drying
363 samples. Figure 8b illustrates the desorption isotherm to relate relative humidity and the degree of
364 saturation. It also illustrates the saturation function (assuming two different values for the saturation
365 coefficient (i.e., $n = 4$ and $n = 5$)). This illustrates that once the relative humidity drops below 65 % to 70
366 % RH, the saturation function is very low.

367 As such, it appears that it may be quite reasonable to design an experiment where the
368 saturation coefficient is determined for a concrete mixture by measuring the conductivity of a sample
369 with two different degrees of saturation (provided they are relatively high). Equation 5 could then be
370 fitted to determine the exponent for the particular mixture design used. For example, this could consist
371 of measuring the conductivity of a sealed sample and then measuring the conductivity of the same
372 sample after vacuum saturation. Assuming the mass of the sample is measured along with the electrical
373 properties, the degree of saturation could be obtained by oven drying the sample after testing and
374 measuring its oven-dried mass. This could then provide an estimate of n for each mixture.

375 A further illustration of this approach can be seen in Figure 9 where the surface resistivity was
376 measured on mortar specimens exposed to drying at 50 +/- 2% relative humidity (1 in. (25 mm) square
377 cross section and a 10.6 inch length (262.5 mm) (Bentz et al. 2012)). It can be noticed that despite the
378 samples not being in equilibrium during the test (i.e., the samples were drying and likely continuing to
379 hydrate slightly) a similar trend emerges for the saturation function. The mixture with a lower w/c
380 would be expected to have a more uniform moisture content and follow the expected function a little
381 more closely than the samples with a higher w/c that likely show some influence of the moisture
382 gradients.

383 **Summary**

384 Tests that measure the electrical conductivity of concrete are sensitive to the degree of
385 saturation of the concrete. This paper explores the potential for testing partially saturated concrete and
386 correcting this data based on its measured degree of saturation to obtain the formation factor, which is
387 a material property. This could have substantial impact when rapid field tests or embedded sensors are
388 used to provide measures of properties related to durability performance. Similarly, this approach could
389 be used to solve the equally important problem of converting measured transport coefficients for
390 saturated concrete to values that would correspond to field conditions with a lower degree of
391 saturation.

392 This paper suggests that the general form of Archie's Law can be written in a way that describes
393 the electrical conductivity of partially saturated concrete, using a stand-alone saturation function. It
394 appears that the saturation function can be written as the degree of saturation raised to an exponent
395 called the saturation coefficient (n). A suggestion for the form of this equation is shown in equation 8
396 which accounts for both drying effects and changes in the pore solution concentration and conductivity
397 during drying. While the saturation coefficient varies from approximately 1.5 to 2.5 for many rocks

398 (shown in this paper for siltstone as 2), it is slightly higher for cement-based materials, ranging from
399 approximately 3.5 to 5.5 for the limited data from experiments. Simulations made using the VCCTL show
400 a coefficient of approximately 5; however these simulations also showed that the saturation coefficient
401 exhibited little variation with changes in the degree of hydration or the water to cement ratio, over the
402 ranges investigated. The use of a saturation value of 4 provided reasonable correlation with the limited
403 experimental data for the plain portland cement-based systems described in this paper.

404 The saturation function in equation 8 accounts for changes in pore solution, pore fluid volume
405 and pore connectivity. The saturation function was used in two examples where the electrical properties
406 were measured, the first being concrete exposed to sealed curing and the second being concretes and
407 mortars exposed to drying. Future studies should be conducted to better understand the response of
408 partially saturated concrete and to obtain experimental values for n for a wider range of concrete
409 mixture compositions. When this work is performed, it would be helpful to describe the pore solution
410 conductivity (or to report the sodium and potassium alkali contents of the cement), so that the role of
411 pore solution concentration can be estimated. It would also be helpful to provide the degree of
412 saturation of the concretes in addition to their measured internal relative humidity.

413 **Acknowledgments**

414 This first author is grateful for support from the Joint Transportation Research Program administered by
415 the Indiana Department of Transportation and Purdue University. The contents of this paper reflect the
416 views of the authors, who are responsible for the facts and the accuracy of the data presented herein,
417 and do not necessarily reflect the official views or policies of the Indiana Department of Transportation,
418 nor do the contents constitute a standard, specification, or regulation.

419 **Disclaimer**

420 Certain commercial products are identified in this paper to specify the materials used and procedures
421 employed. In no case does such identification imply endorsement or recommendation by the National
422 Institute of Standards and Technology or Purdue, nor does it indicate that the products are necessarily
423 the best available for the purpose.

424 **References**

425 Andrade, M. C., Bolzoni, F. and Fullea, J. (2011). "Analysis of the relation between water and resistivity
426 isotherms in concrete", *Materials and Corrosion*, Vol. 62(2), 130-138.

427 Archie, G. E. (2003). "The electrical resistivity log as an aid in determining some reservoir
428 characteristics", *SPE Reprint Series*, (9-16.

429 ASTM C1202 (2010). Standard test method for electrical indication of concrete's ability to resist chloride
430 ion penetration, ASTM International, West Conshohocken, PA.

431 AASTHTO T277 (2007)., Standard method of test for electrical indication of concrete's ability to resist
432 chloride ion penetration, American Association of State Highway and Transportation Officials,
433 Washington, D.C.

434 Barneyback, S. and Diamond, S.(1981). "Expression and analysis of pore fluids from hardened cement
435 pastes and mortars ", *Cem Concr Res* 11, 279.

436 Bentz, D.P. (1998) "Modelling Cement Microstructure: Pixels, Particles, and Property Prediction,"
437 *Materials and Structures*, 32, 187-195

438 Bentz, D.P. and Stutzman, P.E., "Curing, Hydration, and Microstructure of Cement Paste," *ACI*
439 *Materials Journal*, **103**(5), 348-356, 2006

440 Bentz, D. P. (2007). "A virtual rapid chloride permeability test", *Cem Concr Compos*, 29, 723-731.

- 441 Bentz, D.P., "Quantitative Comparison of Real and CEMHYD3D Model Microstructures Using Correlation
442 Functions," Cement and Concrete Research, 36 (2), 259-263, 2006.
- 443 Bentz, D. P., Stutzman, P., Sakulich, A., and Weiss, W. J., (2012), "Study of Early-Age Bridge Deck
444 Cracking in Nevada and Wyoming", NISTIR 7841, January 2012.
- 445 Berke, N. S. and Hicks, M. C. (1992). "Estimating the Life Cycle of Reinforced Concrete Decks and Marine
446 Piles Using Laboratory Diffusion and Corrosion Data", in,.
- 447 Bullard, J. W. , Ferraris, C. F., Garboczi, E. J., Martys, N., Stutzman, P. E. and Terrill, J. E. (2008). "Virtual
448 Cement and Concrete." Chapter 10 in Innovations in Portland Cement Manufacturing. Edited by J.I.
449 Bhatti, F.M. Miller, and S.H. Kosmatka. Portland Cement Association, Skokie, IL.
- 450 Christensen, B. J., Coverdale, R. T., Olson, R. A., Ford, S. J., Garboczi, E. J., Jennings, H. M. and Mason, T.
451 O. (1994). "Impedance spectroscopy of hydrating cement-based materials: measurement,
452 interpretation, and application", J Am Ceram Soc, 77 , 2789-2804.
- 453 Castro, J., Spragg,, R., Kompare, P. and Weiss, W. J. (2010). "Portland Cement Concrete Pavement
454 Permeability Performance", Joint Transportation Research Program, Indiana Department of
455 Transportation and Purdue University, West Lafayette, Indiana.
- 456 Dibella, Carmello (in progress). "Transport and Shrinkage Properties in Plain and Internally Cured ",
457 MStHesis, Purdue University.
- 458 FM 5-578 (2004). "Florida method of test for concrete resistivity as an electrical indicator of its
459 permeability", Florida Department of Transportation, Tallahassee, FL.
- 460 Garboczi, E. J. (1990). "Permeability, diffusivity, and microstructural parameters: A critical review", Cem
461 Concr Res, 20 , 591-601.

- 462 Garboczi, E. J. (1998) Finite Element and Finite Difference Programs for Computing the Linear Electric
463 and Elastic Properties of Digital Images of Random Materials. NISTIR 6269; 211 p. December 1998.
- 464 Garboczi, E. J. and Berryman, J.G. (2000). "New effective medium theory for the diffusivity or
465 conductivity of a multi-scale concrete microstructure model", *Concr Sci Eng*, 2, 88-96.
- 466 Gu, P., Xie, P., Beaudoin, J. J. and Brousseau, R. (1992). « A.C. Impedance Spectroscopy 1 : A New
467 Equivalent Circuit Model for Hydrated Portland Cement Paste », *Cement and Concrete Research* 22,
468 833-840.
- 469 Julio-Betancourt, G. A. and Hooton, R. D. (2004). "Study of the Joule effect on rapid chloride
470 permeability values and evaluation of related electrical properties of concretes", *Cem Concr Res*, 34,
471 1007-1015.
- 472 Hansson, I.L.H. and Hansson, C. M. (1983). « Electrical resistivity measurements of Portland cement
473 based materials », *Cement and Concrete Research*, Vol. 13(5), 675-683.
- 474 Jackson,, N. M. (2011). "Results of round-robin testing for the development of precision statements for
475 the surface resistivity of water saturated concrete", Ponte Vedra Beach, Florida.
- 476 Kessler, R. J., Powers, R. G. and Paredes, M. A. (2005). " Resistivity Measurements of Water Saturated
477 Concrete as an Indicator of Permeability", in: *Corrosion 2005*, NACE International, Houston, TX.
- 478 Li, W., Pour-Ghaz, M., Castro, J., and Weiss, W. J., (2012) "Water Absorption and the Critical Degree of
479 Saturation as it relates to Freeze-Thaw Damage in Concrete Pavement Joints," *ASCE Journal of Civil*
480 *Engineering Materials*
- 481 Martys, N.S., "Diffusion in Partially-Saturated Porous Materials," *Materials and Structures*, 32, pp 555-
482 562 (1999).

- 483 Millington, R. J., and Quirk, J. P., (1961) 'Permeability of Porous Solids,' Transactions of the Faraday
484 Society, 57, pp. 1200-1207
- 485 McCarter, W. J., Forde, M. C. and Whittington, H. W. (1981). "Resistivity characteristics of concrete",
486 Proceedings of the Institution of Civil Engineers (London) Part 1 - Design & Construction, 71,
487 107-117.
- 488 Monfore, G. E. (1968). "The electrical resistivity of concrete", Portland Cement Association, Research
489 and Development Laboratories, Skokie, IL.
- 490 Morris, W., Moreno, E. I. and Sagues, A. A. (1996). "Practical evaluation of resistivity of concrete in test
491 cylinders using a Wenner array probe", Cem Concr Res, 26, 1779-1787.
- 492 Newlands, M. D., Jones, M. R., Kandasami, S. and Harrison, T. A. (2008). "Sensitivity of electrode
493 contact solutions and contact pressure in assessing electrical resistivity of concrete", Mater Struct,
494 41, 621-621-632.
- 495 Powers, T. C., and Brownyard, T.L., (1942) 'Studies of the Physical Properties of Hardened Portland
496 Cement Paste', Bulletin 22 Research and Development Laboratories of the Portland Cement
497 Association, Chicago, Illinois (1948)
- 498 Poursaei, A. and Weiss, W. J. (2009). « An automated electrical monitoring system (AEMS) to assess
499 property development in concrete », Automation in Construction, Vol. 19(4), 485-490.
- 500 Rajabipour, F., Weiss, J. and Shane, J. D., Mason, T. O. and Shah, S. P. (2005) Procedure to interpret
501 electrical
- 502 Rajabipour, F. and Weiss, J. (2007). « Electrical conductivity of drying cement paste », Materials and
503 Structures, Vol. 40(10), 1143-1160.

- 504 Rajabipour, F. (2006). "Insitu electrical sensing and material health monitoring in concrete structures",
505 Ph.D. Dissertation, Purdue University, West Lafayette, Indiana.
- 506 Raupach, M. and Schiessl, P. (1997). « Monitoring system for the penetration of chlorides, carbonation
507 and the corrosion risk for the reinforcement », Construction and Building Materials, Vol. 11(4), 207-
508 214.
- 509 Riding, K. A., Poole, J. L., Schindler, A. K., Juenger, M.C.G. and Folliard, K. J. (2008). "Simplified concrete
510 resistivity and rapid chloride permeability test method", ACI Mater J, 105, 390-394.
- 511 Rupnow, T. D., and Icenogle, P. (2011). "Evaluation of surface resistivity measurements as an alternative
512 to the rapid chloride permeability test for quality assurance and acceptance", Louisiana Department
513 of Transportation, Baton Rouge, LA, pp. 68.
- 514 Samson, E., and Marchand, J., (2007) 'Modeling the Transport of Ions in Unsaturated Cement-Based
515 Materials,' Computers and Structures, 85, pp. 1740-1756
- 516 Schissl, A., Weiss, W. J., Shane, J. D., Berke, N. S., Mason, T.O., and Shah, S. P., (2000) "Assessing the
517 Moisture Profile of Drying Concrete Using Impedance Spectroscopy," Concrete Science and
518 Engineering, Vol. 2, pp. 106-116
- 519 Sellevold, E. J., Larsen, C. K. and Blankvoll, A. A. (1997). « Moisture State of Concrete in a Coastal Ridge »,
520 Special Publication, SP170-42, Vol. 170, 823-834.
- 521 Schlumberger (2011), Oilfield Glossary
- 522 Shane, J. D., Aldea, C. D., Bouxsein, N. F. Mason, T. O., Jennings, H. M. and Shah, S. P. (1999).
523 "Microstructural and pore solution changes induced by the rapid chloride permeability test
524 measured by impedance spectroscopy", Concr Sc Eng, 1, 110-119.

- 525 Shane, J. D. (2000). "Electrical conductivity and transport properties of cement-based materials
526 measured by impedance spectroscopy", Ph.D. Dissertation, Northwestern University, Evanston, IL.
- 527 Snyder, K.A., (2001) "The relationship between the formation factor and the diffusion coefficient of
528 porous materials saturated with concentrated electrolytes: Theoretical and experimental
529 considerations," Concrete Science and Engineering, 3 (12), 216-224, (2001).
- 530 Snyder, K. A., Ferraris, C., Martys, N. S. and Garboczi, E. J. (2000). "Using impedance spectroscopy to
531 assess the viability of the rapid chloride test for determining concrete conductivity", J NIST, 105,
532 497-509.
- 533 Spragg, R, Castro, J., Nantung, T., Parades, M, and Weiss, W. J., (2011) "Variability Analysis of the Bulk
534 Resistivity Measured Using Concrete Cylinders," JTRP Report SPR-3509, FHWA/IN/JTRP-2011/21
535 DOI: 10.5703/1288284314646
- 536 Torquato, S. (2002). "Random heterogeneous materials: microstructure and macroscopic properties",
537 Springer, New York, NY.
- 538 TP95-11 (2011) Draft standard method of test for surface resistivity indication of concrete's ability to
539 resist chloride ion penetration, American Association of State Highway and Transportation Officials,
540 Washington, D.C.
- 541 Tumidajski, P. J., Schumacher, A. S., Perron, S., Gu. P. and Beaudoin, J. J. (1996). « On the relationship
542 between porosity and electrical resistivity in cementitious systems », Cement and Concrete
543 Research, Vol. 26(4), 539-544.
- 544 UNE (2008a), "Concrete durability. Test methods. Determination of the electrical resistivity. Part 1:
545 Direct test (reference method), UNE 83988-1, AENOR, February, 9 pp.

546

547 UNE (2008b), "Concrete durability. Test methods. Determination of the electrical resistivity. Part 2:

548 Four points or Wenner method, UNE 83988-2, AENOR, February, 8pp.

549

550 Weiss, W. J., Shane, J. D., Miseses, A., Mason, T. O. and Shah, S. P. (1999). "Aspects of monitoring

551 moisture changes using electrical impedance spectroscopy", Second symposium on the importance

552 of self desiccation in concrete technology, Lund, Sweden.

553 Whittington, H. W., McCarter, J., and Forde, M. C. (1981). "The conduction of electricity through

554 concrete", Mag Concr Res, 33 , 48-60.

Figure 1
Click here to download high resolution image

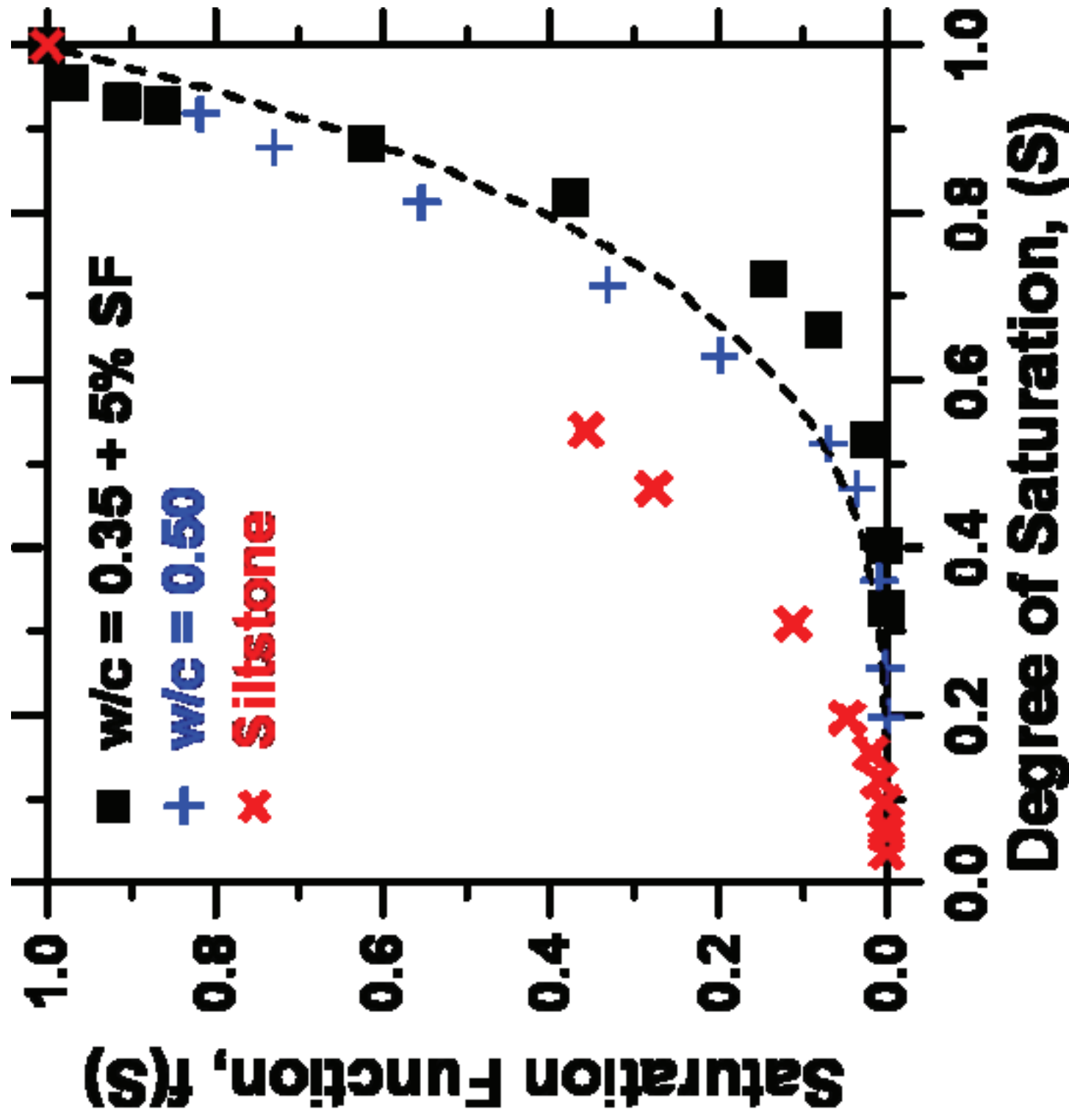


Figure 2

[Click here to download high resolution image](#)



Figure 2b
[Click here to download high resolution image](#)

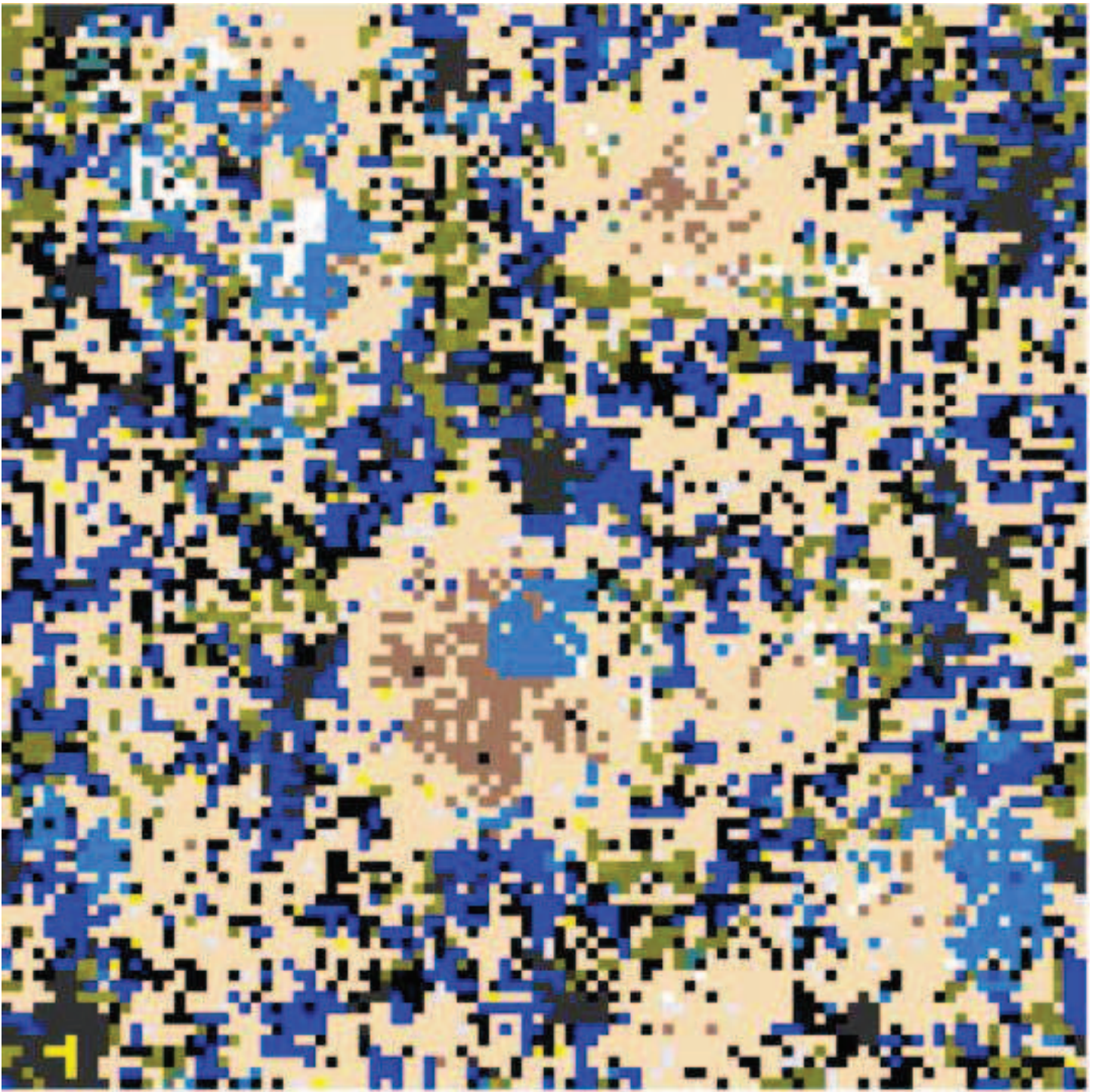


Figure 3
Click here to download high resolution image

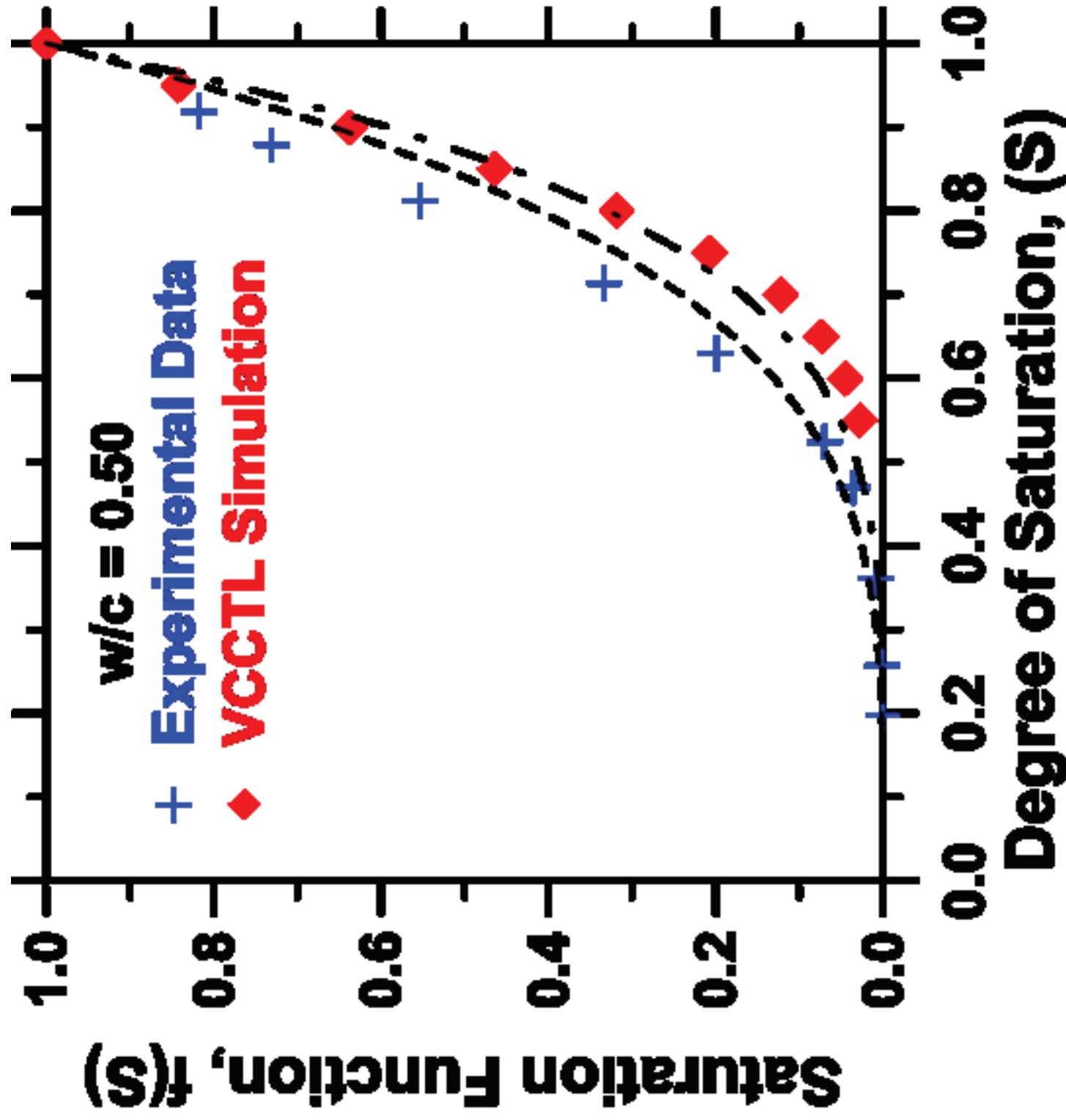
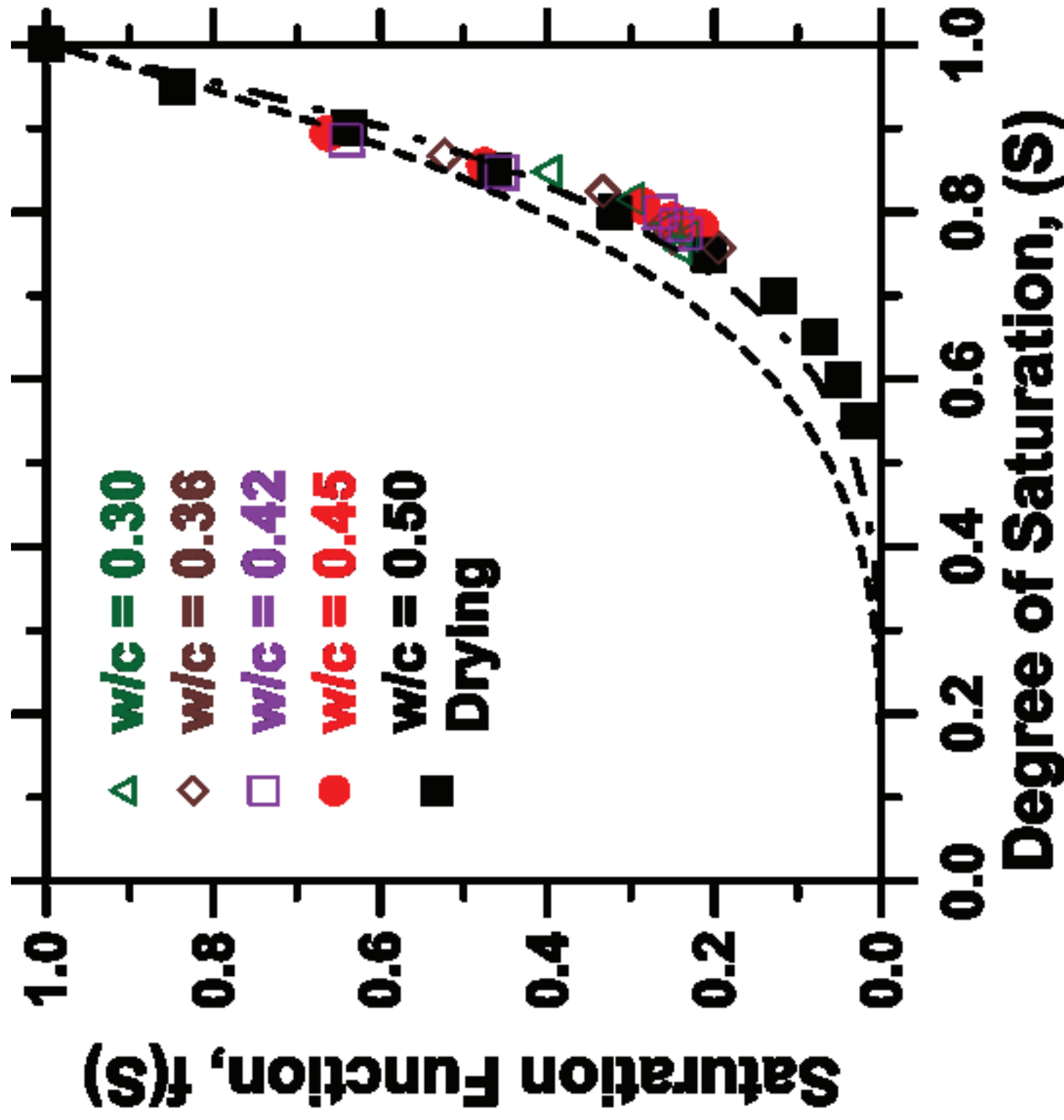


Figure 3b
[Click here to download high resolution image](#)



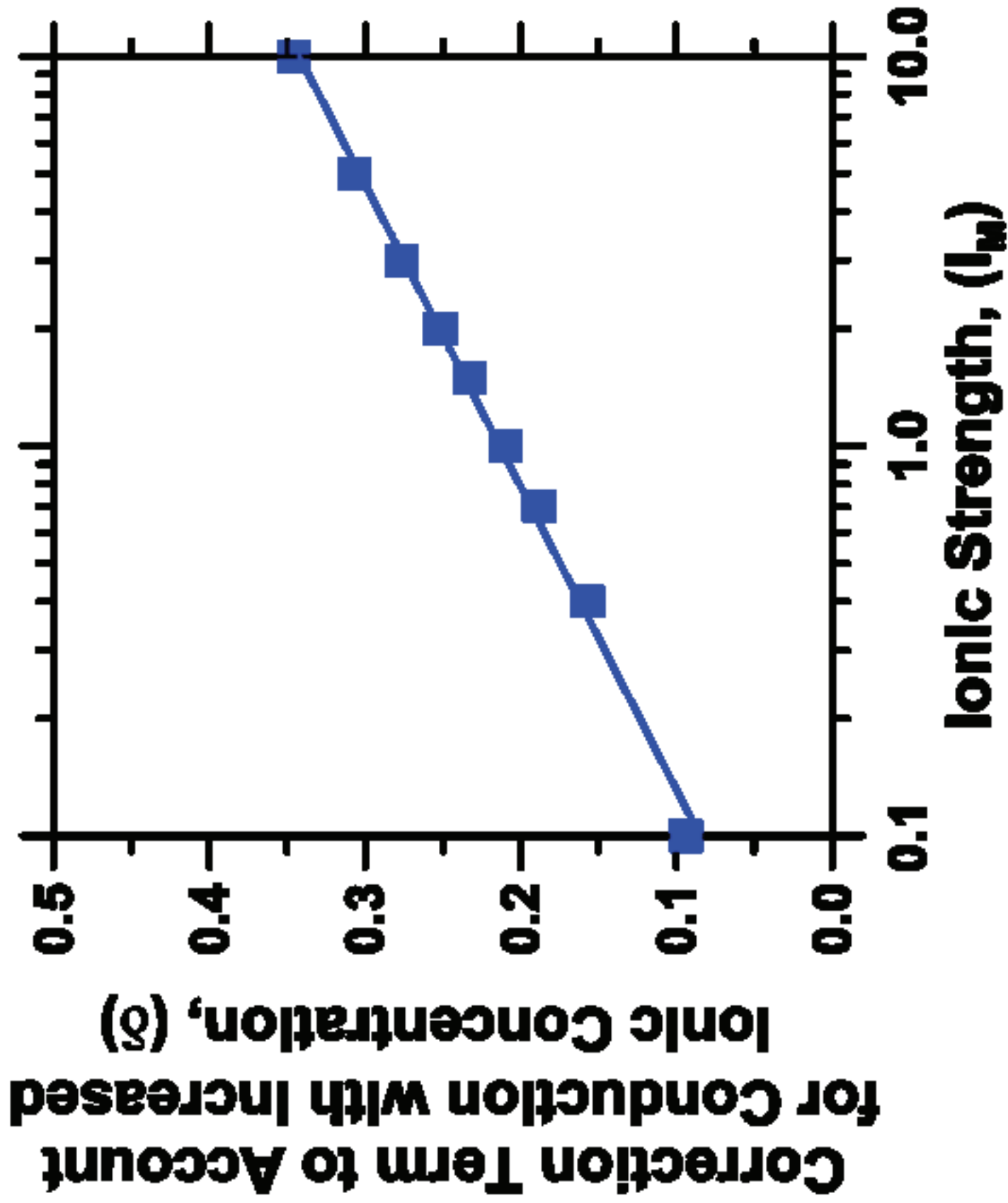


Figure 4
[Click here to download high resolution image](#)

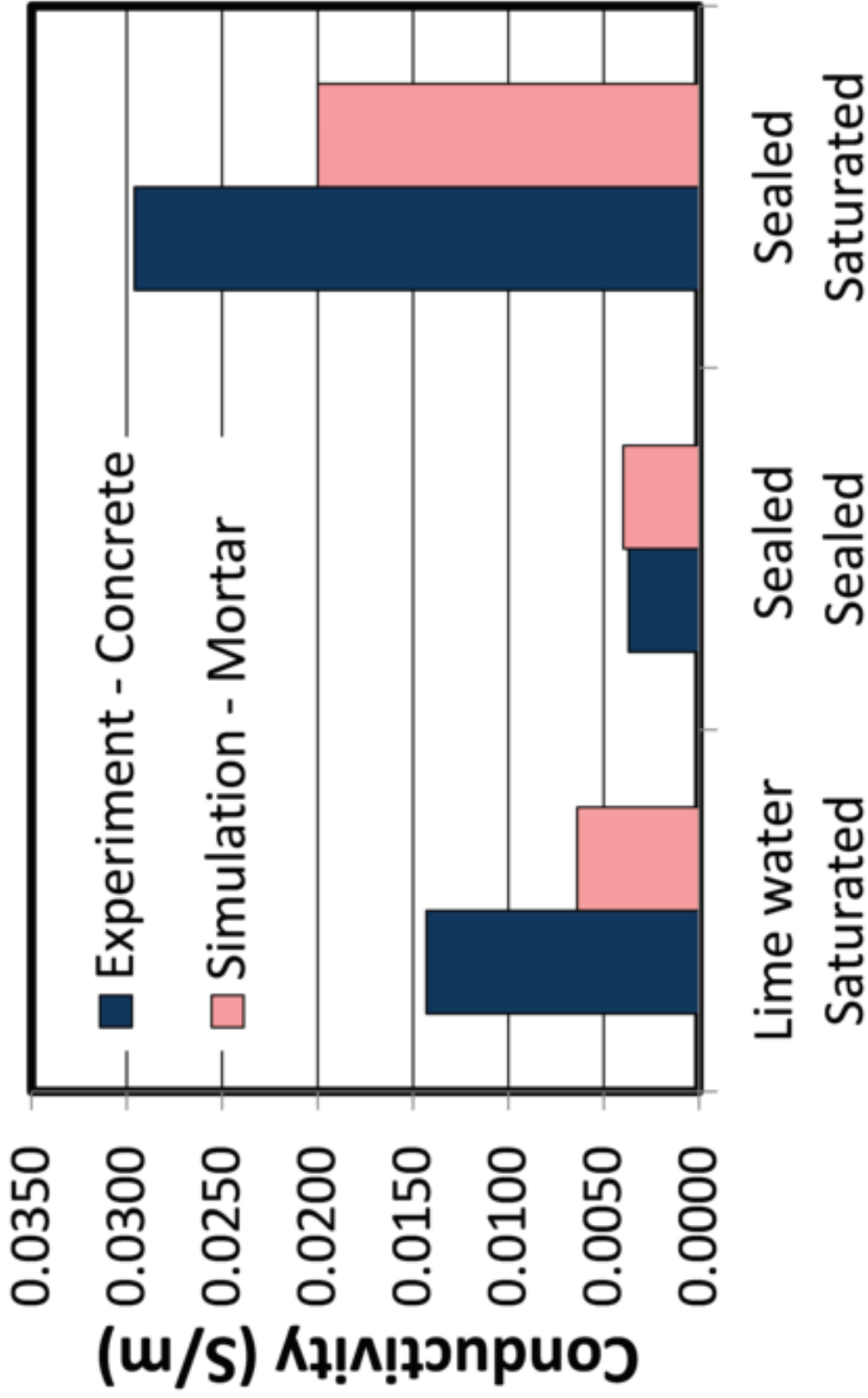


Figure 5
[Click here to download high resolution image](#)

Figure 6a
[Click here to download high resolution image](#)

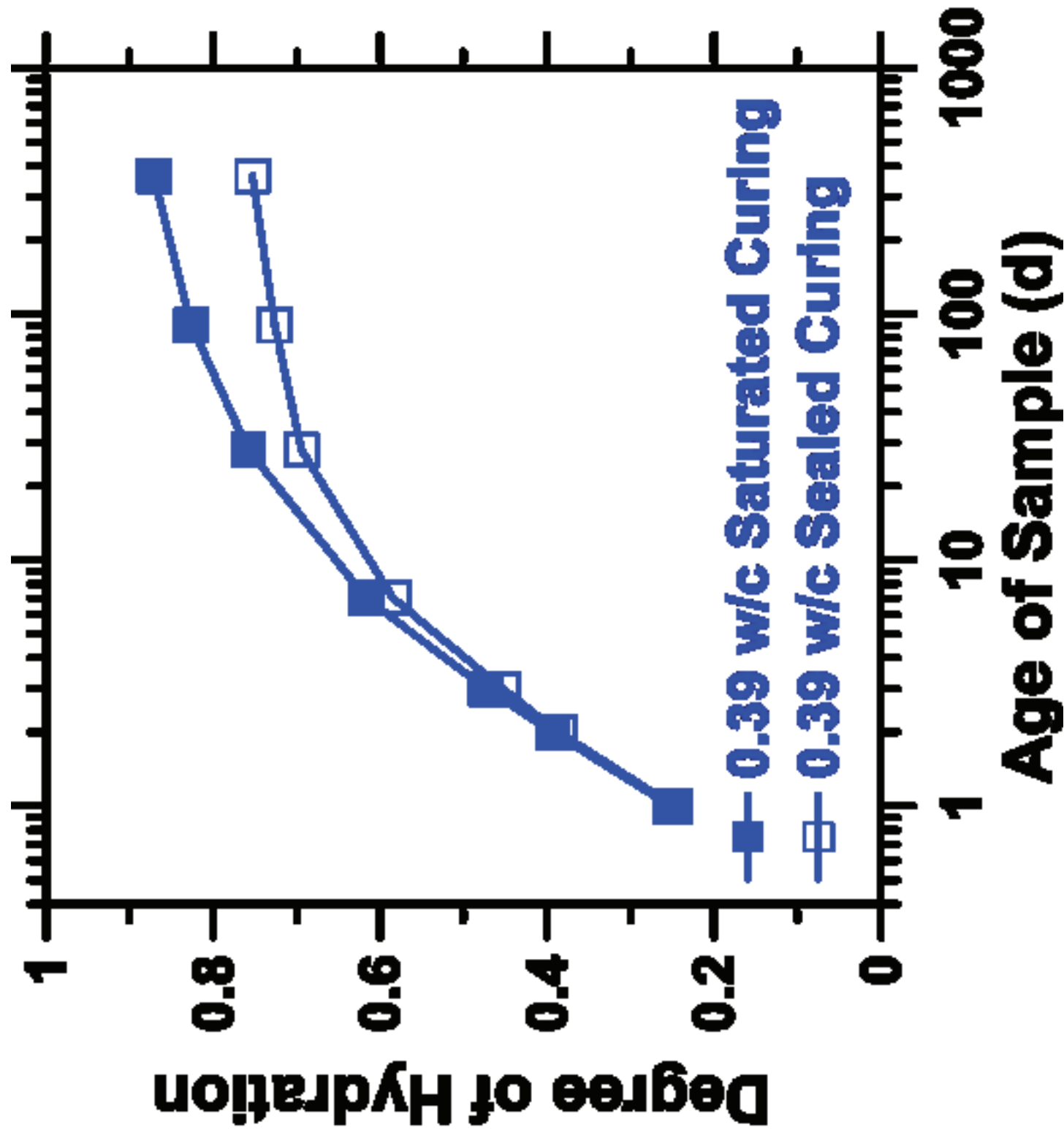


Figure 6b
[Click here to download high resolution image](#)

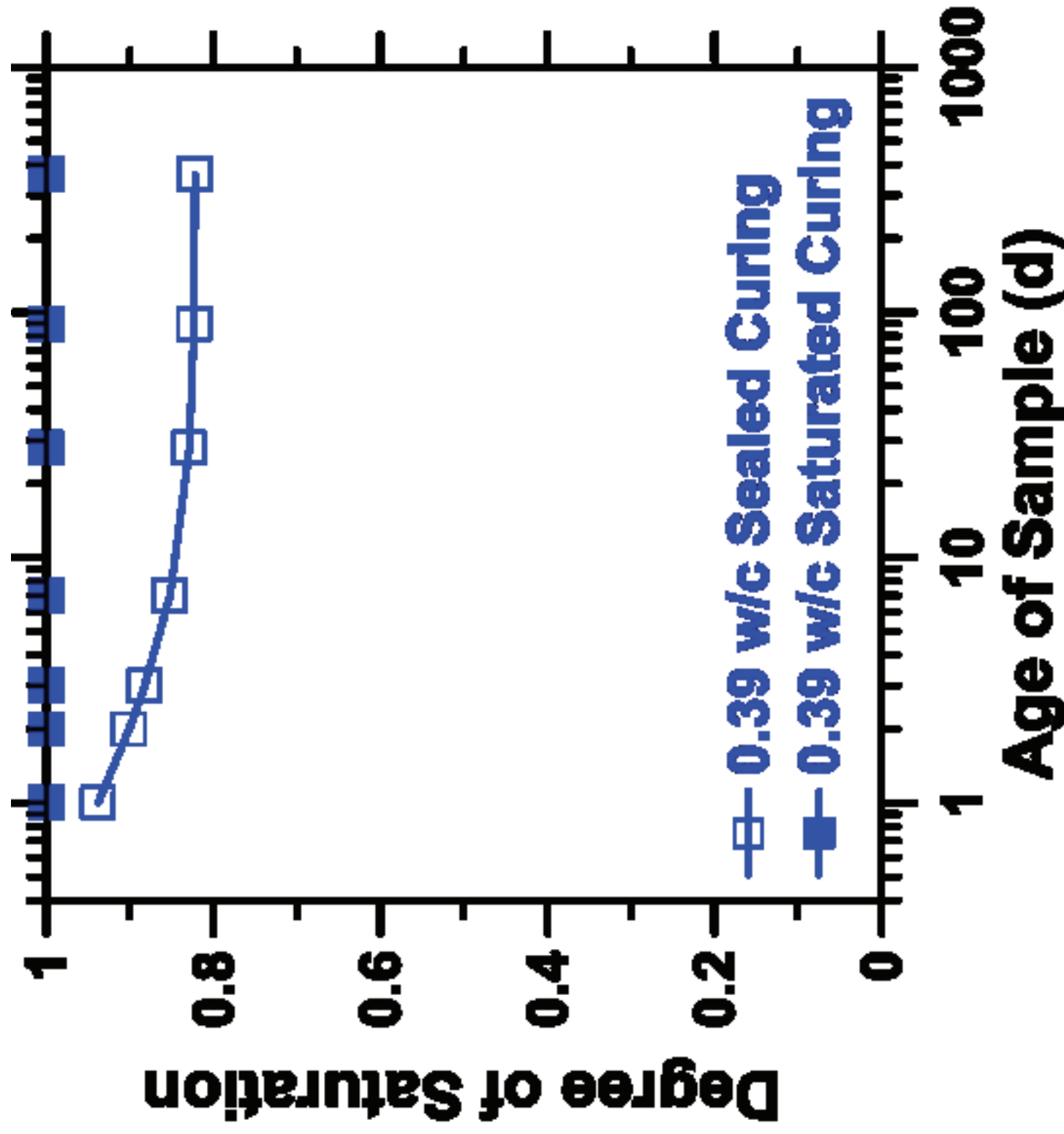


Figure 7a
Click here to download high resolution image

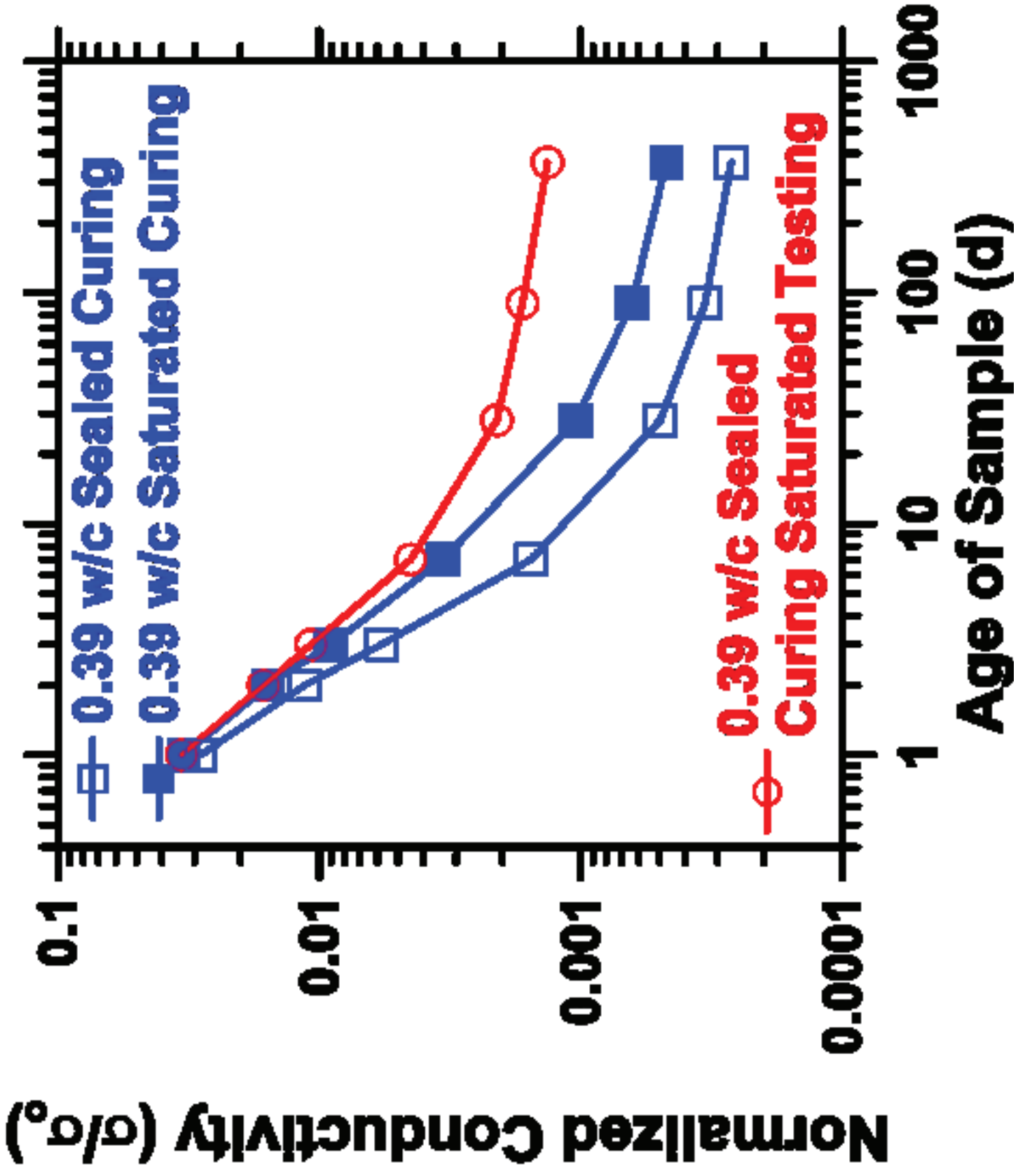


Figure 7b
Click here to download high resolution image

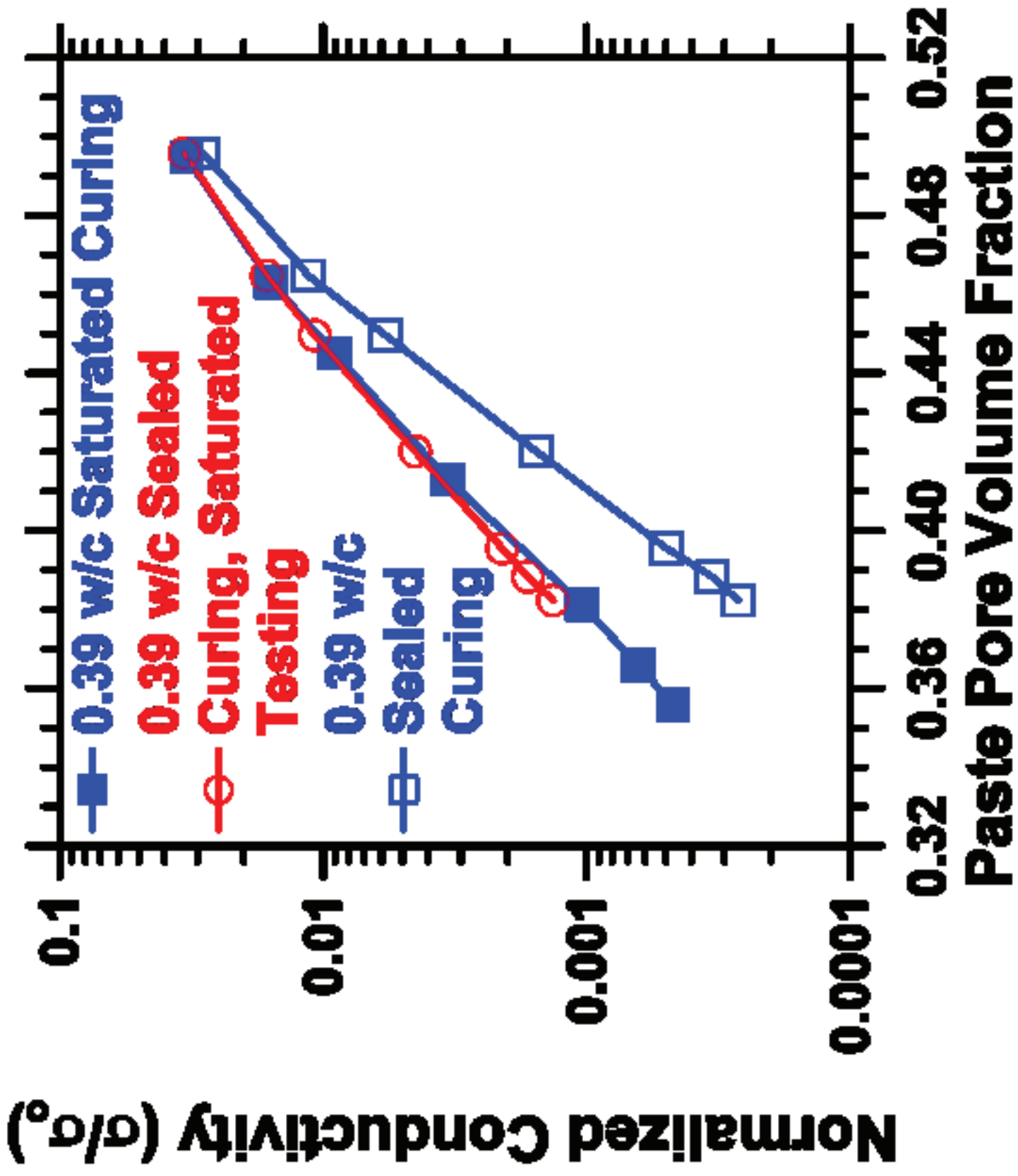


Figure 8a
[Click here to download high resolution image](#)

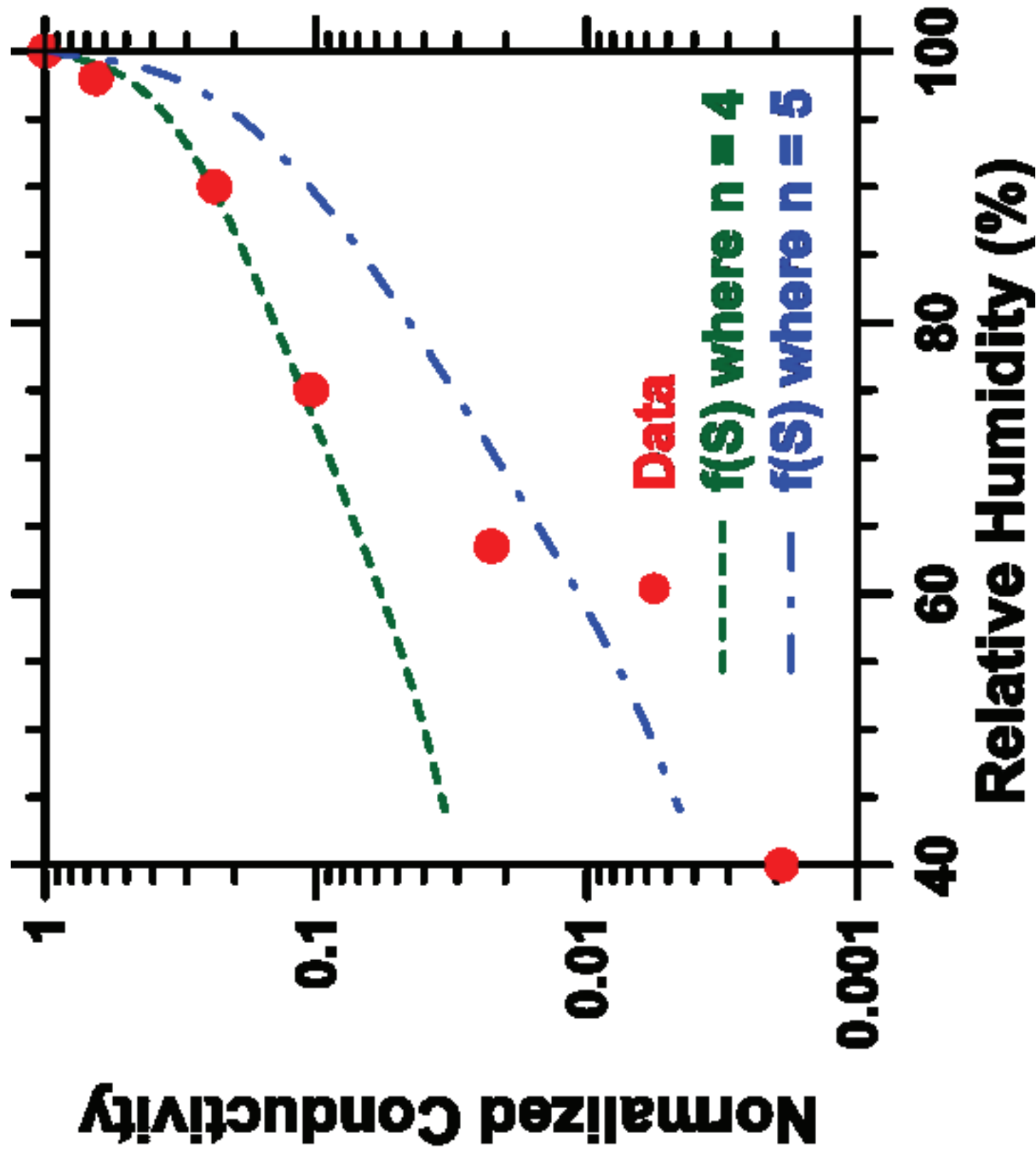


Figure 8b
Click here to download high resolution image

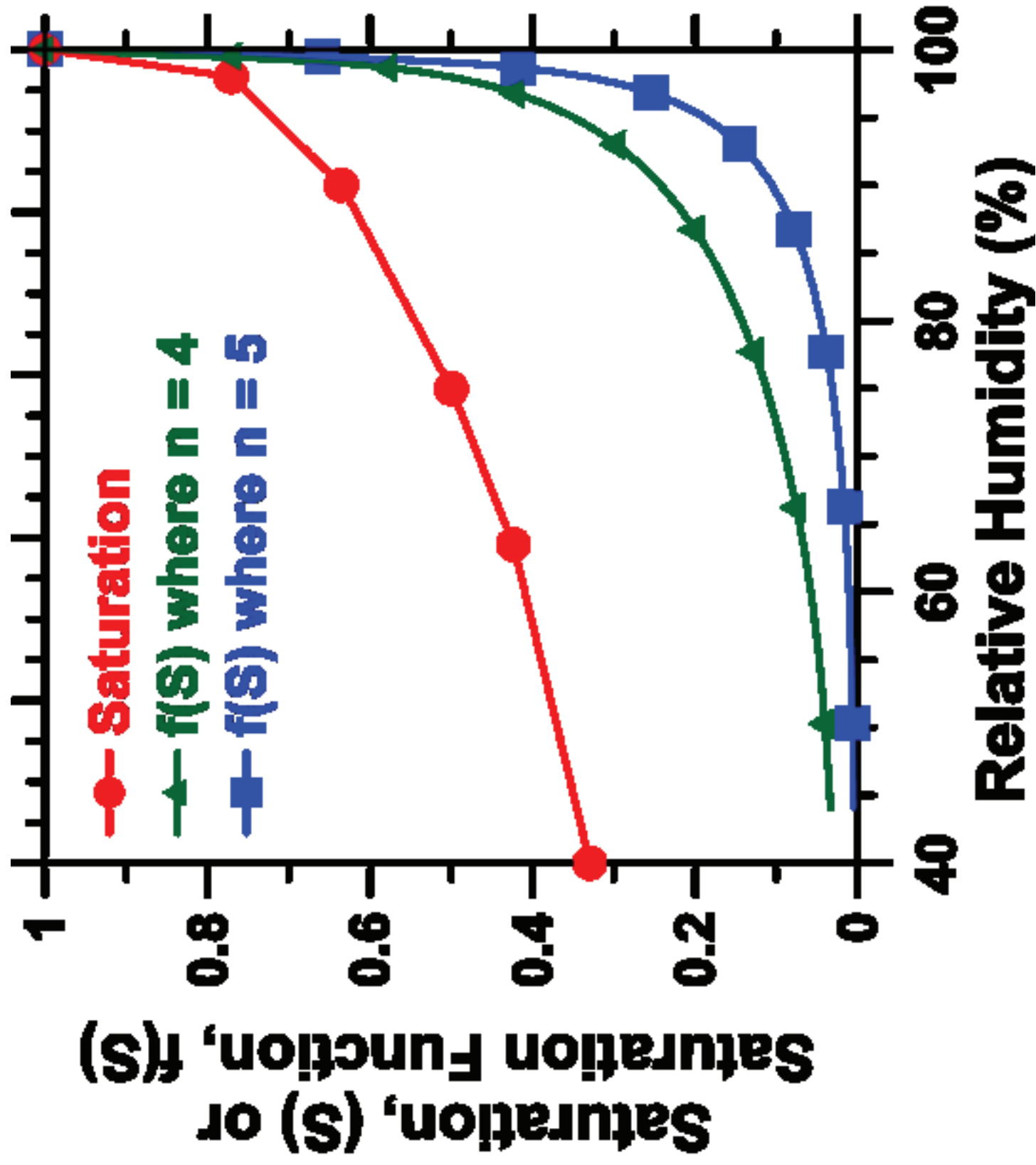
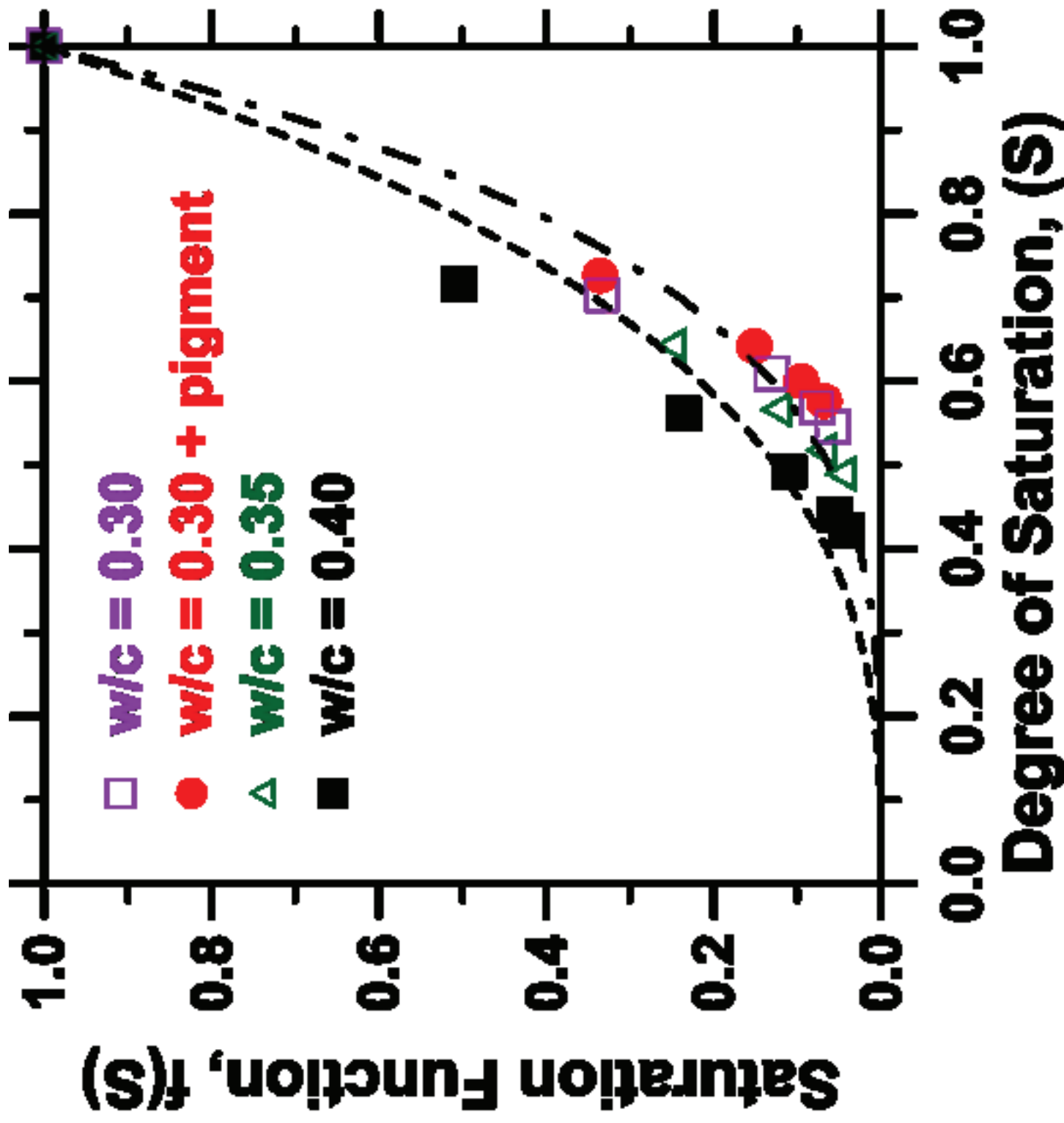


Figure 9
[Click here to download high resolution image](#)



- 1 Figure 1: Experimentally measured saturation coefficients for siltstone and cementitious materials.
2 (Containing data from Rajabipour 2006)
- 3 Figure 2: Microstructural images developed using the VCCTL model for a mortar with a w/c of 0.42 and
4 an aggregate volume of 55 % at a) 3 d and b) 365 d hydrated under saturated conditions. The phases are
5 color-coded as follows: black = capillary porosity, brown = alite, light blue = belite, white = ferrite, beige
6 = C-S-H gel, dark blue = CH, and green = ettringite and monosulfoaluminate combined.
- 7 Figure 3: a) A Saturation Function Interpreted for VCCTL computer simulations b) Calculated saturation
8 functions obtained from a series of simulated microstructures. The dashed curve corresponds to a
9 saturation coefficient $n=4$ and the dotted and dashed line corresponds to a saturation coefficient $n=5$.
- 10 Figure 4: A correction term (δ) to account for the ionic interactions in a pore solution, having an ionic
11 strength I_M when the sample is saturated, as it becomes more concentrated due to drying
- 12 Figure 5: Measured electrical conductivity from RCP tests using a field concrete and simulated mortar
13 with a w/c of 0.39 under different curing and sample conditioning (A maximum coefficient of variation
14 of 3.2% was observed for the experiments)
- 15 Figure 6: Mortar with a w/c of 0.39: a) Degree of hydration and b) Degree of saturation
- 16 Figure 7: Normalized conductivity of mortar with a w/c of 0.39: a) as a function of time and b) as a
17 function of the pore volume in the paste as computed using Powers' model
- 18 Figure 8: a) Normalized conductivity as a function of drying and b) the relationship between relative
19 humidity and saturation for the data
- 20 Figure 9: The application of the saturation function to mortar prisms during drying (the dashed line and
21 dot-dash line denote a $n-1+\delta$ value of 3 and 4, respectively).

SESSION 2: NRMCA

It is understood that concrete can fail due to chloride induced corrosion, sulfate attack, freeze thaw attack and ASR. In this phase rapid index test criteria suitable for specifications will be developed that correlate well with slower performance tests for concrete exposed to chlorides, sulfates, and freeze thaw.

Chloride Ingress - Test Methods, Curing Conditions and Test Ages

Chloride ingress can occur from deicing salts applied in bridge decks in Northern regions as well as concrete exposed to marine conditions. It is well known that when the chloride concentration at the steel rebar exceeds the chloride threshold corrosion can initiate. The chloride diffusion test (ASTM C1556) is understood to be a good performance test. However, that is a very slow test and applicable only for sophisticated laboratories. So rapid index tests were evaluated as follows:

Mixture Proportions and Variables

w/cm	PC	15%FA	30%FA	25%SL	50%SL	7%SF	40%SL+5%SF
0.29	Yes - l						
0.34							Yes - n
0.39	Yes - m	Yes - l	Yes - vl	Yes - l	Yes - vl	Yes - vl	
0.49	Yes - h	Yes - m		Yes - m			
0.62			Yes - h		Yes - h		

where

H – High chloride permeability ($>5 \times 10^{-12} \text{ m}^2/\text{s}$) – 3 mixtures

M – moderate chloride permeability ($3 \text{ to } 5 \times 10^{-12} \text{ m}^2/\text{s}$) – 3 mixtures

L – low chloride permeability ($2 \text{ to } 3 \times 10^{-12} \text{ m}^2/\text{s}$) – 3 mixtures

VL – very low chloride permeability (0.7 to 2×10^{-12} m²/s) – 3 mixtures

N – negligible chloride permeability ($<0.7 \times 10^{-12}$ m²/s) – 1 mixture

The above mixtures were selected keeping the following in mind:

1. Cover a predicted (based on Life 365 computer program) 2 year chloride diffusion coefficient range that is broad – 6.8×10^{-12} to 0.62×10^{-12} m²/s
2. To be able to use rapid index test criteria to choose mixtures with desired classification as indicated above and at the very least rapid index test criteria should help eliminate mixtures with high diffusion coefficients ($>5 \times 10^{-12}$ m²/s)
3. Look at common SCMs like fly ash, slag, silica fume to see if correlation between the rapid index tests criteria and diffusion coefficients are independent of SCM types and dosages
4. w/cm, SCM dosages chosen must cover the ranges normally used in HPC
5. Also some mixtures that would yield high chloride diffusion coefficients (containing high w/cm, high pozzolan) should be made and the rapid index tests should yield high values so that such mixtures will not be selected. Also some mixtures that would yield low chloride diffusion coefficients (containing low w/cm, low or no pozzolan or conductive aggregates) should be made and the rapid index tests should yield low values so that such mixtures will be selected.

Mixture Prepared and Tested Thus Far

All the 13 concrete mixtures have now been cast in 2 phases. Phase I looked at 6 mixtures and the test results are provided in Table 1 where as Phase II looked at 7 mixtures and the test results are provided in Table 2. The common elements of the two phases are:

Crushed coarse aggregate (1.0 in. nominal maximum size) ASTM C33 No. 57, natural sand FM=2.88

Adjusted water reducer or high range water reducer (if any) for desired slump = 5 to 7 in.

Non air entrained concrete mixtures – even though most of these mixtures in practice will contain air our aim here is to determine the validity of the rapid index tests and criteria in classifying mixtures based on their chloride diffusion coefficients. This validation will also hold for air entrained concrete mixtures. Also the use of air entrainment will make the comparisons between mixtures more challenging

Planned Test Methods, Curing Conditions and Test Ages

Normal Curing – Standard moist room curing starts immediately after making the specimens

Accelerated Curing – 7 days of normal curing followed by 21 days of curing in 100F water

For all mixtures measure the following:

Slump, temperature, air content, density, Strength (28 days), Shrinkage (7 days moist curing followed by 90 days of air drying). Shrinkage test is for reference and may be discontinued for future mixtures.

The following durability tests will be conducted for all the mixtures

Durability Tests

- **Rapid Chloride Permeability test – RCPT (ASTM C1202)**

- 28 day accelerated
- 56 day normal curing
- 26 week (182 d) normal curing
- 78 week (546 d) normal curing

- **5 minute Conductivity Test (ASTM C1202 based)**

- 28 day accelerated
- 56 day normal curing
- 26 week (182 d) normal curing
- 78 week (546 d) normal curing

- **Rapid Migration Test - RMT (AASHTO TP 64)**

- 28 day accelerated
- 56 day normal curing
- 26 week (182 d) normal curing
- 78 week (546 d) normal curing

- **Chloride Diffusion Test (ASTM C1556)**

Phase I

- 6m normal curing + 35 days in solution
- 59d normal curing + 16m in solution
- 59d normal curing + cyclic exposure (18 week using 4d in solution/3d at 100F air - 20% rh cycle) in solution.

Phase II

- i) 56d normal curing + 35d in solution
- ii) 6m nc + 35d in solution
- iii) 6m nc + 15m in solution
- iv) 56d nc + cyclic exposure (21 week using 3d in solution/4d at 73F air - 50% rh cycle)
- v) 56d nc + cyclic exposure (75 week using 3d in solution/4d at 73F air - 50% rh cycle)
- vi) 56d nc + 75w cyclic exposure (3d solution+4d air)

- **Sorptivity Test (ASTM C1585)**

- i) 28 day accelerated + 18 d specimen conditioning (C1585)
- ii) 56 day normal curing + 18 d specimen conditioning (C1585)
- iii) 26 week (182 d) normal curing + 18 d specimen conditioning (C1585)

- **Absorption test BS 1881:122 (ASTM Draft)**

- i) 10 day normal curing + 3 d in oven
- ii) 28 day accelerated + 3 d in oven
- iii) 26 week (182 d) normal curing + 3 d in oven

For Phase I the oven temperature was maintained at 105C where as for Phase II it was 60C. The difference followed the development of the ASTM drafts. It was felt that the high oven temperatures will lead to internal micro-cracking of concrete leading to misleading high results that are not reflective of the absorption characteristics of the concrete specimen being tested.

Rapid index tests need to correlate with chloride penetration levels for two real life situations:

- a. when the structures are in a complete or near complete saturation state such as in a submerged marine exposure or possibly bridge decks in high humidity regions where chloride ingress is primarily diffusion controlled. The ASTM C1556 would be the correct comparison test here and the aim would be to observe which of the rapid index tests correlates well with diffusion coefficient (at oldest age). Ideally suitable rapid index test criteria (s) can be chosen so that mixtures can be selected based on the desired level of chloride diffusion coefficient.
- b. when the structures are not completely saturated such as bridge decks in low humidity regions where the chloride ingress could be due to sorption and diffusion. ASTM C1556 conducted in a wet/dry scenario would be the closest comparison test here and the aim would be to observe which of the rapid index tests correlates well with the ingress coefficient (at oldest age). Ideally suitable rapid index test criteria (s) can be chosen so that mixtures can be selected based on the desired level of chloride diffusion coefficient.

Table 1. Yield Adjusted Mixture Proportions and Test Results

Calculated Batch Quantities						
	0.49PC	0.49SL25	0.39SL50	0.49FA15	0.39FA30	0.34SL40SF5
Type I/II cement, lb/yd ³	554	416	306	472	431	382
Slag, lb/yd ³		139	306			277

Flyash, lb/yd ³				83	185	
Silica Fume, lb/yd ³						35
SCM, %	0	25	50	15	30	45
Coarse Agg. (No.57), lb/yd ³	2075	2074	2070	2081	2081	2086
Fine Aggregate, lb/yd ³	1303	1293	1314	1273	1267	1264
Mixing Water, lb/yd ³	272	272	239	273	240	236
w/cm	0.49	0.49	0.39	0.49	0.39	0.34
ASTM C494 Type A, oz/cwt	4.0	4.0	4.0	4.0	4.0	4.0
ASTM C494 Type F, oz/cwt	2.5	2.9	4.3	2.4	5.0	7.8
Fresh Concrete Properties						
ASTM C143, Slump, in.	7 ½	4 ½	8	7	6 ¾	9
ASTM C231, Air, %	1.4	1.7	1.3	1.5	1.6	1
ASTM C138, Density, lb/ft ³	156.5	156.1	157.7	155.7	156.5	159.3
ASTM C1064, Temperature, °F	76	76	75	76	75	75
Hardened Concrete Properties						
ASTM C39, Compressive Strength, psi						
28 days	6,830	7,550	10,520	6,640	7,970	12,440
Draft ASTM Standard, Water Absorption Test at 105 °C, %						
10d normal cure	2.89	2.24	1.69	3.25	2.33	1.43
28d accelerated cure	2.52	1.77	1.34	2.44	1.63	1.26
196d normal cure	2.30	1.80	1.29	2.29	1.44	1.49
ASTM C1202, Rapid Chloride Permeability, Coulombs						
28d accelerated cure	4657	1992	561	2414	723	166
56d normal cure	4674	1912	581	3013	1417	270
196d normal cure	3356	1581	496	1551	340	147
550d normal cure	3891 ⁻	1465 ⁻	394 ⁻	1070 ⁻	174 ⁻	166 ⁻
Draft ASTM Standard, 5 minute Conductivity, Sm⁻¹						
28d accelerated cure	0.0189	0.0083	0.0030	0.0091	0.0030	0.0009

56 normal cure	0.0154	0.0072	0.0034	0.0129	0.0058	0.0013
196d normal cure	0.0099	0.0055	0.0021	0.0057	0.0018	0.0008
550d normal cure	0.0076 ⁻	0.0054 ⁻	0.0018 ⁻	0.0054 ⁻	0.0008 ⁻	0.0009 ⁻
AASHTO TP64, Rate of Penetration (RMT), mm/(V-hr)						
28d accelerated cure	0.065	0.030	0.004	0.046	0.015	0.003
56d normal cure	0.044	0.025	0.006	0.043	0.024	0.002
196d normal cure	0.047	0.016	0.006	0.025	0.006	0.002
550d normal cure	0.048 ⁻	0.017 ⁻	0.003 ⁻	0.017 ⁻	0.005 ⁻	0.001 ⁻
ASTM C157, Length Change (Drying Shrinkage), %						
28 days ⁺	0.035	0.039	0.031	0.029	0.028	0.028
56 days ⁺	0.046	0.048	0.037	0.039	0.036	0.032
90 days ⁺	0.055	0.054	0.044	0.048	0.043	0.039
180 days ⁺	0.062	0.060	0.049	0.054	0.049	0.044
ASTM C 1585, Rate of Water Absorption (Sorptivity), x10⁻⁴ mm/s^{1/2}						
28d accel. cure (Initial/Secondary)	10.4 / 7.5	3.0 [*] / 3.4	1.7 [*] / 1.7	7.5 / 4.6	4.7 [*] / 2.1	2.5 [*] / 0.9
56d normal cure (Initial/Secondary)	9.9 / 6.9	8.5 / 2.6 [*]	2.5 [*] / 1.4	16.6 / 10.7	7.0 [*] / 3.3	4.1 [*] / 1.9 [*]
196d normal cure (Initial/Secondary)	5.9 [*] / 5.5	3.4 [*] / 1.3	3.7 [*] / 1.1	4.2 / 2.4	3.6 [*] / 1.8	1.3 [*] / 0.8
ASTM C 1556, Chloride Diffusion, x 10⁻¹² m²/s						
Case 1 6m nc + 35d in solution	3.29	1.32	0.68	2.31	1.97	0.35
Case 2 59d nc + 16m in solution	12.94	3.09	0.58	4.11	1.07	0.35
Case 3 59d nc + 18w cyclic exposure (4d solution+3d air in 100F and 20% RH)	11.07	3.11	1.24	6.34	3.42	0.82
ASTM C 1556, Surface Chloride, % by weight of concrete						
Case 1	0.78	1.29	1.87	1.77	2.20	1.80
Case 2	1.05	1.20	1.80	1.35	1.60	1.90
Case 3	1.03	1.52	1.63	1.23	1.46	2.10

⁺ Curing period in 70°F, 50% RH environment NOT included 7 days initial wet curing period in water bath

^{*} a correlation coefficient less than 0.98 indicating that the rate cannot be determined according to ASTM C1585

Result of only one specimen

The chloride profiles for the 3 conditions were plotted and the diffusion coefficients calculated.

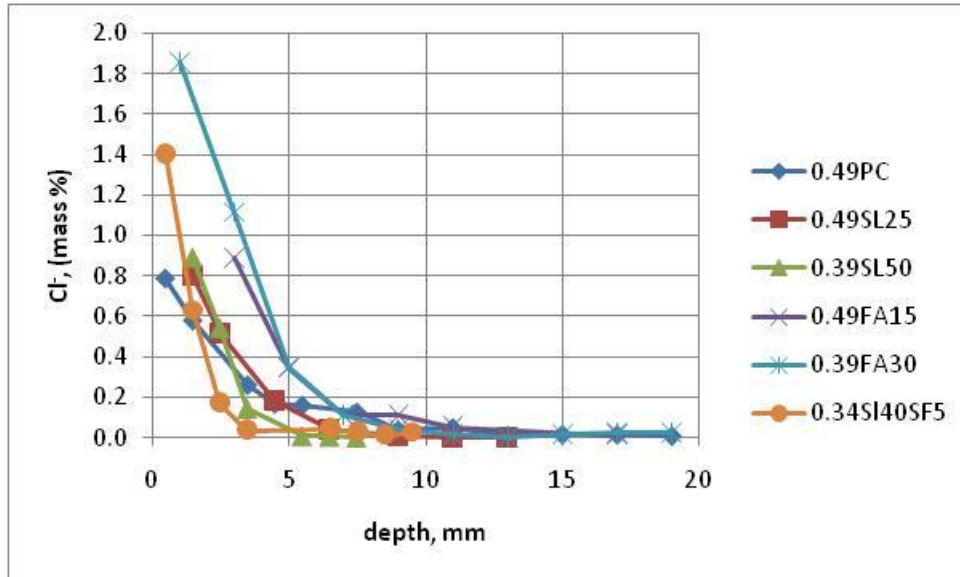


Figure 1a. Chloride profile (ASTM C1556) for 6m normal curing followed by 35d in solution

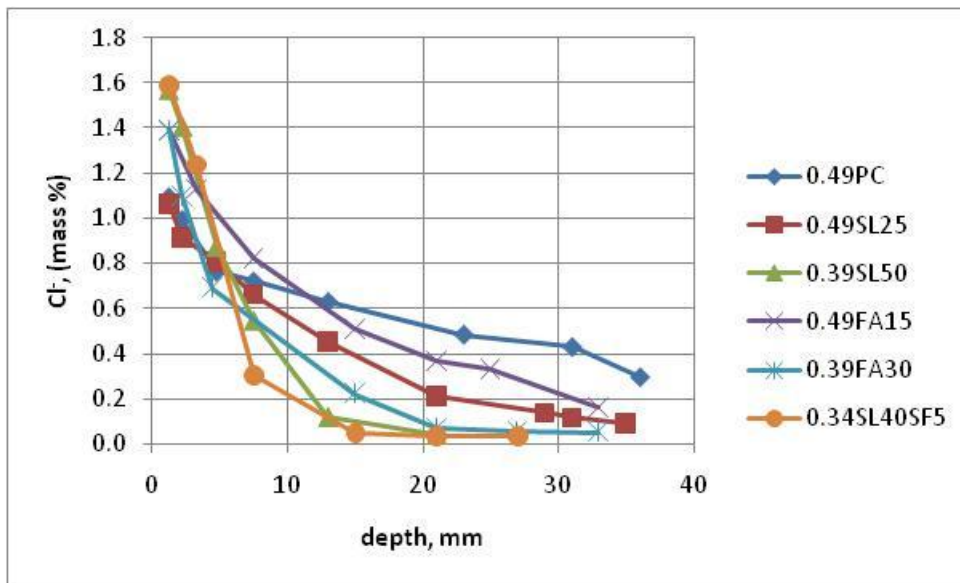


Figure 1b. Chloride profile for 59d normal curing followed by 16m in solution

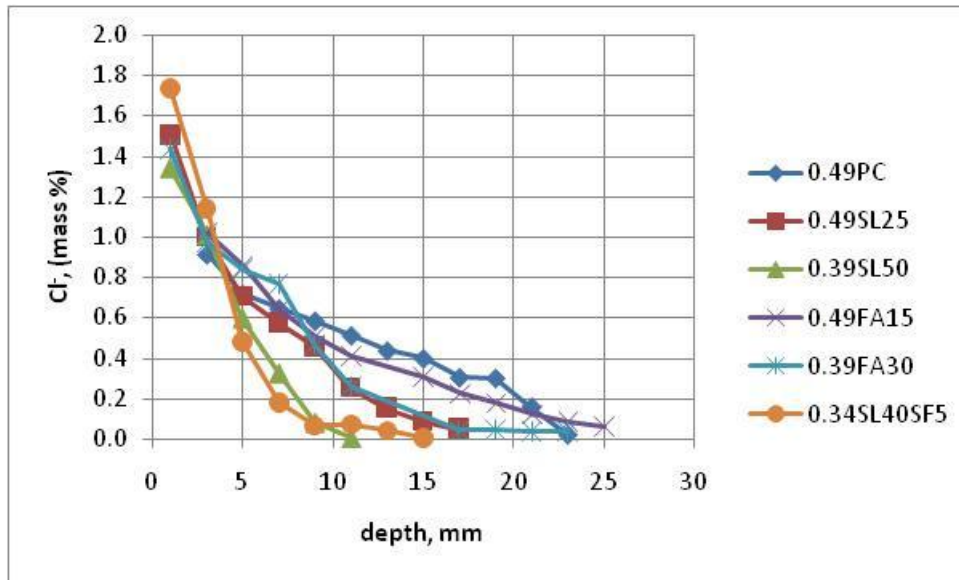


Figure 1c. Chloride profile for 59d normal curing followed by 18 weeks in cyclic exposure

Preliminary Discussions on Chloride Profiles and Diffusion Coefficient Test Results

1. Since the cases depicted in Figures 1b, and 1c show the longest exposure attention is paid to those. Judging by the chloride profiles shown in Figure 1b (59d normal curing+16m in solution) the best performing mixes (showing low chloride ingress) in order were 0.34SL40SF5=0.39SL50<0.39FA30<0.49SL25<0.49FA15<0.49PC. Judging by the chloride profiles shown in Figure 1c (59d normal curing+18 week cyclic exposure) the best performing mixes (showing low chloride ingress) in order were 0.34SL40SF5=0.39SL50<0.49SL25=0.39FA30<0.49FA15<0.49PC. The 0.49SL25 seems to do similar to the 0.39FA30 mixture in the cyclic case whereas the 0.49SL25 shows greater chloride ingress than the 0.39FA30 mixture for the immersed case. The fly ash mixture seems to perform better in long term immersed case as compared to the cyclic case. It is possible that the higher early age sorptivity values of the fly ash mixture as compared to the slag mixture could have contributed to this.
2. Judging by the chloride diffusion coefficient values reported in Table 1 for the mixtures in Figure 1b (59d normal curing+16m in solution) the best performing mixtures (from the lowest diffusion coefficient) in order were 0.34SL40SF5<0.39SL50<0.39FA30<0.49SL25<0.49FA15<0.49PC. Judging by the chloride diffusion coefficient values reported in Table 2 for the mixtures in Figure 1c (59d normal curing+18 week cyclic exposure) the best performing mixtures (from the lowest diffusion coefficient) in order were 0.34SL40SF5<0.39SL50<0.49SL25=0.39FA30<0.49FA15<0.49PC. The rankings of the mixtures based on visual observation of the chloride profiles and the chloride diffusion coefficient calculation is similar except for the 0.35SL40SF5 and 0.39SL50 mixtures which can be due to differences in the surface chloride content estimation. It is the chloride diffusion coefficient value that is used for service life estimation and hence attention would be paid to that in all subsequent data analysis. However it is always

useful to look at the raw chloride profiles to make sure the order of mixtures is generally similar.

3. The chloride diffusion coefficient values vary as follows:
 1. 6m nc + 35d in solution - 0.35 to $3.29 \times 10^{-12} \text{ m}^2/\text{s}$
 2. 59d nc + 16m in solution - 0.35 to $12.94 \times 10^{-12} \text{ m}^2/\text{s}$
 3. 59d nc + 18w cyclic - 0.82 to $11.07 \times 10^{-12} \text{ m}^2/\text{s}$

There is about an order of magnitude between the lowest and highest values in each condition and so it encompasses the broad range of chloride diffusion coefficients that is available with the materials and mixture proportions commonly used by the industry.

Table 2. Yield Adjusted Mixture Proportions and Preliminary Test Results

Calculated Batch Quantities								
	0.39PC	0.39FA15	0.39SL25	0.39SF7	0.62FA30	0.62SL50	0.29PC	0.39PC ^{++R}
Type I/II cement, lb/yd ³	612	520	462	565	349	249	803	612
Slag, lb/yd ³	-	-	154	-	-	249	-	-
Flyash, lb/yd ³	-	92	-	-	149	-	-	-
Silica Fume, lb/yd ³	-	-	-	43	-	-	-	-
SCM, %	0%	15%	25%	7%	30%	50%	0%	0%
Coarse Agg. (No.57), lb/yd ³	2066	2068	2081	2052	2094	2093	2069	2066
Fine Aggregate, lb/yd ³	1331	1296	1331	1307	1216	1258	1183	1331
Mixing Water, lb/yd ³	238	239	240	237	287	290	236	238
w/cm	0.39	0.39	0.39	0.39	0.58	0.58	0.29	0.39
ASTM C494 Type A, oz/cwt	4	4	4	4	3	3	5	4
ASTM C494 Type F, oz/cwt	8.8	8.3	6.9	8.2	-	-	11.7	8.4
Fresh Concrete Properties								
ASTM C143, Slump, in.	5	6 1/2	7 3/4	6	6 1/2	7	8 3/4	7
ASTM C231, Air, %	1.8	1.6	1.2	1.8	1.6	1.4	1.1	1.7
ASTM C138, Density, lb/ft ³	158.1	156.9	158.9	156.5	152.5	154.1	159.7	158.1
ASTM C1064, Temperature, °F	75	75	75	75	75	75	76	76
Hardened Concrete Properties								

ASTM C39, Compressive Strength, psi								
28 days	10,460	9,590	10,300	10,740	3,880	5,380	13,480	9,890
Draft ASTM Standard, Water Absorption Test at 60 °C, %								
56d normal cure	1.03	1.02	1.00	0.82	1.88	1.75	0.91	-
213d normal cure	0.85	0.79	0.91	0.76	1.55	1.40	0.70	-
ASTM C1202, Rapid Chloride Permeability, Coulombs								
28d accelerated cure	2180	1031	1186	276	2495	661	1078	1980
56d normal cure	1722	1557	1272	299	4012	832	1209	-
213d normal cure	1607	563	873	252	1177	572	936	-
Draft ASTM Standard, 5 minute Conductivity, Sm ⁻¹								
28d accelerated cure	0.0101	0.0054	0.0061	0.0014	0.0089	0.0037	0.0061	0.0102
56 normal cure	0.0089	0.0070	0.0058	0.0014	0.0119	0.0034	0.0056	-
213d normal cure	0.0062	0.0026	0.0037	0.0014	0.0042	0.0020	0.0040	-
AASHTO TP64, Rate of Penetration (RMT), mm/(V-hr)								
28d accelerated cure	0.034	0.017	0.013	0.004	0.047	0.007	0.012	0.029
56d normal cure	0.027	0.017	0.011	0.004	0.046	0.012	0.011	-
213d normal cure	0.021	0.009	0.009	0.002	0.033	0.006	0.007	-
ASTM C157, Length Change (Drying Shrinkage), %								
28 days ⁺	0.032	0.037	0.032	0.028	0.041	0.044	0.024	-
56 days ⁺	0.039	0.047	0.038	0.034	0.054	0.052	0.029	-
90 days ⁺	0.042	0.054	0.047	0.043	0.064	0.053	0.030	-
180 days ⁺	0.049	0.056	0.052	0.045	0.066	0.061	0.038	-
ASTM C 1585, Rate of Water Absorption (Sorptivity), x10 ⁻⁴ mm/s ^{1/2}								
28d accel. cure (Initial/Secondary)	-	3.1/2.1	4.7/2.0 [*]	3.3/2.1	9.6/3.8	7.6/2.8	3.1/2.6	9.5/5.2
56d normal cure (Initial/Secondary)	8.3/4.0 [*]	6.1/4.1	***	3.8/2.1 [*]	9.9/7.0	7.1 [*] /2.8 [*]	2.1 [*] /2.9	-
213d normal cure (Initial/Secondary)	4.7 [*] /3.0	2.1 [*] /1.7	3.6 [*] /1.9	2.6 [*] /0.7 [*]	4.6/3.7	5.5 [*] /1.6 [*]	1.6 [*] /1.3 [*]	-
ASTM C 1556, Chloride Diffusion, x 10 ⁻¹² m ² /s								
56d nc + 35d in solution	4.86	2.89	2.21	1.18	8.30	2.90	1.32	-

6m nc + 35d in solution	2.72	1.40	1.19	0.67	8.23	2.02	1.08	-
6m nc + 15m in solution	1.75	0.67	0.77	0.22	0.95	0.55	0.56	-
56d nc + 21w cyclic exposure (3d solution+ 4d air)	2.20	1.51	1.08	0.90	12.08	2.27	1.28	-
56d nc + 75w cyclic exposure (3d solution+ 4d air)	1.96	0.94	0.42	0.35	7.10	1.45	0.53	-
ASTM C 1556, Surface Chloride, % by weight of concrete								
56d nc + 35d in solution	0.96	1.17	1.50	1.23	1.11	1.40	1.10	-
6m nc + 35d in solution	0.94	1.46	1.58	1.27	1.00	1.20	1.46	-
6m nc + 15m in solution	0.80	0.80	1.20	1.20	1.00	1.20	1.10	-
56d nc + 21w cyclic exposure (3d solution+ 4d air)	0.80	1.00	1.30	1.10	1.30	1.30	1.00	-
56d nc + 75w cyclic exposure (3d solution+ 4d air)	1.05	1.00	1.60	1.35	1.30	2.00	1.10	-

[†] Tested at 21d instead of 28d

⁺ Curing period in 70°F, 50% RH environment NOT included 7 days initial wet curing period in water bath

^{*} A correlation coefficient less than 0.98 indicating that the rate cannot be determined according to ASTM C1585

^{**} Exact repeat of designated mixture

^{***} No correlations were found, so data is unavailable

The chloride profiles for the 5 conditions were plotted and the diffusion coefficients calculated.

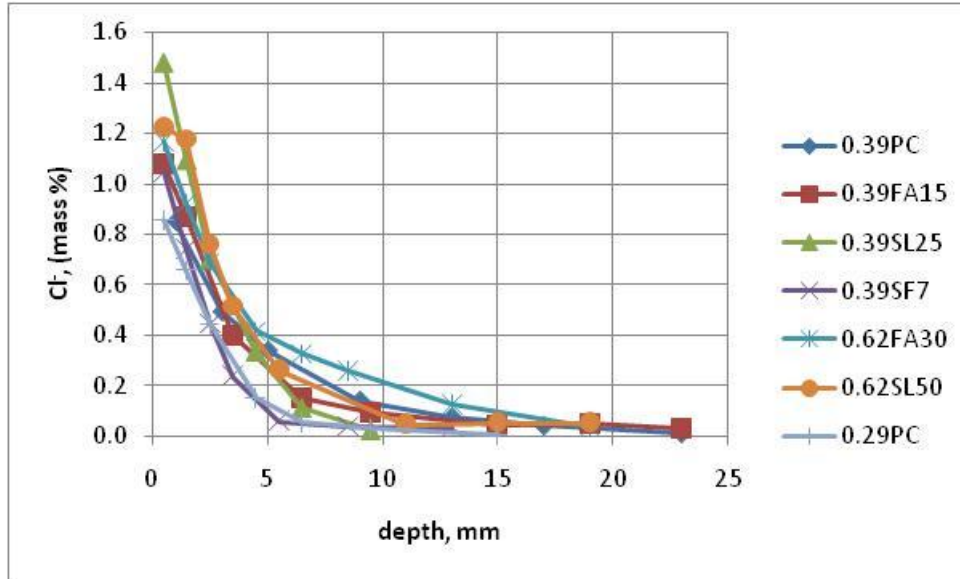


Figure 3a. Chloride profile (ASTM C1556) for 56d normal curing followed by 35d in solution

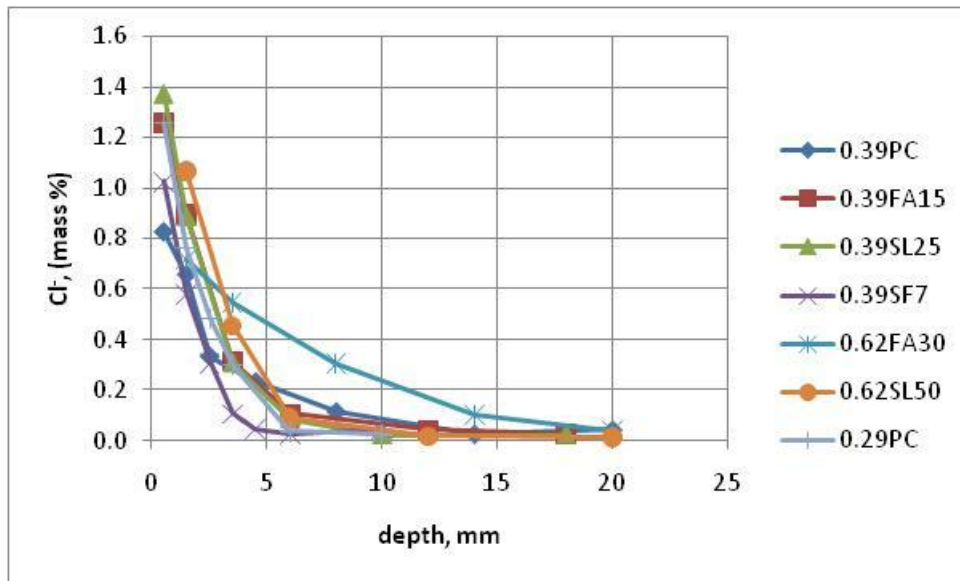


Figure 3b. Chloride Profile for 6 month normal curing followed by 35d in solution

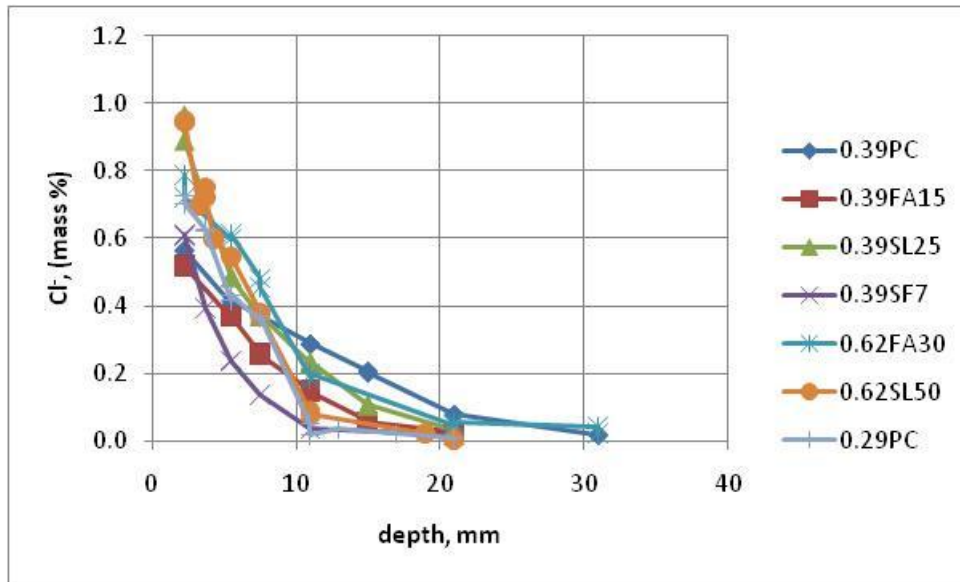


Figure 3c. Chloride Profile for 6m normal curing followed by 15m in solution

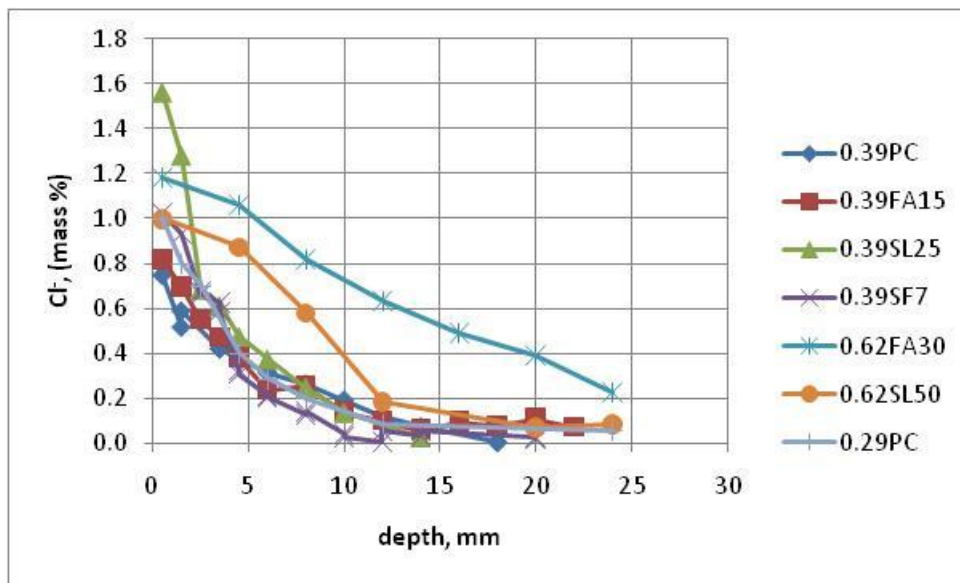


Figure 3d. Chloride Profile for 56d normal curing followed by 21 weeks in cyclic exposure

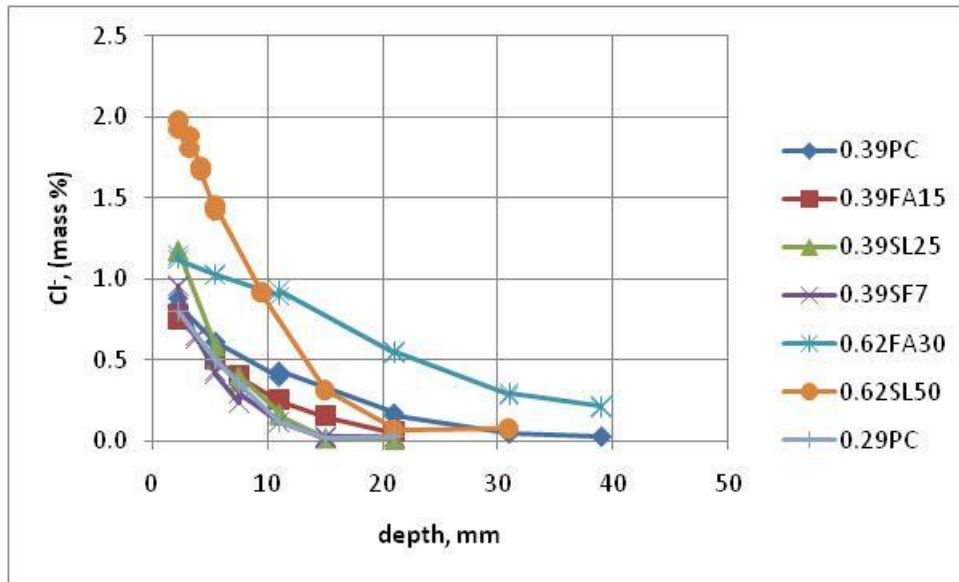


Figure 3e. Chloride Profile for 56d normal curing followed by 75 weeks in cyclic exposure

Preliminary Discussions on Chloride Profiles and Diffusion Coefficient Test Results

- Since the cases depicted in Figures 3c, and 3e show the longest exposure attention is paid to those. Judging by the chloride profiles shown in Figure 3c (6m normal curing+15 m in solution) the best performing mixes (showing low chloride ingress) in order were 0.39SF7<0.29PC=0.62SL50<0.39FA15<0.39SL25=0.62FA30<0.39PC. Judging by the chloride profiles shown in Figure 3e (56d normal curing+75 week cyclic exposure) the best performing mixes (showing low chloride ingress) in order were 0.29PC=0.39SF7=0.39SL25<0.39FA15<0.39PC=0.62SL50<0.62FA30. In the cyclic case the two 0.62 w/cm mixtures did not rank as well as in the immersed case. A similar observation can be made when the 0.29 PC and 0.39SF7 mixture rankings are compared. The cyclic condition is a little different as it involves chloride ingress into a partially saturated concrete surface. From the rankings in the 2 conditions it appears that a lower w/cm is more favorable for a cyclic case possibly due to the tighter pore structure it entails at the concrete surface and also difference in drying rates. Also the 0.39SL25 seems to do slightly better than the 0.39FA15 mixture in the cyclic case whereas the situation is the reverse for the immersed case. The fly ash mixture seems to perform better in long term immersed case as compared to the cyclic case. It is possible that the higher early age sorptivity values of the fly ash mixture as compared to the slag mixture could have contributed to this.
- Judging by the chloride diffusion coefficient values reported in Table 2 for the mixtures in Fig. 3c (6m normal curing+15 m in solution) the best performing mixtures (from the lowest diffusion coefficient) in order were 0.39SF7<0.29PC=0.62SL50=0.39FA15<0.39SL25=0.62FA30<0.39PC. Judging by the chloride diffusion coefficient values reported in Table 2 for the mixtures in Fig. 3e (56d normal curing+75 week cyclic) the best performing mixtures (from the lowest diffusion coefficient) in order were

0.29PC=0.39SF7=0.39SL25<0.39FA15<0.39PC=0.62SL50<0.62FA30. The rankings of the mixtures based on visual observation of the chloride profiles and the chloride diffusion coefficient calculation is identical for the cyclic case (Fig. 5). For the immersed case (Fig. 3c) the difference is negligible and can be explained by the differences in the surface chloride content estimation. It is the chloride diffusion coefficient value that is used for service life estimation and hence attention would be paid to that in all subsequent data analysis. However it is always useful to look at the raw chloride profiles to make sure the order of mixtures is generally similar.

3. The following conditions should apply for all mixtures. For a given duration of chloride exposure the longer the normal curing period the lower should be the chloride diffusion coefficient since concrete undergoes pore refinement under continued hydration. For the same reason for a given duration of normal curing the longer the chloride exposure the lower should be the chloride diffusion coefficient. The above 2 conditions are satisfied for all 7 concrete mixtures. It is tricky to compare the immersed case with the cyclic cases. However, if the diffusion coefficients for each mixtures corresponding to Figs. 3c and 3e are compared it is clear that the values are generally similar for all mixtures except for the two 0.62 w/cm mixtures which showed significantly lower values for the long term immersed case when compared with the cyclic case.
4. The chloride diffusion coefficient values vary as follows:
 1. 56d nc + 35d in solution - 1.18 to 8.30×10^{-12} m²/s
 2. 6m nc + 35d in solution - 0.67 to 8.23×10^{-12} m²/s
 3. 6m nc + 15m in solution - 0.22 to 1.75×10^{-12} m²/s
 4. 56d nc + 21w cyclic - 0.90 to 12.08×10^{-12} m²/s
 5. 56d nc + 75w cyclic - 0.35 to 7.10×10^{-12} m²/s

There is about an order of magnitude between the lowest and highest values in each condition and so it encompasses the broad range of chloride diffusion coefficients that is available with the materials and mixture proportions commonly used by the industry.

Detailed analysis of the correlation between the measured diffusion coefficients and rapid index test results are discussed below. Some of the preliminary results were presented at the 2009 NRMCA Concrete Technology Forum and the 2011 ACI Spring Convention and are summarized below. This is preliminary in nature and will be finalized by the next quarter.

The correlation between the diffusion coefficient results and various rapid index test results (conducted at various ages) are provided in the figures below.

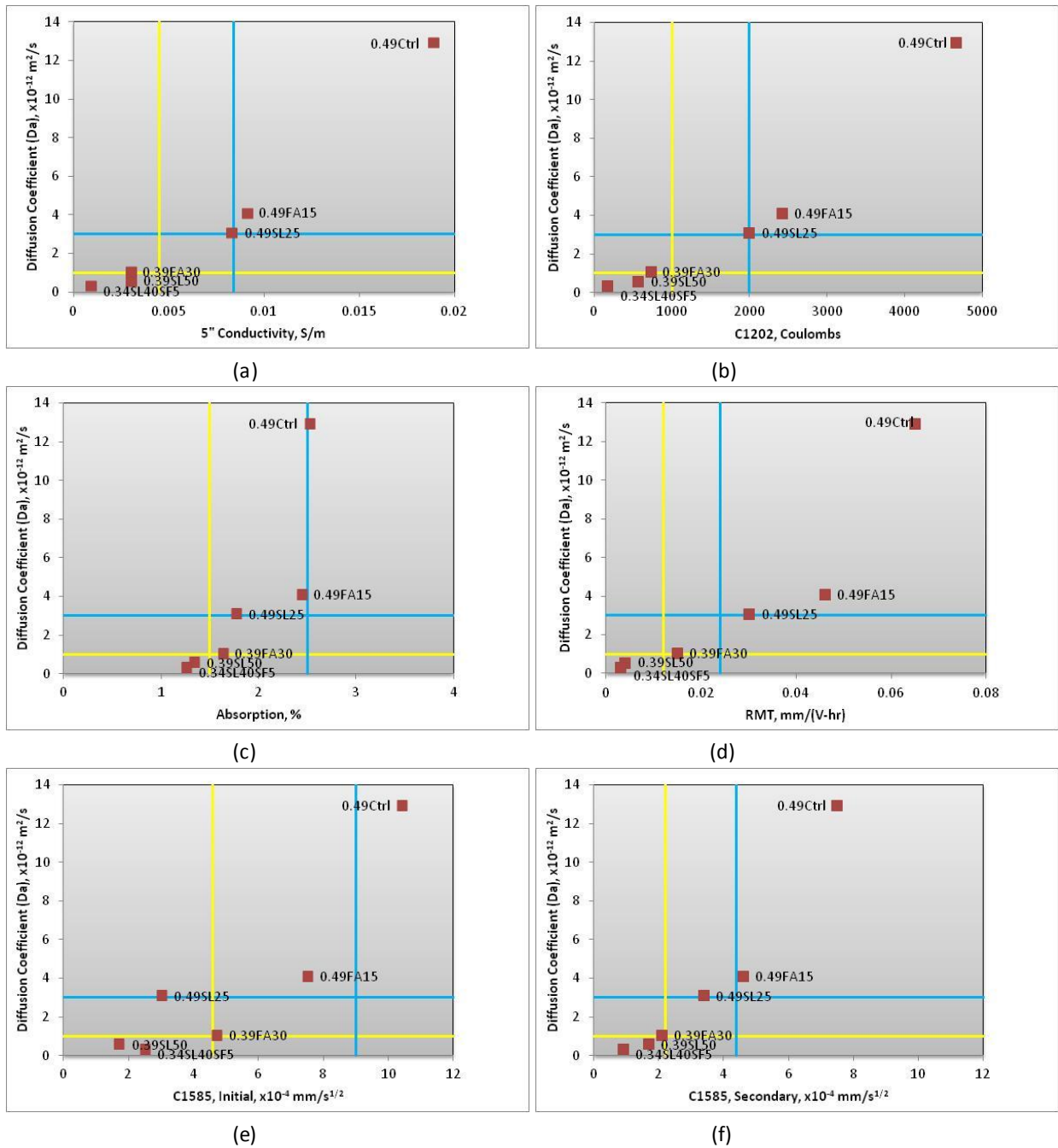


Figure 4. (a) – (f) Correlation between 28 d accelerated rapid index test results and Chloride diffusion coefficients for 59d normal curing followed by 16 months in solution

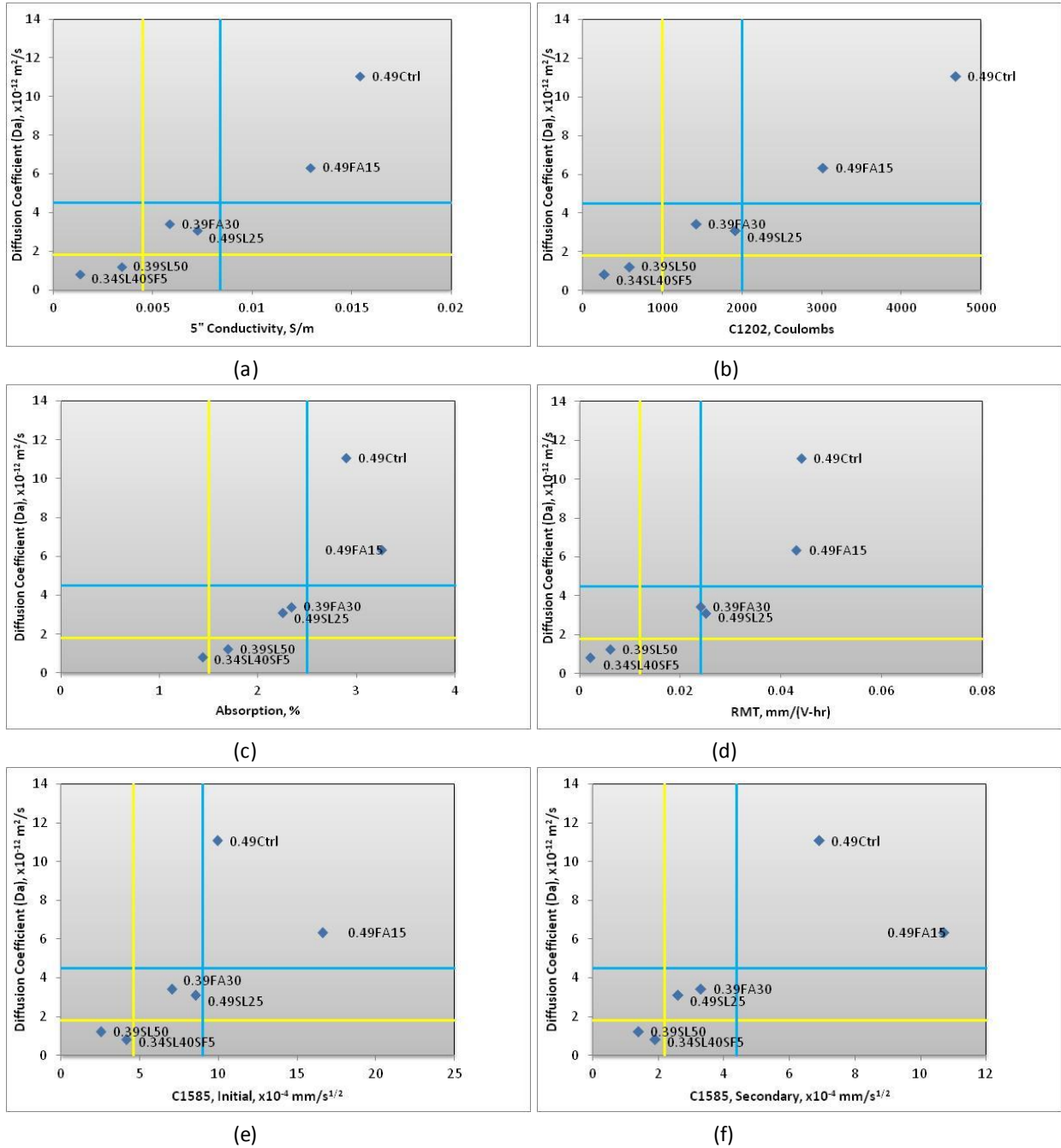


Figure 5. (a) – (f) Correlation between 56 d normal curing rapid index test results and Chloride diffusion coefficients for 59d normal curing followed by 4 months in cyclic exposure (4d in solution + 3d in 100°F/20%RH)

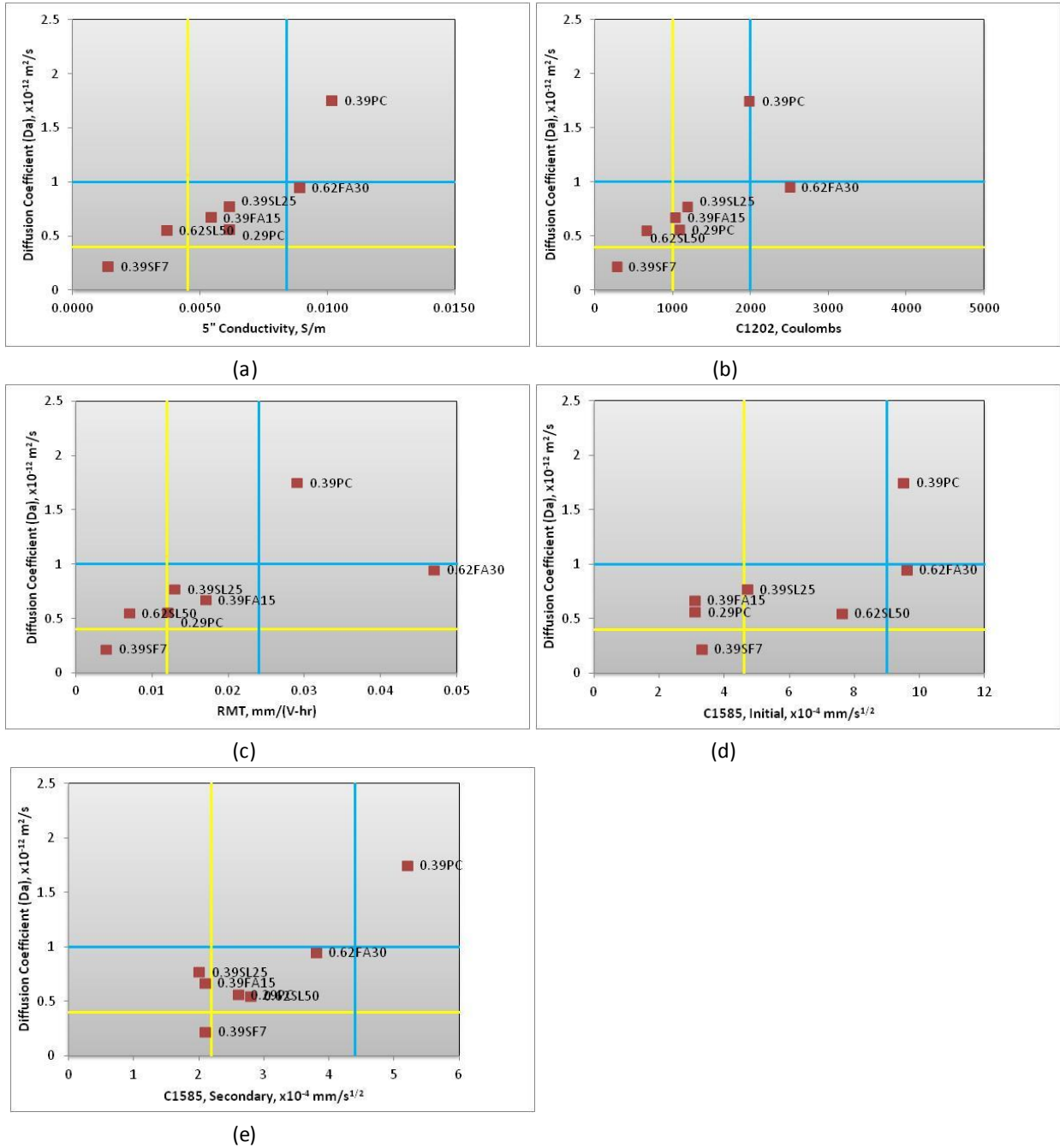


Figure 6. (a) – (f) Correlation between 28 d accelerated rapid index test results and Chloride diffusion coefficients for 6 month normal curing followed by 15 month in solution

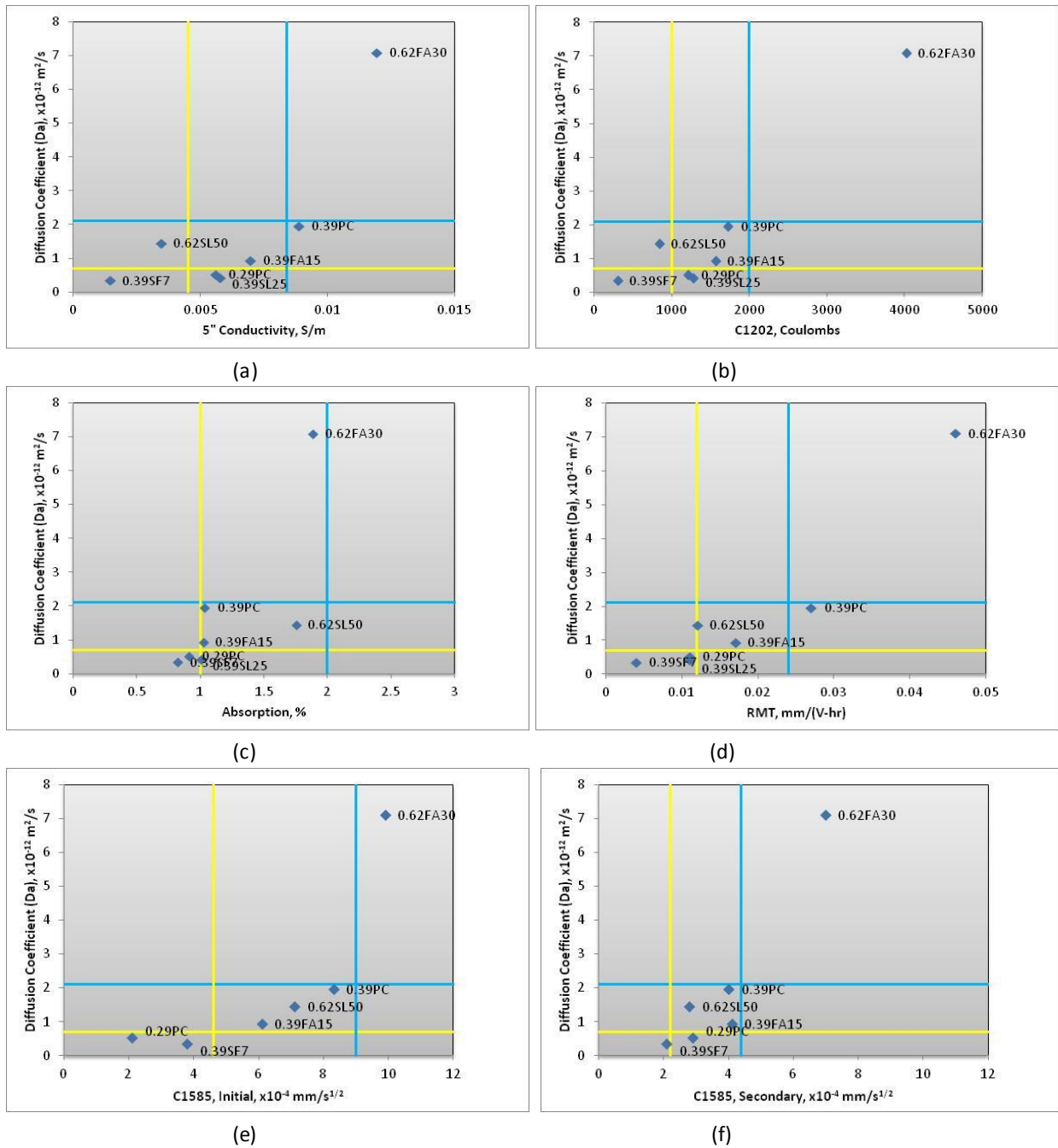


Figure 7. (a) – (f) Correlation between 56 d normal curing test results and Chloride diffusion coefficients for 56d normal curing followed by 18 months in cyclic exposure (3d in solution + 4d in 70°F/50%RH)

Chloride Diffusion Coefficient and Rapid Index Test Results Comparisons

Figure 4 shows that the 28 day accelerated test results for 5 mt. conductivity, RCPT, RMT, and Secondary sorptivity tests correlate well with the chloride diffusion coefficient results attained for 59d normal curing followed by 16 months in chloride solution immersion. Initial sorptivity and absorption test results do not correlate well.

Figure 5 shows that the 56 day test results for 5 mt. conductivity, RCPT, and Secondary sorptivity tests correlate well with the chloride diffusion coefficient results attained for 59d normal curing followed by 4 months cyclic exposure (Each cycle: 4 day in solution+3 days in 100F/20%RH). Initial sorptivity, and absorption test results do not correlate well while RMT was acceptable.

Figure 6 shows that the 28 day accelerated test results for 5 mt. conductivity, RCPT, RMT, and Secondary sorptivity tests correlate well with the chloride diffusion coefficient results attained for 6 month curing followed by 15 months in chloride solution immersion. The 0.62 w/cm mixtures don't correlate well for the electrical tests but even they are not bad - 0.62FA30 is conservative while 0.62SL50 is almost ok. Initial sorptivity test results do not correlate well.

Figure 7 shows that the 56 day test results for RMT, Initial sorptivity, and Secondary sorptivity tests correlate well with the chloride diffusion coefficient results attained for 56d normal curing followed by 18 months in cyclic exposure (3d in solution+4d in 70F/50% RH). RCPT, and 5 mt. conductivity test results don't correlate for the 0.62SL50 mixture; Also the 0.39SL25, and 0.29PC mixture has similar D_a 's as 0.39SF7 but much higher RCPTs. This suggests that silica fume is more effective at reducing RCPT but not as much diffusivity. For same diffusivity one would target lesser RCPT for binary silica fume mixes as opposed to binary slag or fly ash mixes. However this is true only for the cyclic case. Absorption test results do not correlate well.

The limits for the 5mt conductivity, RCPT, RMT, absorption, and Secondary sorptivity are consistent regardless if 56 day or 28 day accelerated test results are considered. However for Initial sorptivity the limits are not consistent.

The coefficient of determinations (R^2) between each of the rapid index test results and the chloride diffusion coefficients for the longest chloride exposures in Table 1 and 2 has been summarized in the following Table. The coefficient of determinations of the 56 day rapid index test results are listed first and the coefficient of determinations of the 28 day accelerated rapid index test results are listed after the slash.

Rapid Index Test	Coefficient of Determination with Diffusion Coefficient			
	56 day/28 day acc			
	59d + 16mo in solution	59d + 4mo cyclic	6mo + 15mo in solution	56d + 18mo cyclic
5 minute Conductivity (Draft ASTM)	0.93/ 1.00	0.96 /0.91	0.78/ 0.90	0.66 /0.43
RCPT (ASTM C1202)	0.95/ 1.00	0.99 /0.93	0.65/ 0.83	0.88 /0.66
Absorption (Draft ASTM)	0.77/ 0.91	0.91/ 0.94	0.10/NA	0.67/NA
RMT (AASHTO TP64)	0.88/ 0.96	0.97 /0.97	0.72/ 0.73	0.89 /0.82
Initial Sorptivity (ASTM C1585)	0.62/ 0.80	0.59/ 0.97	0.44/ 0.50	0.84 /0.72
Secondary Sorptivity (ASTM C1585)	0.63/ 0.99	0.76/ 0.96	0.51/ 0.79	0.88 /0.55

Between the 56 d and 28 d accelerated test results the higher R^2 values have been highlighted in the above Table. For the immersed case the 28 d accelerated rapid index test results had better R^2 values. For the cyclic case in general the 56 d rapid index test results had better R^2 values. The R^2 values for the immersed and cyclic exposure cases have been summarized in the Table below. The average R^2 values for the immersed and cyclic cases as well as the overall averages have been provided. The curing condition that leads to the maximum R^2 value is also provided. For the immersed case the 5 mt conductivity and C1202 have the best R^2 values (>0.90), while RMT, and final sorptivity have acceptable R^2 values (>0.80). Initial sorptivity had poor R^2 value. The 28 d accelerated rapid index test results had the best R^2 values. For the cyclic case RCPT and RMT had the best R^2 values (>0.90), while the remaining tests have acceptable R^2 values (>0.80). The 56 d rapid index test results had the best R^2 values except for initial sorptivity for which the 28d accelerated rapid index test results had better R^2 values. Overall RCPT and RMT had the best R^2 values (>0.90), while 5 minute conductivity and Secondary sorptivity have acceptable R^2 values (>0.80). Initial sorptivity and absorption gave low R^2 values and therefore should not be considered for selecting mixtures based on their chloride diffusion coefficient.

Rapid Index Test	Coefficient of Determination (R^2) with Diffusion Coefficient				
	Immersed	Average for immersed	Cyclic	Average for cyclic	Overall Average/lowest
					t

5 minute Conductivity (Draft ASTM)	1.00/0.90	0.95/28 d acc	0.96/0.66	0.81/56 d	0.88/0.66
RCPT (ASTM C1202)	1.00/0.83	0.92/28 d acc	0.99/0.88	0.94/56 d	0.93/0.83
Absorption (Draft ASTM)	0.91/NA	NA	0.91/0.67	0.79/56 d	NA
RMT (AASHTO TP64)	0.96/0.73	0.85/28 d acc	0.97/0.89	0.94/56 d	0.90/0.73
Initial Sorptivity (ASTM C1585)	0.80/0.50	0.65/28 d acc	0.97/0.72	0.85/28 d acc	0.75/0.50
Secondary Sorptivity (ASTM C1585)	0.99/0.79	0.89/28 d acc	0.76/0.88	0.82/56 d	0.86/0.79

Even though the RCPT test may be a good indicator test for low chloride diffusion coefficients for both the immersed as well as the cyclic exposures in some situations such as in Figure 6 and 7 it can give misleading results. Figures 6, and 7 show that the 0.62SL50 mixture is placed in the wrong quadrant indicating that the measured chloride diffusion coefficients are actually higher than that indicated by the low RCPT, RMT, and 5 mt. conductivity values.

In the following Table the 56 day rapid index results and the chloride diffusion coefficients for the 18 m cyclic exposure is listed. The 56 day RCPT result (832 coulombs) for the 0.62SL50 mixture was lower than that for the 0.39SL25, 0.29PC, and 0.39FA15 mixture (1200 to 1600 coulombs). Yet the diffusion coefficient test results for the 0.62SL50 mixture was 1.5 to 3.5 times higher than those mixtures. A job specification of 1000 coulombs would have allowed the 0.62SL50 mixture and rejected the other mixtures even though they would have attained lower chloride diffusion coefficients! Even the RMT and 5 mt conductivity test results conclude that the 0.62SL50 mixture is similar or better than the 0.39SL25, 0.29PC, and 0.39FA15 mixture. The clearest conclusion though comes from the absorption and sorptivity test results. The 56 day absorption and sorptivity test results were much higher for the 0.62SL50 as compared to the other mixtures indicating that additional sorptivity or absorption criteria may be used to remove the 0.62SL50 mixture. It is interesting to note that for the immersed case the 0.62SL50 mixture does not appear to mislead so much. The 28 d accelerated RCPT result (661 coulombs) for the 0.62SL50 mixture was lower than that for the 0.39SL25, 0.29PC, and 0.39FA15 mixture (about 1100 coulombs). But the diffusion coefficient test results for the 0.62SL50 mixture was 0.7 to 1.0 times that of the other mixtures.

Mix ID	56 day RCPT Coulombs	D _a , 18 m cyclic × 10 ⁻¹² m ² /s	56 day RMT Mm/(V-hr)	56 day conductivity Sm ⁻¹	56 day Initial Sorpt × 10 ⁻⁴ mm/s ^{1/2}	56 day Abs. %
0.62FA30	4012	7.10	0.046	0.0119	9.9	1.88
0.39PC	1722	1.96	0.027	0.0089	8.3	1.03
0.39FA15	1557	0.94	0.017	0.0070	6.1	1.02
0.29PC	1209	0.53	0.011	0.0056	2.1	0.91
0.39SL25	1272	0.42	0.011	0.0058	NA	1.00
0.62SL50	832	1.45	0.012	0.0034	7.1	1.75
0.39SF7	299	0.35	0.004	0.0014	3.8	0.82

The 0.62FA30 mixture has a different story. Fly ash tends to react slowly and therefore the early age rapid index test results of the 0.62FA30 mixture are still high and so they do not lead to incorrect conclusions as the 0.62SL50 mixture.

The 56 day RCPT result (299 coulombs) for the 0.39SF7 mixture was much lower than that for the 0.39SL25, and 0.29PC mixture (1200 coulombs). Yet the diffusion coefficient test results for all 3 mixtures for the 18 m cyclic exposure were similar. Even the RMT and 5 m t conductivity test results conclude that the 0.39SF7 mixture is much better than the 0.39SL25, and 0.29PC mixtures. This suggests that silica fume is more effective at reducing RCPT but not as much the diffusivity. For same diffusivity one would target lesser RCPT for binary silica fume mixes as opposed to binary slag or fly ash mixes. It is interesting to note that this is not true for the immersed case. The 28 d accelerated RCPT result (276 coulombs) for the 0.39SF7 mixture was lower than that for the 0.39SL25, and 0.29PC mixture (about 1100 coulombs). But the diffusion coefficient test results for the 0.39SF7 mixture was 0.30 to 0.40 times that of the other mixtures.

The bigger danger with solely depending on the conductivity based tests is that high w/cm mixtures containing slag or silica fume (high w/cm silica fume mixtures performed similar to high w/cm slag mixtures) can show low early age conductivity values leading to the mistaken conclusion that they would help attain low chloride diffusion coefficients for cyclic exposures. The feasibility of using the Secondary

sorptivity test criteria in addition to the RCPT test criteria to classify mixtures with low chloride diffusion coefficient is investigated below.

From Figure 4-7 the performance criteria for the 4 rapid index test methods that have the best overall R² values can be listed as follows:

Chloride Diffusion Coefficient Level	RCPT, Coulombs	RMT, mm/(V-hr)	5 mt. conductivity, S/m	Sec. Sorptivity, $\times 10^{-4}$ mm/s^{0.5}
Very Low	≤ 1000	≤ 0.012	≤ 0.0045	≤ 2.20
Low	1000 to 2000	0.012 to 0.024	0.0045 to 0.0084	2.20 to 4.40
Moderate	> 2000	> 0.024	> 0.0084	> 4.40

Mixtures are classified just by taking into account the RCPT test and the final sorptivity test for each of the 4 exposures depicted in Figures 4-7.

For the immersed case: rapid index test criteria @ 56 days was used

For the cyclic case: rapid index test criteria @ 28 days accelerated was used

In cases where the classified mixtures according to the 2 rapid index tests are at two different levels of chloride diffusion coefficient conservatively it was decided to take into account the higher chloride diffusion coefficient level. The results are classified in the Table below. When compared to Figure 7 it can be seen this mixture classification based solely on the rapid index test criteria matches exactly their performance levels in chloride diffusion coefficient. The real strength in combining the Secondary sorptivity with the RCPT test criteria is seen in 0.62SL50 mixture which correctly falls in the low category. However it is not perfect as it classified 0.29PC, and 0.39SL25 mixtures as belonging to low category even though they had very low diffusion coefficients. At least the selection based on the rapid index criteria is conservative in successfully eliminating the high w/cm slag cement mixtures.

Chloride Diffusion Coefficient Level	59d + 16mo in solution	59d + 4mo cyclic	6mo + 15mo in solution	56d + 18mo cyclic
Very Low	0.34SL40SF5, 0.39SL50, 0.39FA30	0.34SL40SF5, 0.39SL50,	0.39SF7	0.39SF7
Low	-	0.39FA30, 0.49SL25	0.29PC, 0.39FA15, 0.39SL25, 0.62SL50	0.29PC, 0.39FA15, 0.39SL25, 0.62SL50, 0.39PC
Moderate	0.49SL25, 0.49FA15, 0.49PC	0.49FA15, 0.49PC	0.39PC, 0.62FA30	0.62FA30

On the other hand if just the 56 day RCPT criteria had been considered the following mixture selection would have been made which clearly shows the 0.62SL50 mixture in the incorrect chloride diffusion coefficient level

Chloride D _a Level	56d + 16mo in solution	56d + 4mo cyclic	6mo + 15mo in solution	56d + 18mo cyclic
Very Low	0.34SL40SF5, 0.39SL50, 0.39FA30	0.34SL40SF5, 0.39SL50	0.39SF7, 0.62SL50	0.39SF7, 0.62SL50
Low	-	0.39FA30, 0.49SL25	0.29PC, 0.39FA15, 0.39SL25	0.29PC, 0.39FA15, 0.39SL25, 0.39PC
Moderate	0.49SL25, 0.49FA15, 0.49PC	0.49FA15, 0.49PC	0.39PC, 0.62FA30	0.62FA30

The sorptivity test as well as the calculation of Secondary sorptivity is relatively complex. For it to be useable as an acceptance criterion at least for mixture qualification the following simplification is suggested. The Secondary sorptivity test results were plotted against the mass gain (due to moisture) during the period of the test in which the Secondary sorptivity test result is calculated. This corresponds to the mass gain between 1 d and 7 d after the specimen contacts the water. Figure 8 below shows that there is an excellent correlation between the Secondary sorptivity values and the mass gain. As many as 130 data points corresponding to the whole test program were included. This means that the Secondary sorptivity test criteria can be converted to mass gain. The appropriate conversions for $2.2 \times 10^{-4} \text{ mm/s}^{0.5}$ and $4.4 \times 10^{-4} \text{ mm/s}^{0.5}$ are 1.2 g and 2.4 g respectively. The test also becomes much easier to do. The original specimen mass, mass at 1 day and at 7 days needs to be determined from which the mass gain between 1 and 7 days can be calculated.

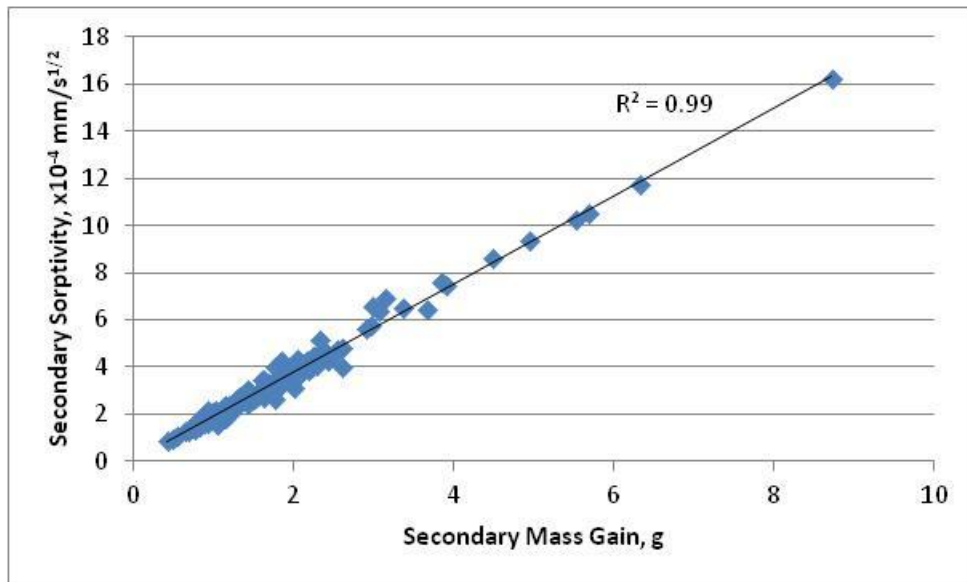


Figure 8. Correlation between Secondary Sorptivity and Mass Gain

The RCPT and 5 minute conductivity test results for all of the Table 1, and 2 mixtures have been in plotted as Figure 9 below. The results indicate a good correlation as expected.

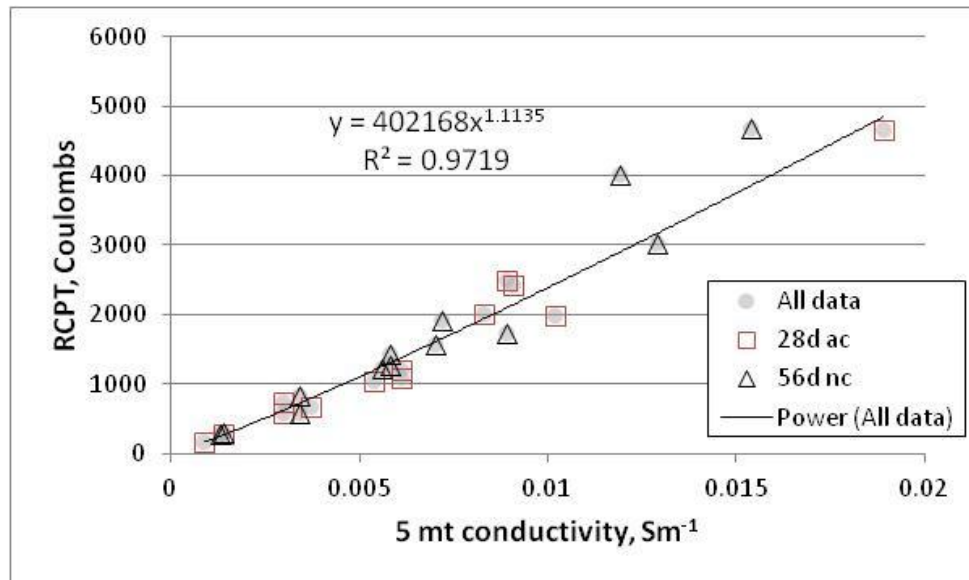


Figure 9. Correlation between RCPT and 5 minute conductivity

Preliminary Conclusions

1. It appears that the RCPT and sorptivity criteria should be used in conjunction with the strength criteria. This would help replace the prescriptive criteria like w/cm, SCM etc. This is very effective at catching the high w/cm, high SCM mixtures as well which are not caught just by the RCPT criteria.
2. The rapid index tests should be conducted at the following conditions:
 - 56 days moist cured for cyclic environments
 - 28 day accelerated for cases immersed in chloride
3. The reliability of the triple performance criteria are being tested against a broader set of mixtures that were cast as part of Tables 3, 4 and 5.
4. The RCPT and 5 minute conductivity test results appear to have a good correlation as expected.

Freeze Thaw - Test Methods, Curing Conditions and Test Ages

Freeze thaw (F-T) attack is another major concrete deterioration mechanism. Capillary sorption and water vapor diffusion are the two principal transport mechanisms that cause critical saturation of capillary pores which is necessary for freeze thaw damage. An air content of 5% to 7% with an air voids spacing factor less than 0.2 μm is typically necessary to maintain adequate freeze thaw resistance. While the air entrainment requirement is acceptable an attempt will be made to develop test and performance criteria as an alternative to the maximum w/cm requirement. ACI 318 states that for F1, F2, F3 categories max w/cm=0.45, min strength=4500 psi, and air content limits. It is clear that a low

w/cm is required to ensure low water penetration and potential for critical saturation. By conducting mixes with different w/cm and various SCM dose and contents we will examine if F-T performance (as measured by no. of cycles for 15% mass loss or relative dynamic modulus of elasticity after 300 cycles) is better correlated with a rapid index test such as sorption or gas permeability criteria than w/cm. If at each w/cm, F-T performance varies widely depending on the test criteria the importance of the test criteria as opposed to w/cm is established. Also it would be determined whether some mixes with low w/cm and higher sorptivity/gas perm can have poorer F-T performance as compared to mixes with higher w/cm and lower sorptivity/gas perm which can again establish the importance of the test criteria as opposed to w/cm.

ACI 318-08 F classes

Moderate F1: Concrete exposed to freezing-and thawing cycles and occasional exposure to moisture

Severe F2: Concrete exposed to freezing-and thawing cycles and in continuous contact with moisture

Very severe F3: Concrete exposed to freezing-and thawing and in continuous contact with moisture and exposed to deicing chemicals

From the test results plots Concrete class F2 can be suggested to have RDM of 60-80% while F3 can have RDM>80% after 300 F-T cycles. It is hoped that these RDM and mass loss correlates with rapid index test criteria such as sorptivity and we can use those test criteria rather than RDM.

For C672 Y axis will be mass loss or visual rating

Mixture Proportions Planned

w/cm	PC	20%FA	30%SL	25%SL+5%SF
0.45	Yes-m		Yes-m	
0.50	Yes-h	Yes-m	Yes-m	Yes-l
0.60	Yes-h			Yes-m

The mixtures have been cast and are shown in Table 3.

Crushed coarse aggregate (1.0" max) no. 57, natural sand FM=2.88

Adjust water reducer or high range water reducer (if any) for desired slump = 5 to 7 in.

Air entrained concrete mixtures – Target 5 to 6% air. Use AEA from same admix manufacturer

Normal Curing – Standard moist room curing starts immediately after making the specimens

Accelerated Curing – 7 days of normal curing followed by 21 days of curing in 100F water

For all mixtures measure the following: Slump, temperature, air content, density, Strength (28 days of moist curing followed by 28 days of air drying), Shrinkage (7 days moist curing followed by 90 days of air drying).

Durability Tests

For all tests at all ages, make 2 cylinders unless otherwise stated. Make 6 extra cylinders for each mix, moist cure for 28 days and then ship 4 to Purdue/UT for gas permeability testing and keep the other 2.

- Rapid Chloride Permeability test (ASTM C1202)
 - i) 28 day accelerated
 - ii) 56 day normal curing
 - iii) 26 week (182 d) normal curing

- ASTM C666. Test 2 replicate specimens as recommended by C666 standard. 28 day moist curing followed by 28 day air drying in 50% RH and 70F and then start C666. Do dynamic modulus, mass change tests as required by C666. Do test until 1000 cycles or visible differences between mixtures which-ever occurs first. Also mixtures should not be tested for >25% mass reduction or 50% relative dynamic modulus of elasticity.

- ASTM C672. Test 2 replicate specimens as recommended by C672 standard. 28 day moist curing followed by 28 day air drying in 50% RH and 70F and then start C672. Do test until 150 cycles or visible differences between mixtures which-ever occurs first. Determine visual rating every 5 cycles.

- Sorptivity Test (ASTM C1585) after:

- i) 28 day accelerated + 18 d specimen conditioning (C1585)
 - ii) 38 day normal curing + 18 d specimen conditioning (C1585)
 - iii) 26 week (182 d) normal curing + 18 d specimen conditioning (C1585)
- Absorption test BS 1881:122 – use latest ASTM draft which states 50C.
 - i) 28 day accelerated + 3 d in oven
 - ii) 56 day normal curing + 3 d in oven
 - iii) 26 week (182 d) normal curing + 3 d in oven

Table 3. Yield Adjusted Mixture Proportions and Preliminary Test Results

Calculated Batch Quantities											
	0.57	0.50	0.50	0.50	0.50	0.60	0.45	0.45	0.57	0.50	0.50
	PC	PC	FA20	SL30	SL25SF5	SL25SF5	PC	SL30	PC ^{***} -R	PC ^{***} -R	SL30 ^{***} -R
Type I/II cement, lb/yd ³	506	539	442	385	385	353	592	414	505	541	382
Slag, lb/yd ³				165	137	126		177			164
Flyash, lb/yd ³			111								
Silica Fume, lb/yd ³					27	25					
SCM, %	0	0	20	30	30	30	0	30	0	0	30
Coarse Agg. (No.57), lb/yd ³	2087	2021	2071	2060	2058	2077	2035	2029	2082	2026	2043
Fine Aggregate, lb/yd ³	1094	1083	1066	1093	1084	1072	1062	1048	1118	1086	1084
Mixing Water, lb/yd ³	290	270	276	275	275	302	267	266	293	270	273
w/cm	0.57	0.50	0.50	0.50	0.50	0.60	0.45	0.45	0.58	0.50	0.50
ASTM C494 AEA, oz/cwt	3.8	4.4	23.5	6.3	4.4	7.0	4.4	6.9	3.8	4.4	4.8
ASTM C494 Type F, oz/cwt		3.1	2.2	3.2	5.5	2.6	8.1	11		6.7	12.8
Fresh Concrete Properties											
ASTM C143, Slump, in.	7	6	6	5	5	6.5	5.25	6	5.5	4.75	7
ASTM C231, Air, %	6	7.2	6	6.2	6.5	6.2	7	7.6	5.8	7.2	7.2
ASTM C138, Density, lb/ft ³	148.1	145.7	147.7	148.1	147.7	147.3	147.3	146.5	148.9	146.1	146.9
ASTM C1064, Temperature, °F	75	75	73	70	72	70	70	70	70	70	68
Hardened Concrete Properties											
ASTM C39, Compressive Strength, psi											

28 days	4,918	4,895	4,101	5,376	6,249	4,844	5,427	5,182	4,738	4,454	5,312
Draft ASTM Standard, Water Absorption Test at 50 °C, %											
28d accelerated cure	-	-	1.41	-	1.24	1.56	1.61	1.2	2.28	1.81	1.47
56d normal cure	1.85	1.65	1.81	1.36	1.44	1.74	1.76	1.39	-	-	-
182d (26w) normal cure	1.67	1.47	1.19	1.45	1.29	1.51	1.49	1.20	-	-	-
ASTM C1202, Rapid Chloride Permeability, Coulombs											
28d accelerated cure	-	-	2014	-	332	516	2630	851 ⁻	5015	3578	1077
56d normal cure	4876	3633	4287	1554	469	848	2957	1143 ⁻	-	-	-
182d (26w) normal cure	5297	3879	2193	1340	532	622	2722	1094	-	-	-
ASTM C157, Length Change (Drying Shrinkage), %											
28 days ⁺	0.045	0.039	0.041	0.049	0.053	0.063	0.036	0.039	-	-	-
56 days ⁺	0.061	0.046	0.050	0.052	0.056	0.069	0.049	0.049	-	-	-
90 days ⁺	0.069	0.054	0.057	0.058	0.065	0.075	0.055	0.055	-	-	-
180 days ⁺	0.076	0.059	0.057	0.063	0.065	0.077	0.058	0.058	-	-	-
ASTM C 1585, Rate of Water Absorption (Sorptivity), x10⁻⁴ mm/s^{1/2}											
28d accelerated cure (Initial/Secondary)	-	-	8.7 ⁺ / 3.0	-	5.4 ⁺ / 1.9	7.1 ⁺ / 3.3	5.9 ⁺ / 4.1	***	17.5 ⁺ / 6.7	10.7 ⁺ / 4.7	***
56d normal cure (Initial/Secondary)	13.7 / 3.6 ⁺	8.1 ⁺ / 3.4	14.1 / 9.8	***	6.0 / 3.2	6.2 / 3.5	***	5.0 / 3.1 ⁺	-	-	-
196d normal cure (Initial/Secondary)	4.3 ⁺ / 1.6 ⁺	2.9 ⁺ / 2.1 ⁺	5.5 ⁺ / 2.3 ⁺	5.0 ⁺ / 1.2 ⁺	***	4.9 ⁺ / 1.7	***	2.7 ⁺ / 1.5	-	-	-
ASTM C 666, Freezing and Thawing Resistance, %											
Durability Factor @ 2,500 c	97	98	95	72	96	96	98	97	-	-	-
Durability Factor @ 3,200 c ^{***}	86	91	82	46	93	91	90	97			
Mass Loss @ 2,500 c	5.0	2.8	5.9	5.9	4.3	6.8	3.7	5.4	-	-	-
Mass Loss @ 3,200 c ^{***}	8.2	5.6	9.2	7.8	6.4	8.8	6.2	5.8			
ASTM C 672, Salt Scaling Resistance											
Visual Rating (0-5) @ 50 cyc	5	3.0	3.0	3.0	2.3	3.8	2.0	0.5	-	-	-
Visual Rating (0-5) @ 180 cyc	5 ⁺⁺	3.5	4.5	3.0	3.6	4.3	2.8	1.5	-	-	-

** Exact repeat of designated mixture

* A correlation coefficient less than 0.98 indicating that the rate cannot be determined according to ASTM C1585

+ Curing period in 70°F, 50% RH environment NOT included 7 days initial wet curing period in water bath

- Result of only one specimen

** Terminated at 75 cycles

*** Result of only one specimen. All FT specimens were taken out of the FT chamber at about 3120 cycles and kept in the moist room for 90 days prior to the final FT exposures for 80 cycles.

+++ No correlations were found, so data is unavailable

At the end of 3120 cycles the specimens were taken out of the F-T machine. They were surface dried, weighed and then subjected to 90 days of moist room curing. The specimens were weighed again and then immediately subjected to 80 F-T cycles. The results at the end of 3200 F-T cycles are also provided in the Table. At the end of the 3200 cycles the specimens were moist cured again for 80 days and then were immediately subjected to 260 F-T cycles. The results at the end of 3500 cycles showed the same trend as the results at the end of 3200 cycles. Therefore the discussions below are primarily focused on freeze thaw performance up to 3200 FT cycles.

Even after 3200 F-T cycles in the ASTM C666 test barring one mix all the other mixes had excellent F-T resistance as shown by durability factors (DF) in excess of 80%. The test data is very consistent with both freeze thaw specimens from a given mixture showing similar results in terms of durability factor and mass loss as seen from the table below. Even that one mix (0.50SL30) may be an outlier as a very similar mix (0.45SL30) has 97% RDM even after 3200 cyc. Further the low RDM of that mix might be due to surface scaling and resulting difficulties in getting the correct RDM.

The mixtures covered a broad range with w/cm varying from 0.45 to 0.60, cementitious systems from straight cement to binary system with fly ash or slag, and ternary blends of slag and silica fume and 56 day RCPT from about 500 to 5000 coulombs. The 28 day strengths varied between 4100 and 6250 psi with most of them between 4100 and 4900 psi. The air contents varied between 6 and 7.6%. Note that generally concrete mixtures with DF>80% after 300 cycles are assumed to have excellent F-T resistance (FHWA grades HPC as: Grade 2 = DF>80%, Grade 1 = DF between 60 and 80% after 300 F-T cycles in C666). On this basis it can be concluded that even if w/cm>0.60, if air content and strengths are adequate DFs should be good and hence mixtures should be F-T durable. Also the mixtures tested varied a great deal in the 56 day rapid index test results (RCPT, sorptivity and absorption) but yet their freeze thaw performance is not compromised. In other words even though the transport properties may not be very good the air void system and compressive strength are primary factors ensuring good freeze thaw behavior of these mixtures.

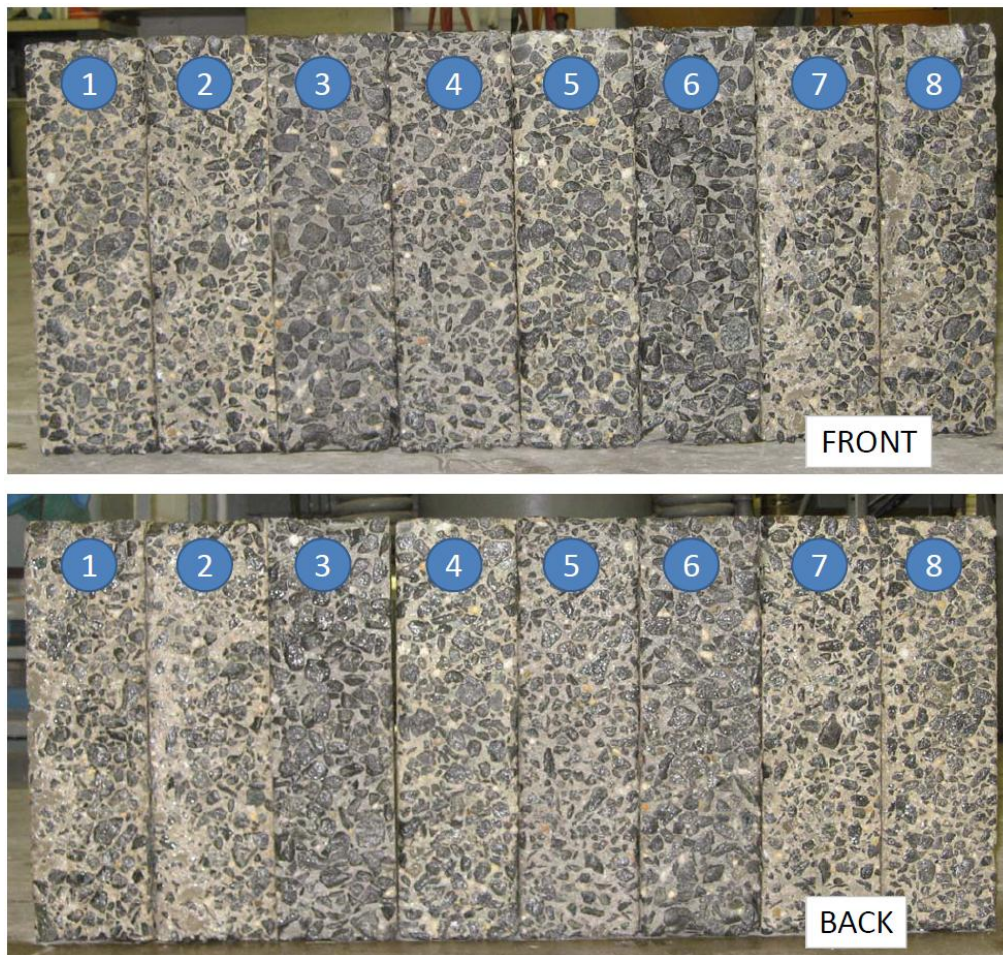


Figure 10. Scaling of C666 prisms after 3200 F-T cycles (numbers signify Mix ID)

Since the F1 class of structures are occasionally exposed to moisture before freezing and will have no snow and ice accumulation (all non horizontal exterior concrete surfaces, and horizontal exterior concrete surfaces not in contact with ground) scaling is certainly not a concern. **On the basis of excellent DFs of mixtures even with w/cm of 0.60 it is suggested that the F1 class should have no w/cm requirement.** F1 class would still have an air content and strength requirement. The 28 day strength of many of these mixtures was between 4100 and 4800 psi suggesting a specified strength requirement of 3500 psi for F1 class is appropriate.

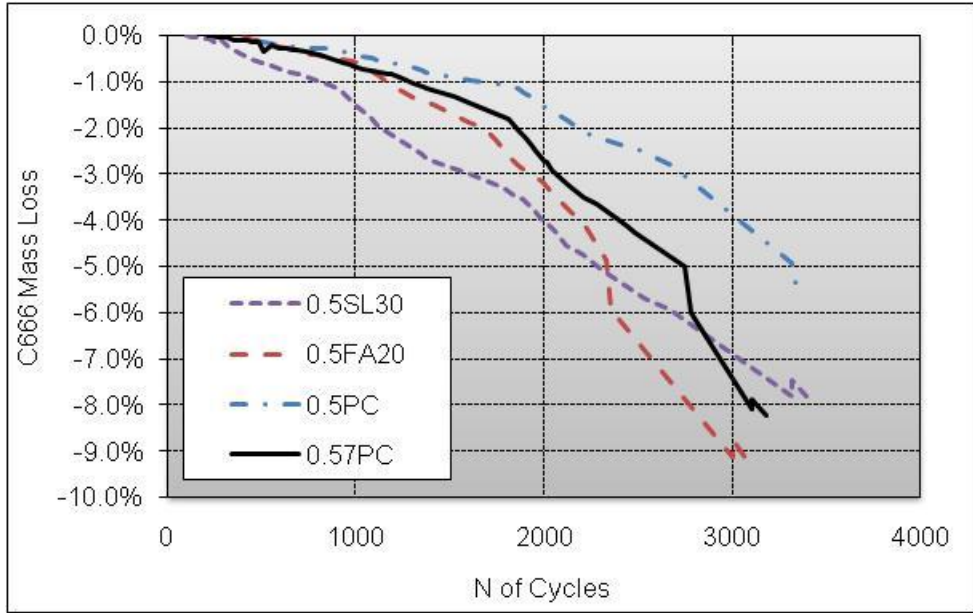
For the F2 class scaling can be an issue in addition to DFs. F2 class of structures is not exposed to salts so that the scaling is mainly due to FT cycles. After 3200 F-T cycles there is C666 scaling mass loss varying between 5.6% and 9.2%. Figure 10 shows the C666 scaling results after 3200 cycles and all mixtures appear to have scaled. Figure 11 shows mass loss increasing as a function of the number of cycles for all mixes. After 300 cyc in the C666 test the mass loss of all mixtures is still below 0.5%

showing hardly any scaling. What is the mass loss limit and the corresponding number of C666 cycles? The Table below classifies the mixtures based on their mass loss performance at different number of cycles.

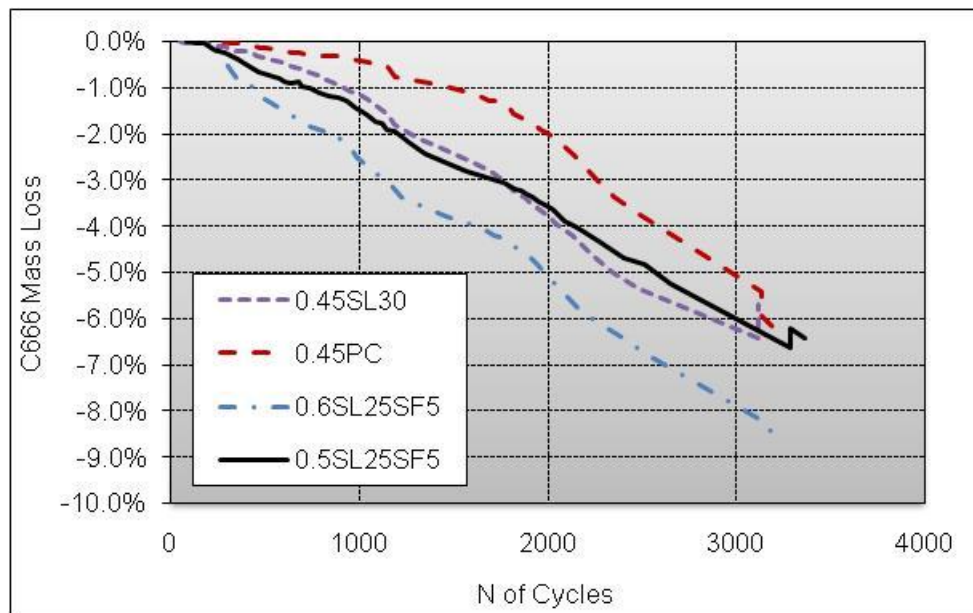
No. of cycles	Mix Classification based on Mass Loss; format is Mass loss, % = Mix ID		
	Good	Average	Poor
1200	0.6 to 1.1% = 1,2,3,7	1.8 to 2.1% = 4,5,8	3.1% = 6
1500	0.8 to 1.5% = 1,2,3,7	2.3 to 2.8% = 4,5,8	3.8% = 6
1900	1.2 to 2.2% = 1,2,7	2.9 to 3.5% = 3,4,5,8	4.6% = 6
2000	1.5 to 2.0% = 2,7	2.7 to 3.9% = 1,3,4,5,8	5.0% = 6
2500	2.8 to 3.7% = 2,7	4.3 to 5.4% = 1,5,8	5.9 to 6.8% = 3,4,6
3200	5.6 to 6.4% = 2,5,7,8	7.8 to 9.2% = 1,3,4,6	

From the Table it is obvious that Mixtures 2, 7 are the consistent best formers. Based on our findings a w/cm limit of 0.50, specified strength of 4000 psi and 6% air content should lead to less scaling which is more or less consistent with the current ACI 318 F2 requirements. Figure 12 shows that barring the absorption test and sorptivity test none of the rapid index criteria, or w/cm, air content, compressive strength correlates with freeze thaw performance as measured by the C666 durability factor. A key reason may be that even after 3200 cycles very little FT failure has taken place (i.e. DFs are largely >80%). Figure 13 shows that none of the rapid index criteria, or w/cm, compressive strength correlates with freeze thaw performance as measured by the C666 scaling mass loss. Air content seems to have a correlation. However it is not practical to have consistently over 7%. C666 scaling mass loss measurements are not well established measurement criterion as C666 durability factor and so the lack of correlation is not surprising. However from what one understands about the mechanism of freeze thaw and scaling the following can be stated:

1. Scaling is freeze thaw failure that occurs at the concrete surface. It is important for the surface layer of concrete not to be critically saturated. Having adequate air contents at the concrete surface delays the time taken for critical saturation and hence scaling.
2. Everything else being the same concrete of higher strength can resist scaling pressures better.
3. The role of w/cm is unclear. It is possible that a lower w/cm concrete may delay the time taken to attain critical saturation and hence may be beneficial.
4. All of the above can also be stated for freeze thaw resistance of concrete i.e. not just surface scaling.

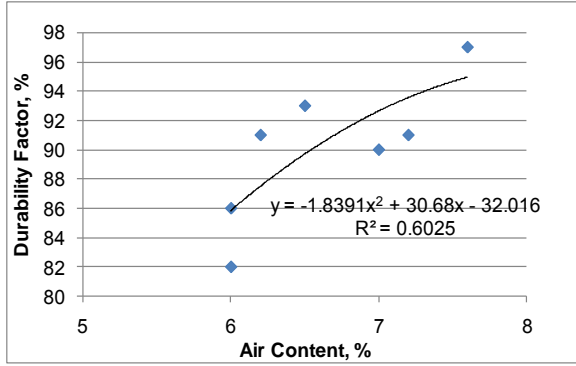


(a)

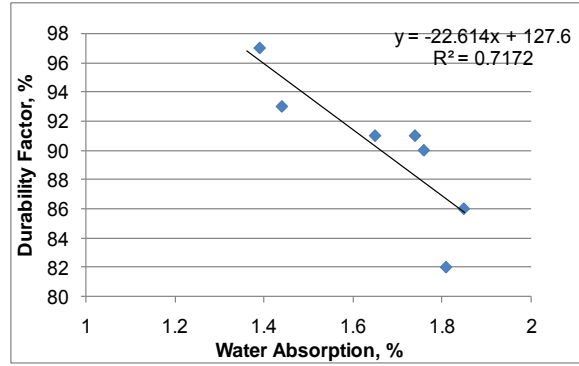


(b)

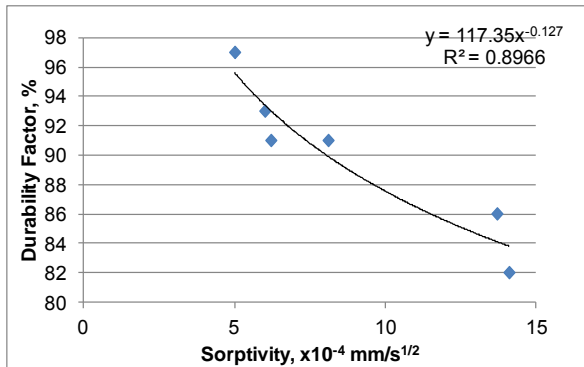
Figure 11. C666 mass loss vs N of cycles



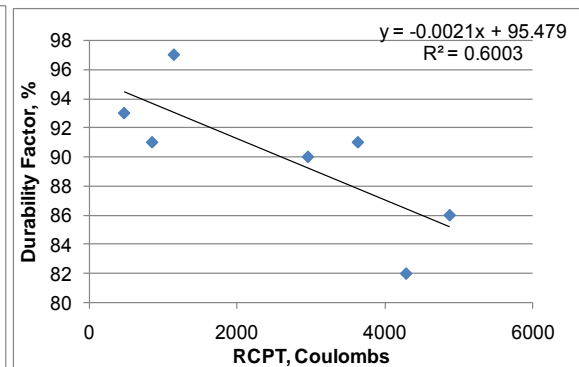
(a)



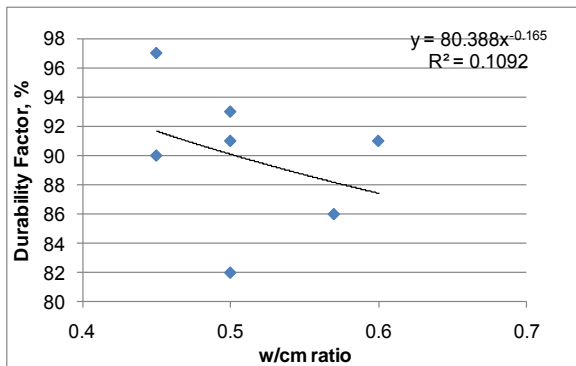
(b)



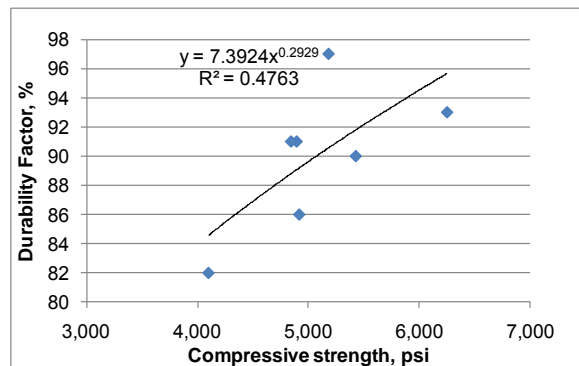
(c)



(d)

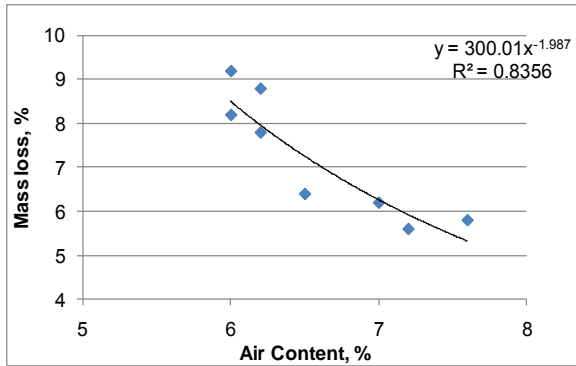


(e)

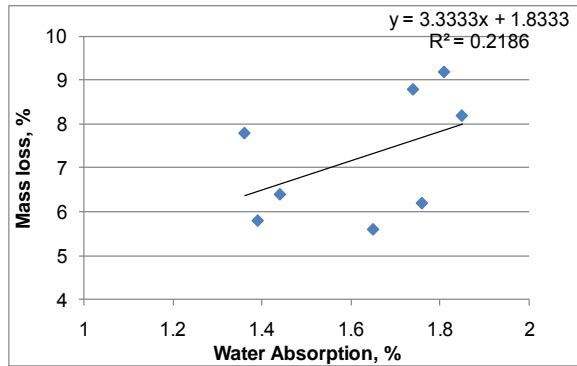


(f)

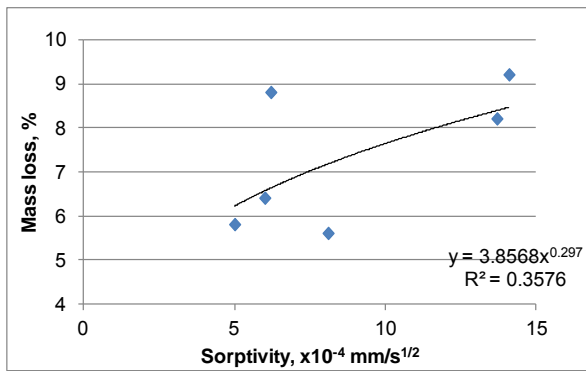
Figure 12. (a) – (f) Correlation between durability factor after 3200 cycles and fresh air content, various rapid index tests



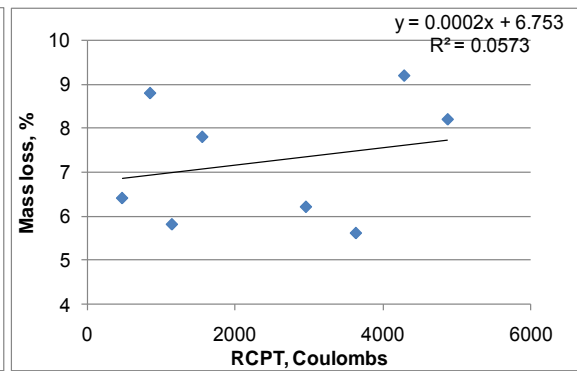
(a)



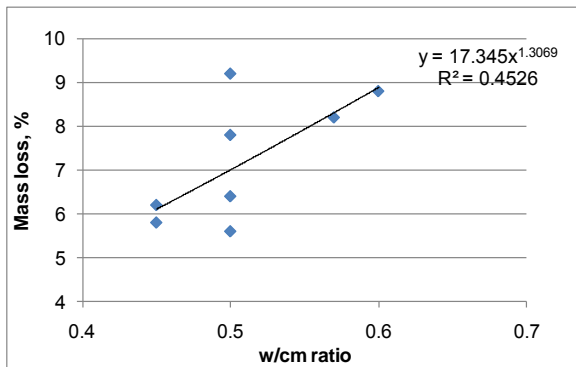
(b)



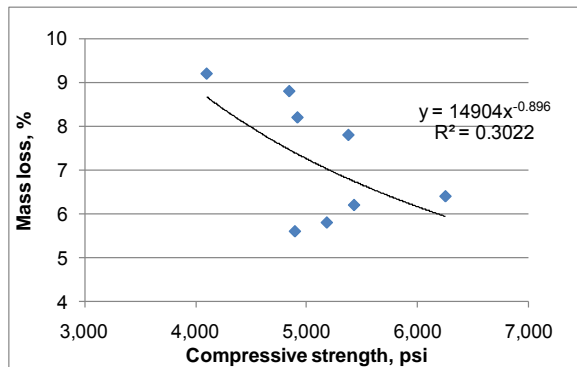
(c)



(d)



(e)



(f)

Figure 13. (a) – (f) Correlation between mass loss after 3200 cycles and fresh air content, various rapid index tests

For the F3 class deicer salt scaling is an issue in addition with regular FT scaling and DFs. ASTM C672 Scaling tests have been completed and the visual ratings are given based on the following table from C672.

Rating	Condition of Surface
0	No scaling
1	Very slight scaling (1/8 in. depth max, no coarse aggregate visible)
2	Slight to moderate scaling
3	Moderate scaling (some coarse agg visible)
4	Moderate to severe scaling
5	Severe scaling (coarse agg visible over entire surface)

Since visual ratings are somewhat subjective they were given by 4 engineering staff members and the ratings averaged for each mixture. The ratings between the staff members were fairly consistent. Ratings after 50, and 180 freeze thaw cycles are provided in Table 3, except for Mixture 0.57PC for which the scaling after 75 cycles was so severe that the mix had to be terminated.

After 180 cycles mixture performance varied widely from a rating of 1.5 to a high in excess of 5. Figure 14 shows the actual surface appearance of the various mixtures and the corresponding visual ratings of scaling.

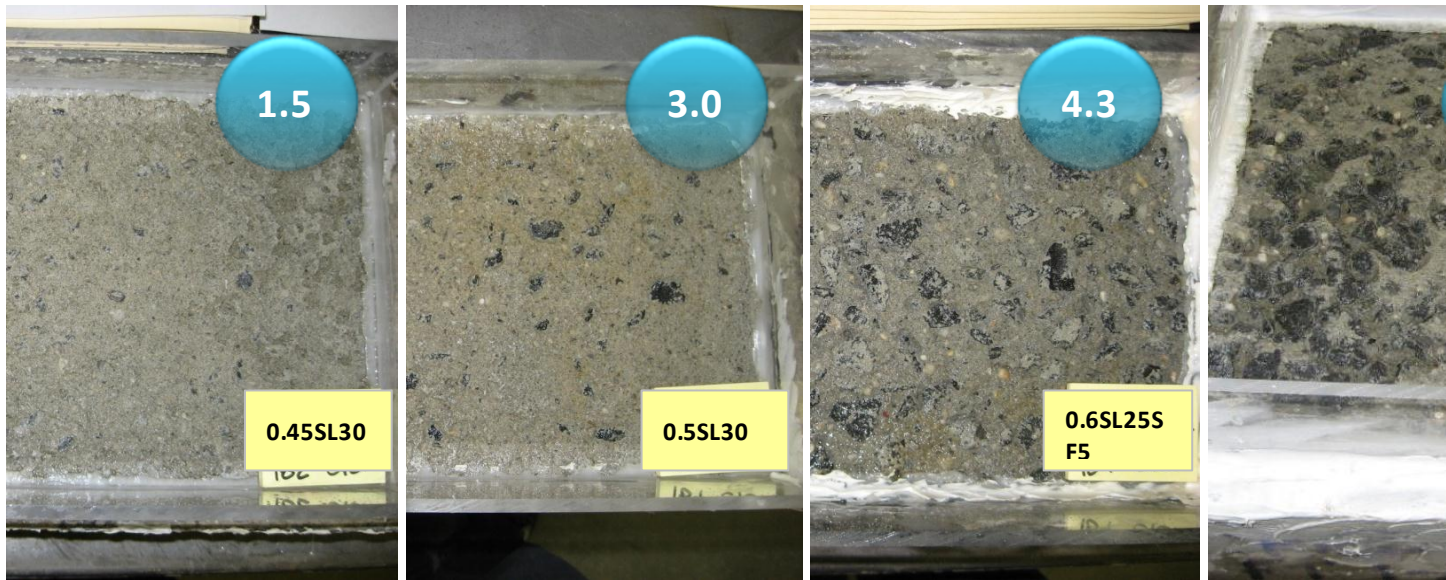


Figure 14. Slabs subjected to ASTM C672 salt scaling after 180 FT cycles

Correlation between salt scaling test visual ratings and rapid index test results

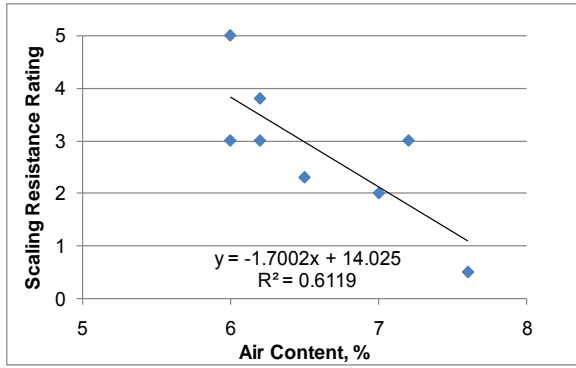
It should be kept in mind that the scaling resistance is evaluated after 50 cycles. Goodspeed et al. in their article HPC Defined have stated that a visual rating after 50 cycles of:

0,1 corresponded to the HPC performance Grade 3

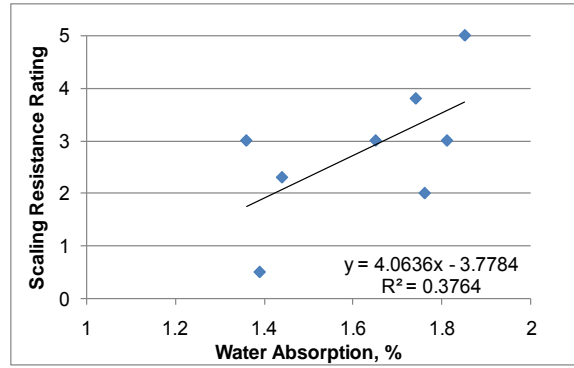
2,3 corresponded to the HPC performance Grade 2

4,5 corresponded to the HPC performance Grade 1

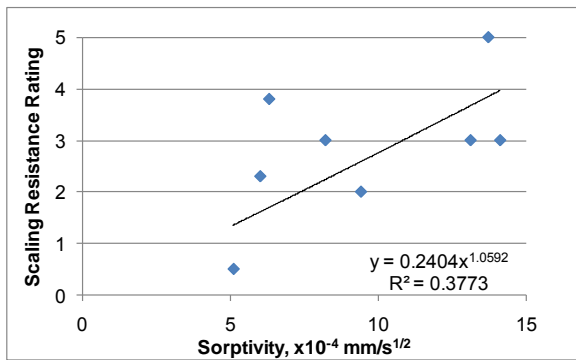
Correlations between the visual ratings after 50 cycles and fresh air content and between the visual ratings after 50 cycles and the various rapid index tests such as absorption, sorptivity and rapid chloride permeability are drawn in Figure 15 a-f. None of the rapid index test results correlate well with the ASTM C672 mass loss. It does not appear possible to select rapid index test criteria as an alternative to ASTM C672 to select mixtures with good scaling resistance. The ratings do appear to correlate somewhat with air content and w/cm which are the current requirements in ACI 318 for concrete exposed to Class F3.



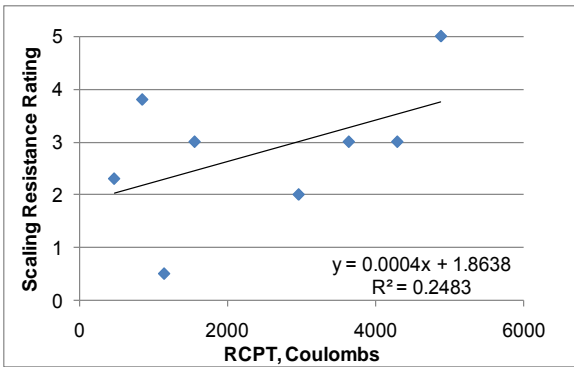
(a)



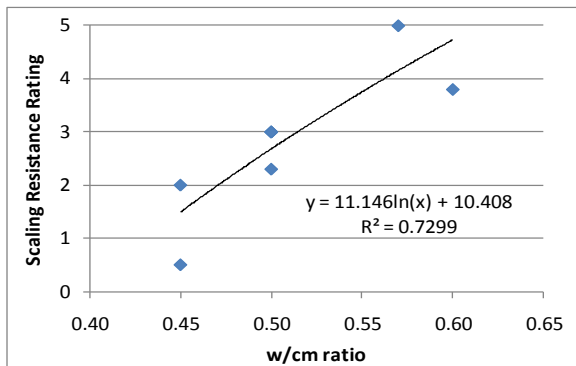
(b)



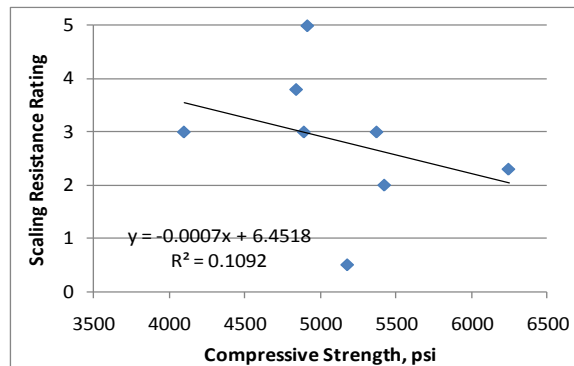
(c)



(d)



(e)



(f)

Figure 15. (a) – (f) Correlation between the visual ratings after 50 cycles and fresh air content, various rapid index tests

Conclusions and Planned Work on Freeze Thaw over Next 2 Quarters

From our understanding of the mechanisms of freeze thaw failure (bulk and scaling) it appears that it would be worthwhile for us to explore if there is a critical degree of saturation (DOS) for FT failure such as C666 DFs, and mass loss. If it is established that there is such a critical DOS then mixtures that increase the time to critical degree of saturation are likely to be more freeze

thaw resistant. The time to critical degree of saturation can be estimated by the sorptivity test (ASTM C1585) and the moisture content of the specimen at 100% saturation (M_{100}). M_{100} is determined by oven drying the specimen until there is a less than 2 g mass decrease and then repeatedly vacuum saturating the specimen until there is a less than 2 g mass increase. The following test program is therefore planned:

Variables

Aim: 1. To determine if there is a critical degree of saturation for FT failure such as C666 DFs, and mass loss; 2. To determine the time to critical DOS

DOS – 4 levels: ~100%, 92%, 86%, right after moist cure (M_C). % is calculated as ratio of M_{100} .

Mixtures – 4: 0.45PC (3 to 4% air), 0.45PC (6 to 7%), 0.65PC (3 to 4%), 0.65SL35 (3 to 4%) – w/cm, air content, and SCM are the parameters being varied.

So 4 mixes x 4 DOS = 16 cases

Crushed coarse aggregate (1.0" max) no. 57, natural sand FM=2.88

Adjust water reducer or high range water reducer (if any) for desired slump = 5 to 7 in.

Use AEA from same admix manufacturer

Standard moist room curing starts immediately after making the specimens

For all mixtures measure the following:

1. Slump, temperature, air content, density
2. Strength at 28 and 56 d – 4 4x8
3. 56 day RCPT – 1 4x8 – 2 tests on the same cut face
4. 56 day Sorptivity (C1585) – 1 4x8 – 2 tests on the same cut face that is exposed to water extend test to 1 year (decide at 6 months), after Day 9 take readings every 28 days
5. Air void – 1 4x8 (hold)

Calculate M_{100} on 2 3x6 as follows:

After 28 day moist cure get SSD weight and then oven dry at 105C for 48 h. Weight it after it cools down and then back in oven for 24 h again weigh. Keep doing that till mass change is

less than 0.1% or 2 g whichever is higher (2 g will be higher). Then vacuum saturate (VS) the 2 specimens per C1202. Measure SSD weight after 18 h water immersion period. Again subject specimen to VS and weigh again. Keep doing this till – mass change is less than 2 g. The final weight is M_{100} . After this dry specimens in 70F, 50% RH room and measure time of drying to get to 86% and 92% DOS levels.

Do Freeze thaw (ASTM C666) with following modifications:

3x6 cylinders – 2/DOS/mix – 2x4=8/mix. Make 4 3x6 extra per mix

After 28 day moist curing remove 6 3x6 cylinders from moist room (call them 100-1, 100-2, 92-1, 92-2, 86-1, 86-2). Get SSD weight.

Then dry them in 140F room for 7 days. Weigh it.

Then VS per C1202. Measure SSD weight after 18 h water immersion period. Again subject specimen to VS and weigh again. Keep doing this till – mass change is less than 2 g.

After the final VS remove 4 of the 6 cylinders (the 86's, and 92's - leave the 100's submerged in water). The 4 cylinders should be dried to reach 86% and 92% as follows:

86% and 92% DOS is reached by monitoring mass change of specimens in the 70F and 50% RH room. The earlier measurements on oven dry specimens should give an estimate of the time needed to reach the 86% and 92% DOS levels.

As soon as the 92's reach 92% DOS seal them in a plastic sheet. At the same time remove the 100's (2 cylinders) that are still submerged in water. Measure the SSD weight. These are the ~100%DOS specimens (based on past experience this should be >95% DOS). Seal the 100's also in a plastic sheet.

Remove 2 -3x6 cylinders from the moist room (call them M_c -1, M_c -2). Measure the SSD weight. This is the DOS right after moist cure (M_c). Typically M_c is about 75 to 82% of M_{100} . Seal the M_c 's also in a plastic sheet.

As soon as the 86's reach 86% DOS seal those also in a plastic sheet.

As soon as each of the 8 specimens are sealed in a plastic sheet they should also be put inside a heat shrinkage wrap.

After this all 8 specimens are to be kept for a minimum of 3 days to allow moisture to redistribute before commencing freezing and thawing testing. This is similar to the paper by Li et al. Measure mass after 3 days and record new DOS (if the seal is good there should be no mass loss and DOS should be same).

Place two 3x6 belonging to the same RH in 1 FT container. That way you can accommodate all 16 cases at the same time.

Remove specimens at 25, 50, 75, 100 and then every 50 cycles up to 600 cycles (decide to 300 cycles) – remove them from the bags and measure DF and mass loss; take pics if interesting features are observed such as deterioration scaling, cracking etc.

Try to avoid repeated opening, closing – so make all 4 mixes on same day or 2 on 1 day and other 2 after 4 days (i.e. when the 25 cycles comes up) – this way you take all measurements each time.

Sulfate Resistance - Test Methods, Curing Conditions and Test Ages

Sulfate attack is another major concrete deterioration mechanism. Water soluble sulfates penetrate concrete by a combination of capillary sorption and diffusion. Three mechanisms are recognized:

- 1 Physical sulfate attack – generally by salt crystallization of certain sulfate salts
- 2 Chemical attack of aluminate phases in to form calcium sulfo-aluminate hydrates and gypsum.
- 3. Chemical attack on the calcium silicate hydrate matrix at cooler temperatures (thaumasite formation)

Note: The thaumasite sulfate attack mechanism is less common and is not addressed in this test program.

Concrete resistance to sulfate attack is governed by 2 factors:

- 1. Cementitious type – Increasing C3A in portland cement portion in concrete decreases its sulfate resistance. Aluminate phases from SCMs can also sometimes contribute to this effect – more likely in some Class C fly ashes or some higher alumina content slags from off shore.
- 2. Low permeability – that reduces the rate of penetration of sulfates into the concrete. The ACI 318 building Code recognizes 3 exposure classes of sulfate exposure in increasing severity based on concentration of water soluble sulfates in soil or water – S1, S2, and S3 and establishes the following (Table A) minimum requirements for concrete mixtures for adequate sulfate resistance:

Table A. ACI 318 Building code Requirements for Concrete Exposed to Sulfate

Category	CM type or Performance Equivalent	w/cm, strength
S0	None	None

S1	Type II or ASTM C1012 <0.1% at 6 mos	0.50, 4000 psi
S2	Type V or ASTM C1012 <0.1% at 12 mos	0.45, 4500 psi
S3	Type V+pozz or slag or ASTM C1012 < 0.1% at 18 mos	0.45, 4500 psi

In ACI 318-08, ASTM C1012 expansion criteria are recognized as an alternative to the prescriptive requirements for the allowable types of cementitious materials.

The maximum w/cm limit is invoked to control the permeability of concrete. Besides w/cm, however, the permeability of concrete is also impacted by the composition of the cementitious materials. The aim of this task to develop rapid index test and performance criteria as an alternative to the maximum w/cm requirements. It is clear that a low w/cm is required to ensure low sulfate ingress by sorption and diffusion. Low permeability of concrete is an important factor to control both the physical and chemical forms of sulfate attack.

By testing concrete mixtures with different w/cm and cementitious types (including SCM types and contents) we will examine if concrete performance against sulfate attack (as measured by USBR 4908 method B) is better correlated with ASTM C1012 and a rapid index test alternative to w/cm criteria. Rapid index tests that will be evaluated include rapid chloride permeability (and conductivity), sorption or gas permeability.

USBR4908 is a test that was used by the US Bureau of Reclamation on historical research on sulfate resistance. It is a long term test on concrete and is not suited for inclusion in code or specification criteria. The evaluation of rapid index test results relative to performance in the USBR4908 will allow establishment of such required performance criteria. The test involves immersing 3x6 in. cylindrical concrete specimens in 10% sodium sulfate solutions for an extended period and measuring expansions periodically. An expansion of 0.5% is considered as failure and the test is expected to last at least 12-18 mos.

It is proposed that all concrete mixtures be subjected to an immersion period of 18 mos with the expansions recorded. Mixtures that show higher resistance to sulfate attack will result in lower expansions in the USBR test. By separating out mixtures into 3 categories based on their USBR expansion levels it will be possible to select mixtures that will perform in the different sulfate exposure classes S1, S2, and S3 – mixtures with the lowest USBR expansion levels could be used for S3 exposure category and so on.

Additionally, partially submerged specimens in test solutions will be performed at the same sulfate concentration. This is intended to simulate sorption and wicking of sulfates in structures and the condition of physical sulfate attack.

The results will be interpreted as follows:

It is expected that two mixtures with different composition of cementitious materials could have the same performance in the USBR test due to different levels of sulfate ingress (permeability) into the concrete. It is proposed to tie the rapid index test criteria that measures a permeability property to the C1012 expansion levels (see Table B).

The process of developing these rapid index criteria is proposed to be accomplished by the following 3 plots.

Plot 1 will have 12 mo or 18 mo USBR expansions on the Y axis and rapid index test results on X axis. Plot only those mixtures (from the 20+ mixtures tested as per Table C) that satisfy the ASTM C1012 expansion criteria for the S1 exposure class but that fail that for exposure classes S2, and S3. Three different USBR expansion levels as suggested in column 2 of Table b will be used to delineate expansions in the USBR test on concrete specimens for the 3 exposure classes (these may need to be revised later based on the test results). Record the corresponding rapid index test criteria.

Plot 2 should have mixtures that satisfy the ASTM C1012 expansion criteria for the S2 exposure class but that fail that for exposure class S3. The same three expansion criteria for the USBR expansions will be used. Record the corresponding rapid index test criteria.

Plot 3 should have mixtures that satisfy the ASTM C1012 expansion criteria for S3 exposure class. The same three expansion criteria for the USBR expansions will be used. Record the corresponding rapid index test criteria.

The final outcome is expected to be along the following lines

This allows the two criteria to offset each other and can be established based on the USBR concrete performance testing – a more conservative result in the C1012 might permit a less conservative criteria in the rapid index for permeability and vice versa.

Table B. Interpretation of USBR expansion Results and Development of Rapid Index test Criteria

Category	USBR expansion	C1012	Rapid index (assume RCPT coulombs)
S1	0.4 to 0.6%	<0.1% at 6 mos	3000
		<0.1% at 12 mos	4000
		<0.1% at 18 mos	4000
S2	0.2 to 0.4%	<0.1% at 6 mos	2000

		<0.1% at 12 mos	3000
		<0.1% at 18 mos	4000
S3	<0.2%	<0.1% at 6 mos	NA
		<0.1% at 12 mos	1500
		<0.1% at 18 mos	2000

Table C. Mixture Proportions Planned

Category	w/cm	Cement	No SCM	15%FA	20%FA	30%FA	25%SL	35%SL	50%SL
S0	0.50	Type I	1-cement						
S1	0.50	Type II	1-cement						
	0.40	Type I		Yes			Yes		
	0.50	Type I		Yes			Yes		
	0.60	Type I		Yes			Yes		
S2	0.45	Type V	2-cements						
	0.40	Type II			Yes			Yes	
	0.50	Type II			Yes			Yes	
	0.60	Type II			Yes			Yes	
S3	0.40	Type V				Yes			Yes
	0.50	Type V				Yes			Yes
	0.60	Type V				Yes			Yes

For S1, 0.50, test 1 Type II control mix

For S2, 0.45, test 2 Type V control mixes

So there are a total of 22 mixtures – 18 with SCMs and 4 without. Some of these mixtures may be optimized if possible without losing research objective.

The mixtures that have been struck off have been cast as of now and are shown in Table 4.

Crushed coarse aggregate (1.0" max) no. 57, natural sand FM=2.88

FA will be Class F fly ash.

Adjust water reducer or high range water reducer (if any) for desired slump = 5 to 7 in.

Non air entrained concrete.

Need a Type I with relatively high C3A so its not too similar to the Type II

Planned Test Methods, Curing Conditions and Test Ages (Lab)

Mortar

ASTM C1012. Conduct C1012 tests. C1012 is normally done on mortar at a constant w/cm = 0.485. Therefore there will be a total of 10 mixtures - 6 SCM mixtures (2 with Type I, 2 with Type II, 2 with Type V) and 4 PC only mixtures. Consider 2 for replication at high and low expansion level. Conduct C1012 for 18 mos – some of mixtures with lower SCMs may be stopped earlier. Take periodic expansion readings as per C1012.

Concrete

Normal Curing – Standard moist room curing starts immediately after making the specimens

Accelerated Curing – 7 days of normal curing followed by 21 days of curing in 100F water

For all concrete mixtures measure the following: Slump, temperature, air content, density, Strength (4x8 cyl at 28 days of moist curing).

Durability Tests

For all tests at all ages, make 2 cylinders unless otherwise stated. Make 6 extra cylinders for each mix, moist cure for 28 days and then ship 4 to Purdue/UT for gas permeability testing and keep the other 2.

- Rapid Chloride Permeability test (ASTM C1202)
 - i) 28 day accelerated
 - ii) 56 day normal curing
 - iii) 52 week normal curing

- USBR4908 fully immersed method B. Test 3 prisms per mix. Start after 28 days of moist curing and 28 days of air drying (everything else similar to USBR 4908 requirements). Conduct test for 36 mos or as instructed. Take periodic expansion readings. Follow USBR test method for other requirements.
- USBR4908 partially immersed (same 10% solution as above). Test 3 prisms per mix. Start after 28 days of moist curing and 28 days of air drying (everything else similar to USBR 4908 requirements). Conduct test for 36 mos or as instructed. Take periodic expansion readings. The specimens are immersed half way following the procedure in the NIST report. Figure 14 shows the test set up. The partially immersed specimens were made for the high and low w/cm and PC only mixes. Mass change will also be measured to determine if there is surface spalling at the wet zone.
- Sorptivity Test (ASTM C1585) after :
 - i) 28 day accelerated + 18 d specimen conditioning (C1585)
 - ii) 56 day normal curing + 18 d specimen conditioning (C1585)
 - iii) 52 week normal curing + 18 d specimen conditioning (C1585)
- Absorption test BS 1881:122 – use latest ASTM draft
 - i) 28 day accelerated + 3 d in oven
 - ii) 56 day normal curing + 3 d in oven
 - iii) 52 week normal curing + 3 d in oven



Figure 14 USBR half immersed specimens in the container

If at each w/cm, sulfate performance varies depending on the test criteria the importance of the test criteria as opposed to w/cm is established. Also it would be determined whether some mixes with low w/cm and higher sorptivity/gas perm can have poorer sulfate performance as compared to mixes with higher w/cm and lower sorptivity/gas perm which can again establish the importance of the test criteria as opposed to w/cm.

This task does not consider the development of a more rapid test for C1012. Options include smaller specimen size/paste or higher temperature soln. exposure.

Some of the initial concrete mixtures are being cast at the moment.

Table 4 and Table 5 shows the results from all 22 concrete mixtures cast. At the moment all the rapid index test results are available. For the USBR fully immersed and partially immersed conditions 9 to 12 mo test data is available at this point and 12 mo data for all mixtures should become available by January 2012. For the fully immersed case the following are being measured – 1. Length change; 2. Mass change; 3. Visual rating/pictures. For the partially immersed case the following are being measured – 1. Scaling length; 2. Mass change; 3. Visual rating/pictures. Ambient RH will continue to be measured at 2 locations – one at 1 in. above the solution and the other near the top of the specimen. The 12 mo USBR data in Table 4 and 9 mo data in Table 5 is available and is discussed below.

For the fully immersed case the length change vs age is plotted in Figure 15. There is expansion with increasing age with the higher w/cm mixtures having higher expansions both in the case of slag and fly ash mixtures. The expansion levels are still very low. For the 0.5 w/cm PC mixtures the mixture with the lower C_3A (0.5PC-II) content had a lower expansion level as expected. The mass change vs age is plotted in Figure 16. Thus far there has been a mass increase as a result of absorption. The higher w/cm mixtures have had higher mass increases as a result of their absorption. Both the 0.6 w/cm slag and fly ash mixtures have shown a sharp mass decrease at a later age. This is primarily due to the corners of the prisms breaking off. Pictures taken at 12 mos for all the fully immersed specimens shown in Figure 17 confirm this. Figure 20, 21, and 22 show that length change, mass loss and visual pictures of all of the Table 5 mixtures at age of 9 months has not shown any deterioration.

For the partially immersed case mass loss has not been found to give good results thus far and is not reported. However scaling length has been measured. This is the length of scaling from the surface of the solution upwards. Scaling occurs because the sulfate solution is absorbed by the concrete migrates upwards evaporates from the top surface leaving behind salt crystals

which can expand when they absorb moisture causing scaling and cracking. This is described as physical sulfate attack and does not require the chemical sulfate attack reaction. The measured scaling lengths are plotted for the different mixtures in Figure 18, and 23. Once again the low w/cm (0.40) mixtures had lower scaling lengths when compared to the higher w/cm mixtures (0.60) for both the fly ash and slag cement cases. The other interesting finding from Figure 18 is that the two 0.50 PC mixtures had the similar scaling lengths even though the C₃A contents were quite different (8% vs 12%). This confirms that the failure is not due to chemical sulfate attack. Figure 19, and 24 shows the scaling details for the partially immersed specimens. For the portion of the specimens that has been immersed in the sulfate solutions Figure 19 shows that the two 0.60 w/cm mixtures and the PC mixture with the higher C₃A showed more significant mass loss.

Correlations between the rapid index test results and USBR expansion results would prove interesting. However such an exercise can be done only after at least 24 mo of USBR testing. For the fully immersed case length change might be the most promising way of classifying the mixtures. For the partially immersed case scaling length might be the most promising way of classifying the mixtures. At the end of the 18 months the following destructive testing can be conducted – 1. At least 2 cubes/specimen (3 in.) will be sawn off and tested for compressive strength for the immersed case; For the partially immersed case at least 1 cube will be sawn off and tested from the immersed part. Higher strength loss will be indicative of poorer sulfate resistance. 2. Sulfate ingress can be measured for both cases. Also to accelerate the deterioration process of the partially immersed case weekly cycling has been started between the 73F and 100F rooms starting this Fall.

Table 6 shows the ASTM C1012 mortar test results for the 10 mixtures that have been cast. 9 month C1012 expansions and the originally expected sulfate exposure classes are also listed.

Table 4. Yield Adjusted Mixture Proportions and Preliminary Test Results

Calculated Batch Quantities	1	2	3	4	5	6	7	8
	0.4SL25-I	0.5SL25-I	0.6SL25-I	0.5PC-I	0.4FA15-I	0.5FA15-I	0.6FA15-I	0.5PC-II
Cement Type	I	I	I	I	I	I	I	I/II
Type I/II cement, lb/yd ³	457	419	378	559	519	476	413	557
Slag, lb/yd ³	152	140	126					
Flyash, lb/yd ³					92	84	73	
SCM, %	25	25	25	0	15	15	15	0

Coarse Agg. (No.57), lb/yd ³	2060	2055	2079	2056	2062	2061	2068	2050
Fine Aggregate, lb/yd ³	1302	1247	1260	1256	1277	1277	1272	1253
Mixing Water, lb/yd ³	244	279	283	279	244	280	291	279
w/cm	0.40	0.50	0.56	0.50	0.40	0.50	0.60	0.50
ASTM C494 Type A, oz/cwt	3	3	3	3	3	3	3	3
ASTM C494 Type F, oz/cwt	9.15	5.64	0	3	10.29	3.3	2	2.41
Fresh Concrete Properties								
ASTM C143, Slump, in.	5.50	6.50	6.50	7.00	4.00	4.00	7.00	5.25
ASTM C231, Air, %	1.6	1.7	1.2	1.4	1.6	1.4	1.2	2.0
ASTM C138, Density, lb/ft ³	156.9	154.1	153.7	154.5	156.1	153.7	153.3	154.1
ASTM C1064, Temperature, °F	72	72	72	73	72	72	72	72
Hardened Concrete Properties								
ASTM C39, Compressive Strength, psi								
28 days	9,540	7,700	5,710	5,690	8,400	5,980	4,630	6,440
Draft ASTM Standard, Water Absorption Test at 50 °C, %								
28d accelerated cure	0.62	0.79	1.34	1.33	0.61	0.88	1.13	1.31
56d normal cure	0.63	0.75	1.17	1.04	0.61	0.83	1.01	1.23
52w normal cure	0.55	0.65	0.87	0.72	0.38	0.64	0.86	0.73
ASTM C1202, Rapid Chloride Permeability, Coulombs								
28d accelerated cure	728	1104	1842	3132	509	968	1849	3459
56d normal cure	704	1161	1947	2947	913	1593	2627	3610
52w normal cure	649	1004	1253	2365	353	526	963	3132
ASTM C 1585, Rate of Water Absorption (Sorptivity), x10⁻⁴ mm/s^{1/2}								
28d accelerated cure (Initial/Secondary)	2 [*] /1.1 [*]	2.8 [*] /1.7 [*]	4.2 [*] /2.2 [*]	6.3 [*] /4.8	1.8 [*] /1.3 [*]	2.5 [*] /1.9 [*]	5.2 [*] /3.1 [*]	7.2/3.8 [*]
56d normal cure (Initial/Secondary)	3.1 [*] /2	5/2.6 [*]	8.1/3 [*]	5.8 [*] /3.3 [*]	4 [*] /2.4 [*]	5.7/2.6 [*]	7.4/4.2 [*]	6.2/4.3
52w normal cure (Initial/Secondary)	4.6 [*] /1.4	4.9 [*] /1.6 [*]	7.7 [*] /2.5	6.8 [*] /3.8	**	7.2 [*] /1.9 [*]	9.9 [*] /2.8 [*]	4 [*] /4.8
USBR 4908 Fully Immersed Method B (10% solution), %								
Length Change @ 12 months	0.032	0.041	0.040	0.096	0.028	0.038	0.043	0.044

Length Change @ 18 months	On-going	On-going	On-going	On-going	On-going	On-going	On-going	On-going
Mass Change @ 12 months	0.60	1.03	0.74 ⁺	1.38	0.81	1.28	1.33 ⁺	1.64
Mass Change @ 18 months	On-going	On-going	On-going	On-going	On-going	On-going	On-going	On-going
USBR 4908 Partially Immersed (10% solution), inch								
Scaling Distance @ 12 months	0.00	-	1.38	1.29	0.54	-	1.71	1.33
Scaling Distance @ 18 months	On-going	-	On-going	On-going	On-going	-	On-going	On-going

* A correlation coefficient less than 0.98 indicating that the rate cannot be determined according to ASTM C1585

⁺ Both ends' corners of the specimen crumbled and fell off resulted in mass reduction instead of mass gain due to physical sulfate attack

** No correlations were found, so data is unavailable

Note. Type I cement had C₃A content of 12% whereas Type I/II cement had C₃A content of 8%.

Table 5. Yield Adjusted Mixture Proportions and Preliminary Test Results

Calculated Batch Quantities	9	10	11	12	13	14	15	16	17	18	19	20	21	22
	0.4FA20-II	0.5FA20-II	0.6FA20-II	0.4SL35-II	0.5SL35-II	0.6SL35-II	0.4FA30-V1	0.5FA30-V1	0.6FA30-V1	0.4SL50-V1	0.5SL50-V1	0.6SL50-V1	0.45PC-V1	0.45PC-V2
Cement Type	I/II	I/II	I/II	I/II	I/II	I/II	V-1	V-1	V-1	V-1	V-1	V-1	V-1	V-2
Type I/II cement, lb/yd ³	487	448	387	391	361	316								
Type V cement, lb/yd ³							429	392	343	300	281	245	577	581
Slag, lb/yd ³				210	195	170				300	281	245		
Flyash, lb/yd ³	122	112	97				184	168	147					
SCM, %	20	20	20	35	35	35	30	30	30	50	50	50	0	0
Coarse Agg. (No.57), lb/yd ³	2057	2061	2062	2030	2046	2073	2069	2062	2088	2028	2070	2086	2049	2065
Fine Aggregate, lb/yd ³	1262	1216	1259	1279	1238	1267	1245	1194	1256	1271	1247	1270	1286	1296
Mixing Water, lb/yd ³	244	280	290	240	278	302	245	280	294	240	281	304	260	262
w/cm	0.40	0.50	0.60	0.40	0.50	0.62	0.40	0.50	0.60	0.40	0.50	0.62	0.45	0.45
ASTM C494 Type A, oz/cwt	3	3	3	3	3	3	3	3	3	3	3	3	3	3
ASTM C494 Type F, oz/cwt	4.67	1.8	0	5.84	2.16	0	4.58	0	0	1.17	0.72	0	2.5	2.5
Fresh Concrete Properties														
ASTM C143, Slump, in.	4.5	6.75	5	7	5	4.5	4.75	6.75	7	7	5.5	6	4.5	6.5

ASTMC231, Air, %	1.6	1.8	1.7	3.2	2.1	1.7	2	1.5	1	1.7	1.8	1.3	1.9	1.6
ASTMC138, Density, lb/ft ³	155.3	153.3	152.5	154.5	153.3	153.7	155.3	152.5	153.7	154.1	154.9	154.5	155.3	156.5
ASTMC1064, Temperature, °F	74	75	75	72	72	72	70	70	70	71	70	70	72	74
Hardened Concrete Properties														
ASTM C39, Compressive Strength, psi														
28 days	7,490	5,310	3,990	10,020	6,740	5,730	7,610	4,870	3,590	7,500	7,500	6,200	8,800	7,720
Draft ASTM Standard, Water Absorption Test at 50 °C, %														
28d accelerated cure	0.96	1.45	1.81	0.69	1.02	1.14	0.91	1.46	1.98	1.08	1.09	1.30	1.12	1.30
56d normal cure	0.92	1.38	1.65	0.78	1.08	1.29	0.93	1.47	1.86	1.07	1.12	1.52	1.14	0.96
364d normal cure	0.59	0.93	1.18	0.60	0.84	0.97	0.65	0.99	1.29	0.94	1.09	1.32	0.75	1.14
ASTM C1202, Rapid Chloride Permeability, Coulombs														
28d accelerated cure	1147	1776	3081	576	789	1143	592	1434	2618	470	487	586	2845	3437
56d normal cure	1848	2662	3856	705	943	1790	1543	3731	4772	593	887	1077	3456	3905
364d normal cure	354	660	1080	441	621	889	362	554	759	393	447	535	2861	3184
ASTM C 1585, Rate of Water Absorption (Sorptivity), x10⁻⁴ mm/s^{1/2}														
28d accelerated cure (Initial/Secondary)	1.8 [*] /1.6	2.1 [*] /2.9	3.8 [*] /4	**	4.2 [*] /2.3	5 [*] /2.4 [*]	3.2 [*] /1.3 [*]	7.8 [*] /2.5	15.2 [*] /4.4 [*]	**	5.3 [*] /1.5 [*]	6.2 [*] /1.6 [*]	5.4 [*] /2	8.6 [*] /3.3 [*]
56d normal cure (Initial/Secondary)	6/2.8 [*]	8.3 [*] /4.1	22/11.1 [*]	5.4 [*] /1.7 [*]	7.1 [*] /2.2 [*]	12.9/2.2 [*]	6.4/2.6 [*]	6.7 [*] /1.7 [*]	9.4/4	**	4.3/1.4 [*]	6.9/1.8 [*]	6.5 [*] /2.9	10.3/4.9
364d normal cure (Initial/Secondary)	3.4/1.7	3.4 [*] /2	6 [*] /4.4 [*]	2.3 [*] /0.8 [*]	6.4/2	**	1.2 [*] /1.1 [*]	**	5.8 [*] /1.5 [*]	**	2.4 [*] /1 [*]	3.8 [*] /1.1 [*]	2.1 [*] /-	3.7 [*] /**
USBR 4908 Fully Immersed Method B, %														

Length Change @ 9 months	0.028	0.031	0.035	0.026	0.028	0.042	0.033	0.032	0.035	0.028	0.028	0.031	0.033	0.027
Length Change @ 18 months	On-going													
Mass Change @ 9 months	1.16	1.75	2.41	0.66	1.07	1.46	1.19	2.30	2.95	0.98	1.20	1.56	1.19	1.19
Mass Change @ 18 months	On-going													
USBR 4908 Partially Immersed														
Scaling Distance @ 9 months	1.19	-	1.81	0.38	-	1.81	0.81	-	1.69	1.56	-	1.88	0.38	0.56
Scaling Distance @ 18 months	On-going	-	On-going	On-going	On-going									

* A correlation coefficient less than 0.98 indicating that the rate cannot be determined according to ASTM C158

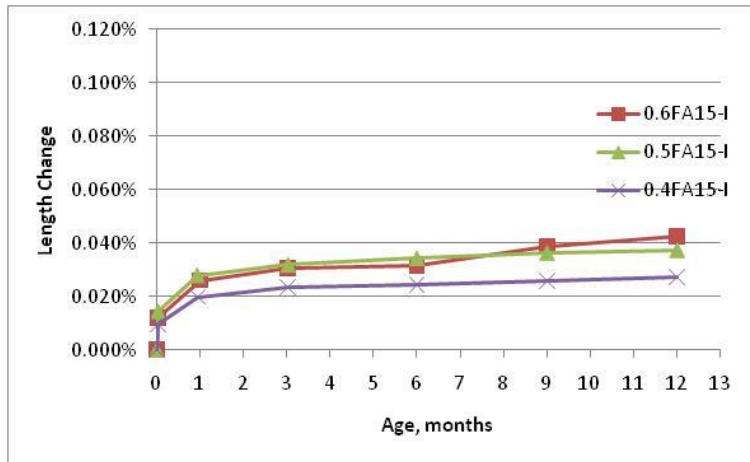
** No correlations were found, so data is unavailable

Note. Type I/II, V-1, and V-2 cements had C₃A content of 8%, 3%, and 5%, respectively.

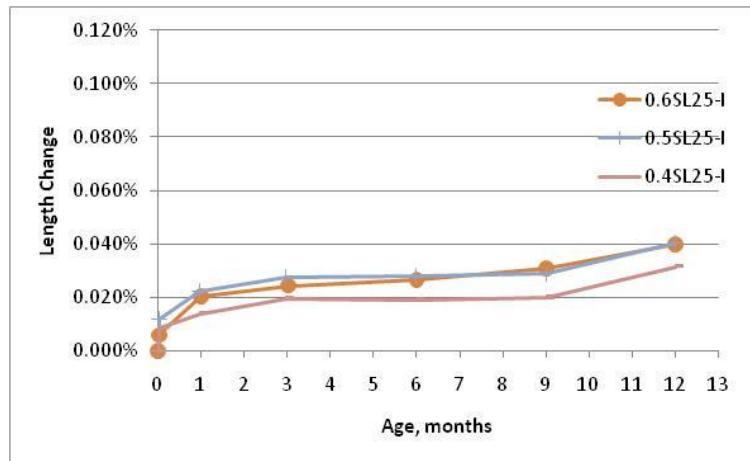
Table 6. ASTM C1012 Mortar Mixture Proportions and Preliminary Test Results

Mix No.	1	2	3	4	5	6	7	8	9	10
Cement Type	I	I/II	V-1	V-2	I	I/II	V-1	I	I/II	V-1
C ₃ A (Cement mill cert.), %	12	8	3	5	12	8	3	12	8	3
Slag, %					25	35	50			
Flyash, %								15	20	30
Batch Quantities										
Cement, g	500	500	500	500	375	325	250	425	400	350
Slag cement, g					125	175	250			
Flyash, g								75	100	150
Graded Standard Sand, g	1375	1375	1375	1375	1375	1375	1375	1375	1375	1375
Water, g	243	243	243	243	243	243	243	243	243	243
w/cm	0.49	0.49	0.49	0.49	0.49	0.49	0.49	0.49	0.49	0.49
Fresh Mortar Properties										
ASTM C1064, Temperature, °F	74	75	75	75	75	75	72	77	74	73
ASTM C1437, Flow, %	92	111	122	116	108	108	118	89	107	121
ASTM C109, At Immersion into Sulfate Solution										
Age, days	1.9	1.8	1.3	1.9	1.8	2.0	5.8	6.8	3.8	6.0
Compressive strength, psi	2,850	3,381	2,925	3,169	2,894	2,931	4,019	2,850	2,850	2,856
ASTM C1012, Sulfate Expansions										
9 month, %	1.073	0.100	0.032	0.040	0.039	0.040	0.023	0.052	0.040	0.022
12 month, %	ongoing									
18 month, %	ongoing									
Coeff. Var. - 9 month, %	47	6	16	7	2	13	12	44	13	21
Coeff. Var. - 12 month, %	ongoing									
Coeff. Var. - 18 month, %	ongoing									
Expected sulfate class	S0	S1	S2	S2	S1	S2	S3	S1	S2	S3

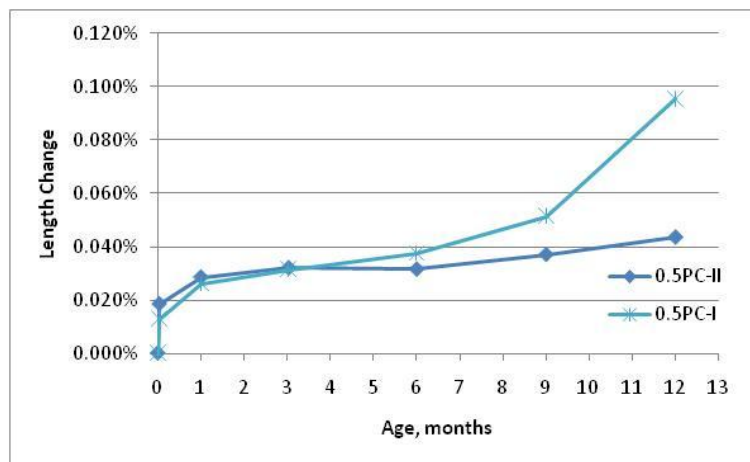
Note. Type I cement had C₃A content of 12% whereas Type I/II cement had C₃A content of 8%.



(a)



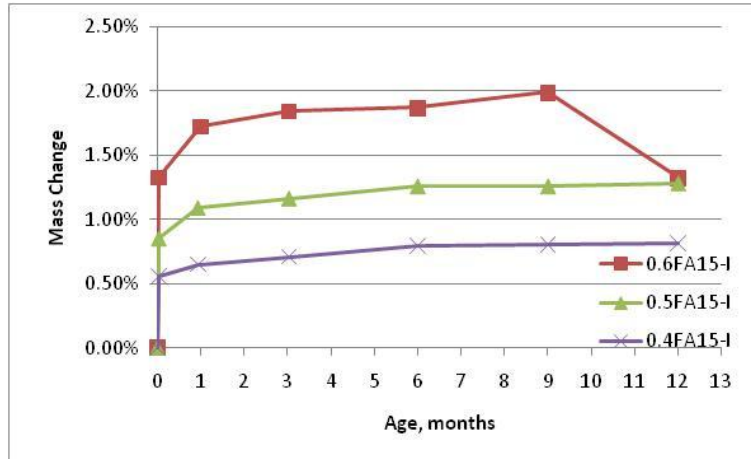
(b)



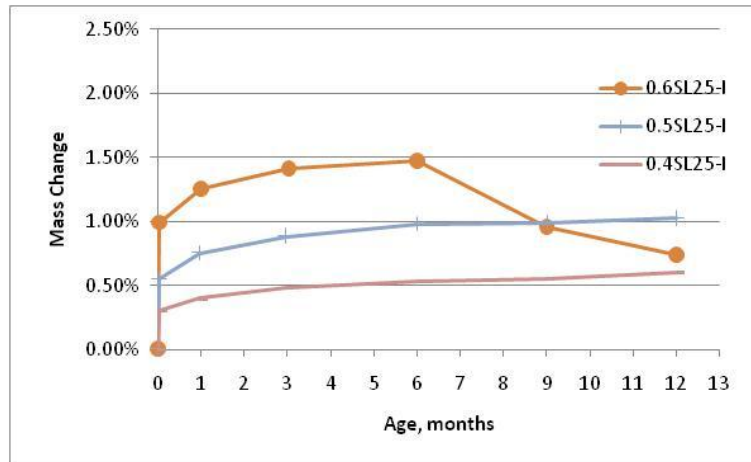
(c)

Figure 15 USBR Fully Immersed Condition Length Change (Mixtures 1-8)

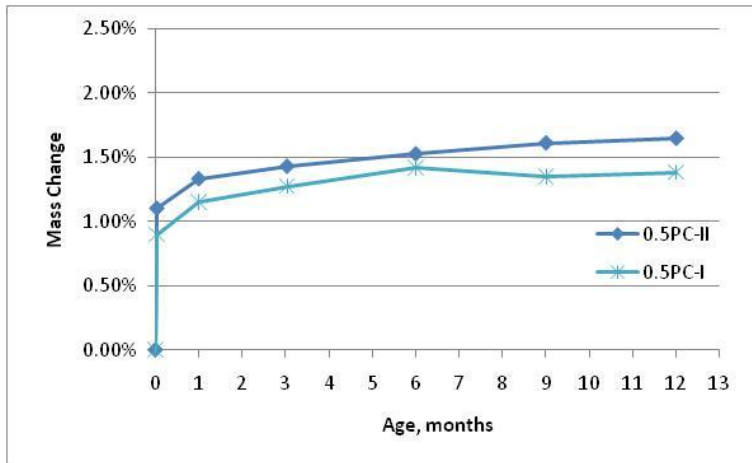
(a) 15% fly ash mixtures at various w/cm ratios, (b) 25% slag cement mixtures at various w/cm ratios, and (c) portland cement mixtures (I C₃A=12%, II C₃A=8%)



(a)



(b)



(c)

Figure 16 USBR Fully Immersed Condition Mass Change (Mixtures 1-8)

(a) 15% fly ash mixtures at various w/cm ratios, (b) 25% slag cement mixtures at various w/cm ratios, and (c) portland cement mixtures (I C₃A=12%, II C₃A=8%)



(a)



(b)



(c)

Figure 17 USBR Fully Immersed Sample Pictures after 12 months

(a) 15% fly ash mixtures at various w/cm ratios, (b) 25% slag cement mixtures at various w/cm ratios, and (c) portland cement mixtures

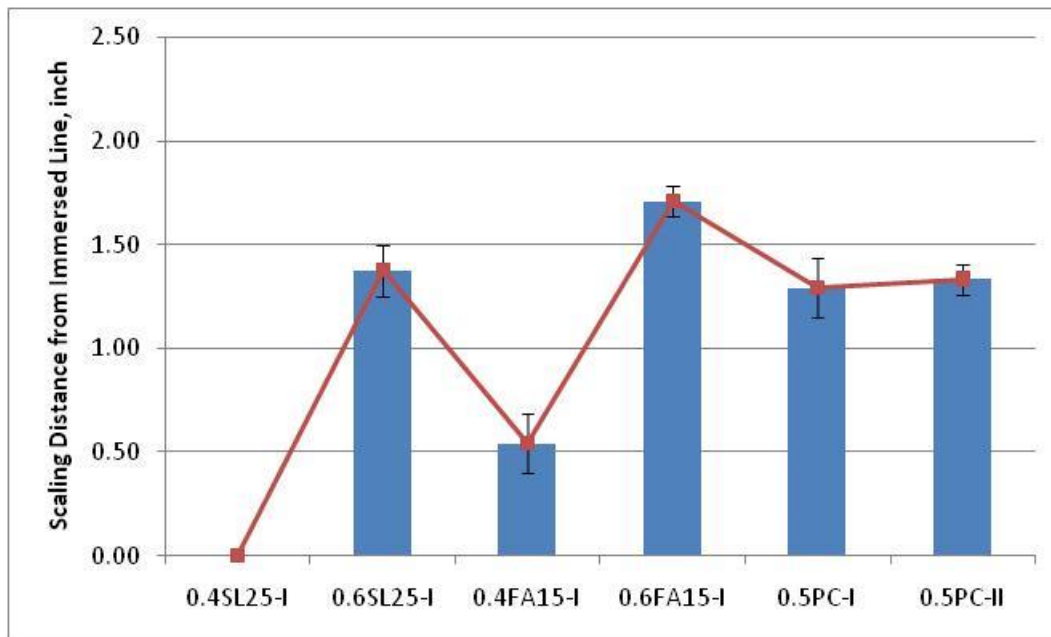
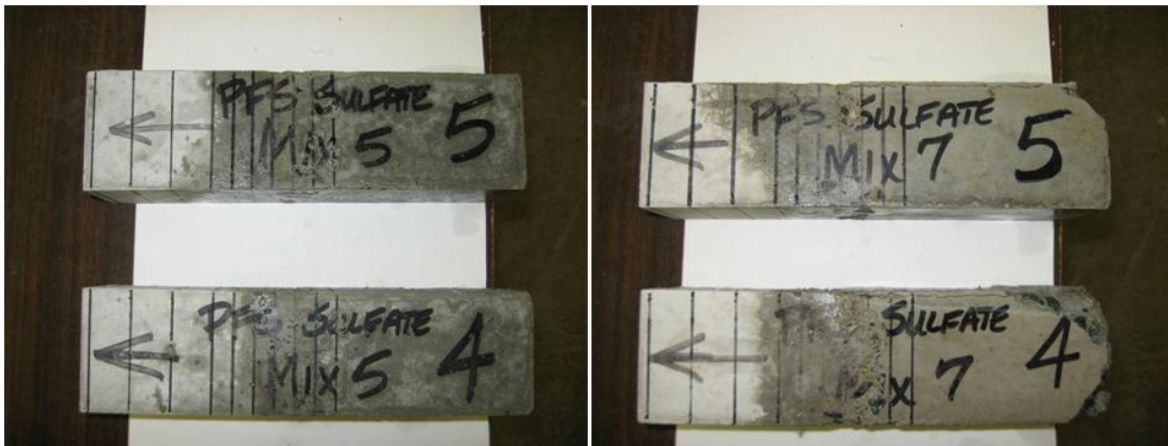


Figure 18 USBR Half Immersed Condition Scaling Distance from Immersion Line after 12 months

Error Bars indicates ± 1 standard deviation for the testing of three specimens



(a)



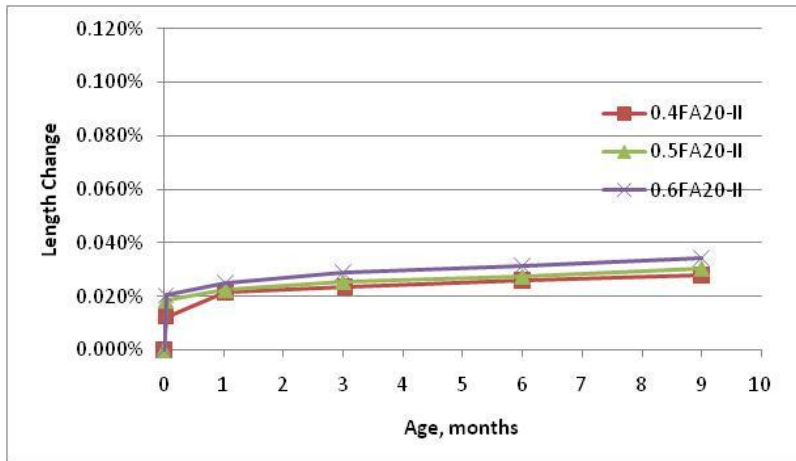
(b)



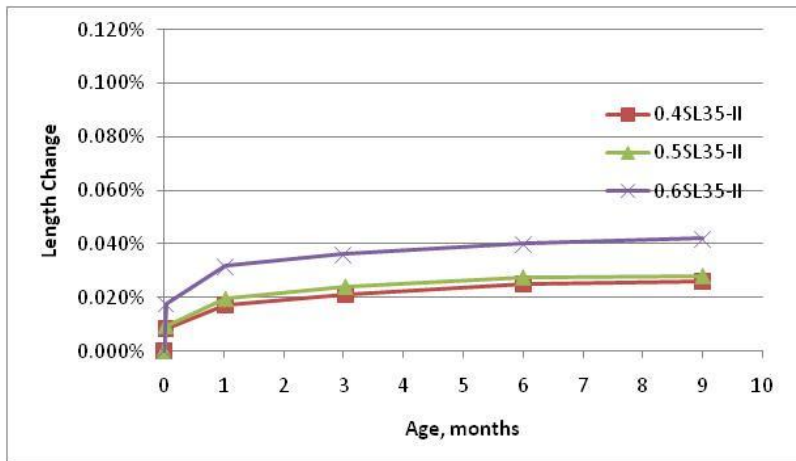
(c)

Figure 19 USBR Half Immersed Sample Pictures after 12 months

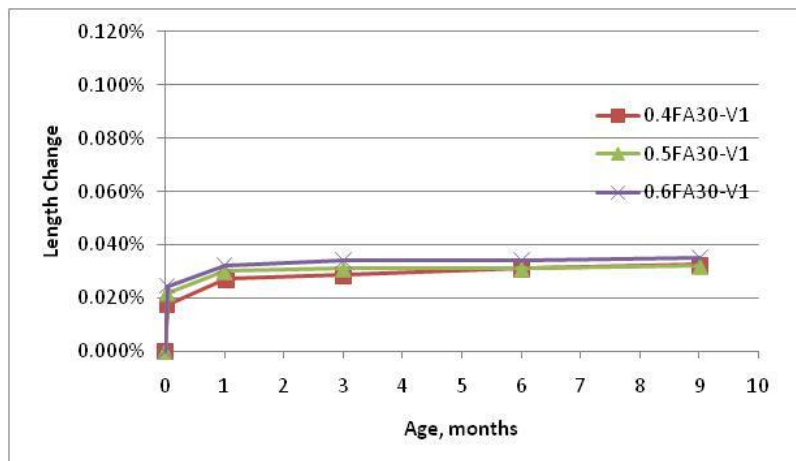
(a) 25% slag cement mixtures, (b) 15% fly ash mixtures, and (c) portland cement mixtures



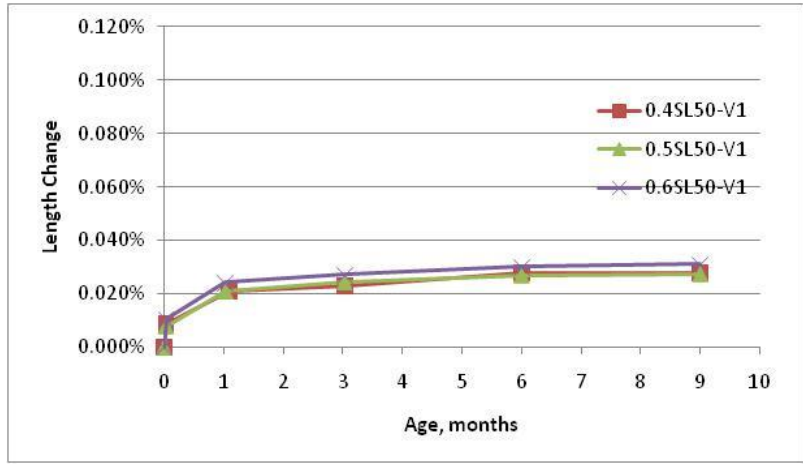
(a)



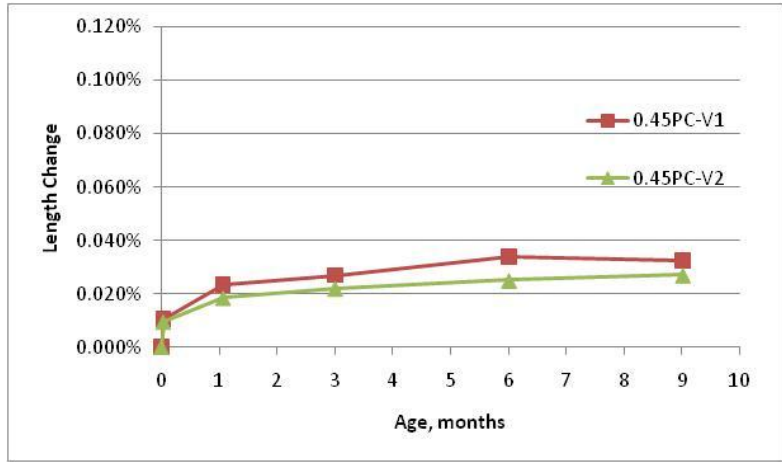
(b)



(c)



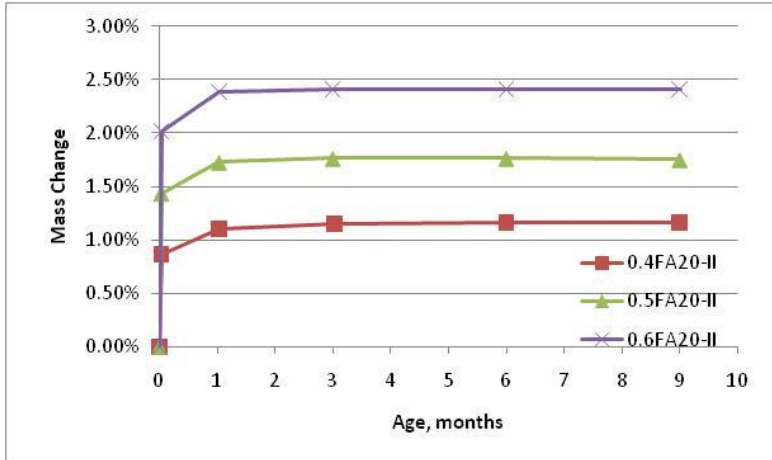
(d)



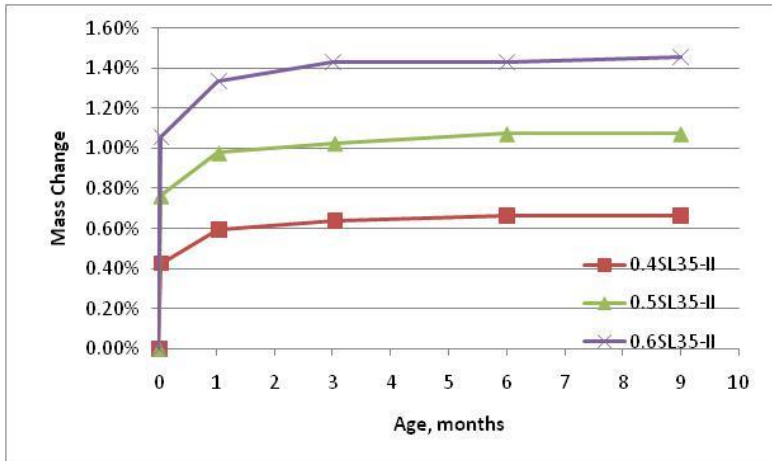
(e)

Figure 20 USBR Fully Immersed Condition Length Change (Mixtures 9-22)

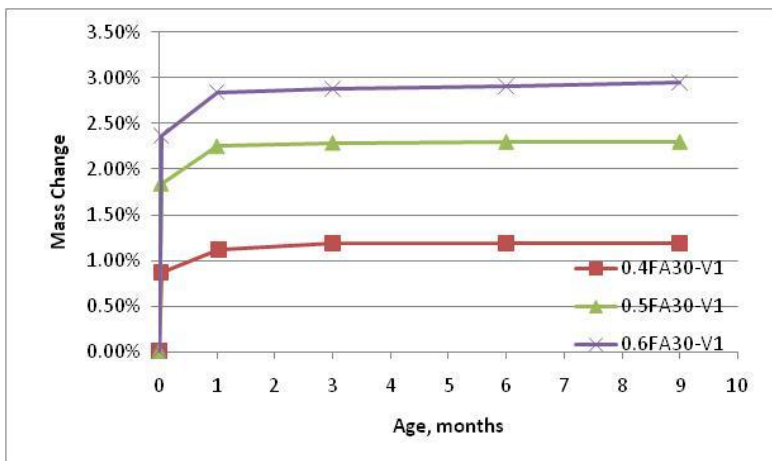
(a) 20% fly ash mixtures at various w/cm ratios, (b) 35% slag cement mixtures at various w/cm ratios, (c) 30% fly ash mixtures at various w/cm ratios, (d) 50% slag cement mixtures at various w/cm ratios, and (e) portland cement mixtures (V1 C₃A=3%, PC-V2 C₃A=5%)



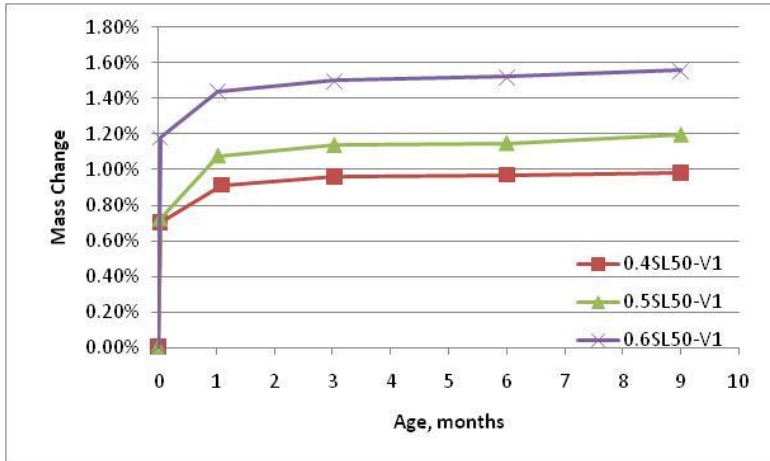
(a)



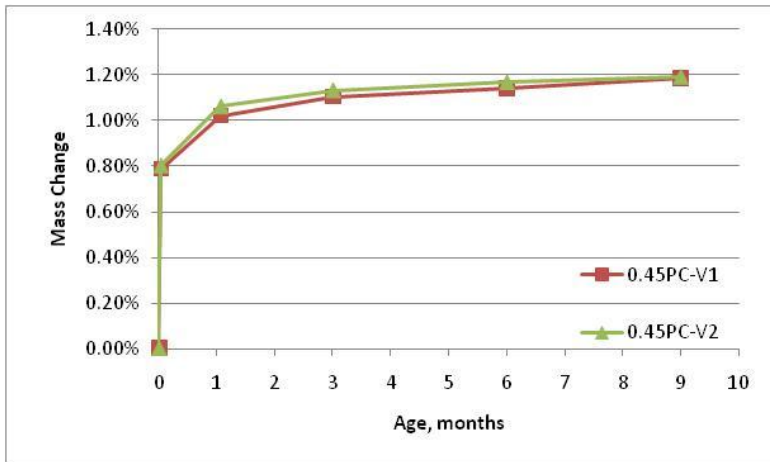
(b)



(c)



(d)



(e)

Figure 21 USBR Fully Immersed Condition Mass Change (Mixtures 9-22)

(a) 20% fly ash mixtures at various w/cm ratios, (b) 35% slag cement mixtures at various w/cm ratios, (c) 30% fly ash mixtures at various w/cm ratios, (d) 50% slag cement mixtures at various w/cm ratios, and (e) portland cement mixtures (PC-V1 C₃A=3%, PC-V2 C₃A=5%)



(a)



(b)



(c)



(d)



(e)

Figure 22 USBR Fully Immersed Sample Pictures after 9 months

(a) 20% fly ash mixtures at various w/cm ratios, (b) 35% slag cement mixtures at various w/cm ratios, (c) 30% fly ash mixtures at various w/cm ratios, (d) 50% slag cement mixtures at various w/cm ratios, and (e) portland cement mixtures

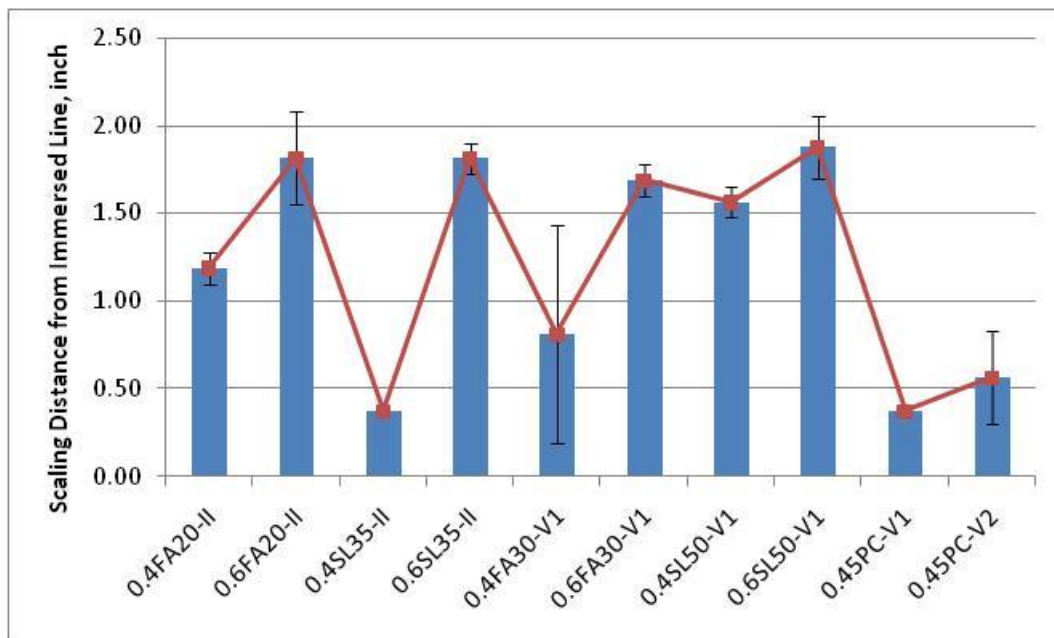
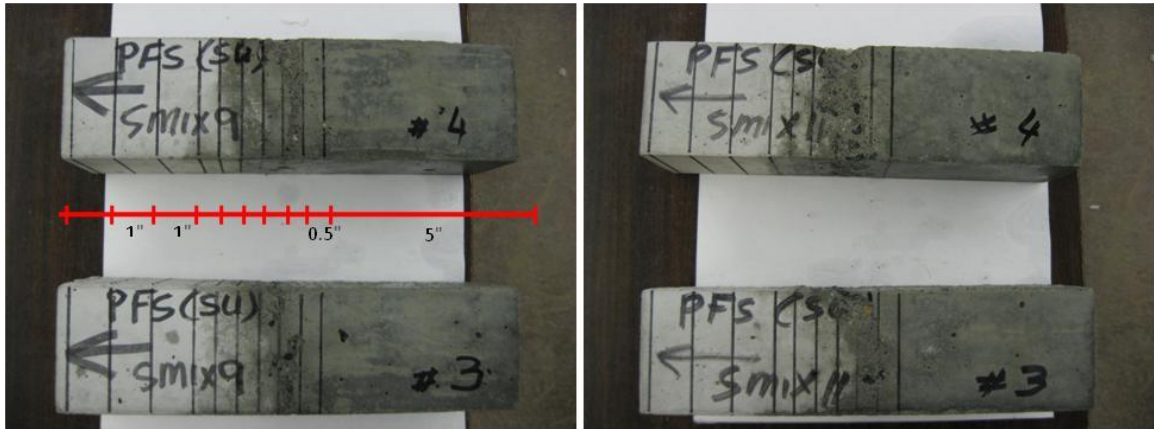


Figure 23 USBR Half Immersed Condition Scaling Distance from Immersion Line after 9 months

Error Bars indicates ± 1 standard deviation for the testing of two specimens



(a)



(b)



(c)



(d)



(e)

Figure 24 USBR Half Immersed Sample Pictures after 9 months

(a) 20% fly ash mixtures, (b) 35% slag cement mixtures, (c) 30% fly ash mixtures, (d) 50% slag cement mixtures, and (e) portland cement mixtures